FINITE ELEMENT STABILITY ANALYSIS OF THIN-WALLED STEEL STRUCTURES

A Thesis submitted for

the Degree of

DOCTOR OF PHILOSOPHY

by

MOHAMED TAHER MOHAMED NEMIR

Department of Civil Engineering

University of Salford

September 1985

CONTENTS

DECLARATION

None of the material contained in this thesis has been submitted in support of an application for another degree or qualification of this or any other university or institution of learning.

MOHAMED TAHER
September 1985

ABSTRACT

Recent applications in the use of light gauge steel members have been concerned with developing large scale systems built entirely from cold-formed steel members. An explicit analysis of such structures is complicated by the different phenomena that the structure may be prone to during loading. In particular, elastic buckling phenomena is an important consideration in the design of such structures since the load at which buckling occurs often provides a close upper bound to the carrying capacity of the structure.

The first part of this two-part thesis (Part I, Chapters1-8) has been devoted to general methods of analysis of the torsional-flexural buckling of thin-walled structures. A review of previous investigations and the available methods of solution is presented. A general finite element formulation of the torsional-flexural buckling of thin-walled structures has been derived. The resulting elastic geometric matrix can be used to analyse structures with monosymmetrical members. It also includes the effect of sectorial-monosymmetry for cross-sections without any axis of symmetry. A general transformation matrix has been developed to allow for the application of the finite element method to the three-dimensional elastic stability analysis of space and portal frames. The validity and accuracy of the new finite element formulation have been checked by analysing a number of different elastic lateral buckling problems for which exact or highly accurate solutions by other techniques are available.

An experimental program was carried out on simply supported cold-formed steel z-beams. The first part of this program was undertaken to check the validity of the finite element calculations of the bimoments caused by nonuniform torsion. The second part was devoted to elastic lateral buckling of z-beams under combined bending and torsion.

The second part of this thesis (Part II, Chapter 9) deals with the analysis of hipped roof structures with corrugated steel roof sheeting. A simple theoretical model has been suggested. The model has been used to perform an elastic linear analysis of the behaviour of two types of the hipped roof structures. The theoretical results are compared with previous experimental results for these two structures.

ACKNOWLEDGEMENTS

I would like to express my gratitude to my supervisor, Professor J.M. Davies, who introduced me to the subject and gave valuable advice throughout the project, and to Professor E.R. Bryan, for his continued interest and encouragement throughout the period of study.

I also wish to express my thanks to the Structural Laboratory staff and in particular to Mr. W. Deakin, Mr. S. Abed Elhafiz for his preparation of the graphs, and to Mrs. L.C. Rycroft for typing the manuscript.

LIST OF MAIN SYMBOLS

S_y Static moment of area about y-axis

S_z Static moment of area about z-axis

I_y Second moment of area about y-axis

I_z Second moment of area about z-axis

I_o Polar moment of inertia

A Area of cross section

$\bar{\omega}_m$ Sectorial co-ordinate at point m

S_ω Sectorial static moment of area

I_ω Second sectorial moment of area (warping constant)

J Torsion constant of the cross section

E Modulus of elasticity

G Shear modulus

u Displacement in x-direction

v Shear center displacement in y-direction

w Shear center displacement in z-direction

θ_x Angle of twist of the cross section

ψ Angle of rotation about z-axis

ϕ Angle of rotation about y-axis

χ Warping of the cross section

x,y,z Local co-ordinate system of axes

X,Y,Z Global co-ordinate system of axes

ℓ_1, m_1, n_1 Direction cosines of the local x-axis with respect to the global axes X, Y and Z respectively

ℓ_2, m_2, n_2 Direction cosines of the local y-axis with respect to the global axes X, Y and Z respectively

ℓ_3, m_3, n_3 Direction cosines of the local z-axis with respect to the global axes X, Y and Z respectively

K_E Member elastic stiffness matrix

K_G Member geometric matrix

ℓ Span of the member

$\bar{t}_i$ Member transformation matrix

B Bimoment (warping moment)

M_y Bending moment about y-axis

M_z Bending moment about z-axis

Q_y Shear force in y-direction

Q_z Shear force in x-direction

P_x Compressive axial force

β_y Coefficient of monosymmetry about y-axis

β_z Coefficient of monosymmetry about z-axis

β_ω Coefficient of sectorial monosymmetry

k Bending - twisting parameter

LIST OF FIGURES AND TABLES

(Figures and tables are presented at the end of the relevant chapter).

CHAPTER 2

CHAPTER 3

Table

CHAPTER 9

Fig.

Table

LIST OF PHOTOGRAPHIC PLATES

CHAPTER 5

CHAPTER 7

P A R T (I)

CHAPTER ONE

INTRODUCTION

The conventional analysis of linearly elastic structures carrying static loads is always performed under the assumption that stable equilibrium exists between internal and external forces. This includes neglecting the reduction of the stiffness due to the change of the structure geometry. However, with the increase in the value of the static load the structure may be prone to the effect of one of the stability phenomena. A condition of instability exists when the structure starts to lose its stiffness. This is characterised by the fact that the deformations of the structure corresponding to a given load factor can reach infinite values for arbitrarily small (infinitesimal) load increments. If the entire structure remains perfectly elastic until buckling commences, this type of buckling is called elastic buckling. The load level at this stage is defined as the elastic buckling load or the elastic critical load.

In the fundamental case of buckling it is assumed that a thin-walled long column with open cross section buckles by flexure in the plane of the least rigidity. However, under uniform axial compression a column with cruciform cross sectional shape buckles torsionally while its longitudinal axis remains straight. In general, buckling of columns takes place in a combined torsional and flexural mode. The in-plane displacements of the cross section can be analysed as a translation of the shear center and a rotation about it.

A beam bent in the plane of the greatest flexural rigidity may buckle laterally in a similar manner. The flexural-torsional buckling load may represent the ultimate strength of thin-walled unbraced beams.

For more than 25 years the common use of cold-formed members in building has been almost limited to secondary systems such as the roof purlins and the side beams of steel frameworks. The use of cold-formed steel members for primary

systems, such as portal and space frames has been comparatively rare. This may be due to the lack of information concerning the behaviour of such structures and the need for theoretical techniques to analyse the different phenomena that may occur during loading. However, recent applications have been concerned with developing steel portal and space frames built entirely of cold-formed members.

The design of plane frames built of hot-rolled members is often based on the in-plane behaviour alone. For such consideration to be valid, the resistance of the frame to the out of plane displacements must be sufficiently high. Light gauge steel portal frames, however, have a high tendency to twist, warp, and buckle laterally under in-plane loading. Torsional-flexural buckling is an important consideration in the design of such frames.

Although the torsional-flexural buckling of single span and continuous beams has been extensively studied, little has been reported about the torsional-flexural buckling of plane and space frames. Most of the studies carried out in this field were limited to certain frame shapes and special loading conditions.

The finite element method is well recognised as a powerful technique to be used for the linear analysis of complex and irregular structural systems. During the last 15 years, the method has been extended by many investigators to deal with torsional-flexural buckling problems. However, the application of the method has generally been limited to single span or continuous beams.

The study reported in the first part of this thesis (Part I) was undertaken in order to establish a finite element formulation for the torsional-flexural buckling of thin-walled beams, columns and frames. The new formulation was aimed to be applicable to any cross sectional shape.

The first part of this thesis (Part I) contains eight chapters. An introduction is presented in the present chapter. Chapter two is devoted to three main items, namely,

a) Review of the general theory of the torsional-flexural behaviour of thin-walled structures.

b) Methods used to analyse the torsional-flexural buckling.

c) Review of previous studies on the torsional-flexural buckling.

The derivation of the new finite element elastic stiffness and geometric matrices is presented in chapter three. The derivation is based on Vlasov's concept (1) of the torsional-flexural behaviour of thin-walled structures. The chapter also includes a new transformation matrix for the three-dimensional buckling analysis of plane and space frames.

Chapter four presents a review of the different techniques used to predict the critical load from the elastic instability equation. It also includes the illustration of the finite element computer program used in this study.

Chapter five is devoted to the calculations of the bimoments caused by the nonuniform torsion of a thin-walled structure. The finite element solutions for a number of problems are compared to closed form, highly accurate solutions and to experimentally determined bimoments.

Chapter six presents the results of a theoretical study made by the finite element method to examine the validity and accuracy of the new formulation. Finite element solutions for a number of previously presented problems are given with the comparison with other solutions of these problems.

Chapter seven deals with the lateral buckling of simply supported cold-formed Z-beams with end warping free. An experimental program was carried out to test five of these beams under different types of bending and torsional loading. The measured values of the displacements and critical loads are compared to the corresponding finite element solutions.

The observations and conclusions of the present study are given in chapter eight.

CHAPTER TWO

Torsional-Flexural Buckling of Thin-Walled Structures

2.1. UNIFORM AND NONUNIFORM TORSION

A thin-walled member exhibits warping displacements when it is twisted by uniform torque if the flanges at the end cross sections have no longitudinal restraint. Under such conditions warping is the same for all cross sections and the only stresses produced are the shearing stresses at each cross section of the member. The warping of the cross section of a twisted I-beam is shown in fig. 2.1. During twisting, plane sections do not remain plane, only the web remains plane while the flanges rotate bodily in two opposite directions.

If some longitudinal restraint is applied to the flanges at any cross section, or if the torque varies along the length of the member, the flanges will then be forced to take up a curvature in the longitudinal direction. As shown in fig. 2.2, where a cantilever beam is twisted by a concentrated torque T applied at the free end, the curvature of the flanges varies along the member and the flanges appear as being under two equal, but opposite bending moments, acting in their own plane. The combination of the two bending moments induced in the flanges as a result of the nonuniform torque is called a bimoment. The longitudinal stresses caused by the bimoment can be very large and must be considered in the analysis. At any cross section the acting torque T can be divided into two parts:

a) T_s due to St.venant shear stresses, and

b) T_w due to the normal stresses induced by the bimoment.

The present chapter contains three main parts, namely:

1. Review of the general theory of torsional-flexural behaviour of thin-walled structures.

2. The different methods which can be used to analyse the torsional-flexural buckling of thin-walled structures and the validity of each method.

3. Review of the previous studies carried out to analyse the torsional-flexural buckling of thin-walled structures.

2.2. COMBINED TORSIONAL-FLEXURAL BEHAVIOUR OF PRISMATIC MEMBERS

2.2.1. Basic assumptions

The basic assumptions of the theory of torsional-flexural behaviour of thin-walled prismatic members as given by Vlasov (1) are:

a) The material of the structure is perfectly elastic.

b) Small deflection theory is adopted.

c) The member retains its cross-sectional shape while undergoing all deformations during loading but may warp perpendicular to the plane of the cross section.

d) The shear deformations of the middle surface of the member can be neglected.

2.2.2. Torsional-flexural behaviour of prismatic member

The subject prismatic member with an arbitrarily chosen cross section is shown in fig. 2.3. The member is defined with respect to a rectangular co-ordinate system which is right handed. Axes y and z coincide with the two principal axes of the cross section while x coincides with the longitudinal centroidal axis of the member.

The in-plane displacement of an arbitrary point m with co-ordinates y and z (fig. 2.4) can be represented by the two components v_m and w_m in y and z directions respectively. These two components are given by,

$$v_m = v - (z_o - z)\,\theta_x \qquad (2.1)$$

$$w_m = w + (y_o - y)\,\theta_x \qquad (2.2)$$

in which, y_o and z_o are the shear center co-ordinates, v and w are the displacements of the shear center and θ_x is the angle of twist of the cross section. The two in-plane displacements v_m and w_m are replaced in fig. 2.5 by another two components, t_m in the direction tangential to the cross section at m and n_m in the direction perpendicular to the tangent.

The tangential component t_m is given by,

$$t_m = v \sin \alpha + w \cos \alpha + H \theta_x \qquad (2.3)$$

where,

$$H = (y_o - y) \cos \alpha - (z_o - z) \sin \alpha \qquad (2.4)$$

The shear strain at point m in the middle surface is given by,

$$\gamma_{sh} = \frac{\partial t_m}{\partial x} + \frac{\partial u_m}{\partial s} \qquad (2.5)$$

where, u_m is the longitudinal displacement at point m. Applying the fourth assumption of the theory, the shear strain γ_{sh} can be set to zero, hence,

$$\frac{\partial u_m}{\partial s} = - \frac{\partial t_m}{\partial x} \qquad (2.6)$$

Substituting for t_m from equation 2.3, and integrating with respect to s from s = o to s, the expression of the longitudinal displacement u_m becomes,

$$u_m = u_o - \grave{w} z - \grave{v} y - \grave{\theta}_x \int_o^s H \, ds \qquad (2.7)$$

where, u_o is the displacement, in x-direction, of point p from which s is measured, z and y are the Cartesian co-ordinates at point m, $\grave{w}$ and $\grave{v}$ are the first derivatives of the shear center displacements with respect to x axis,

and θ'_x is the first derivative of the angle of twist θ_x with respect to x. The first three terms of equation 2.7 represent the effect of the axial load P_x, bending moment M_y and bending moment M_z acting at the cross section. The fourth term of equation 2.7 represents the warping displacement caused by the nonuniform torsion.

The integration $\int_o^s H\, ds$ is known as the sectorial co-ordinate of point m.

2.2.3. Sectorial proporties of the cross section

2.2.3.1. Sectorial co-ordinate (ω)

As shown in fig. 2.6 the sectorial co-ordinate ω_m of point m represents double the area swept by the radius r when moving along the middle line of the cross section from the origin p where s = o up to point m. The sectorial co-ordinate is taken positive when the radius r is rotating in the positive direction, that is to say counterclockwise about the shear center . The distribution of the sectorial co-ordinates for a Z-cross section is shown in fig. 2.7.

2.2.3.2. Sectorial static moment of area

The sectorial static moment at m on the middle line of the cross section is given by,

$$S_{\omega_m} = \int_o^s \omega\, dA \qquad (2.8)$$

In which, A is the area of the cross section.

As for the Cartesian co-ordinates, the principal origin g of the sectorial co-ordinates is the point on the middle line of the cross section at which S_ω = o. The actual values of the sectorial co-ordinates can be calculated with respect to this origin.

2.2.3.3. Second sectorial moment of area (warping constant)

The warping constant is a geometrical characteristic of the cross section and is given by,

$$I_\omega = \int_A \bar{\omega}^2 \, dA \qquad (2.9)$$

where, $\bar{\omega}$ is calculated with respect to the principal origin of the sectorial co-ordinates g.

It can be concluded that, in the theory of thin-walled structures, any point m on the middle line of the cross section is defined by the three co-ordinates y, z and $\bar{\omega}$. The statical moments of area which are required to calculate the shear stresses at m are S_y, S_z and S_ω. The corresponding second moments of area for the cross section are I_y, I_z and I_ω.

2.2.4. First order equilibrium equations of combined torsional-flexural behaviour.

The differential equations of equilibrium describing the first order torsional and flexural behaviour of a thin-walled prismatic member are,

$$- E A \frac{du}{dx} = P_x \qquad (2.10)$$

$$- E I_z \frac{d^4 v}{dx^4} = q_y \qquad (2.11)$$

$$- E I_y \frac{d^4 w}{dx^4} = q_z \qquad (2.12)$$

$$GJ \frac{d^2 \theta_x}{dx^2} - E I_\omega \frac{d^4 \theta_x}{dx^4} = m_x \qquad (2.13)$$

In which, P_x is the normal force in x-direction, q_y and q_z are the uniformly distributed loads in y and z directions respectively and m_x is the acting torque per unit length.

2.2.5. Basic theory of torsional-flexural buckling

The beam-column with doubly symmetrical I cross section shown in fig. 2.8 is loaded by a central thrust P_x with biaxial eccentricities e_z and e_y which are constant along the length ℓ of the beam. If the initial deflection, due to the bending couples, is considered as very small, the second-order effect of the central thrust P_x on the bending stresses can be neglected and the normal stress at any point is given by,

$$f = -\frac{P_x}{A} - \frac{P_x e_y y}{I_z} - \frac{P_x e_z z}{I_y} \qquad (2.14)$$

In investigating the stability of the initially deflected beam, Timoshenko (2) assumed that up to the moment of buckling the beam is essentially in a state of flexural equilibrium. At the moment of buckling, however, additional deflections are produced and the beam passes to a new form of equilibrium which is flexural-torsional.

By calculating the intensities of the distributed lateral loads and torque produced by the initial compressive stresses when acting on the slightly displaced cross section, Timoshenko (2) presented the differential equations of equilibrium for the flexural-torsional buckling of the beam. These equations are,

$$EI_z \frac{d^4v}{dx^4} + P_x \frac{d^2v}{dx^2} + P_x e_z \frac{d^2\theta_x}{dx^2} = o \qquad (2.15)$$

$$EI_y \frac{d^4w}{dx^4} + P_x \frac{d^2w}{dx^2} - P_x e_y \frac{d^2\theta_x}{dx^2} = 0 \qquad (2.16)$$

$$EI_\omega \frac{d^4\theta_x}{dx^4} - (GJ - P_x \frac{I_o}{A}) \frac{d^2\theta_x}{dx^2} + P_x e_z \frac{d^2v}{dx^2} - P_x e_y \frac{d^2w}{dx^2} = o \qquad (2.17)$$

where, in addition to the previously given notations, the constant I_o represents the polar moment of inertia about the shear center.

Vlasov (1) showed that if a longitudinal force P_x is applied to the cross section at a point where the sectorial co-ordinate $\bar{\omega}$ is not equal to zero, this force can produce bimoments. He added the normal stresses caused by the bimoment to the three terms in equation (2.14) and studied the torsional-flexural buckling of the beam when the initial form of equilibrium is torsional-flexural. Vlasov's concept for the general case of torsional-flexural buckling is the basis of the new finite element formulation of the torsional-flexural buckling of thin-walled prismatic element presented in chapter three of this thesis.

2.3. METHODS OF ANALYSING ELASTIC STABILITY PROBLEMS

2.3.1. General

Methods used to analyse the elastic stability problems of thin-walled structures may be classified as equilibrium methods, energy methods and numerical methods. Equilibrium methods are based on the solution of the differential equations of equilibrium which represent the buckled form of the structure. On the other hand, energy methods and numerical methods do not require the solution of the differential equilibrium equations.

2.3.2. Equilibrium methods

The differential equations of equilibrium representing the elastic lateral buckling of a given thin-walled structure are linear and homogeneous. The coefficients of these equations depend on the geometric and elastic characteristics of the structure and on the load factors.

There are two procedures to derive the differential equations of equilibrium:

a) By calculating the internal forces caused by the initial stresses of the loading system when acting on the slightly displaced member and considering the equilibrium between the external and internal forces at the moment of buckling (1,2).

b) By applying the principle of stationary energy and using the calculus of variations concept to derive the differential equations of equilibrium from the energy expression (3).

The methods which can be used to solve the differential equations of equilibrium may be classified as exact (closed form) methods, and approximate methods.

2.3.2.1. Exact (closed form) solutions

If a single load parameter is considered, the coefficients of the differential equations can be expressed in terms of this parameter. This parameter, together with the deformations, are the unknown quantities of the equations.

The exact solution of the differential equilibrium equations is based on choosing suitable functions to represent the deformed state of the structure. These functions must satisfy the boundary and loading conditions of the structure.

After substituting the assumed functions in the equilibrium equations and constructing the matrix of the coefficients, the determinant of this matrix is considered as the stability criterion.

One of the few examples of elastic torsional-flexural buckling of beams that can be solved exactly, is that of a simply supported I-beam carrying a thrust P_x with eccentricity e_y which is constant along the length ℓ of the be.m. The differential equilibrium equations for this case can be derived from equations 2.15-2.17 (section 2.2.5), and these equations become,

$$EI_z \frac{d^4v}{dx^4} + P_x \frac{d^2v}{dx^2} = o \qquad (2.18)$$

$$EI_y \frac{d^4w}{dx^4} + P_x \frac{d^2w}{dx^2} - P_x e_y \frac{d^2\theta_x}{dx^2} = o \qquad (2.19)$$

$$EI_\omega \frac{d^4\theta_x}{dx^4} - (GJ - P_x \frac{I_o}{A})\frac{d^2\theta_x}{dx^2} - P_x e_y \frac{d^2w}{dx^2} = o \qquad (2.20)$$

The end conditions for a simply supported beam are:

$$v = w = \theta_x = o \qquad \text{at } z = o \text{ and } z = \ell \qquad (2.21)$$

$$\frac{d^2v}{dx^2} = \frac{d^2w}{dx^2} = \frac{d^2\theta_x}{dx^2} = o \qquad \text{at } z = o \text{ and } z = \ell \qquad (2.22)$$

These conditions are satisfied by taking v, w, and θ_x in the form,

$$v = A_1 \sin \frac{\pi x}{\ell}\ ,\ w = A_2 \sin \frac{\pi x}{\ell}\ ,\ \theta_x = A_3 \sin \frac{\pi x}{\ell} \qquad (2.23)$$

Substituting by these functions into equations (2.18),(2.19), and (2.20) the differential equations of equilibrium become,

$$(EI_z \frac{\pi^2}{\ell^2} - P_x)\ A_1 = o \qquad (2.24)$$

$$(EI_y \frac{\pi^2}{\ell^2} - P_x)\ A_2 + P_x \cdot e_y \cdot A_3 = o \qquad (2.25)$$

$$P_x \cdot e_y \cdot A_2 + (EI_\omega \frac{\pi^2}{\ell^2} + GJ - P_x \frac{I_o}{A})A_3 = o \qquad (2.26)$$

The first of these equations (eq. 2.24) shows that the buckling in the plane of symmetry is independent and the corresponding buckling load is the same as the Euler load. The second and third equations (eq. 2.25 and 2.26) show that the lateral buckling in the xy plane and the torsional buckling are coupled. The corresponding critical load can be obtained by equating to zero the determinant of these two equations. This condition is given by,

$$\Delta = \begin{bmatrix} (F_y - P_x) & P_x e_y \\ P_x e_y & \frac{I_o}{A}(F_\phi - P_x) \end{bmatrix} = o \qquad (2.27)$$

in which,

$$F_y = EI_y \frac{\pi^2}{\ell^2} \qquad F_\phi = \frac{A}{I_o}(EI_\omega + GJ\frac{\pi^2}{\ell^2}) \qquad (2.28)$$

By expanding the determinant Δ, the equation from which the critical load can be calculated is given by,

$$P_x^2 - \bar{K}P_x(F_y+F_\phi) + KF_y F_\phi = o \qquad (2.29)$$

where $$\bar{K} = \frac{i_o^2}{(i_o^2 - e_y^2)} \quad \text{and} \quad i_o^2 = \frac{I_o}{A} \qquad (2.30)$$

The smallest positive solution of equation 2.29 gives the critical buckling load.

Unfortunately, exact (closed form) solutions of the differential equations of equilibrium are comparatively rare and limited to simple structures. There are, however, some approximate methods to solve the equilibrium equations and these methods will be explained now.

2.3.2.2. Approximate solutions of the differential equations

a) Infinite series solution

In some cases the solution of the governing differential equations of equilibrium can be carried out by assuming a suitable finite series to represent the deformations. This series must satisfy the loading and constraint conditions of the problem. The accuracy of the method depends on the number of terms taken from the series. Timoshenko (2) used

the method to study the lateral buckling of an I-beam subjected to a concentrated load. He used a trigonometric series to represent the angle of twist θ_x. In another application Trahair (4) showed that a Taylor series expansion can be used to express the twisted shape θ_x of the buckled beam.

b) Iterative integration method

Another approximate method for the solution of the differential equations of equilibrium is the iterative integration method. The method is known as the Stodola-Vianello method (3) and is sometimes called the successive approximation method.

The method is based on integrating numerically the differential equations of equilibrium starting from an initial approximation for the deformed shape of the structure. This assumed shape must satisfy the boundary conditions. The numerical integration of the differential equations of equilibrium results in a new improved representation for the deformed shape of the structure. Then the procedure can be repeated to obtain a third estimate for the assumed function. In this way a series of functions can be generated, where each function corresponds to a certain value of the buckling load. The procedure can be continued until the desired accuracy is obtained. The applications of the iterative integration method have shown excellent agreement with the closed form solutions for beam and column stability problems (2,3,4).

c) Finite difference solution

The finite difference method is an approximate method for solving complex differential equations. The method can be applied to stability problems to give approximate values for buckling loads in some cases when the differential equations of equilibrium cannot be solved in closed form.

The method is based on replacing the differential equation,which is applicable over a certain range of an independent variable x , by a finite number of algebric equations, one for each of a number of points within the range of x. At each point, the differential operators of the dependent function f(x) are represented by finite difference approximations which can be given as combinations of the values of f(x) of neighbouring points,assuming some polynomial shape for the f(x) values. The boundary conditions of the differential equations are represented in the same way. The solution of the resulting homogeneous equations gives the desired unknowns of the problem.

The application of the method to buckling problems can be demonstrated by analysing the lateral buckling of a simply supported I-beam loaded by a uniform bending moment M (3). The governing differential equation of the buckled form of the beam is given by,

$$EI_\omega \frac{d^4\theta}{dx^4} - GJ \frac{d^2\theta}{dx^2} - \frac{M^2}{EI_y}\theta = o \qquad (2.31)$$

The boundary conditions are,

$$\theta = \frac{d^2\theta}{dx^2} = o \qquad \text{at } x = o \text{ and } x = \ell \qquad (2.32)$$

Dividing the span ℓ of the beam into n equal parts of width $b = \ell/n$ the values of θ at the end and interior points are given by,

$$\theta_o, \theta_1, \theta_2, \cdots, \theta_{i-1}, \theta_i, \theta_{i+1}, \cdots, \theta_{n-1}, \theta_n \qquad (2.33)$$

If the interval width b is chosen sufficiently small,the slope of the function θ at the ith point may be approximated by the slope of any of the two straight lines AB or BC (fig. 2.9) and then,

$$(\frac{d\theta}{dx})_{i(left)} \simeq \frac{\theta_i - \theta_{i-1}}{b}, \text{and } (\frac{d\theta}{dx})_{i(right)} \simeq \frac{\theta_{i+1} - \theta_i}{b} \quad (2.34)$$

The differential operators $\frac{d^2\theta}{dx^2}$, and $\frac{d^4\theta}{dx^4}$ at the ith point can also be given by,

$$(\frac{d^2\theta}{dx^2})_i = \frac{\theta_{i+1} - 2\,\theta_i + \theta_{i-1}}{b^2} \quad (2.35)$$

$$(\frac{d^4\theta}{dx^4})_i = \frac{\theta_{i+2} - 4\,\theta_{i+1} + 6\,\theta_i - 4\,\theta_{i-1} + \theta_{i-2}}{b^4} \quad (2.36)$$

Substituting the approximate values of the differential operators in the differential equation (eq. 2.31), the difference equation which is valid at any point i is given by,

$$\theta_{i+2} - K_1\theta_{i+1} + K_2\theta_i - K_1\theta_{i-1} + \theta_{i-2} = o \quad (2.37)$$

where $$K_1 = 4 + \frac{GJ\,\ell^2}{EI_\omega\, n^2} \quad (2.38)$$

and $$K_2 = 6 + 2\,\frac{GJ\,\ell^2}{EI_\omega\, n^2} - \frac{M^2\,\ell^4}{E^2 I_\omega I_y\, n^4} \quad (2.39)$$

and the boundary conditions give,

$$\theta_o = \theta_n = o \qquad \theta_{-1} = -\theta_1 \text{ and } \theta_{n+1} = -\theta_{n-1} \quad (2.40)$$

Equation 2.37 is valid at n-1 points. It represents a system of linear homogeneous equations in the n-1 unknown values of the rotation θ_i. The approximate value of the buckling moment M_c can be calculated by setting equal to zero the determinant of the coefficients of these equations.

The accuracy of the solution may be improved either by increasing the number of intervals into which the span ℓ is divided or by improving the accuracy of the representation of the differential operators. However, each of these two modifications increases the labour of solving the simultaneous equations and makes the method unsuitable for hand calculations. A finite differences computer program can then be developed to obtain more accurate results.

d) Finite integral solution

The finite integral method is an approximate technique for solving complex differential equations. The method is based on considering the differential equation as an integral equation in the highest derivative of the dependent variable f(x). As for the finite difference method the length ℓ of the beam is divided into a number of equal parts n of width b where $b = \ell/n$. The integral equation is then replaced by a finite number of homogeneous equations one for each point. The dependent variable f(x) and its lower derivatives are replaced by a combination of the values of the highest derivatives of f(x).

The application of the method can be illustrated by analysing the lateral buckling of a simply supported beam with a narrow rectangular cross section loaded by uniform bending moment. The governing differential equation is given by,

$$\frac{d^2\theta}{dx^2} + \bar{K}\,\theta = 0 \qquad (2.41)$$

where, $\bar{K} = M^2/GJ \cdot EI_y$ (2.42)

Equation 2.41 can be rewritten in integral form,

$$R + \bar{K}\left(\int_0^x \int_0^x R\,dx\,dx + Ax + B\right) = 0 \qquad (2.43)$$

where , $R = \frac{d^2\theta}{dx^2}$

The constants of integration A, and B can be determined from the boundary and symmetry conditions. These conditions are,

$$\theta = o \quad \text{at } x = o \quad \text{and } (\frac{d\theta}{dx}) = o \quad \text{at } x = \ell/2 \qquad (2.44)$$

Substituting these two conditions in equation 2.43 gives,

$$A = -\int_o^{\ell/2} R\, dx \qquad \text{and} \qquad B = o \qquad (2.45)$$

As in the finite difference method, the function R may be approximated by a parabola fitted to three adjacent values of R; this parabola is given by,

$$R = ax^2 + bx + c \qquad (2.46)$$

in which,

$$a = \frac{R_{i+1} - 2R_i + R_{i-1}}{2b^2}, \quad b = \frac{R_{i+1} - R_{i-1}}{2b} - 2a\, x_i \quad \text{and,}$$

$$c = R_i - a\, x_i^2 - b\, x_i \qquad (2.47)$$

The integrals of θ are given by,

$$\int_{x_{i-1}}^{x_i} R\, dx = \frac{b}{12}(5\, R_{i-1} + 8\, R_i - R_{i+1}) \qquad (2.48)$$

$$\int_{x_{i-1}}^{x_{i+1}} R\,dx = \frac{b}{12}\,(4R_{i-1} + 16\,R_i + 4\,R_{i+1}) \qquad (2.49)$$

By making the second integral of the function R and substituting in equation 2.43 the integral equation becomes,

$$R_i - \frac{\bar{K}b^2}{144}\,(12\,R_{i-1} + 154\,R_i + 60\,R_{i+1}) = o \qquad (2.50)$$

Equation 2.50 is valid at n-1 points. It represents a system of linear homogeneous equations. The critical buckling moment M_c can be calculated by equating to zero the determinant of the coefficients of these equations. More details about the applications of the method to the stability problems can be found in references 5, 6, and 7.

2.3.3. Energy methods

2.3.3.1. General

The use of the energy method to solve the problems of elastic stability is based on the principle of the stationary value of energy which characterizes the equilibrium condition in an elastic system. This principle can be stated as: "the amount of total potential energy of an elastic structure does not change when the structure passes from its configuration of equilibrium to an infinitesimally near adjacent configuration". This can be expressed as,

$$U = U_w + V = \text{Stationary} \qquad (2.51)$$

where,

U is the total potential energy, U_w is the potential of the applied load, and V is the strain energy.

Equation 2.51 can be rewritten in the form,

$$\delta U_w + \delta V = \delta\,(U_w + V) = 0 \qquad (2.52)$$

in which, δU_w is the increase in the potential energy of the acting load and is equal to minus the work done by the load during the virtual displacement, and δV is the increase in the strain energy of the structure.

The use of the method to solve stability problems often leads to approximate values of the critical buckling load. The solution depends on using approximate deformation shapes that satisfy the boundary conditions of the problem. The accuracy of the solution depends on how close the assumed deformation shapes compared to the exact ones.

Timoshenko (2) was the first to use the energy method for the approximate solution of elastic stability problems. At about the same time, Ritz (3) published his general method for the direct solution of minimum problems in mathematical physics. Ritz's method is quite general and it has many applications in stability problems. The method was later extended and refined by many investigators (3). The application of Ritz's method to elastic stability problems is illustrated in the next section.

2.3.3.2. The Ritz method

Considering the elastic lateral buckling of a simply supported beam with narrow rectangular cross section loaded by uniform bending moment M, the total potential energy U is given by,

$$U = GJ \int_0^{\ell} \left(\frac{d^2\theta}{dx^2}\right)^2 dx - \frac{M^2}{EI_y} \int_0^{\ell} \left(\frac{d\theta}{dx}\right)^2 dx \qquad (2.53)$$

The angle of rotation θ_x can be expressed by the finite series,

$$\theta_x = b_1\psi_1 + b_2\psi_2 + \cdots \quad \cdots + b_n\psi_n \qquad (2.54)$$

where, ψ-terms are arbitrarily chosen functions of x called co-ordinate functions. These functions must satisfy the same boundary conditions as the angle of rotation θ_x. The b-terms are a corresponding set of parameters.

Substituting from equation 2.54 into the energy expression (eq. 2.53) the total energy U can be given by,

$$U = f_1(b_1, \ldots, b_n) - \frac{M^2}{EI_y \cdot GJ} f_2(b_1, \ldots, b_n) \qquad (2.55)$$

in which, f_1 and f_2 are quadratic forms of the parameters $b_1, \ldots, b_n$ which are the variables of the problem. Applying the principle of stationary energy (eq. 2.52) the stability conditions are given by,

$$\frac{\partial U}{\partial b_i} = o \qquad (i = 1,2, \ldots, n) \qquad (2.56)$$

Equation 2.56 represents a system of n linear homogeneous equations from which the critical buckling moment M_c can be calculated by equating to zero the determinant of the coefficients of these equations.

The accuracy of Ritz's method may be improved by increasing the number of terms of the finite series taken to represent the dependent function θ_x. However, success or failure in applying the method depends mainly on the proper choice of the co-ordinate functions ψ. These functions can be polynomials or transcendental functions. The only restriction is that they must satisfy the boundary conditions of the problem. However, in the majority of cases satisfactory results can be obtained only when the co-ordinate functions ψ form a system of orthogonal functions (3).

2.3.4. Numerical techniques based on the displacement method

2.3.4.1. General

The use of the closed form and energy solutions for analysing elastic stability problems is limited to simple structures such as single span beams and beam-columns. The difficulty of applying such methods to solve the more complex structures, such as continuous beams and frames, arises from the amount of calculations needed to solve the large sets of the resulting differential equations.

The advent of the electronic digital computer has made possible a completely new approach to deal with large sets of simultaneous equations. Nevertheless, the matrix formulation of large sets of equations has long been recognised as the most convenient way of representing the load-displacement relationship to meet the nature of the routine calculations involved in computer programming.

During the last twenty five years the applications of matrix methods have been extended to the analysis of elastic stability problems. However, most of these studies have been devoted to certain types of stability problems. The methods used in these applications can be divided into two main types, namely,

1. The member stiffness-matrix method (with specific boundary conditions).

2. The finite element method.

Both methods will now be reviewed and discussed with regard to their applications in elastic stability problems.

2.3.4.2. Member stiffness-matrix method

In the conventional analysis of elastic plane frames, the derivation of member stiffness factors is based on the assumption that the member carries bending moments and shear forces only. On the other hand, the differential equations of equilibrium governing the second-order behaviour of a beam-column member, include the effect of the direct axial strains caused by axial forces. Thus, in comparison to the first-order stiffness matrix of an elastic member, the second-order matrix contains the same stiffness factors but modified by multiplying factors called stability functions. Values of stability functions depend on the ratio between the acting axial force and the value of Euler buckling load.

Credit probably goes to Livesley (8) for being the first to use the matrix stiffness method to analyse the in-plane elastic buckling of steel frameworks. He described a

computer program to carry out the analysis and predict the in-plane elastic buckling load for two-dimensional frames loaded at column tops.

Renton (9) followed the same procedure to derive the stiffness matrix of the elastic torsional-flexural buckling of thin-walled members. He used this matrix to analyse the elastic stability problem of symmetrical space frames. His method has some limitations as it is applicable only to certain types of cross sections and to frames loaded only at the column tops.

Chu and Rametsreiter (10) extended Renton's method to study the large deflection symmetrical and asymmetrical buckling modes of space frames. Later, Razzaq and Naim (11), used the same method to analyse the elastic stability of rigid-jointed unbraced single-story single-bay orthogonal space frames subjected to equal and unequal concentrated column top loads.

Chaudhary (12) based his stiffness matrix on the closed form solution of the differential equilibrium equations for torsional-flexural buckling of thin-walled structures given by Vlasov (1). Aly and Sato (13), however, have shown in a later discussion of Chaudhary's proposed matrix,that the accuracy of this matrix is subject to question.

The derivation of the second-order stiffness matrix given by Renton (9) for the torsional-flexural buckling of axially loaded thin-walled column,is based on the closed form solution of the Eulerian differential equations given by Kappus (14). These differential equations are,

$$EI_z \frac{d^4v}{dx^4} + P_x\left(\frac{d^2v}{dx^2} - z_o \frac{d^2\theta_x}{dx^2}\right) = o \qquad (2.57)$$

$$EI_y \frac{d^4w}{dx^4} + P_x\left(\frac{d^2w}{dx^2} + y_o \frac{d^2\theta_x}{dx^2}\right) = o \qquad (2.58)$$

$$GJ \frac{d^2\theta_x}{dx^2} - EI_\omega \frac{d^4\theta_x}{dx^4} - P_x\left(y_o \frac{d^2w}{dx^2} - z_o \frac{d^2v}{dx^2} + i_o^2 \frac{d^2\theta_x}{dx^2}\right) = o \quad (2.59)$$

in which, y_o and z_o are the co-ordinates of the shear center with regard to the centroid.

The solution of the differential equations (2.57 - 2.59) for skew or double symmetrical section is given by,

$$v = v_a \cos \mu_z x + v_b \sin \mu_z x + \alpha_1 x + \alpha_o \quad (2.60)$$

$$w = w_a \cos \mu_y x + w_b \sin \mu_y x + \beta_1 x + \beta_o \quad (2.61)$$

$$\theta = \theta_a \cosh \mu_\phi x + \theta_b \sinh \mu_\phi x + \psi_1 x + \psi_o \quad (2.62)$$

where, v_a, v_b, w_a, w_b, θ_a, θ_b, α_1, β_1, ψ_1, α_o, β_o, and ψ_o are independent constants of integration which can be evaluated from the end conditions and,

$$\mu_y^2 = \frac{P_x}{EI_y}, \quad \mu_z^2 = \frac{P_x}{EI_z} \text{ and } \mu_\phi^2 = \frac{I}{EI_\omega}(GJ - P_x i_o^2) \quad (2.63)$$

In solving the differential equations of equilibrium (2.57-2.59) with the chosen displacement functions (2.60-2.62), Renton (9) assumed that the joints are sufficiently stiff for warping to be neglected. The load acting at the two ends of the member can then be given by,

$$M_y = -P_x (w_a \cos\mu_y x + w_b \sin\mu_y x) \quad (2.64)$$

$$M_z = P_x (v_a \cos\mu_z x + v_b \sin\mu_z x) \quad (2.65)$$

$$M_x = (GJ - P_x i_o^2)\, \psi_1 \quad (2.66)$$

$$P_y = -P_x \beta_1, \quad \text{and} \quad P_z = -P_x \alpha_1 \quad (2.67)$$

The last four equations (2.64-2.67) define equal and opposite pairs of moments or forces acting at the ends. The stiffness matrix of the member can then be given by,

$$K = \begin{bmatrix} a_{11} & & & \\ a_{12} & a_{22} & \text{Symmetric} & \\ a_{13} & a_{23} & a_{33} & \\ a_{14} & a_{24} & a_{34} & a_{44} \end{bmatrix} \qquad (2.68)$$

where, the submatrices $[a_{11}]$, $[a_{12}]$, ... and $[a_{44}]$ are given in Appendix A.2.1.

2.3.4.3. Finite element method

The finite element method is a numerical technique whose active development has been pursued for a relatively short period of time. The method was originally developed to solve structural engineering problems, but the natural base of its theory makes it applicable to problems in many fields of engineering.

The basic concept of the method, when used in structural engineering problems, is that a whole structure can be represented by an assemblage of subdivisions (the finite elements). A set of displacement functions is used to describe (approximately) the deformed state of the structure in terms of the displacements at the nodal points. The solution is formulated for each typified unit and then combined to obtain the solution for the whole structure.

In the conventional analysis of elastic linear structure by the finite element method, the energy concept is often used to derive the first-order stiffness matrix of the element. The energy concept can also be employed in elastic buckling problems to establish the second order load displacement relationship. In elastic buckling problems, however, the conventional linear stiffness matrix $[K_E]$ is supplemented by another matrix $[K_G]$ called geometric

(stability) matrix. This matrix represents the elastic effect of the applied load on the buckling deformations.

For conditions of stable equilibrium, where the load factor is of a value less than its critical value, the element stiffness equation given by the first variation of the potential energy expression becomes,

$$\{P\} = \left[K_E\right]\{\Delta\} + \left[K_G\right]\{\Delta\} \qquad (2.69)$$

in which, $\{\Delta\}$ is the nodal displacement vector.

Eq. 2.69 describes the second order behaviour of the element.

In elastic stability problems it is usually assumed that prebuckling deformations have taken place and that the analysis is being conducted at a near buckling state.
Eq. 2.69 can be modified to,

$$\{dP\} = \left[\left[K_E\right] + \left[K_G\right]\right]\{d\Delta\} \qquad (2.70)$$

in which, $\{d\Delta\}$ is the matrix of vanishing small increments of the displacements and $\{dP\}$ is the matrix of corresponding forces.

At the critical load, more than one equilibrium state is possible and the deformations of the structure corresponding to a given load factor can reach infinite values for arbitrarily small (infinitesimal) load increments. Thus at the buckling stage eq. 2.70 becomes,

$$\left[\left[K_E\right] + \lambda_c\left[K_G\right]\right]\{d\bar{\Delta}\} = o \qquad (2.71)$$

where, $\{d\bar{\Delta}\}$ represents the buckling deformations and λ_c is an instability parameter (eigenvalue).

The analysis begins with a chosen value of the applied load from which the individual element end forces are calculated through a pre buckling analysis. The end forces can then be used to formulate the geometric matrix $\left[K_G\right]$. The critical

load is equal to the instability parameter λ_c times the chosen value of the load factor. The instability problem then becomes an eigenvalue problem of finding the instability parameter (eigenvalue) λ_c from the nontravial solution of eq. 2.71. Such solution exists when,

$$\left| \bar{K}_E \right| + \lambda_c \left| \bar{K}_G \right| = 0 \qquad (2.72)$$

in which, $\left|\bar{K}_E\right|$ and $\left|\bar{K}_G\right|$ are the two determinants corresponding to the stiffness matrices $[K_E]$ and $[K_G]$ respectively.

The simplicity and broad application potential of the finite element method to structural stability problems was made clear in a study of the beam-column problem reported by Rodden, et al (15), in 1963. In the same year Gallagher and Padlog (16) published a similar study in which they suggested cubic polynomials to represent the in-plane displacements of the beam-column member. Many applications of the method to elastic stability problems have since been presented; however, up to 1969 these applications were devoted to the in-plane flexural buckling (17,18,19,20).

The extension of the finite element method to deal with elastic torsional-flexural buckling problems has been coupled with the growing use of light gauge steel members. Light gauge steel members, with their low torsional rigidity, have a high tendency to buckle in torsional or combined torsional-flexural modes. The basic theory of torsional-flexural buckling has been well established and explained by many authors (1,2,3). However, the applications of the theory have been limited to simple and regular structural systems. The finite element technique provides a very effective tool to cope with large scale and complex structures such as space frameworks.

Krahula (21) presented a finite element formulation of the first order torsional-flexural behaviour of thin-walled elements basing his derivation on the closed form solution of the differential equilibrium equations. Krajcinovic (22),

however, was the first to extend the scope of the finite element technique to elastic torsional-flexural buckling of thin-walled members. He used the energy method together with trigonometric displacement functions to derive the elastic stiffness matrix $[K_E]$ and the geometric (instability) matrix $[K_G]$. He concluded that in comparison to the exact solution the method gives an upper bound estimate for the elastic buckling load (22,23).

Barsoum and Gallagher (24) presented a finite element formulation for the torsional and lateral instability analysis of beam-column members based on an approximate representation of the flexural and torsional displacement of the member. They used the energy concept to derive the elastic matrix $[K_E]$ and the geometric matrix $[K_G]$. The method showed an excellent agreement with exact solutions of beam, column, and beam-column problems (24,25). The same procedure was followed by many investigators to analyse the elastic torsional-flexural buckling of continuous beams (26,28), unbraced and braced portal frames (27), and one bay symmetrical space frames loaded at column tops (28).

The finite element formulations presented so far lack generality and consistency. These formulations are applicable only to members with doubly symmetrical cross sections. Furthermore, the effect of external bimoment, which may be of great importance in light gauge steel members, has not been considered.

In the next chapter (chapter 3), a new finite element formulation is presented. This formulation is based on Vlasov's concept (1) of the general behaviour of thin-walled members. The technique is valid for any cross sectional shape, and it includes new terms representing the bimoment influence for sections with no axes of symmetry.

2.4. LITERATURE REVIEW OF PREVIOUS STUDIES OF TORSIONAL-FLEXURAL BUCKLING PROBLEMS

2.4.1. Single span elements

The elastic torsional and torsional-flexural buckling of thin-walled columrs loaded by either axial or eccentric

thrust has been extensively studied and explained by many authors (1,2,3,29,30). Renton (32) presented the direct solution for axially loaded thin-walled bars with open cross section. Studies by Culver (31) were devoted to the closed form solution of torsional-flexural buckling of simply supported beam-columns with open cross section. A comprehensive study carried out by Pekoz, et al (33), on eccentrically loaded cold-formed columns with single symmetrical open cross sections, has led to a simple but sufficiently accurate design procedure for such columns.

The general theory of torsional-flexural buckling of single span beams with doubly symmetrical cross sections,having either simply supported or fixed end conditions,has been presented by many investigators (1,2,3,34). A comprehensive literature survey of the work done in this subject has been presented by Lee (35). Nethercot (36) has also presented another survey of the investigations concerning the lateral buckling of single span beams up to 1970. In addition, Nethercot and Rockey (37) presented a simple design procedure for rapid estimation of the lateral buckling loads of simply supported I-beams. This procedure is based on introducing a lateral buckling coefficient in the critical moment expression, similar to the plate buckling coefficient. The procedure is valid for a wide variety of load cases and supporting conditions.

The superior accuracy of the finite integral technique,in comparison to the finite difference method,for solving differential equations was made clear in the important paper presented by Brown and Trahair (5). This technique was used by Trahair and Kitipornchai(38) to provide a simple linear approximation for the elastic lateral buckling load of simply supported stepped I-beams loaded with central concentrated loads. In another paper, using the same technique, Trahair and Kitipornchai(39) reported a comprehensive study of the lateral buckling of simply supported tapered I-beams. Another important application of the finite integral technique is that presented by Anderson and Trahair (40) concerning the elastic

lateral buckling of monosymmetric I-beams and cantilevers. They concluded that "the effect of monosymmetry is such that the critical load is larger when the tension flange is the smaller of the two flanges". Later in another publication Kitipornchai and Trahair (41) refined the procedure and provided simple design expressions for the elastic critical loads of monosymmetric I-beams and cantilevers.

During the last 15 years the scope of the finite element method has been extended to cover torsional-flexural buckling analysis. The accuracy of the method has been confirmed for simple stability problems for which exact solutions are available (22,24,25,26). Nethercot and Rockey (42) used the finite element formulation presented by Barsoum and Gallagher (24) to analyse the torsional-flexural buckling of single span I-beams having different support conditions at each end. They developed simple expressions for the lateral buckling moment of beams loaded by either equal or unequal end moments.

More recently Roberts (43) has presented a new approach to deal with elastic stability problems based on complete expressions for the strains including second order terms. The validity of some of these expressions has been checked by analysing a number of conventional stability problems using the energy method (43,44). However, it has been reported that the method can be extended to solve more complex problems by means of a suitable numerical technique(43).

2.4.2. Continuous beams

Under working conditions, the majority of the single span beamsdesigned as being simply supported are subjected to considerable elastic restraints,either because of the size of the end connections or due to the bracing system provided to prevent buckling. These restraints increase the elastic stability of the beam and may, in some cases, even change the mode of failure.

The effect of individual end restraints on the elastic stability of single span beams has been the subject of

many theoretical and experimental studies. Flint (45) pointed out the importance of considering the influence of the elastic end restraints in the design of single span I-beams. He conducted an experimental and theoretical study of the effect of elastic lateral bracing on the elastic buckling load. Flint (45) carried out his theoretical analysis using the energy method. However, the analysis lacks the generality and is slightly in error, due to the neglect of the warping rigidity of the I-beam.

In 1955, Austin et al (46) reported a theoretical study of the effect of flexural end restraints on the elastic buckling behaviour of single span I-beams under in-plane cases of loading. The beam was considered fully restrained against twisting at both ends. They applied a successive approximation procedure to solve the differential equations of equilibrium and presented a number of charts for evaluating the critical load for single span I-beams loaded with in-plane loading, provided that the flexural stiffnesses of the elastic end restraints are known.

Trahair (47) reported an investigation of the influence of individual symmetrical end restraints on the elastic lateral buckling load of single span I-beams. The elastic restraints considered were: major axis rotation, minor axis rotation and torsional restraints, while end sections were either free to warp or fully restrained with respect to warping.

In continuous beam structures, each span is elastically restrained against bending about major and minor axes and warping by the adjacent spans (or span) attached to it. The elastic stability of continuous beams was first analysed by Salvadori (48), who presented a lower bound approximation for the elastic lateral buckling load of narrow rectangular continuous beams. He treated the beam as a series of single span beams simply supported with respect to the minor axis bending and subjected to external major axis moments at the supports.

Trahair (49) extended the method used in reference (47) to the elastic lateral buckling of I-beam elements with any combination of symmetrical end restraints provided that the end twisting is prevented. He presented tables for the elastic buckling load and proposed an approximate technique, based on these tables, for evaluating the lateral buckling load of continuous beams, beams supported by cross beams and one bay symmetrical portal frames. In another paper Trahair (6) showed how to calculate the elastic buckling load for single span I-beams with unsymmetrical end restraint using the tables given in reference (49).

The interaction buckling behaviour of two-span and symmetrical three-span continuous beams loaded with either central concentrated loads or uniformly distributed loads and fully restrained against twisting and lateral movement at the interior supports, has been investigated by Trahair (50,51). Trahair (50) proposed an approximate procedure to calculate the elastic torsional-flexural buckling load of narrow rectangular continuous beams by considering the inter-action effect between the spans during buckling. For a given span the procedure starts by reducing the minor axis bending and warping rigidities of the adjacent spans according to their in-plane bending moment values. Such reduced rigidities can be used to evaluate the end restraining effect on the span under consideration and then the buckling load can be estimated from previously presented tables (47,49). Trahair (50) also suggested a much easier technique to evaluate the lateral buckling loads of continuous beams from a simple interaction graph. This technique can be expressed for the two-span continuous beam shown in fig. 2.10.a, by the interaction graph shown in fig. 2.10.b, in which:

i) point 1 represents the lateral buckling load for the left span when the right span is unloaded;

ii) point 2 represents the lateral buckling load for the right span when the left span is unloaded, and

iii) point 3 is the point of zero interaction, when the loading condition is such as to make both spans critical at the same time.

In addition, Trahair (51) presented a comprehensive experimental study concerning the interaction buckling behaviour of continuous I-beams loaded by central concentrated loads in order to verify the theoretical procedure given in references 47, 49, 50. He tested a series of high strength aluminium I-section continuous beams under different combinations of central concentrated loads. The general level of agreement between the experimental and analytical results was good.

The studies reported by Hartmann (52,54,55) and Hartmann and Munse (53) were devoted to the effect of elastic lateral bracing on the lateral instability of rigid-jointed structures. Hartmann's analytical procedure (52,53) has been based on numerically integrating the differential equations of equilibrium, together with the continuity equations at the interior joints. Hartmann (54) used the method to investigate the effects of continuity and of the individual stiffness of lateral bracing on the lateral buckling behaviour of continuous I-beams loaded by central concentrated loads. He concluded that the approximate lower bound estimate of the critical load given by Salvadori (48) gives the actual critical load only if the loading condition is such as to make all spans buckle simultaneously without any interaction in the buckling plane. In a later discussion of Hartmann's paper (54), Trahair (56) showed that both Hartmann's procedure (54) and Salvadori's lower bound method lead to correct values of the buckling load only if all individual spans are critical at the same time. Trahair (56) also concluded that while the accuracy of Salvadori's method is not always good, especially for I-section beams, the Hartmann solution gives slightly overestimated values of the buckling load. However, in order to verify his procedure, Hartmann (55) conducted an experimental study on narrow rectangular two-span continuous beams loaded with different combinations of central concentrated loads and laterally supported by elastic bracing at the interior support. In general, the experimental results were in a good agreement with the analytical procedure.

With the extension of the finite element method to cover the elastic buckling problems, Powell and Klingner (26) applied the method to continuous beams. They checked their finite element formulation by analysing a two-span continuous I-beam with the same dimensions, properties, and loading conditions of that tested by Trahair (51). The comparison showed that the theoretical results are, in general, below the corresponding experimental results.

Nethercot and Trahair (57) suggested a simple method for hand calculations of the elastic buckling loads of laterally continuous beams. The method is based on using a moment modification factor m to allow for the type of loading and an effective length factor K to allow for the elastic restraints at the two ends of the segment under consideration. The critical bending moment M_c can then be calculated from,

$$M_c = m\,(\pi\sqrt{EI_y\,GJ})\,\frac{(\sqrt{1 + \pi^2 EI_\omega/GJ\,K^2\ell^2})}{K\ell} \qquad (2.73)$$

Nethercot and Trahair gave an empirical formula for evaluating the moment factor m and developed a chart for the effective length factor K.

Later Dux and Kitipornchai (58) extended the method for numerical calculations of the elastic lateral buckling load. They treated the critical segment, together with the two adjacent segments, as a sub-assemblage and provided a stiffness matrix for it. They also presented new charts for the effective length K which reflects the restraining effect of the adjacent segments. The results of their technique showed a good agreement with the more accurate finite element solution.

2.4.3. Three-dimensional buckling analysis of plane and space frames

In a three-dimensional frame analysis the acting load, or the resulting deflections, or both, lie in three-

dimensional space. The exact analysis of such behaviour is complicated. On the other hand, it has been proved that the simplified procedure of treating the structure as a series of two-dimensional frames restricted to move only in their own plane may not provide the correct description of the true behaviour of the structure.

The comprehensive theoretical study reported by Hartmann (53), was devoted to the effects of lateral continuity and of individual elastic lateral bracing stiffnesses on the torsional-flexural buckling behaviour of plane frames. The study is restricted to single-story single-bay doubly symmetrical I-section frames with not more than two members meeting at a joint. Three cases of loading were considered in the study, namely: a) a lateral (sway) force applied at the top of one column, b) two equal transverse forces applied at the shear center of each of the two third points of the beam, and c) two axial loads applied at the column tops. Hartmann (53) showed that in comparison to his proposed method, Salvadori's lower bound procedure (48) can give reasonable values for the buckling load of the frame provided that the beam is considered fully restrained against warping at both ends. In another paper, Hartmann reported an experimental study concerning the effect of elastic stiffness of lateral bracing on the torsional-flexural buckling of narrow rectangular plane frames loaded by an in-plane lateral (sway) force at the top of one column. The comparison between the experimental results and the corresponding theoretical values showed that the analytical technique (53) can be used to predict the critical load with good accuracy.

The study reported by Renton (9) (Sec.2.3.4.2) resulted in a matrix formulation for the torsional-flexural buckling analysis of axially loaded thin-walled columns with either doubly symmetric or monosymmetric or skew cross sections. In order to check the validity of the method Renton (9) carried out some tests on rigid-jointed symmetrical space frames loaded by different combinations of lateral and transverse forces applied at column tops. The analytical results showed a satisfactory agreement with the test results.

Chu and Rampetsreiter (10) suggested a method to analyse the large deflection buckling of space frames based on the constant load technique. In this technique the load factor is maintained at a certain level and the deflection that provides the balancing internal forces has to be calculated through an iteration process. The load can then be increased to new value and again the procedure can be repeated to draw the load-deflection relationship from which the buckling load can be evaluated. Chu and Rampetsreiter used the stiffness matrix developed by Renton (9) for small deflection buckling and described a procedure to modify the stiffness and transformation matrices at every load level to include the effect of the shortening caused by the compressive axial forces.

Razzaq and Naim (11) reported a numerical study of the elastic torsional-flexural buckling of rigid-jointed symmetrical space frames with I-cross section members under different combinations of axial transverse loads applied at column tops. The analysis was based on the stiffness matrix presented by Renton (9) and extended by Chu and Rampetsreiter (10). The results showed that the effective length approach of calculating the critical load of plane or space frames may lead to underestimated values of the buckling load as it does not consider the three-dimensional interaction of the frame members.

Trahair (59) suggested that the elastic buckling behaviour of a three-dimensional steel frame can be predicted by considering the biaxial bending and torsion of the individual members of the frame, together with the interaction effect between these members. He presented a finite integral solution for the differential equations governing the torsional-flexural buckling of biaxially loaded beam-column members with elastic end restraints.

Vacharajittiphan and Trahair (60) reported a theoretical and experimental study of the torsional-flexural buckling of one-bay symmetrical portal frame with members having doubly symmetrical I-section. Loads were concentrated at the two

column tops and at the center of the beam. The analytical procedure was based on using the finite integral technique to predict the elastic buckling load from the solution of the governing differential equations. The interaction behaviour of two types of fixed base portal frame was experimentally predicted and the comparison between the theoretical and experimental interaction curves showed a satisfactory agreement. In another paper the two authors (61) extended the analytical procedure to solve any shape of doubly symmetric I-portal frames under in-plane loading.

Morino (62), reported a comprehensive study of the types of failure to which a space frame may be prone. He considered three modes of failure, namely, a) plastic mechanism failure, b) elastic buckling failure, and c) elasto-plastic failure. The elastic buckling analysis was carried out using the matrix displacement method and the critical load was predicted by the determinental approach for two modes of buckling, namely, a) twisting modes, and b) sway modes.

Citipitioglu (63) presented an analytical study of the elastic buckling of one-story one-bay space frames loaded by vertical loads at the column tops using the matrix displacement method and taking into account the pre-buckling moments. He concluded that considering the pre-buckling moments may reduce the calculated value of the buckling load by not more than 10%.

The warping behaviour at rigid joints between frame members at different inclinations forms a complex problem. Such behaviour depends on the joint angle, the individual lengths, the cross sectional shapes of the members meeting at the joint and the stiffness arrangement at the joint itself. In dealing with rigid jointed frames most of the researchers, however, have assumed that the joints are sufficiently stiff for warping to be prevented (9,10,11,53,60,61,62). Vacharajittiphan and Trahair (64), however, reported a comprehensive finite element study concerning the warping and distortional behaviour of rigid joints between I-section members. They presented approximate expressions to evaluate

the warping restraint stiffness at a given joint according to the type and number of stiffeners and the angle of the joint. In comparison to the finite element analysis these expressions have proved to give very conservative values of the warping restraint stiffness.

The different factors effecting the stability of structural building frames have been reviewed by Birnstiel and Iffland (65). They suggested a procedure to include the effects of geometric nonlinearity, material nonlinearity and axial load in a general stability analysis of three-dimensional structures. In order to include the effect of axial forces on the bending stiffness, they followed the procedure given by Renton (9) which dictates the use of proper stability functions to modify the conventional stiffness matrix of a three-dimensional member.

To demonstrate the validity and accuracy of their finite element formulation of the lateral stability analysis of beam-columns, Tebedge and Tall (28) gave alternative solutions for a variety of previously solved stability problems. For example, they analysed the symmetrical space frame which was investigated by Morino (62) and the comparison showed a good agreement between the two procedures.

2.4.4. The contribution made by this study

The finite element method has proved to be the most generally applicable technique for analysing the torsional-flexural buckling of regular and irregular beam and column problems. However, the majority of the previously discussed applications of the method were limited to two dimensional systems (22,23,25,26,42,57).

The effect of the out of plane bending (M_z) was considered in the geometric matrix given by Barsoum and Gallagher (24). However, the positive direction taken for this bending is inconsistent with the sign conventions adopted in the study. Furthermore, the elastic stiffness matrix given by the authors is not identical (in signs) to the conventional stiffness matrix. Thus a proper transformation matrix is needed in order to perform a three-dimensional

frame analysis. Applications of the formulation given by Barsoum and Gallagher were limited to beam and column problems only (24,42,57).

The geometric matrix presented by Tebedge and Tall (28), is identical to that given by Barsoum and Gallagher (24), and although the elastic stiffness matrix was not given in the paper, the procedure leads to the same stiffness matrix. The transformation matrix used by Tebedge and Tall (28) is inconsistent with both the stiffness and geometric matrices. The only space frame problem solved in the paper to check the validity of the formulation is that given by Morino (62) in which the columns of the frame were loaded equally on their tops and no bending moments were involved.

The study reported in the first part of this thesis was undertaken in order to present a general finite element formulation that can be used for the three-dimensional buckling analysis of framed structures, and that is not limited by the deficiencies of the previous formulations mentioned above. The new formulation is based on the general theory of torsional-flexural buckling of thin-walled structures presented by Vlasov (1). The effect of externally acting bimoments in the general case of loading is included. This effect appears only if the cross section of the member has no axis of symmetry. For such sections a new sectorial characteristic called the "sectorial monosymmetric" constant (β_ω) is introduced.

A finite element computer program is described in chapter 4. The program can be used for first order, second order, and buckling analysis of elastic structures. The accuracy of the elastic stiffness matrix when used to evaluate the bimoments caused by nonuniform torsion is discussed in chapter 5. The validity and accuracy of the new finite element formulation when employed to analyse buckling problems are discussed in chapter 6. To check the validity of the new terms which reflect the effect of the external bimoments, an experimental and theoretical study of the torsional-flexural behaviour of simply supported Z-beams is presented in chapter 7.

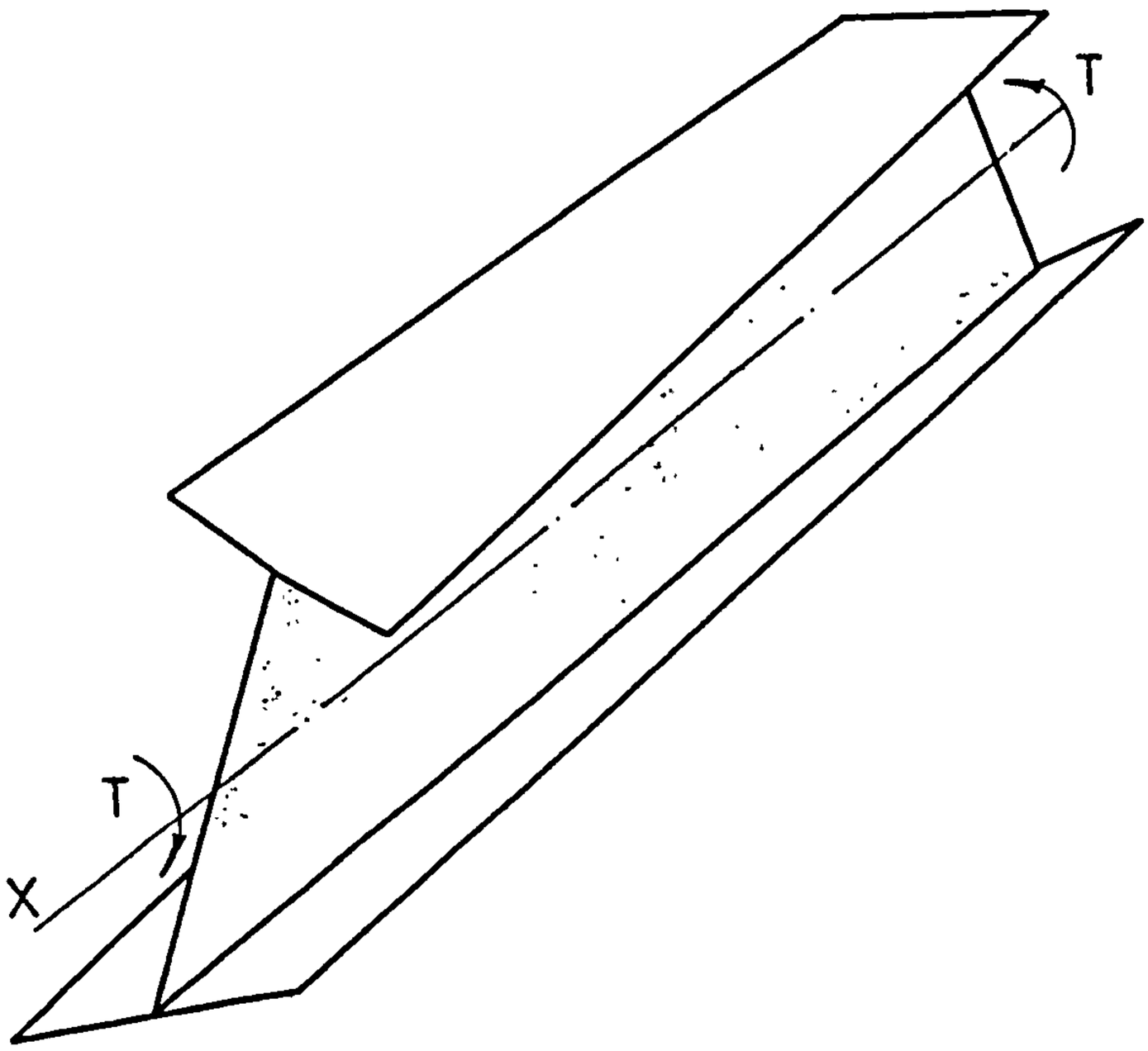

Fig. 2.1 Warping Of Doubly Symmetrical I - Beam

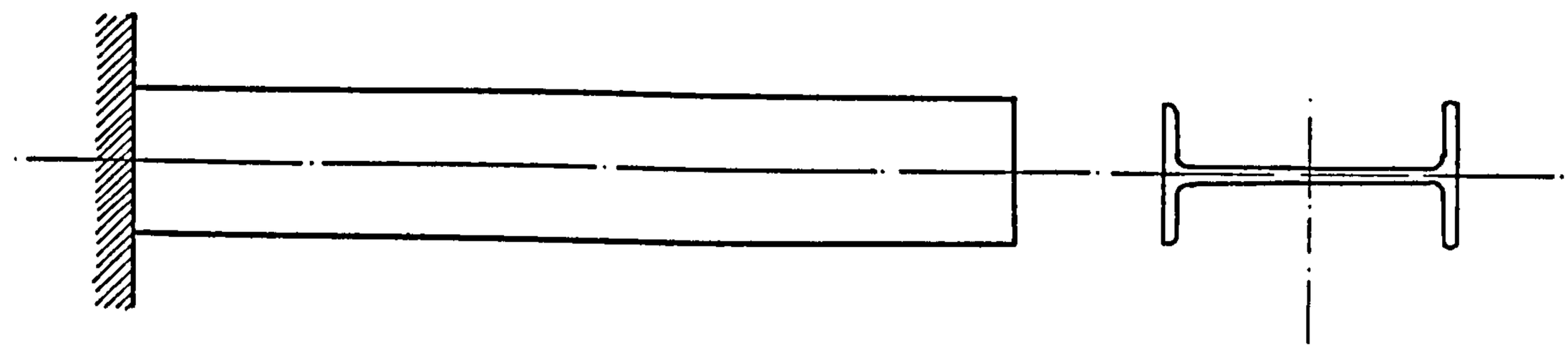

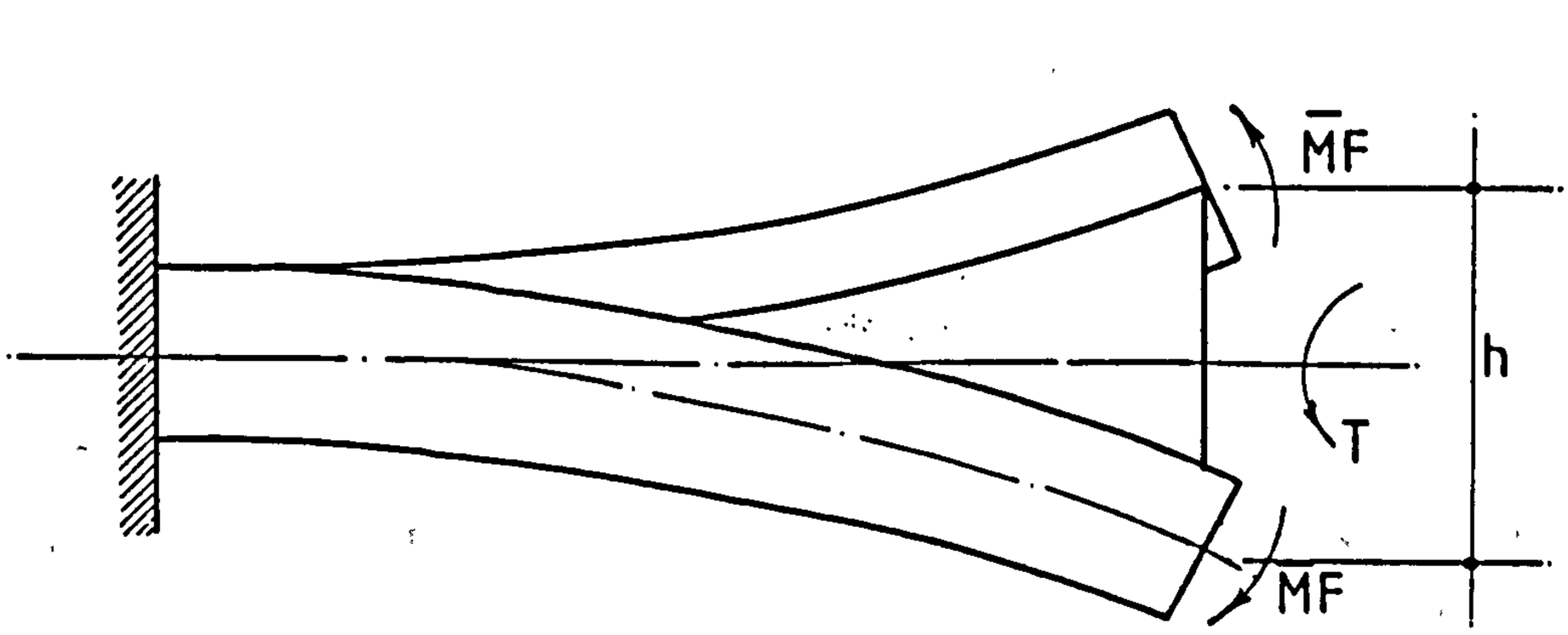

Fig. 2.2 Warping Of Cantilever Beam

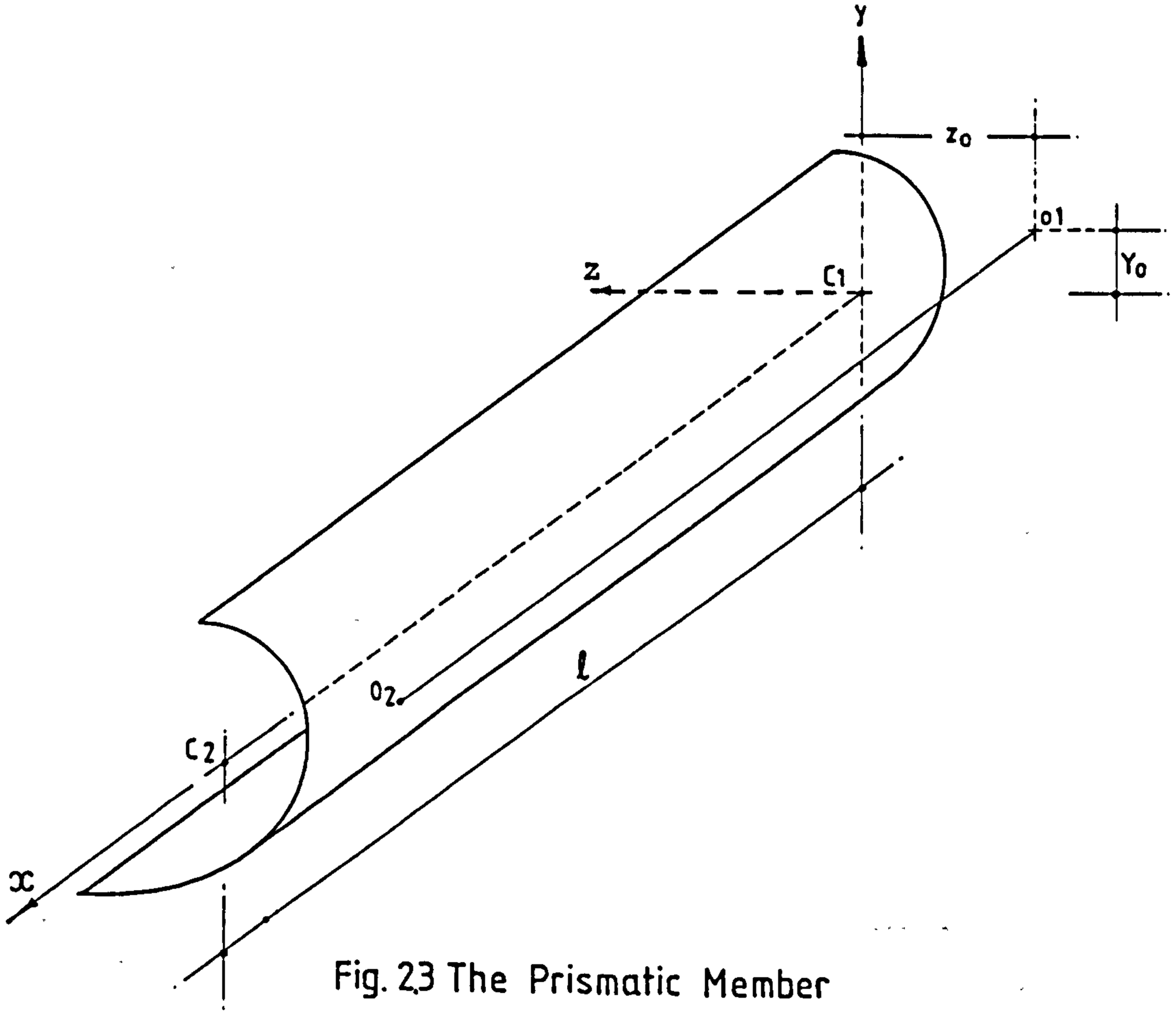

Fig. 23 The Prismatic Member

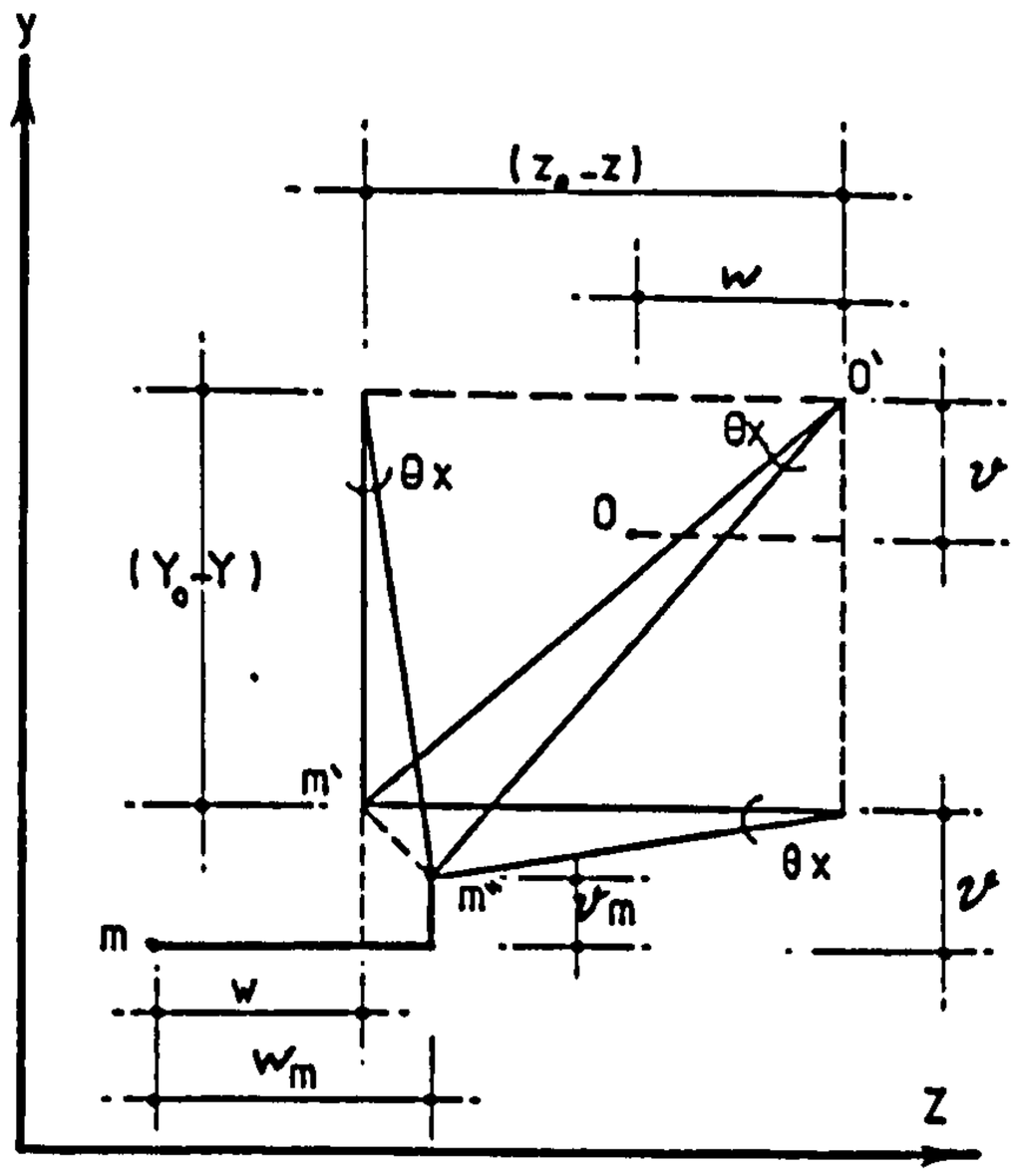

Fig. 24 Torsional–Flexural Displacements Of Point (m)

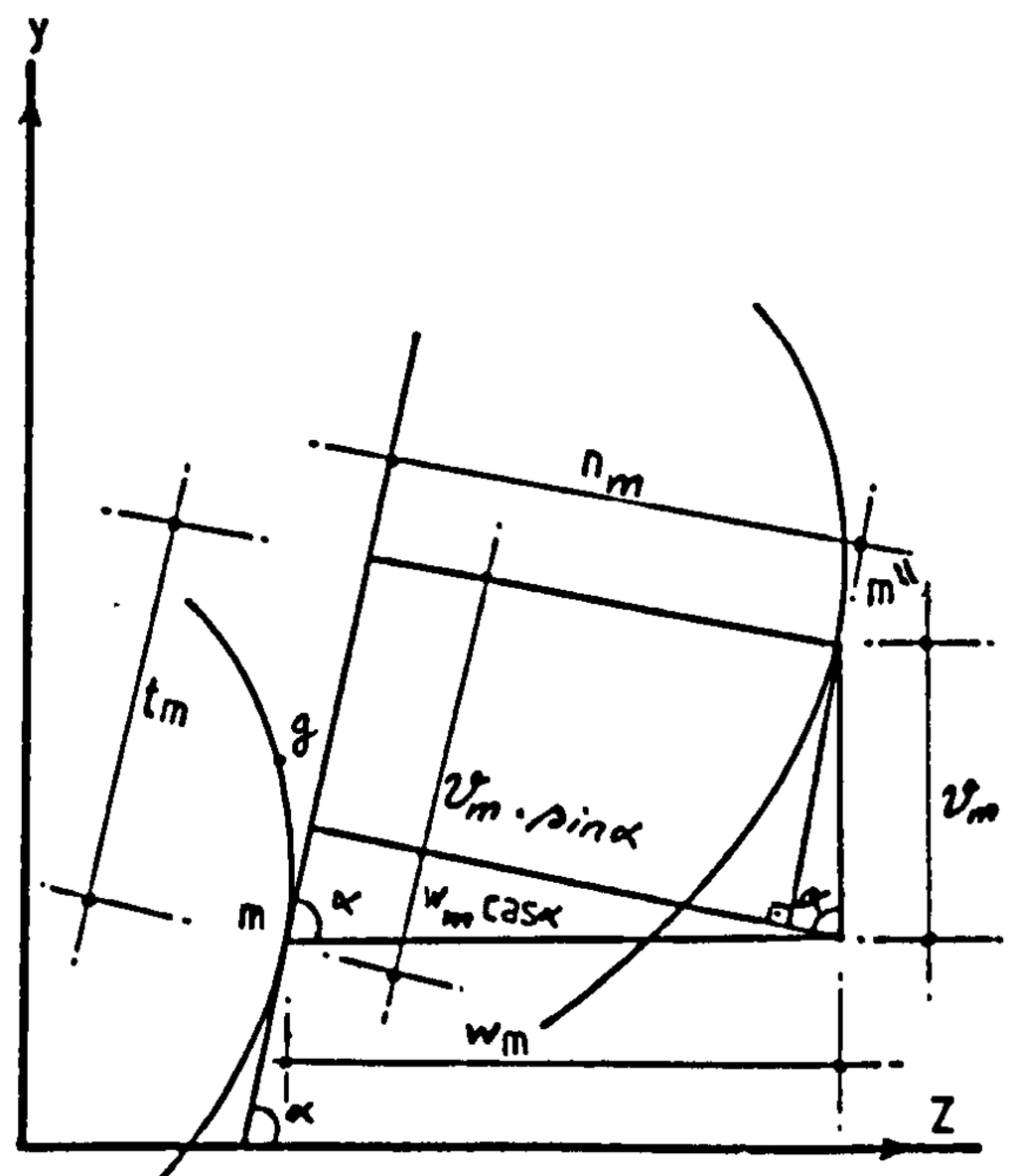

Fig. 25 Normal And Tangential Displacements

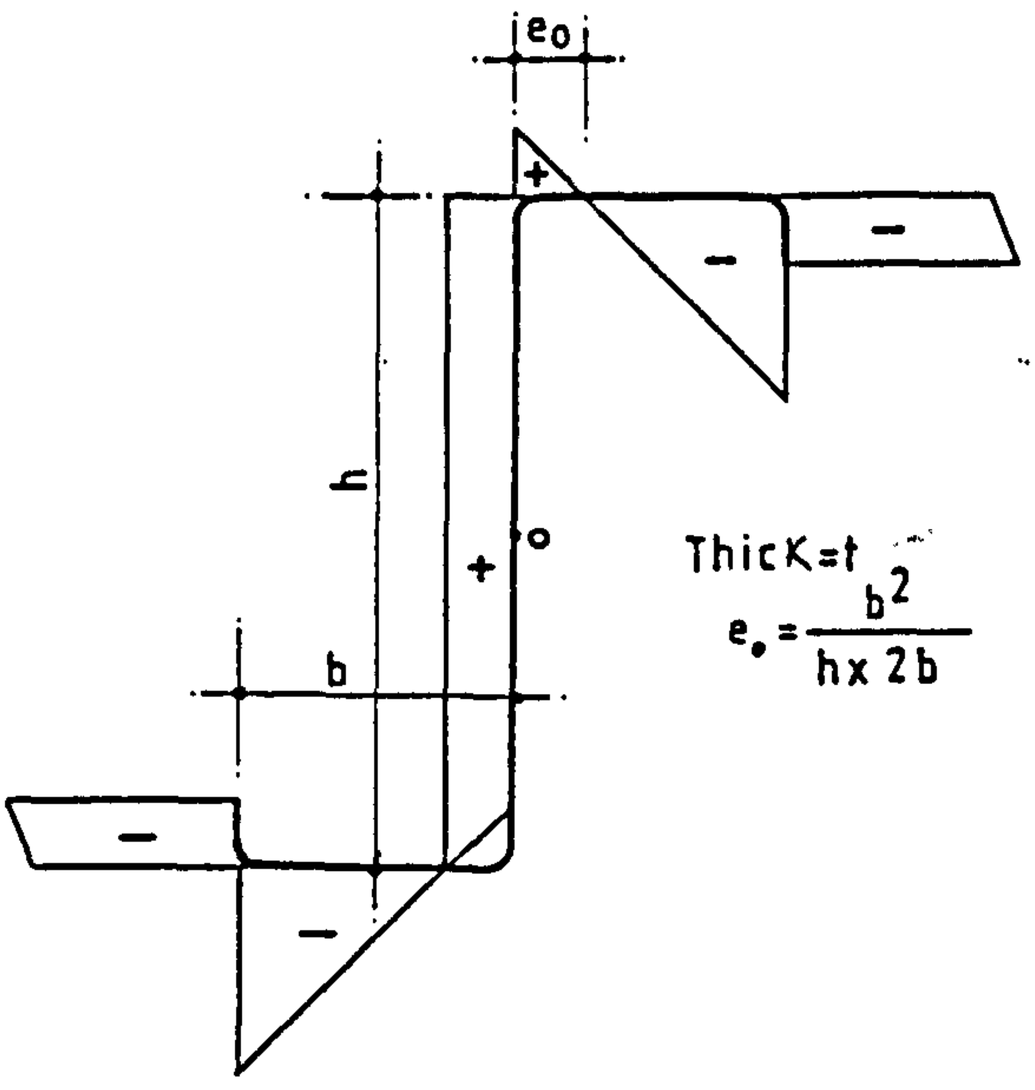

Fig. 2.7 Distribution Of The Sectorial Coordinates For Z. Section

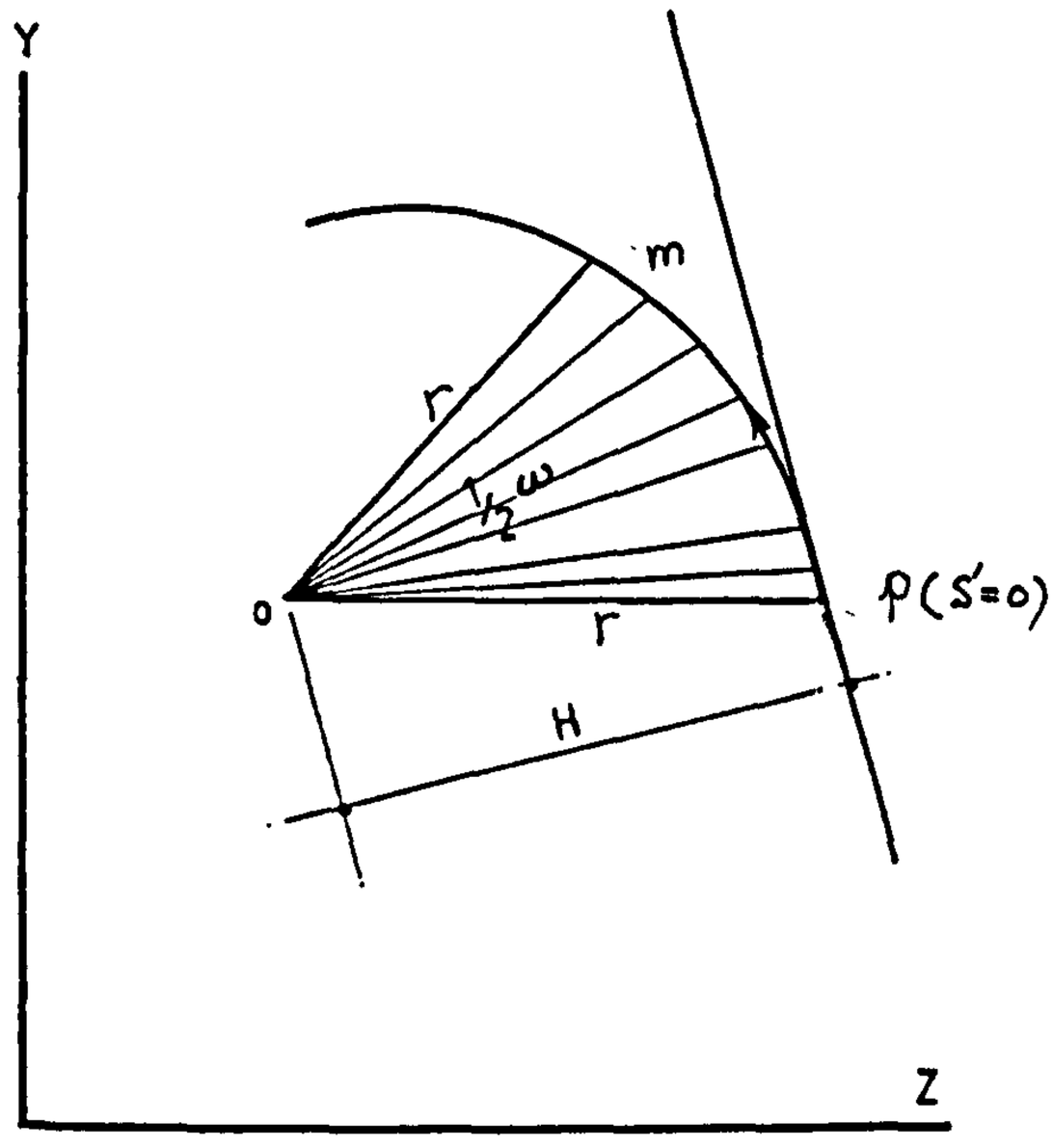

Fig. 2.6 Sectorial Coordinates.

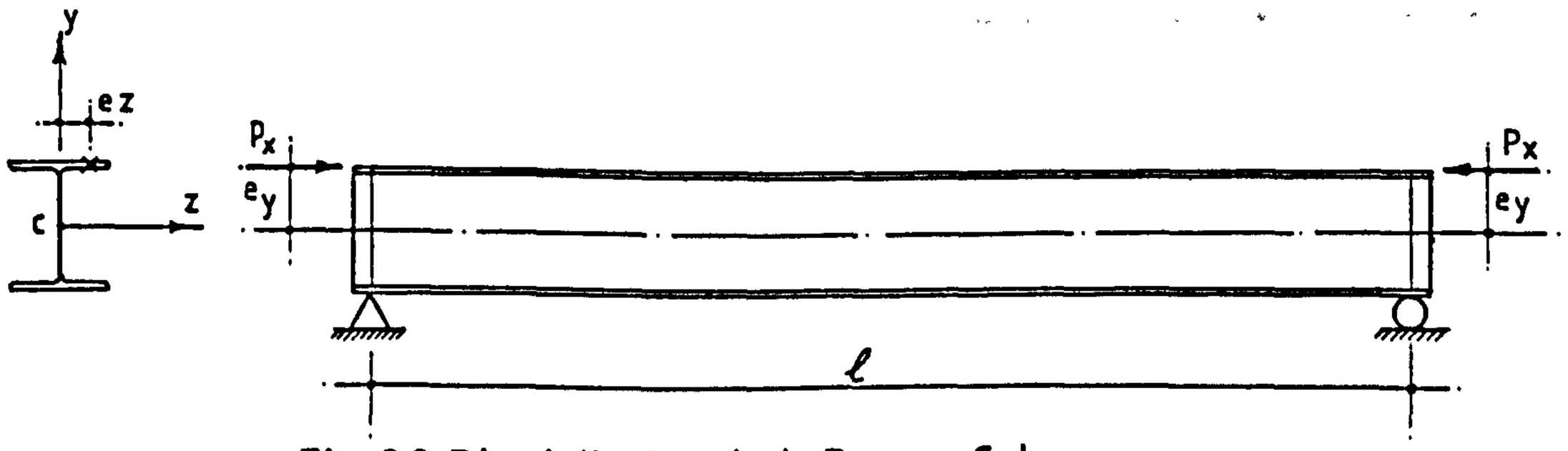

Fig. 2.8 Biaxially Loaded Beam - Column

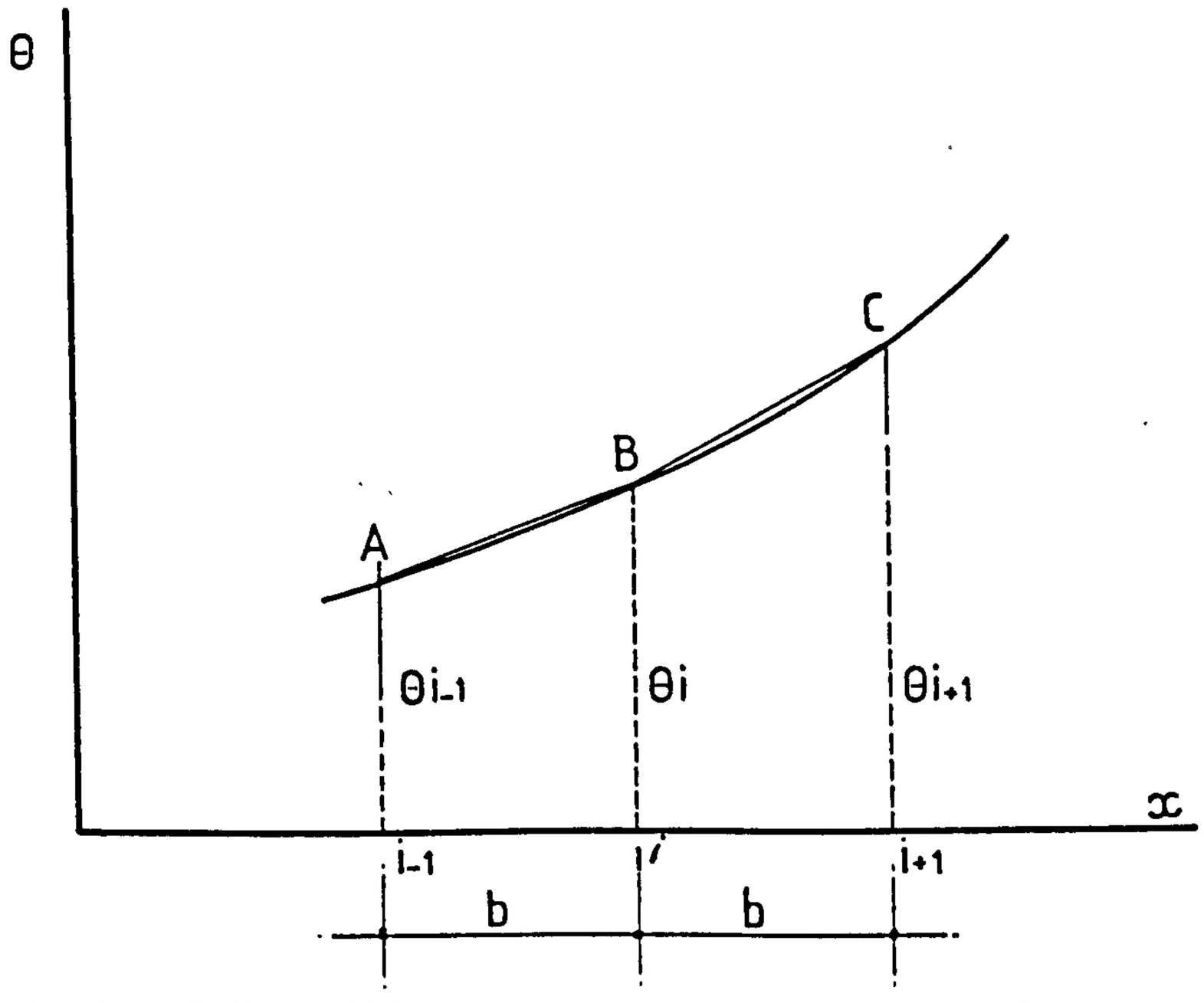

Fig . 2.9 Finite Difference Approximation For The Angle Of Twist θ

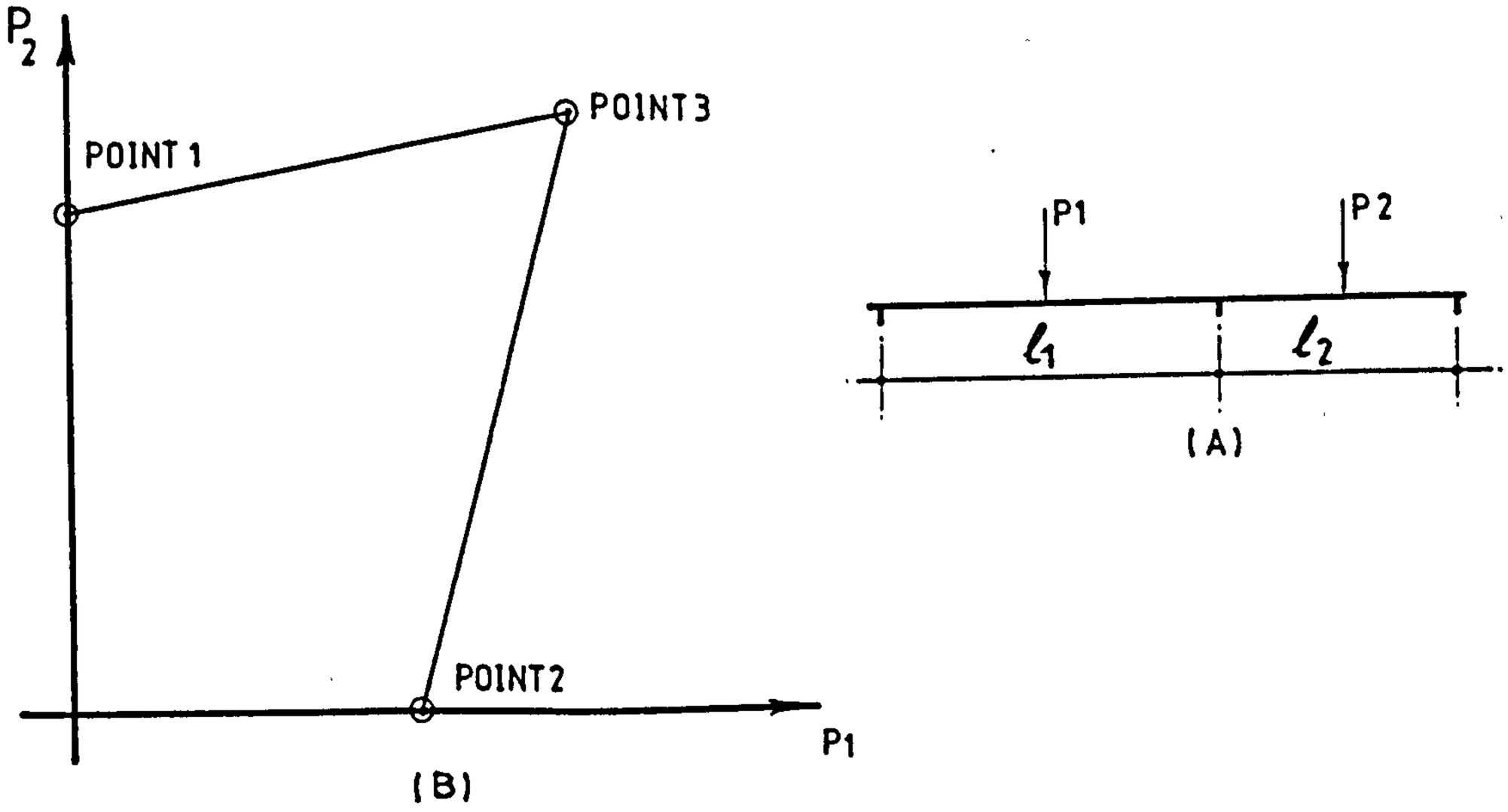

Fig. 2.10 Approximate Interaction Curve For A Continuous Beam (Ref. 50)

CHAPTER THREE

Finite Element Formulation of the Elastic Three-Dimensional Buckling Behaviour of Thin-walled Systems

3.1. GENERAL

A finite element formulation for the elastic three-dimensional buckling behaviour of thin-walled members is presented in this chapter. The formulation is based on the theory of torsional-flexural behaviour as described by Vlasov (1).

Vlasov showed that self-balancing longitudinal forces applied to points of the cross section of a thin-walled beam-column member can distort the cross section. The warping of the cross section by either longitudinal or transverse load-applied out of the shear center can give rise to the normal stresses in the cross section. The generalized force corresponding to these normal stresses is called bimoment.

It is assumed, in the analysis presented herein, that at the moment of buckling, the structure passes from a torsional-flexural equilibrium state to another torsional-flexural equilibrium but critical state. The bimoment stresses are included as the fourth term to be added to the conventional three terms of the equation of normal stresses.

The energy concept has been used to derive the elastic matrix and the geometric matrix describing the buckling behaviour of the element. The derivation of these matrices has been based on the small deformation theory. Pre-buckling deformations are considered as very small, in comparison to the buckling deformations, and so their effect can be neglected.

3.2. BIMOMENT

The basic concept of bimoment was explained by Vlasov (1) for the case shown in fig. 3.1. Fig. 3.1.a. shows a cantilever beam with doubly symmetric I-cross section

subjected to an eccentric axial force P_x. According to the elementary theory of bending, the eccentric force P_x is equivalent to a combined system of axial thrust P_x and pure bending in the two principal planes yx and zx. However, if the warping of the cross section is considered (theory of thin-walled structures) another system of longitudinal forces (fig. 3.1.e) must be added to the three components given by the elementary beam theory (fig. 3.1.b-3.1.d). As shown in fig. 3.1.e. the additional system of forces gives two equal and opposite bending moments acting in the planes of the two flanges. This system is called a bimoment.

The bimoment, caused by either an eccentric longitudinal force (fig. 3.1.e) or by a nonuniform torsion of transverse loads (fig. 2.2) is given by the expression.

$$B = \bar{M}_F \times h \qquad (3.1)$$

where, B is the bimoment, $\bar{M}_F$ is the flange in-plane bending moment, and h is the distance between the centroids of the two flanges. In terms of the normal stress σ_x in the cross section, the bimoment B can also be given by,

$$B = \int_A \sigma_x \, \bar{\omega} \, dA \qquad (3.2)$$

in which, $\bar{\omega}$ is the sectorial co-ordinate.

The theory of bimoment and bimoment distribution in single span and continuous beams has been presented by many investigators (79-84). A review of these studies and the different methods of calculating the bimoment, including the finite element method with full comparison between the results of such methods are presented in chapter 5 of this thesis. Also presented in the same chapter is an experimental study of the warping stresses caused by nonuniform torsion of Z-beams.

If the bimoment B_x acting at a given cross section (x = const.) is known, the longitudinal normal stresses σ_B caused by this bimoment can be evaluated from the expression,

$$\sigma_B = \frac{B_x \bar{\omega}}{I_\omega} \tag{3.3}$$

in which, I_ω is the warping constant of the cross section.

3.3. STRAIN ENERGY

The subject prismatic element with an arbitrarily chosen cross section is shown in fig. 2.3. Equation 2.7 gives the longitudinal displacement u_m at an arbitrary point m. Equation 2.7 can be rewritten in a more general form given by,

$$u_m = u - \grave{w} z - \grave{v} y - \grave{\theta}_x \bar{\omega} \tag{3.4}$$

where, u is the average longitudinal displacement of the cross section (the longitudinal displacement caused by central thrust), and $\bar{\omega}$ is the sectorial co-ordinate with respect to the sectorial origin. The longitudinal normal strain can then be expressed by the equation,

$$\varepsilon_m = \grave{u} - \acute{w} z - \acute{v} y - \acute{\theta}_x \bar{\omega} \tag{3.5}$$

The strain energy of the element can be divided into two main parts, namely, 1) strain energy due to normal stresses, and 2) strain energy due to shear stresses.

3.3.1. Strain energy due to normal stresses

The strain energy U_1 caused by the normal stresses is given by,

$$U_1 = \frac{E}{2} \int_V \varepsilon_m^2 \, dV \tag{3.6}$$

in which, E is the modulus of elasticity of the material and V is the volume of the element.

Substituting for ε_m from eq. 3.5 and knowing that x and y are measured with respect to the principal axes ox and oy and the sectorial co-ordinate $\bar{\omega}$ is evaluated with respect to the sectorial origin, the strain energy U_1 due to normal stresses becomes,

$$U_1 = \frac{E}{2} \int_o^\ell (A \cdot \dot{u}^2 + I_y \cdot \ddot{w}^2 + I_z \cdot \ddot{v}^2 + I_\omega \cdot \ddot{\theta}_x^2)\, dx \quad (3.7)$$

3.3.2. Strain energy due to shear stresses

The shear strain due to shear forces is small and can be neglected (3). The strain energy U_2 due to torsional shear is given by,

$$U_2 = \frac{1}{2} \int_o^\ell GJ \cdot \dot{\theta}_x^2\, dx \quad (3.8)$$

in which, GJ is the torsional stiffness of the element.

The total strain energy U_s for the element is the sum of U_1 and U_2 and is given by,

$$U_s = \frac{1}{2} \int_o^\ell (EA\dot{u}^2 + EI_y\ddot{w}^2 + EI_z\ddot{v}^2 + EI_\omega\ddot{\theta}_x^2 + GJ\dot{\theta}_x^2)\, dx \quad (3.9)$$

3.4. THE POTENTIAL OF THE APPLIED LOAD

The general expression of the normal stresses σ_x acting on the cross section x = constant in the precritical state is,

$$\sigma_x = -\frac{P_x}{A} - \frac{M_y}{I_y} z - \frac{M_z}{I_z} y + \frac{B}{I_\omega} \bar{\omega} \quad (3.10)$$

in which, P_x is the axial thrust, M_y and M_z are the two bending moments about the principal axes oy and oz respectively, and B is the bimoment.

The shear stress τ is given by,

$$\tau = \frac{M'_y}{tI_y} S_y + \frac{M'_z}{tI_z} S_z - \frac{B'}{tI_\omega} S_\omega \qquad (3.11)$$

where, t is the thickness of the cross section at the point where τ is considered, M'_y, M'_z and B' are the first derivatives of the bending moments M_y and M_z and the bimoment B, S_y and S_z are the static moments of the considered part of the cross section about oy and oz axes and S_ω is the sectorial static moment of the same part. The static moments of area are given by,

$$S_y = \int_o^s t\, y\, ds, \quad S_z = \int_o^s t\, z\, ds, \text{ and } S_\omega = \int_o^s t\, \omega\, ds \qquad (3.12)$$

The transition of the element from the stable equilibrium state to the critical state is associated with the appearance of critical deformations. At the critical state the effect of the initial normal stresses σ_x acting on the deformed cross section can be presented in the form of three fictitious loads,

a) $\bar{q}_y$ fictitious distributed lateral load in y direction;

b) $\bar{q}_z$ fictitious distributed lateral load in z direction;

c) $\bar{m}_x$ fictitious distributed torque about the shear centers longitudinal axis.

The evaluation of the lateral loads $\bar{q}_y$ and $\bar{q}_z$ for the case when the bimoments B is equal to zero has been discussed by Vlasov (1). The intensities of these lateral loads are given by the expressions,

$$\bar{q}_y = - P_x(v'' - z_o\theta_x'') - (M_y\theta_x)'' \qquad (3.13)$$

$$\bar{q}_z = - P_x(w'' + y_o\theta_x'') + (M_z\theta_x)'' \qquad (3.14)$$

The potential of these loads becomes,

$$V_1 = - \frac{1}{2}\int_o^\ell P_x(v'' - z_o\theta_x'')v\,dx - \frac{1}{2}\int_o^\ell (M_y\theta_x)''v\,dx \qquad (3.15)$$

$$V_2 = - \frac{1}{2}\int_o^\ell P_x(w'' + y_o\theta_x'')w\,dx + \frac{1}{2}\int_o^\ell (M_z\theta_x)''w\,dx \qquad (3.16)$$

Vlasov (1) showed that if the acting bimoment in the precritical stage B is equal to zero, the intensity of the fictitious distributed torque is given by,

$$\begin{aligned}\bar{m}_{x_1} = &- P_x(y_o\,w'' - z_o\,v'' + y_o^2\,\theta_x'' + z_o^2\,\theta_x'' + i_y^2\,\theta_x'' + i_z^2\,\theta_x'') \\ &- M_y(v'' - \beta_y\,\theta_x'') - M_y'\,\beta_y\,\theta_x' + M_z(w'' - \beta_z\,\theta_x'') \\ &- M_z'\,\beta_z\,\theta_x' \end{aligned} \qquad (3.17)$$

in which, y_o and z_o are the co-ordinates of the shear center, i_y and i_z are the radii of gyration about y and z axes, β_z and β_y are geometrical characteristics of the cross section determined by the two equations,

$$\beta_y = \frac{1}{I_y}\left(\int_A z^3\,dA + \int_A z\,y^2\,dA\right) - 2\cdot z_o \qquad (3.18)$$

$$\beta_z = \frac{1}{I_z}\left(\int_A y^3\,dA + \int_A y\,z^2\,dA\right) - 2\cdot y_o \qquad (3.19)$$

In the general case of loading ($B \neq o$) the effect of the initial bimoment B, when acting on the slightly deformed cross section, results in an additional distributed torque $\Delta\bar{m}_x$. The intensity of this torque can be determined by the equation (1),

$$\Delta\bar{m}_x = \beta_\omega \, (B \, \theta''_x + B' \, \theta'_x) \qquad (3.20)$$

where, β_ω is a new geometrical characteristic of the cross section given by,

$$\beta_\omega = \frac{1}{I_\omega} \int_A \bar{\omega} \, (y^2 + z^2) \, dA \qquad (3.21)$$

The total value of the uniform torque $\bar{m}_x$ is,

$$\bar{m}_x = \bar{m}_{x_1} + \Delta\bar{m}_x \qquad (3.22)$$

The potential of the applied load V_T is the sum of the potentials of the fictitious lateral loads q_y and q_z and of the distributed torque $\bar{m}_x$. Thus this potential can be obtained from the equation,

$$V_T = V_1+V_2+V_3 = \frac{1}{2} \left[\int_o^\ell P_x(-w \cdot w'' - v \cdot v'' - y_o(w\theta'_x + \theta_x w') \right.$$

$$+ z_o \, (v \, \theta''_x + \theta_x v'') - i_o^2 \, \theta_x \, \theta''_x)$$

$$- M_y(\theta_x v'' + v \, \theta''_x + \beta_y \cdot \theta_x \cdot \theta''_x) - M'_y(2 \, \theta'_x v + \beta_y \cdot \theta_x \cdot \theta'_x) - M''_y \cdot \theta_x \cdot v$$

$$+ M_z(\theta_x w'' + w \, \theta''_x - \beta_z \, \theta_x \, \theta''_x) + M'_z(2 \, \theta'_x w - \beta_z \, \theta_x \, \theta'_x) + M''_z \, \theta_x \cdot w$$

$$\left. + B \, \beta_\omega \, \theta_x \, \theta''_x + B' \beta_\omega \, \theta_x \, \theta'_x \right] dx \qquad (3.23)$$

in which, i_o is the polar radius of gyration with respect to the shear center.

3.5. POTENTIAL ENERGY IN TERMS OF THE EXTERNAL JOINT LOADS

As shown in fig. 3.2. the element is subjected to the action of the following loads:

a) Bending moment M_y with values M_{y_1} and M_{y_2} at end 1 and 2 respectively,

b) Bending moment M_z with values M_{z_1} and M_{z_2} at end 1 and 2 respectively,

c) Shearing force Q_y with values Q_{y_1} and Q_{y_2} at end 1 and 2 respectively,

d) Shearing force Q_z with values Q_{z_1} and Q_{z_2} at end 1 and 2 respectively,

e) Twisting moment M_x about the shear center axis with values M_{x_1} and M_{x_2} at end 1 and 2

f) Bimoment B with values B_1 and B_2 at end 1 and 2

g) Axial force P_x with eccentricities e_y and e_z with respect to the centroid.

The average bending moment M_y in the element (fig. 3.3) can be given by,

$$M_y = \frac{1}{2}(M_{y_1} - M_{y_2}) + \frac{1}{2} Q_{z_1} x + \frac{1}{2} Q_{z_2}(\ell - x) + P_x e_z \quad (3.24)$$

The average bending moment M_z (fig. 3.4) is,

$$M_z = \frac{1}{2}(M_{z_1} - M_{z_2}) + \frac{1}{2} Q_{y_1} x + \frac{1}{2} Q_{y_2}(\ell - x) + P_x e_y \quad (3.25)$$

One assumption is made in order to simplify the analysis, that is to consider $\theta_x v'' = v\,\theta_x''$ and $\theta_x w'' = w\,\theta_x''$ and by subsituting for the end forces from eq. 3.24 and 3.25 and their derivatives the potential of the applied load (eq. 3.23) becomes,

$$V_T = \frac{1}{2} P_x \int_o^\ell (-v \cdot v'' - w \cdot w'' - 2 C_z \cdot v'' \cdot \theta_x + 2 C_y \cdot w'' \theta_x - C_o \cdot \theta_x \theta_x'') \, dx$$

$$- \frac{1}{4} \int_o^\ell (M_{y_1} - M_{y_2} + Q_{z_1} x + Q_{z_2}(\ell - x)) (2 v'' \theta_x + \beta_y \theta_x \theta_x'') \, dx$$

$$+ \frac{1}{4} \int_o^\ell (M_{z_1} - M_{z_2} + Q_{y_1} x + Q_{y_2}(\ell - x)) (2 w'' \theta_x - \beta_z \theta_x \theta_x'') \, dx$$

$$- \frac{1}{4} \int_o^\ell (Q_{z_1} - Q_{z_2}) (2 \theta_x' v + \beta_y \theta_x' \theta_x) \, dx$$

$$+ \frac{1}{4} \int_o^\ell (Q_{y_1} - Q_{y_2}) (2 \theta_x' w - \beta_z \theta_x' \theta_x) \, dx$$

$$+ \frac{1}{2} \beta_\omega \int_o^\ell (B \theta_x \theta_x'' + B' \theta_x \theta_x') \, dx \qquad (3.26)$$

where, $C_y = (e_y - y_o)$, $C_z = (e_z - z_o)$ and,

$$C_o = i_o^2 + e_y \beta_y + e_z \beta_z \qquad (3.27)$$

It can be noted that in eq. 3.26 the bimoment B has not been replaced by its values at end 1 and 2. The treatment of the bimoment by an approximate solution of the differential equation of nonuniform torsion will be given in section 3.7.

3.6. DERIVATION OF THE ELEMENT MATRICES

The derivation of the element matrices requires a suitable functional representation of the displaced behaviour of the element. The general form of each displacement function is given by,

$$\delta = d_i \cdot \Delta_i \qquad (3.28)$$

in which, δ is the displacement component, d_i are shape functions which often take the form of polynomials of the co-ordinate x, and Δ_i is a set of nodal displacements.

The shape functions used herein are those suggested by the exact solutions of axial and flexural behaviour of the element (24,26,28). The displacement components can be given by,

$$\{u\} = \left[d_u\right] \{u_i\} \qquad u = d_1u_1 + d_2u_2 \tag{3.29.a}$$

$$\{v\} = \left[d_v\right] \{v_i\} \qquad v = d_3v_1 + d_4v_2 + d_5\psi_1 + d_6\psi_2 \tag{3.29.b}$$

$$\{w\} = \left[d_w\right] \{w_i\} \qquad w = d_3w_1 + d_4w_2 + d_5\phi_1 + d_6\phi_2 \tag{3.29.c}$$

$$\{\theta_x\} = \left[d_\theta\right] \{\theta_i\} \qquad \theta_x = d_3\theta_{x1} + d_4\theta_{x2} + d_5\chi_1 + d_6\chi_2 \tag{3.29.d}$$

in which, u_1, v_1, w_1, θ_{x1} and u_2, v_2, w_2, θ_{x2} are the displacement components at end 1 and 2 respectively and,

$$\psi_{1_2} = -\left(\frac{dv}{dx}\right)1_2 \ , \quad \phi_{1_2} = -\left(\frac{dw}{dx}\right)1_2, \text{ and } \quad \chi_{1_2} = -\left(\frac{d\theta_x}{dx}\right)1_2 \tag{3.30}$$

The shape functions d_i are given by,

$$d_1 = 1 - \frac{x}{\ell} \quad , \qquad d_2 = \frac{x}{\ell} \tag{3.31.a}$$

$$d_3 = 1 + 2\left(\frac{x}{\ell}\right)^3 - 3\left(\frac{x}{\ell}\right)^2 \tag{3.31.b}$$

$$d_4 = -2\left(\frac{x}{\ell}\right)^3 + 3\left(\frac{x}{\ell}\right)^2 \tag{3.31.c}$$

$$d_5 = -\frac{x^3}{\ell^2} + 2\frac{x^2}{\ell} - x \tag{3.31.d}$$

$$d_6 = -\frac{x^3}{\ell^2} + \frac{x^2}{\ell} \tag{3.31.e}$$

From eq. 3.9 the strain energy U_s can be written as,

$$U_s = \frac{1}{2}\int_V \{\varepsilon\}^T \left[D\right]\{\varepsilon\}\, dV \tag{3.32}$$

in which, $\{\varepsilon\}$ is the strain vector, $\{\varepsilon\}^T$ is the transpose of the strain vector and $[D]$ is the matrix representing the generalized Hookean constant.

Substituting for the strain ε from eq. 3.28 the strain energy U_s becomes,

$$U_s = \{\Delta_i\}^T [K_E] \{\Delta_i\} \tag{3.33}$$

where, $[K_E]$ is the element stiffness matrix which can be evaluated from the integration,

$$[K_E] = \frac{1}{2} \int_V \{d_i'\}^T [D] \{d_i'\} \, dV \tag{3.34}$$

Following the same procedure, the potential of the applied load V can be given by the expression,

$$V = - \{\Delta_i\}^T [K_G] \{\Delta_i\} \tag{3.35}$$

in which, $[K_G]$ is the element geometric matrix which can be written as,

$$[K_G] = \int_V \{d_i\}^T [P] \{d_i\} \, dV \tag{3.36}$$

where, $[P]$ is the matrix of the applied external loads. The total potential energy U_p of the element is then given by the expression,

$$U_p = \{\Delta_i\}^T \left[[K_E] + [K_G] \right] \{\Delta_i\} \tag{3.37}$$

Applying Castigliano's first theorem the element stiffness equation becomes,

$$\{P\} = \left[[K_E] + [K_G] \right] \{\Delta_i\} \tag{3.38}$$

The condition of elastic instability is characterised by the fact that at the buckling load the second variation of the total potential energy of the system is equal to zero. This condition leads to an expression for the buckling criterion which is given by,

$$\left|\bar{K}_E\right| + \lambda \left|\bar{K}_G\right| = 0 \qquad (3.39)$$

in which $\left|\bar{K}_E\right|$ is the determinant of the stiffness matrix $\left[K_E\right]$, $\left|\bar{K}_G\right|$ is the determinant of the geometric matrix $\left[K_G\right]$, and λ is the instability parameter (eigenvalue).

3.7. EVALUATION OF THE BIMOMENT TERMS IN THE GEOMETRIC MATRIX

The actual distribution of the bimoment B along the element is given by,

$$B_{(x)} = B_1 \frac{\sinh k(\ell-x)}{\sinh k\ell} + B_2 \frac{\sinh kx}{\sinh k\ell} + B_{t(x)} \qquad (3.40)$$

in which, B_1 is the bimoment at end 1 of the element, B_2 is the bimoment at end 2, $B_{t(x)}$ is the bimoment at any cross section of the element due to the applied torsional loading and k is the bending-twisting parameter given by,

$$k = \sqrt{\frac{GJ}{EI_\omega}} \qquad (3.41)$$

Vlasov (1) showed that the bimoment $B_{h(x)}$ caused by a horizontal thrust P_x when acting at point e on the cross section, where the sectorial co-ordinate is ω_e, can be given by,

$$B_{h(x)} = - P_x \omega_e \frac{\cosh kx}{\cosh \frac{k\ell}{2}} \qquad (3.42)$$

The total bimoment in the general case of loading becomes,

$$B_{(x)} = B_1 \frac{\sinh k(\ell-x)}{\sinh k\ell} + B_2 \frac{\sinh kx}{\sinh k\ell} + B_{t(x)} - P_x\omega_e \frac{\cosh kx}{\cosh \frac{k\ell}{2}} \quad (3.43)$$

For a given value of the parameter k eq. 3.43 can be simplified to,

$$B_{(x)} = B_1F_1(x) + B_2F_2(x) + B_{t(x)} - P_x\omega_eF_3(x) \quad (3.44)$$

By substituting for $\mathcal{B}(x)$ in eq. 3.26 the potential energy of the bimoment becomes,

$$V_B = \frac{1}{2}\beta_\omega\left[\int_o^\ell (B_1F_1(x) + B_2F_2(x) + B_{t(x)} - P_x\omega_eF_3(x))\theta_x\theta''_x + (B_1F_1(x) + B_2F_2(x) + B_{t(x)} - P_x\omega_eF_3(x))\theta_x\theta'_x\right]dx \quad (3.45)$$

In making the integrations in eq. 3.45 two simplifications have been made in order to keep the orthogonality of the approximate shape functions d_i, used to define the angle of rotation θ_x, and to keep the symmetry of the resulting geometric matrix. These two simplifications are,

1. The term $\theta_x\theta''_x$ has been replaced by $-\theta'^2_x$.

2. The second term which includes $\theta_x\theta'_x$ has been neglected as it proves to disturb the symmetry of the resulting coefficients in the geometric matrix. The potential energy of the bimoment V_B can then be given by,

$$V_B = -\frac{1}{2}\beta_\omega\int_o^\ell\left[(B_1F_1(x) + B_2F_2(x) + B_{t(x)} - P_x\omega_eF_3(x))\theta'^2\right]dx \quad (3.46)$$

The integrations of eq. 3.46 have been carried out numerically. For example to calculate $\int_o^\ell B_1F_1(x)\theta'^2\ dx$, for

a given value of kℓ (eq. 3.41), a unit bimoment $B_1 = 1$ was applied at end 1 of the element assuming that the other end (end 2) is fully fixed. The distribution of the bimoment ($F_1(x)$) was calculated using the elastic stiffness matrix (first order) given by eq. 3.34. This approximate distribution of the bimoment has proved to be in very good agreement with the actual distribution given by eq. 3.40 as will be discussed in chapter 5 of this thesis. The bimoment B(x) due to $B_1 = 1$ was then integrated with functions $d_i^{\backprime 2}$ of $\theta_x^{\backprime 2}$ using a suitable subroutine presented in Appendix A.3.1. The procedure was repeated for $B_2 = 1$ and $M_x = 1$ to evaluate the potential V_B in terms of the end forces B_1, B_2, M_x and the end twisting and warping θ_{x1}, θ_{x2}, and χ_1, χ_2. The resulting coefficients are tabulated in Appendix A.3.2 for kℓ values starting from kℓ = 0 up to kℓ = 10.0. As an approximation, $F_3(x)$ has been treated as being equal to $F_2(x)$ and that $P_x\omega_e$ is an external end bimoment to be added to B_1 and B_2.

3.8. STIFFNESS MATRIX

By substituting for the derivatives of the shape functions $d_i^{\backprime}$ in eq. 3.34 and integrating with respect to the volume of the element V the elastic stiffness matrix $[K_E]$ can be given by,

$$
\left[K_E\right] = \left[\begin{array}{c|ccccccc|ccccccc}
 & u_1 & v_1 & w_1 & \theta_{x1} & \phi_1 & \psi_1 & \chi_1 & u_2 & v_2 & w_2 & \theta_{x2} & \phi_2 & \psi_2 & \chi_2 \\
\hline
u_1 & a_{11} & & & & & & & & & & & & & \\
v_1 & & a_{22} & & & & & & & & & & & & \\
w_1 & & & a_{33} & & & & & & & & & & & \\
\theta_{x1} & & & & a_{44} & & & & & & & & & & \\
\phi_1 & & & a_{53} & & a_{55} & & & & & & & & & \\
\psi_1 & & a_{62} & & & & a_{66} & & & & & & & & \\
\chi_1 & & & & a_{74} & & & a_{77} & & & & & & & \\
\hline
u_2 & b_{11} & & & & & & & c_{11} & & & & & & \\
v_2 & & b_{22} & & & & b_{26} & & & c_{22} & & & & & \\
w_2 & & & b_{33} & & b_{35} & & & & & c_{33} & & & & \\
\theta_{x2} & & & & b_{44} & & & b_{47} & & & & c_{44} & & & \\
\phi_2 & & & b_{53} & & b_{55} & & & & & c_{53} & & c_{55} & & \\
\psi_2 & & b_{62} & & & & b_{66} & & & c_{62} & & & & c_{66} & \\
\chi_2 & & & & b_{74} & & & b_{77} & & & & c_{74} & & & c_{77}
\end{array}\right] \quad \text{Symmetric} \qquad (3.47)
$$

where,

$$
\left.\begin{array}{lll}
a_{11} = \dfrac{EA}{\ell} & b_{11} = -a_{11} & c_{11} = a_{11} \\
a_{22} = \dfrac{12EI_z}{\ell^3} & b_{22} = -a_{22} & c_{22} = a_{22} \\
a_{33} = \dfrac{12EI_y}{\ell^3} & b_{33} = -a_{33} & c_{33} = a_{33} \\
a_{44} = \dfrac{1{\cdot}2GJ}{\ell} + \dfrac{12EI_\omega}{\ell^3} & b_{44} = -a_{44} & c_{44} = a_{44}
\end{array}\right\}
$$

$$
\begin{aligned}
a_{55} &= \frac{4EI_y}{\ell} & b_{55} &= \frac{2EI_y}{\ell} & c_{55} &= a_{55} \\
a_{66} &= \frac{4EI_z}{\ell} & b_{66} &= \frac{2EI_z}{\ell} & c_{66} &= a_{66} \\
a_{77} &= \frac{2GJ\cdot\ell}{15} + \frac{4EI_\omega}{\ell}, & b_{77} &= \frac{-GJ\cdot\ell}{30} + \frac{2EI_\omega}{\ell}, & c_{77} &= a_{77} \\
a_{53} &= \frac{-6EI_y}{\ell^2} & b_{53} &= a_{53} & c_{53} &= -a_{53} \\
a_{62} &= \frac{-6EI_z}{\ell^2} & b_{62} &= a_{62} & c_{62} &= -a_{62} \\
a_{74} &= \frac{-GJ}{10} - \frac{6EI_\omega}{\ell^2} & b_{74} &= a_{74} & c_{74} &= -a_{74} \\
b_{35} &= -b_{53} & b_{26} &= -b_{62} & b_{47} &= -b_{74}
\end{aligned}
\qquad (3.48)
$$

It can be noted from eq. 3.48 that the stiffness matrix K_E resulting from the finite element analysis and based on an approximate representation of the element behaviour is identical to the conventional stiffness matrix given by a virtual work analysis except for the signs of a_{62}, b_{62}, c_{62}, a_{26}, b_{26} and c_{26}. This is due to the sign of the bending moments M_{z1} and M_{z2} which follows the shape functions representing the displacement v. However, in section 3.10 a suitable transformation matrix, to be used in a three dimensional analysis in conjunction with stiffness matrix K_E, is presented.

3.9. GEOMETRIC MATRIX

By substituting for the derivatives of the shape functions $\grave{d}_i$ and the external end forces in eq. 3.36 and integrating with respect to the volume of the element V the geometric stiffness matrix can be given by,

$$
\left[K_G\right] = -
\begin{array}{c|c|c|c|c|c|c|c|c|c|c|c|c|}
 & u_1 & v_1 & w_1 & \theta_{x1} & \phi_1 & \psi_1 & \chi_1 & u_2 & v_2 & w_2 & \theta_{x2} & \phi_2 & \psi_2 & \chi_2 \\
\hline
u_1 & & & & & & & & & & & & & & \\
\hline
v_1 & & d_{22} & & & & & & & & & & & & \\
\hline
w_1 & & & d_{33} & & & & & & & & & & & \\
\hline
\theta_{x1} & & d_{42} & d_{43} & d_{44} & & & & & & & & & & \\
\hline
\phi_1 & & & d_{53} & d_{54} & d_{55} & & & & & & & & & \\
\hline
\psi_1 & & d_{62} & & d_{64} & & d_{66} & & & & & & & & \\
\hline
\chi_1 & & d_{72} & d_{73} & d_{74} & & & d_{77} & & & & & & & \\
\hline
u_2 & & & & & & & & & & & & & & \\
\hline
v_2 & & e_{22} & & e_{24} & & e_{26} & e_{27} & & f_{22} & & & & & \\
\hline
w_2 & & & e_{33} & e_{34} & e_{35} & & e_{37} & & & f_{33} & & & & \\
\hline
\theta_{x2} & & e_{42} & e_{43} & e_{44} & e_{45} & e_{46} & e_{47} & & f_{42} & f_{43} & f_{44} & & & \\
\hline
\phi_2 & & & e_{53} & e_{54} & e_{55} & & e_{57} & & & f_{53} & f_{54} & f_{55} & & \\
\hline
\psi_2 & & e_{62} & & e_{64} & & e_{66} & e_{67} & & f_{62} & & f_{64} & & f_{66} & \\
\hline
\chi_2 & & e_{72} & e_{73} & e_{74} & e_{75} & e_{76} & e_{77} & & f_{72} & f_{73} & f_{74} & f_{75} & f_{76} & f_{77} \\
\hline
\end{array}
\qquad \text{Symmetric} \qquad (3.49)
$$

in which,

$$d_{22} = \frac{1.2 \cdot P_x}{\ell} \qquad f_{22} = d_{22} \qquad e_{22} = -\, d_{22}$$

$$d_{33} = \frac{1.2 \cdot P_x}{\ell} \qquad f_{33} = d_{33} \qquad e_{33} = -\, d_{33}$$

$$d_{44} = \frac{1.2\ C_o\ P_x}{\ell} + 0.3 \left[\frac{2(M_{y1}-M_{y2})}{\ell} + Q_{z1} + Q_{z2}\right] \beta_y + 0.3 \left[\frac{2(M_{z1}-M_{z2})}{\ell} + Q_{y1} + Q_{y2}\right] \beta_z + \left[\frac{K_{b1}\ (B_1-B_2)}{\ell} + K_{t1}\ M_x\right] \beta_\omega$$

$$e_{44} = -\, d_{44} \qquad f_{44} = d_{44}$$

$$d_{55} = \frac{2\ P_x\ \ell}{15} \qquad e_{55} = -\, \frac{P_x\ \ell}{30} \qquad f_{55} = d_{55}$$

$$d_{66} = \frac{2\ P_x\ \ell}{15} \qquad e_{66} = -\frac{P_x\ \ell}{30} \qquad f_{66} = d_{66}$$

$$d_{77} = \frac{2\ P_x\ C_o\ \ell}{15} + \left[\frac{(M_{y1} - M_{y2})\ell}{15} + \frac{Q_{z1}\ \ell^2}{60} + \frac{Q_{z2}\ \ell^2}{20}\right] \beta_y$$

$$+ \left[\frac{(M_{z1} - M_{z2})\ell}{15} + \frac{Q_{y1}\ \ell^2}{60} + \frac{Q_{y2}\ \ell^2}{20}\right] \beta_z$$

$$+ \left[K_{b2}\ (B_1 - B_2)\ \ell + K_{t2}\ M_x\ \ell^2\right] \beta_\omega$$

$$e_{77} = \frac{-P_x\ C_o\ \ell}{30} - \left[\frac{(M_{y1} - M_{y2})\ \ell}{60} + \frac{(Q_{z1} + Q_{z2})\ \ell^2}{120}\right] \beta_y$$

$$- \left[\frac{(M_{z1} - M_{z2})\ \ell}{60} + \frac{(Q_{y1} + Q_{y2})\ \ell^2}{120}\right] \beta_z$$

$$- \left[(K_{b4}\ (B_1 - B_2)\ \ell + K_{t4}\ M_x\ \ell^2\ \right] \beta_\omega$$

$$f_{77} = \frac{2\ P_x\ C_o\ \ell}{15} + \left[\frac{(M_{y1} - M_{y2})\ell}{15} + \frac{Q_{z1}\ \ell^2}{20} + \frac{Q_{z2}\ \ell^2}{60}\right] \beta_y$$

$$+ \left[\frac{(M_{z1} - M_{z2})\ \ell}{15} + \frac{Q_{z1}\ \ell^2}{20} + \frac{Q_{z2}\ \ell^2}{60}\right] \beta_z$$

$$+ \left[K_{b1}\ (B_1 - B_2)\ \ell + K_{t1}\ M_x\ \ell^2\ \right] \beta_\omega$$

$$d_{42} = \frac{1.2\ P_x\ C_z}{\ell} + \frac{0.6\ (M_{y1} - M_{y2})}{\ell} + 0.05\ Q_{z1} + 0.55\ Q_{z2}$$

$$e_{42} = \frac{-1.2\ P_x\ C_z}{\ell} - \frac{0.6\ (M_{y1} - M_{y2})}{\ell} - 0.55\ Q_{z1} - 0.05\ Q_{z2}$$

$$d_{43} = \frac{-1.2\ P_x\ C_y}{\ell} - \frac{0.6\ (M_{z1} - M_{z2})}{\ell} - 0.05\ Q_{y1} - 0.55\ Q_{y2}$$

$$e_{43} = \frac{1.2\ P_x\ C_y}{\ell} + \frac{0.6\ (M_{z1} - M_{z2})}{\ell} + 0.55\ Q_{y1} + 0.05\ Q_{y2}$$

$$f_{42} = -\ e_{42} \qquad e_{24} = -\ d_{42}$$

$$f_{43} = -\ e_{43} \qquad e_{34} = -\ d_{43}$$

$$d_{62} = -\ 0.10\ P_x \qquad e_{62} = d_{62} \qquad d_{62} = -\ d_{62} \qquad e_{26} = -\ d_{62}$$

$$d_{53} = -\ 0.10\ P_x \qquad e_{53} = d_{53} \qquad f_{53} = -\ d_{53} \qquad e_{35} = -\ d_{53}$$

$$d_{72} = -\ 0.10\ P_x.C_z - 0.05\ (M_{y1} - M_{y2}) - 0.05\ Q_{z2}\ \ell$$

$$e_{72} = -\ 0.10\ P_x.C_z - 0.05\ (M_{y1} - M_{y2}) - 0.05\ Q_{z1}\ \ell$$

$$f_{72} = -\ C_{72} \qquad e_{27} = -\ d_{72}$$

$$d_{73} = 0.10\ P_x\ C_y + 0.05\ (M_{z1} - M_{z2}) + 0.05\ Q_{y2}\ \ell$$

$$e_{73} = 0.10\ P_x\ C_y + 0.05\ (M_{z1} - M_{z2}) + 0.05\ Q_{y1}\ \ell$$

$$f_{73} = -\ e_{73} \qquad e_{37} = -\ d_{73}$$

$$d_{54} = 1.10\ P_x\ C_y + 0.55\ (M_{z1} - M_{z2}) + 0.10\ Q_{y1}\ \ell + 0.45\ Q_{y2}\ \ell$$

$$e_{54} = 0.10\ P_x\ C_y + 0.05\ (M_{z1} - M_{z2}) - 0.05\ Q_{y1}\ \ell + 0.10\ Q_{y2}\ \ell$$

$$f_{54} = -\ 1.10\ P_x\ C_y - 0.55\ (M_{z1} - M_{z2}) - 0.45\ Q_{y1}\ \ell - 0.10\ Q_{y2}\ \ell$$

$$e_{45} = -\ 0.10\ P_x\ C_y - 0.05\ (M_{z1} - M_{z2}) - 0.10\ Q_{y1}\ \ell + 0.05\ Q_{y2}\ \ell$$

$$d_{64} = -\ 1.10\ P_x\ C_z - 0.55\ (M_{y1} - M_{y2}) - 0.10\ Q_{z1}\ \ell - 0.45\ Q_{z2}\ \ell$$

$$e_{64} = -\ 0.10\ P_x\ C_z - 0.05\ (M_{y1} - M_{y2}) + 0.05\ Q_{z1}\ \ell - 0.10\ Q_{z2}\ \ell$$

$$f_{64} = 1.10\ P_x\ C_z + 0.55\ (M_{y1} - M_{y2}) + 0.45\ Q_{z1}\ \ell + 0.10\ Q_{z2}\ \ell$$

$$e_{46} = 0.10\ P_x\ C_z + 0.05\ (M_{y1} - M_{y2}) + 0.10\ Q_{z1}\ \ell - 0.05\ Q_{z2}\ \ell$$

$$d_{74} = -\ 0.10\ P_x\ C_o - \left[0.05\ (M_{y1} - M_{y2}) + 0.05\ Q_{z1}\ \ell\right]\beta_y$$
$$- \left[0.05\ (M_{z1} - M_{z2}) + 0.05\ Q_{y1}\ \ell\right]\beta_z$$
$$- \left[K_{b3}\ (B_1 - B_2) + K_{t3}\ M_x\ \ell\right]\beta_\omega$$

$$
\begin{aligned}
e_{74} &= -\,0.10\,P_x\,C_o - \left[0.05\,(M_{y1} - M_{y2}) + 0.05\,Q_{z2}\,\ell\right]\beta_y \\
&\quad - \left[0.05\,(M_{z1} - M_{z2}) + 0.05\,Q_{y2}\,\ell\right]\beta_z \\
&\quad - \left[K_{b3}\,(B_1 - B_2) + K_{t3}\,M_x\,\ell\right]\beta_\omega
\end{aligned}
$$

$$
\begin{aligned}
f_{74} &= -\,e_{74} \qquad\qquad e_{47} = -\,d_{74} \\
d_{75} &= \frac{-\,2\,P_x\,C_y\,\ell}{15} - \frac{(M_{z1} - M_{z2})\ell}{15} - \frac{Q_{y1}\,\ell^2}{60} - 0.05\,Q_{y2}\,\ell^2 \\
e_{75} &= \frac{P_x\,C_y\,\ell}{30} + \frac{(M_{z1} - M_{z2})\ell}{60} + \frac{Q_{y2}\,\ell^2}{60} \\
f_{75} &= \frac{2\,P_x\,C_y\,\ell}{15} - \frac{(M_{z1} - M_{z2})\ell}{15} - 0.05\,Q_{y1}\,\ell^2 - \frac{Q_{y2}\,\ell^2}{60} \\
e_{57} &= \frac{P_x\,C_y\,\ell}{30} + \frac{(M_{z1} - M_{z2})\ell}{60} + \frac{Q_{y1}\,\ell^2}{60} \\
d_{76} &= \frac{2\,P_x\,C_z\,\ell}{15} + \frac{(M_{y1} - M_{y2})\ell}{15} + \frac{Q_{z1}\,\ell^2}{60} + 0.05\,Q_{z2}\,\ell^2 \\
e_{76} &= -\,\frac{P_x\,C_z\,\ell}{30} - \frac{(M_{y1} - M_{y2})\ell}{60} - \frac{Q_{z2}\,\ell^2}{60} \\
f_{76} &= \frac{2\,P_x\,C_z\ell}{15} + \frac{(M_{y1} - M_{y2})\ell}{15} + 0.05\,Q_{z1}\,\ell^2 + \frac{Q_{z2}\,\ell^2}{60} \\
e_{67} &= \frac{-\,P_x\,C_z\,\ell}{30} - \frac{(M_{y1} - M_{y2})\ell}{60} - \frac{Q_{z1}\,\ell^2}{60}
\end{aligned}
\qquad (3.50)
$$

in which, K_{b1}, K_{b2}, K_{b3}, K_{b4}, K_{t1}, K_{t2}, K_{t3}, and K_{t4} are the coefficients resulting from the numerical integration of eq. 3.46. Values of these coefficients for different $k\ell$ values $\left(k = \sqrt{\frac{GJ}{EI_\omega}}\right)$ are presented in Appendix A.3.2.

In comparison with the geometric matrix presented by Barsoum and Gallagher (24), or that derived by Tebedge (28), or those presented by Powell (26), Krajcinovic (22,23), it can be noted that the new geometric matrix given by eq. 3.49 includes more terms which allow for more buckling cases to be

analysed. The advantages of the new geometric matrix can be stated as follows:

1. The matrix can be used to analyse members having monosymmetric cross section. It includes the geometric characteristics β_y and β_z which reflect the effect of monosymmetry on the buckling behaviour of the member. The validity and accuracy of the new matrix has been examined by analysing a number of beam and cantilever problems for which experimental or finite integral solutions are already available (ref. 40) as will be explained in chapter 6 of this thesis.

2. The analysis has been carried out considering that up to buckling the bending deformations of the structure are accompanied by torsion and at the moment of buckling the structure passes to another flexural-torsional equilibrium shape. The effect of the bimoment caused by the external load is included in the geometric matrix. This effect is valid only for cross sections without any axis of symmetry. For these sections a new geometric constant β_ω reflecting the effect of sectorial monosymmetry is evaluated. In chapter 7 of this thesis an experimental and theoretical study (based on the new formulation) on cold-formed simply supported Z-beams loaded with concentrated loads is presented. The comparison of the results is also presented as a check of the validity of the bimoment terms in the geometric matrix.

3. The signs of the terms which include M_{z1}, M_{z2}, Q_{y1} and Q_{y2} have been changed according to the sign conventions considered for the shape functions used to represent the displacements v and ψ. Together with the transformation matrix given in the following section (section 3.10) the new formulation can be used for a three dimensional buckling analysis. The validity and accuracy of the formulation have been examined by analysing a number of portal and space frame problems for which an analytical or experimental results are already available and the comparison is presented in chapter 6.

3.10. TRANSFORMATION OF AXES

The system of axes for the subject prismatic element has been defined at the beginning of the previous chapter and is shown in fig. 2.3. The x - axis was defined as coinciding with the centroidal line of the element while y and z axis coincide with the principal axes of the cross section. The three axes form a right-handed system.

In order to carry out a general three dimensional frame analysis all forces and deflections must be stated in terms of one global system of axes. The transformation from a member local axes to the global system can be done through a matrix operation involving the use of a suitable transformation matrix.

Jennings and Majid (67) presented a general procedure for the first order elastic analysis of rigidly jointed space frames in which they took into account the secondary effect of the misalignment of the members using two displacement transformations. The procedure can be described by the following steps:

1. For a given member in a space frame structure if $\left[\bar{\delta}\right]$ is the column vector of the displacements at the two end joints of the member with respect to the global system of co-ordinates and $\left[\delta\right]$ is the column vector corresponding to the components of these displacements in the local co-ordinate system of the member, the compatibility conditions give,

$$\left[\delta\right] = \left[a_i\right]\left[\bar{\delta}\right] \qquad (3.51)$$

in which, a_i is the member transformation matrix given by,

$$\left[a_i\right] = \begin{bmatrix} r_i & o & o & o \\ o & r_i & o & o \\ o & o & r_i & o \\ o & o & o & r_i \end{bmatrix} \qquad (3.52)$$

and,

$$\left[r_i\right] = \begin{bmatrix} \ell_1 & m_1 & n_1 \\ \ell_2 & m_2 & n_2 \\ \ell_3 & m_3 & n_3 \end{bmatrix} \tag{3.53}$$

in which (as shown in fig. 3.5), ℓ_1, m_1, n_1 are the direction cosines of the local x axis with respect to the global X, Y, and Z axes respectively, ℓ_2, m_2, n_2 are the direction cosines of the local y axis and ℓ_3, m_3, n_3 are the direction cosines of the local z axis.

2. The contribution K_i of member i to the overall stiffness matrix of the frame can be given by,

$$\left[K_i\right] = \left[a_i\right]^T \left[k_i\right] \left[a_i\right] \tag{3.54}$$

in which, k_i is the local stiffness matrix of the member.

3. To include the secondary effects caused by the misalignment of the members in the analysis of space frames, Jennings and Majid (67) suggested the use of a misalignment matrix and performing a double transformation of the displacements. Fig. 3.6 shows the misalignment of a given member 1-2 where AB is the line connecting joints A and B of the frame, P_{c1} is the departure at end 1 from joint A in X-direction, P_{c2} is the departure at end 2 from joint B in X-direction, q_c and r_c are the departures of the member netural axis from the line of joints AB in Y and Z-directions respectively. Jennings and Majid presented a misalignment matrix $\left[\bar{m}\right]$ in terms of the departures P_{c1}, P_{c2}, q_c and r_c. The two displacement transformations lead to the general transformation matrix $\left[\bar{a}_i\right]$ which can be evaluated from the following equation,

$$\left[\bar{a}_i\right] = \left[a_i\right] \left[\bar{m}\right] \tag{3.55}$$

Fig. 3.4 shows the positive directions of the end moments M_{z1}, and M_{z2} in the positive directions which have been adopted in the analysis for the angles of rotation ψ_1 and ψ_2. Positive directions of ψ_1 and ψ_2 have been dictated by the use of the shape functions d_3, d_4, d_5 and d_6 for the approximate representation of the displacement v (eq. 3.31.a-e). In order to carry out a three dimensional frame analysis based on the finite element formulation given in the previous sections of this chapter, the transformation matrix $[a_i]$ has to be modified, first according to the sign conventions of M_{z1} and M_{z2}, and secondly to include the warping transformation.

According to the positive directions of ψ_1 and ψ_2, the transformation matrix $[a_i]$ can be modified to the matrix $[t_i]$ where,

$$[t_i]=\begin{bmatrix} r_i & o & o & o \\ o & \bar{r}_i & o & o \\ o & o & r_i & o \\ o & o & o & \bar{r}_i \end{bmatrix} \qquad (3.56)$$

and,

$$[\bar{r}_i]=\begin{bmatrix} \ell_1 & m_1 & n_1 \\ \ell_2 & m_2 & n_2 \\ -\ell_3 & -m_3 & -n_3 \end{bmatrix} \qquad (3.57)$$

The analysis of the warping behaviour at the joints of a framed structure presents a complex problem (9). In a comprehensive study concerning the warping behaviour of rigid-jointed double symmetric I-plane frames Vacharajittiphan and Trahair (64) reported that the warping behaviour depends on the angle of the joint and on the number and type of stiffeners used at the joint. Nevertheless, the results of their investigation are far from being applicable in a large three

dimensional frame analysis. Previous studies on rigid jointed frames have assumed that the joints are sufficiently stiff for warping to be neglected (7,9,10,11,12,28,52,53). For members meeting at 180^{o} angle, the continuity condition at the joint is such that the warping of one member is elastically restrained by the other. The transformation matrix given by eq. 3.56 has been modified to include the transformation of the warping as the seventh degree of freedom at the joint. The submatrix $\left[\overline{r}_i\right]$ given by eq. 3.57 can be replaced by the submatrix $\left[\grave{r}_i\right]$ where,

$$\left[\grave{r}_i\right] = \begin{bmatrix} \ell_1 & m_1 & n_1 & o \\ \ell_2 & m_2 & n_2 & o \\ -\ell_3 & -m_3 & -n_3 & o \\ o & o & o & 1 \end{bmatrix} \qquad (3.58)$$

For rigidly jointed frames the boundary conditions at the corner joints are such that the warping of the joint is prevented.

The general transformation matrix $\left[\overline{t}_i\right]$, which can be used together with the stiffness and geometric matrices given in the previous sections for a three-dimensional second order and/or buckling analysis of frame and which include the secondary effect of the misalignment of the member axes, is given by,

$$\left[\overline{t}_i\right] = \begin{bmatrix} r_i & r_{oi} & o & o \\ o & \grave{r}_i & o & o \\ o & o & r_i & \grave{r}_{oi} \\ o & o & o & \grave{r}_i \end{bmatrix} \qquad (3.59)$$

in which, r_i is given by eq. 3.53, $\grave{r}_i$ is given by eq. 3.57, r_{oi} and $\grave{r}_{oi}$ are given by the following equations,

$$\left[r_{oi}\right] = \begin{bmatrix} b_1 & b_4 & b_7 & o \\ b_2 & b_5 & b_8 & o \\ b_3 & b_6 & b_9 & o \\ o & o & o & o \end{bmatrix} \qquad (3.60)$$

and,

$$\left[\grave{r}_{oi}\right] = \begin{bmatrix} b_1 & b_4 & b_7 & o \\ \grave{b}_2 & \grave{b}_5 & \grave{b}_8 & o \\ \grave{b}_3 & \grave{b}_6 & \grave{b}_9 & o \\ o & o & o & o \end{bmatrix} \qquad (3.61)$$

where,

$$b_1 = - r_c \ell_2 + q_c \ell_3 \qquad b_2 = - r_c \ell_1 - P_{c1} \ell_3 \qquad (3.62.a)$$

$$b_3 = q_c \ell_1 + P_{c1} \ell_3 \qquad b_4 = - r_c m_2 + q_c m_3 \qquad (3.62.b)$$

$$b_5 = - r_c m_1 - P_{c1} m_3 \qquad b_6 = q_c m_1 + P_{c1} m_3 \qquad (3.62.c)$$

$$b_7 = - r_c n_2 + q_c n_3 \qquad b_8 = - r_c n_1 - P_{c1} n_3 \qquad (3.62.d)$$

$$b_9 = q_c n_1 + P_{c1} n_3 \qquad (3.62.e)$$

and, $\grave{b}_2$, $\grave{b}_3$, ..., $\grave{b}_9$ are obtained by switching P_{c1} to P_{c2} in b_2, b_3, ... b_9 respectively.

The buckling analysis of a given structure starts with the choice of an arbitrary value of the load factor and

by performing a linear elastic analysis the individual element end forces are found. By using these forces to form the geometric matrix the instability condition can then be illustrated by eq. 3.39. The critical load is the lowest root of this equation.

There are a number of methods for solving the stability equation. These methods are reviewed in the next chapter. Attention is focused on Southwell plot method. This method is employed in a finite element computer program to predict the buckling load from a second order flexural-torsional analysis of the structure. Chapter four also includes a detailed description of this computer program.

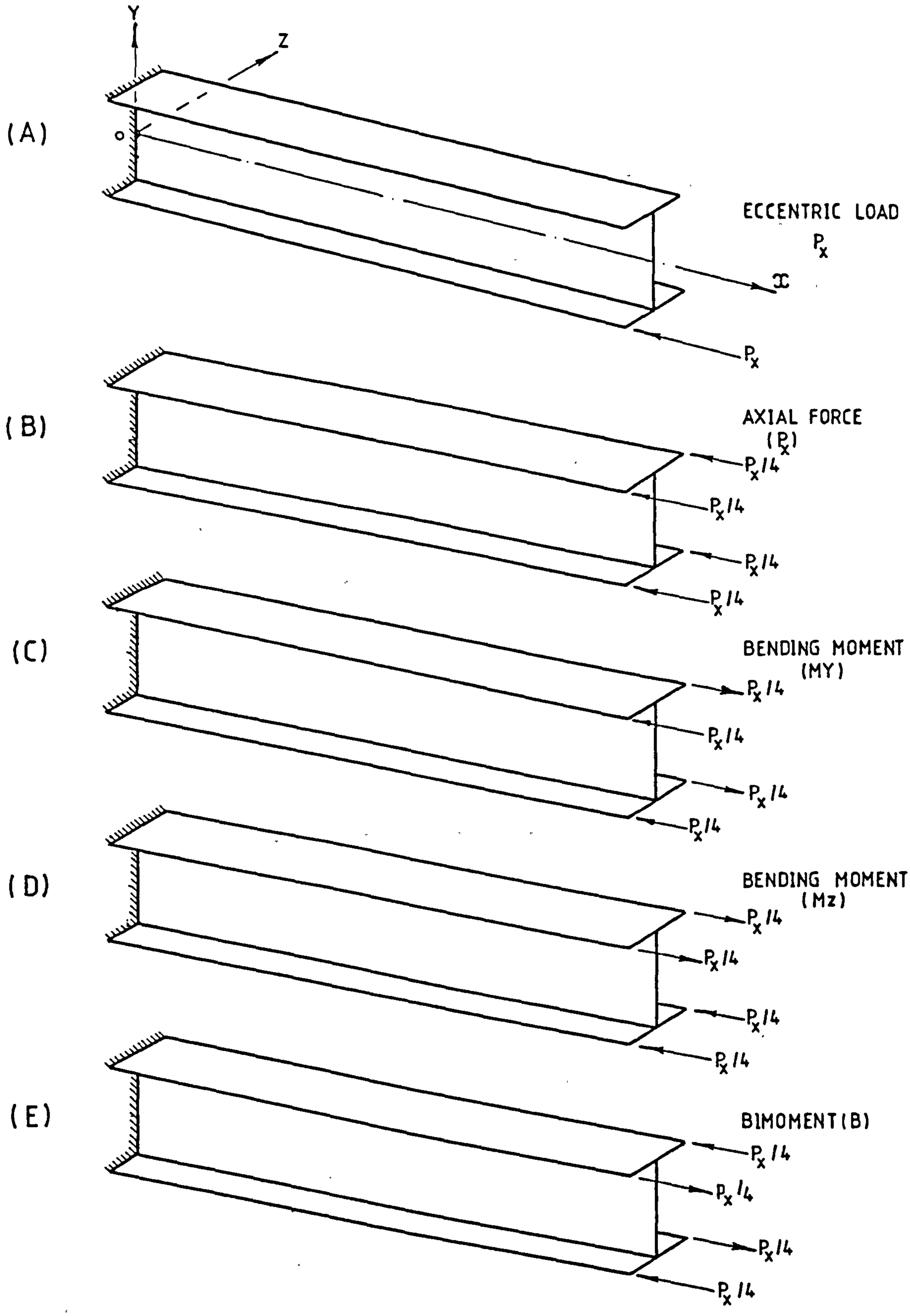

Fig.3.1 Analysis Of The Eccentric Axial Load P_x

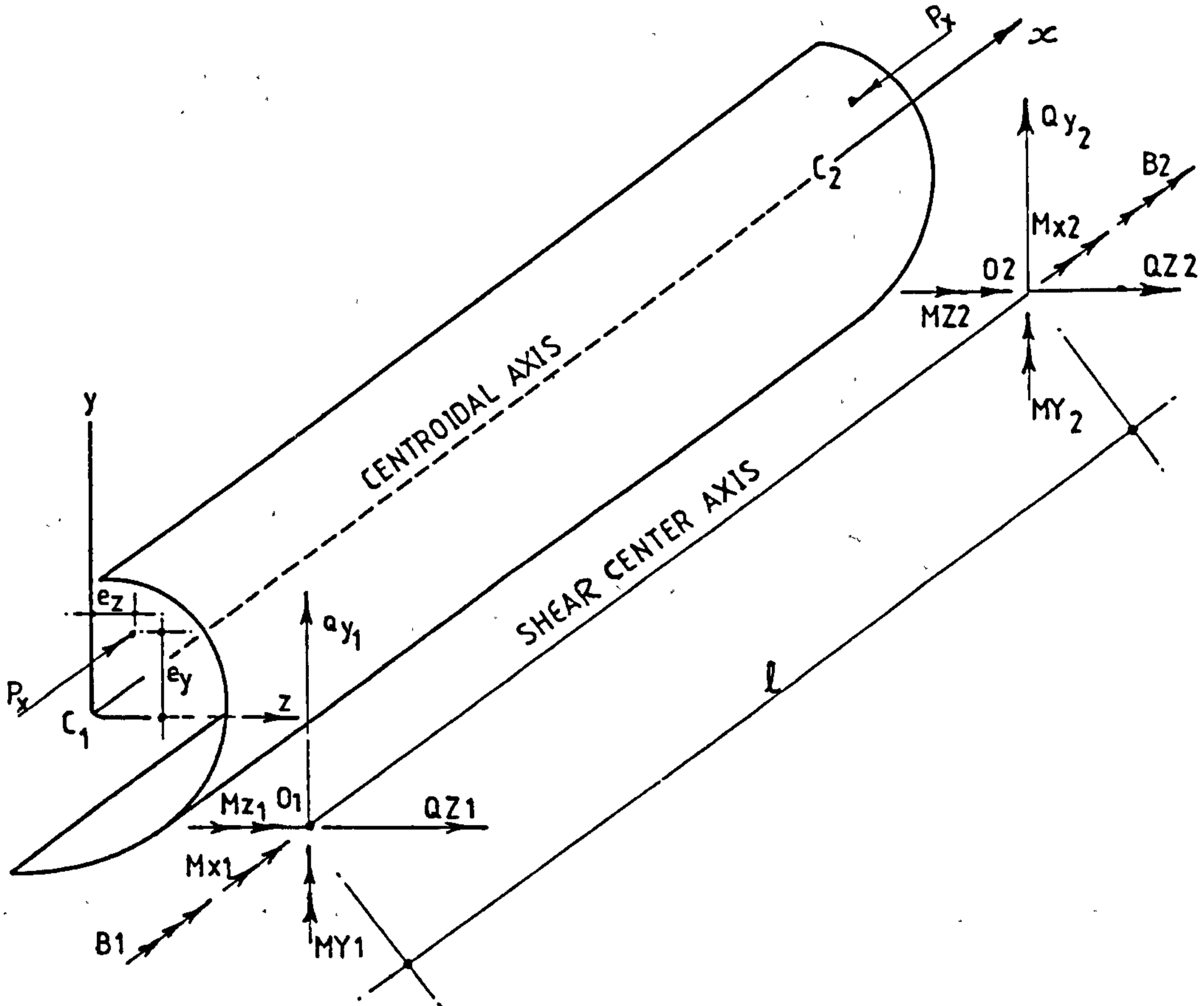

Fig. 3.2 Element End Forces.

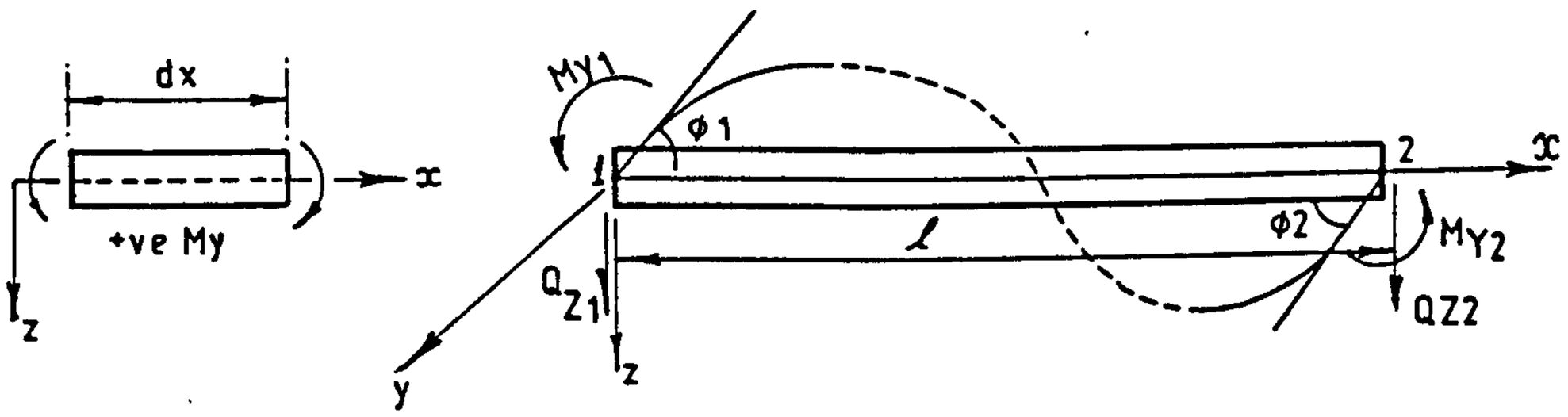

Fig. 3.3 Bending My

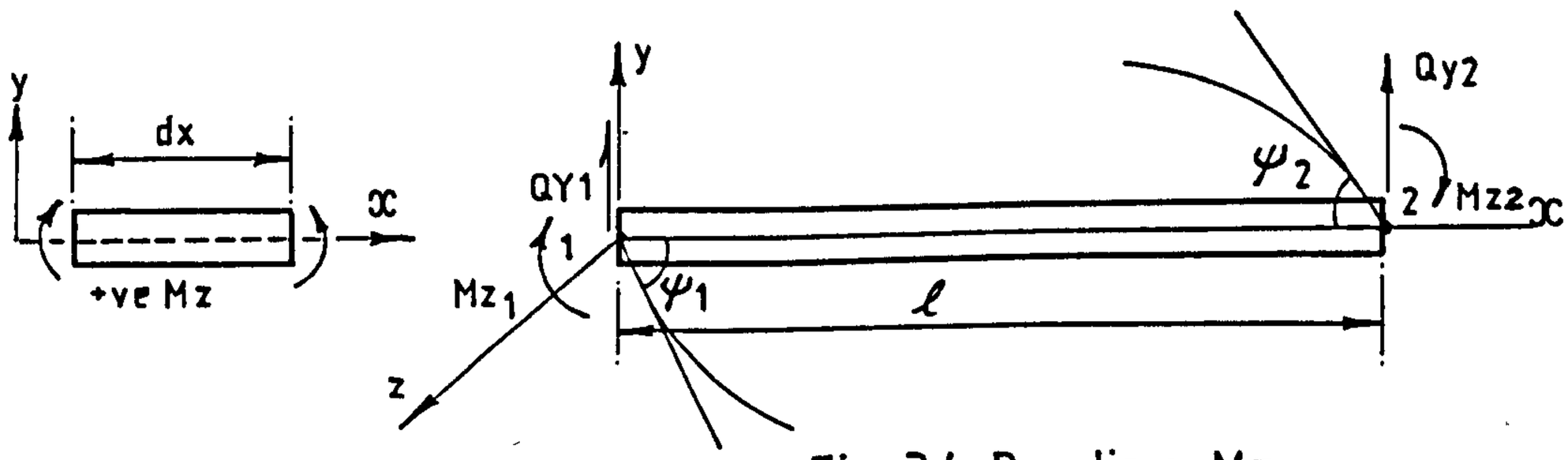

Fig. 3.4 Bending Mz

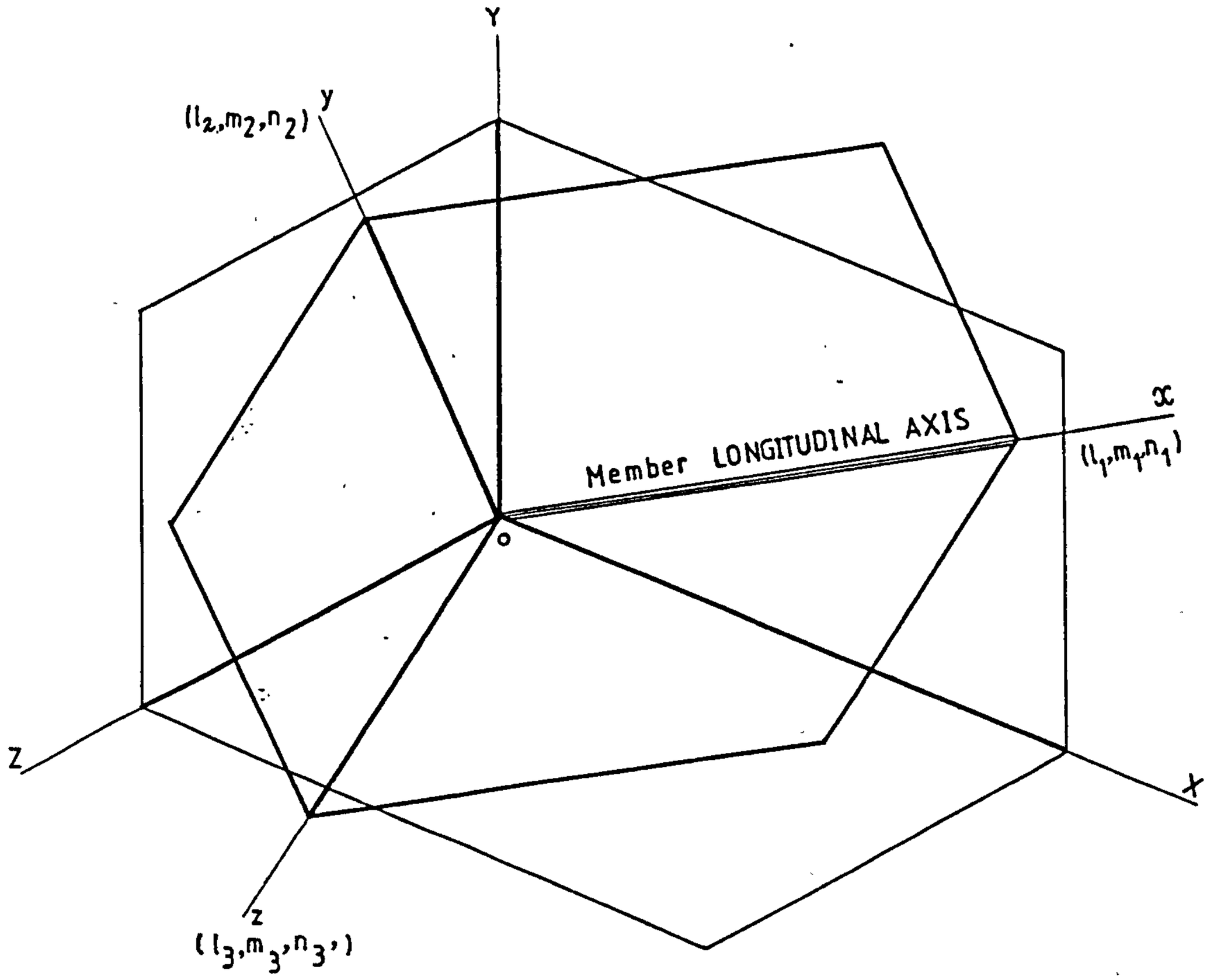

Fig.3.5 Direction Cosines Between Local And Global Axes

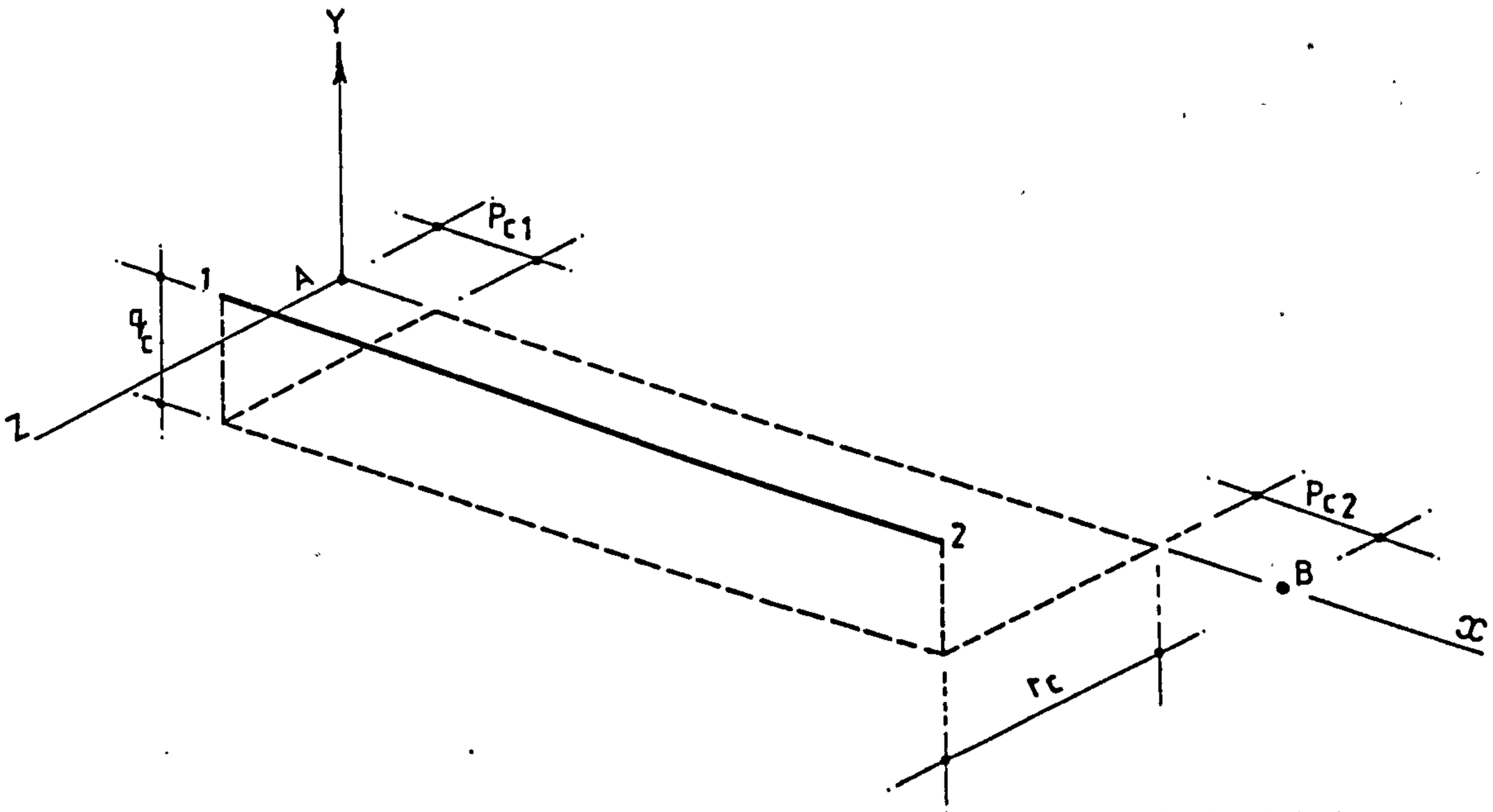

Fig.3.6 Misalignment Of Member Ends From Specified Joint Positions

CHAPTER FOUR

Prediction of the Buckling Load

4.1. THE BUCKLING CRITERION

The second-order behaviour of a framed structure having n joints can be expressed by the following equation,

$$\{F_n\} = \left[\left[K_{ee}\right] + \left[K_{gg}\right]\right]\{\Delta_n\} \qquad (4.1)$$

where, $\{F_n\}$ is the column vector of the external load acting at the joints of the frame, $\left[K_{ee}\right]$ is the overall elastic stiffness matrix of the frame, $\left[K_{gg}\right]$ is the overall elastic geometric matrix, and $\{\Delta_n\}$ is the joint displacement vector. The term $\left[\left[K_{ee}\right] + \left[K_{gg}\right]\right]$ which represents the second-order matrix of the structure can be obtained from the transformation operation,

$$\left[\left[K_{ee}\right] + \left[K_{gg}\right]\right] = \sum_{n}^{i=1} \left[\bar{t}_i\right]^T \left[\left[K_E\right] + \left[K_G\right]\right] \left[\bar{t}_i\right] \qquad (4.2)$$

in which, $\left[K_E\right]$ and $\left[K_G\right]$ are the member stiffness and geometric matrices in the local co-ordinate system, $\left[\bar{t}_i\right]$, and $\left[\bar{t}_i\right]^T$ are the member transformation matrix and its transpose.

The member stiffness and geometric matrices $\left[K_E\right]$, $\left[K_G\right]$ are given by equations 3.47 and 3.48 respectively, and the transformation matrix $\left[\bar{t}_i\right]$ is given by eq. 3.59.

In an elastic stability analysis, the applied load on the structure is regarded as a fixed loading pattern multiplied by some factor λ. The critical load F_{cr} can be defined as the load F multiplied by the smallest value of λ at which the displacements of the structure become indeterminate (bifurcation of equilibrium).

This condition can be mathematically represented by the following relationship,

$$\left[\left[K_{ee}\right] + \lambda \left[K_{gg}\right]\right]\{\bar{\Delta}_n\} = o \qquad (4.3)$$

in which, $\{\bar{\Delta}_n\}$ is the column vector of the buckling deformations.

For the non-trivial solution of eq. 4.3 the determinantal condition is given by,

$$\left|\bar{K}_{ee}\right| + \lambda \left|\bar{K}_{gg}\right| = o \qquad (4.4)$$

in which, $\left|\bar{K}_{ee}\right|$ and $\left|\bar{K}_{gg}\right|$ are the determinants of the stiffness and geometric matrices respectively. The critical load can then be defined as the lowest root of eq. 4.4.

Equation 4.4 is known as the buckling criterion. Below the first (lowest) critical load the determinant has a positive value. When the load is exceeded, the determinant becomes negative. The critical load can be determined by systematically searching for the load at which the determinant first changes its sign.

4.2. SOLUTION OF THE STABILITY EQUATION

4.2.1. Eigenvalue solution

The general form of the eigenvalue problems can be represented by the equation,

$$\left[\left[A\right] - \lambda\left[B\right]\right]\{\bar{X}\} = o \qquad (4.5)$$

in which $\left[A\right]$, and $\left[B\right]$ are symmetrical matrices, λ is a scalar called the eigenvalue, and $\{\bar{X}\}$ is a column vector called the eigenvector. Equations 4.4 and 4.5 are directly analogous. Thus the stability equation (eq. 4.4) can be treated as an eigenvalue problem. The lowest eigenvalue λ multiplied by the load factor gives the first (lowest) critical load of the structure.

Equation 4.5 has solutions other than zero only if the determinant of the coefficients vanishes. This condition can be represented by the following equation,

$$\begin{bmatrix} a_{11} - \lambda_i b_{11} & a_{12} - \lambda_i b_{12} \cdots a_{1n} - \lambda_i b_{1n} \\ a_{21} - \lambda_i b_{21} & a_{22} - \lambda_i b_{22} \cdots a_{2n} - \lambda_i b_{2n} \\ \vdots & \vdots \qquad\qquad \vdots \\ a_{n1} - \lambda_i b_{n1} & a_{n2} - \lambda_i b_{n2} \cdots a_{nn} - \lambda_i b_{nn} \end{bmatrix} = 0 \qquad (4.6)$$

The characteristic equation of the system can be derived by expanding eq. 4.6. The n roots resulting from the solution of the characteristic equation are the n eigenvalues(λ values) of eq. 4.5. The eigenvector $\{\bar{X}_i\}$ corresponding to any eigenvalue λ_i can be evaluated by substituting for λ_i in eq. 4.5 and solving for the ratios of the elements in $\{\bar{X}_i\}$.

The solution of eq. 4.5, by any of the computer-based methods, is often based on converting the problem into a standard eigenvalue problem, (69), which can be described by the equation,

$$\left[\left[H\right] - \lambda \left[I\right]\right] \{\bar{X}\} = o \qquad (4.7)$$

where, the matrix H is given by,

$$\left[H\right] = \left[B\right]^{-1} \left[A\right] \qquad (4.8)$$

and $\left[I\right]$ is the identity matrix.

The solution of eq. 4.7 can be carried out using one of the computer-based methods for solving the eigenvalue problems. These methods can be divided into two main groups, namely, transformation methods and iterative methods (69). The transformation methods can be used when all the eigenvalues and eigenvectors are required. The iterative methods

can be applied when one or few eigenvalues and eigenvectors only are required. More details about these methods can be found in references 69, 70 and 71.

4.2.2. Prediction of the buckling load from the load-displacement curve

This method is based on performing a second-order analysis of the structure and predicting the critical load from the load-displacement relationship. The procedure starts by analysing the structure under a small value of the load factor in order to identify the largest component of the lateral displacements Δ_ℓ. The load factor is then increased by a small positive increment and the corresponding value of the lateral displacement Δ_ℓ is to be calculated from a second-order analysis. The procedure is repeated in order to draw the load-displacement relationship until the curve becomes relatively flat. The maximum value of the load, from the curve, represents the critical load of the structure. The increments of the load must be kept small in order to avoid arriving at higher buckling modes.

4.2.3. Southwell method

Southwell (72) proposed an analytical technique for calculating the Euler buckling load of a real column using a load-deflection plot made for loads below the buckling load itself.

The method was later refined and applied by many investigators to predict the buckling loads for different types of stability problems such as beam-column (73), plane frameworks (74), plane trusses (75), and unbraced plane frames with flexible joints (76).

Southwell's method can briefly be illustrated as follows:

If an elastic strut is not quite straight initially and if the initial imperfection of the central line at the mid-length of the strut is equal to $\bar{v}$, the differential equation of equilibrium is,

$$\frac{d^2v}{dx^2} + \frac{P_x}{EI_z}(\bar{v} + v) = o \qquad (4.9)$$

in which, v is the additional deflection, P_x is the axial compressive force, and EI_z is the flexural rigidity of the strut.

Both v and $\bar{v}$ can be represented by Fourier sine series with coefficients $\bar{v}_n$ and v_n, respectively (75). By substituting in eq. 4.9 the load-deflection relationship becomes,

$$v_n = \frac{\bar{v}_n}{\frac{P_n}{P} - 1} \qquad (4.10)$$

in which, P_n is the nth critical load for the perfect strut.

The first critical load P_{cr} can be calculated from the equation,

$$\delta \cong v_1 = \frac{\bar{v}_1}{\frac{P_{cr}}{P} - 1} \qquad (4.11)$$

in which, δ is the total deflection of the strut at its center.

Equation 4.11 represents a rectangular hyperbola whose asymptotes are the axis P and the horizontal line $P = P_{cr}$ (77). Equation 4.11 can be rewritten in another form given by,

$$P_{cr} \cdot \frac{\delta}{P} = \delta + \bar{v}_1 \qquad (4.12)$$

Equation 4.12 describes the standard Southwell plot which is shown in fig. 4.1. The critical buckling load P_{cr} can be calculated from the slope of the plot.

Fig. 4.2 shows an alternative representation of eq. 4.12 known as the modified Southwell plot. The plot

represents a linear relationship between $P/_{\delta}$ and P. The critical load P_{cr} is given by the intercept with the P axis, while the inverse slope gives v_1.

The modified Southwell plot is used in the finite element computer program to predict the buckling load from a second-order analysis as will be illustrated in the next part of this chapter.

4.3. THE COMPUTER PROGRAM

The main routines of the finite element computer program used in the study reported in this thesis were already developed by Davies[1]. The program has been modified to include the geometric matrix and the transformation matrix which are presented in chapter three.

The computer program can be used for the following types of analysis:

a) Conventional elastic analysis of framed structures with maximum seven degrees of freedom at each joint (mode of analysis = o).

b) Second-order torsional-flexural analysis of framed structures (mode of analysis = 12).

c) Torsional-flexural buckling analysis of framed structures (mode of analysis = 2).

The input data for a given problem consists of the following:

1. Joints : Each joint of the structure, including the supports, has to be numbered and identified by its co-ordinates with respect to the adopted global system of co-ordinates. Degrees of freedom must also be given according to the restraining conditions at the joint.

2. Members : The members connecting the joints are divided into groups according to their elastic and cross sectional properties. Each member is identified by four integer numbers, the first refers to the group of the member, the second and third identify the two end joints

[1] Professor of Structural Engineering, University of Salford.

of the member, while the fourth number specifies a third joint chosen to define the principal plane of the member.

3. Loads : The applied loads are identified in the data sheet by the number of the loaded joint, the direction at which the load is applied (an integer from 1 to 7), and by the value of the load.

The flow chart of the computer program is shown in fig. 4.4. The program consists mainly of the following sub-routines:

a) Main subroutine, b) Subroutine MAPP,
c) Subroutine SPACE, d) Subroutine BARS,
e) Subroutine SOLVE, and f) Subroutine STORE.

The main subroutine contains the basic organization and the iteration process to calculate the elastic critical load using the modified Southwell plot.

The procedure of calculating the torsional-flexural buckling load for a given structure starts by applying a small value of the load factor and by solving for the displacements the largest component of the deflection can be identified. An infinitesimal value of the load can then be applied at the critical joint in the critical direction in order to start the buckling displacements.

The instability problem is linearized by carrying out a doubly iterative process. At each load level the singularity of the determinant $\left[\bar{K}_{ee.} + \lambda \bar{K}_{gg}\right]$ is checked. At each load level, also, an inner iteration is performed to find out the correct value of the displacement. This operation is carried out by solving repeatedly the second-order equation for the displacements until the percentage difference between two consecutive values of the critical displacement is less than the adopted value for the tolerance. This step is shown in fig. 4.3.

Fig. 4.5. shows the flow chart of the inner iteration technique to calculate the correct value of the critical

displacement Δ_{cr} at a given value of the load factor. The prediction of the critical load factor λ_{cr} using the modified Southwell plot is illustrated by the flow chart in fig. 4.6. The procedure continues until the percentage difference between two consecutive predictions of λ_{cr} becomes less than the tolerance (0.005). A complete listing of the main subroutine, which includes the double iteration process, is given in Appendix A.4.1.

The method used to solve the linear matrix equations is based on making use of the sparse nature of the stiffness matrices and operating on the non-zero elements only. The method has the advantage of preplanning the storage so that the exact size of each submatrix generated during the solution is evaluated and appropriate storage is reserved and addressed before the actual solution starts. The basic theory of the method will now be explained in more detail.

The load-displacement relationship for an elastic structure having n joints can be described by the stiffness equation, $F = K \cdot \delta$. If this equation is expanded it can be rewritten as,

$$\begin{bmatrix} F_1 \\ F_2 \\ \vdots \\ F_n \end{bmatrix} = \begin{bmatrix} K_{11} & K_{12} \ldots K_{1n} \\ K_{21} & K_{22} \ldots K_{2n} \\ \vdots & \vdots \quad \vdots \\ K_{n1} & K_{n2} \ldots K_{nn} \end{bmatrix} \begin{bmatrix} \delta_1 \\ \delta_2 \\ \vdots \\ \delta_n \end{bmatrix} \qquad (4.13)$$

where, the individual K terms are submatrices associated with the n joints of the structure.

For the part of the structure which is shown in fig. 4.7, the submatrix equations of this part are given by,

$$\left[\begin{array}{c} F_b \\ F_c \\ F_d \\ F_e \\ \hline F_t \end{array}\right] = \left[\begin{array}{cccc:c} K_{bb} & & & & K_{bt} \\ & K_{cc} & & & K_{ct} \\ & & K_{dd} & & K_{dt} \\ & & & K_{ee} & K_{et} \\ \hline K_{tb} & K_{tc} & K_{td} & K_{te} & K_{tt} \end{array}\right] \left[\begin{array}{c} \delta_b \\ \delta_c \\ \delta_d \\ \delta_e \\ \hline \delta_t \end{array}\right] \qquad (4.14)$$

where, the K submatrices of the above equation are of a size depending on the number of degrees of freedom of the joints.

Equation 4.14 can be rewritten in a partitioned form as follows,

$$\left[\begin{array}{c} F_a \\ \hline F_t \end{array}\right] = \left[\begin{array}{c:c} K_{aa} & K_{at} \\ \hline K_{ta} & K_{tt} \end{array}\right] \left[\begin{array}{c} \delta_a \\ \hline \delta_t \end{array}\right] \qquad (4.15)$$

By eliminating joint t from the analysis (fig. 4.8), the following relationships are obtained,

$$K^*_{aa} = K_{aa} - K_{at}\ K_{tt}^{-1}\ K_{ta} \qquad (4.16)$$

$$F^*_a = F_a - K_{at}\ K_{tt}^{-1}\ F_t \qquad (4.17)$$

After calculating δ_a, δ_t can be evaluated by substituting for δ_a in eq. 4.15. By repeating the application of eq. 4.16 and 4.17, the number of joints in the analysis reduces until for the last joint the displacement can be calculated from the following equation,

$$\delta_n = K^{*\,-1}_{nn}\ F^*_n \qquad (4.18)$$

The sparse matrix K_{aa} is replaced by the dense matrix K^*_{aa}. As the stiffness matrix is symmetrical, K_{at} is the

transpose of K_{ta} so that it is sufficient to store only one of them. The elimination equations (eq. 4.16 and 4.17) show that it is only necessary to store the two matrices K_{tt}^{-1} and K_{ta} (or their product).

The solution starts with a simple operation to establish a list of the joints at a near optimum order of elimination together with the joint connections including the imaginary connections which will be created during the solution. The order of elimination and the connection list do not include the joints with no degrees of freedom.

The elimination order is performed by selecting, at each stage, to eliminate next the joint, or one of the joints, with the lowest sum of degrees of freedom for the joints to which it is connected, i.e. the joint with the smallest size for its connection matrix, K_{aa}^{*}, in eq. 4.16. The connection list is contained in a two-dimensional integer array,MAP. The number of degrees of freedom for a given joint m is specified in a one-dimensional array JS, while another array, NM, is used to specify the sum of the number of the degrees of freedom of the joints connected to joint m, i.e. the size of K_{aa}^{*} at the current stage of the elimination process. The integer array JDF is used to specify, in a binary form, the active degrees of freedom at each joint. During the preliminary mapping the solution process continues updating the arrays MAP and NM up to the last joint of the structure. A complete list of the subroutine MAPP which includes the procedure of preliminary mapping is given in Appendix A.4.2.

The subroutine SPACE includes the formulation of the elastic stiffness matrix and the transformation matrix given by Jennings and Majid (67). It can be used for first-order analysis of framed structures provided that six degrees of freedom are considered at each joint.

The subroutine BARS includes the formulation of the elastic stiffness and geometric matrices for the second-order and stability analysis of thin-walled structures. It also contains the formulation of the transformation matrix, which

is presented in chapter three, for performing a three-dimensional stability analysis of frames. A complete list of the subroutine BARS is given in Appendix A.4.3.

The stiffness and load matrix elements are stored in two linear arrays, in the working store, namely ADDR, and WADDR respectively. Having completed the mapping operation, the complete stiffness matrix for the structure is built up, member by member, in the form of submatrices which are entered at the appropriate addresses. The solution then proceeds by eliminating the joints one at a time according to the previously arranged elimination list using eq. 4.16 and 4.17. During the elimination process, stiffness terms of the form K_{tt}^{-1} and $K_{at} \cdot K_{tt}^{-1}$ and the modified load submatrices F_a^*, are written up to the backing store. These terms are required later for the evaluation of the joint displacements and member forces.

The joint displacements and member forces are evaluated using eq. 4.17 and 4.18. These calculations are performed using the subroutine SOLVE. A complete list of this subroutine is given in Appendix A.4.4.

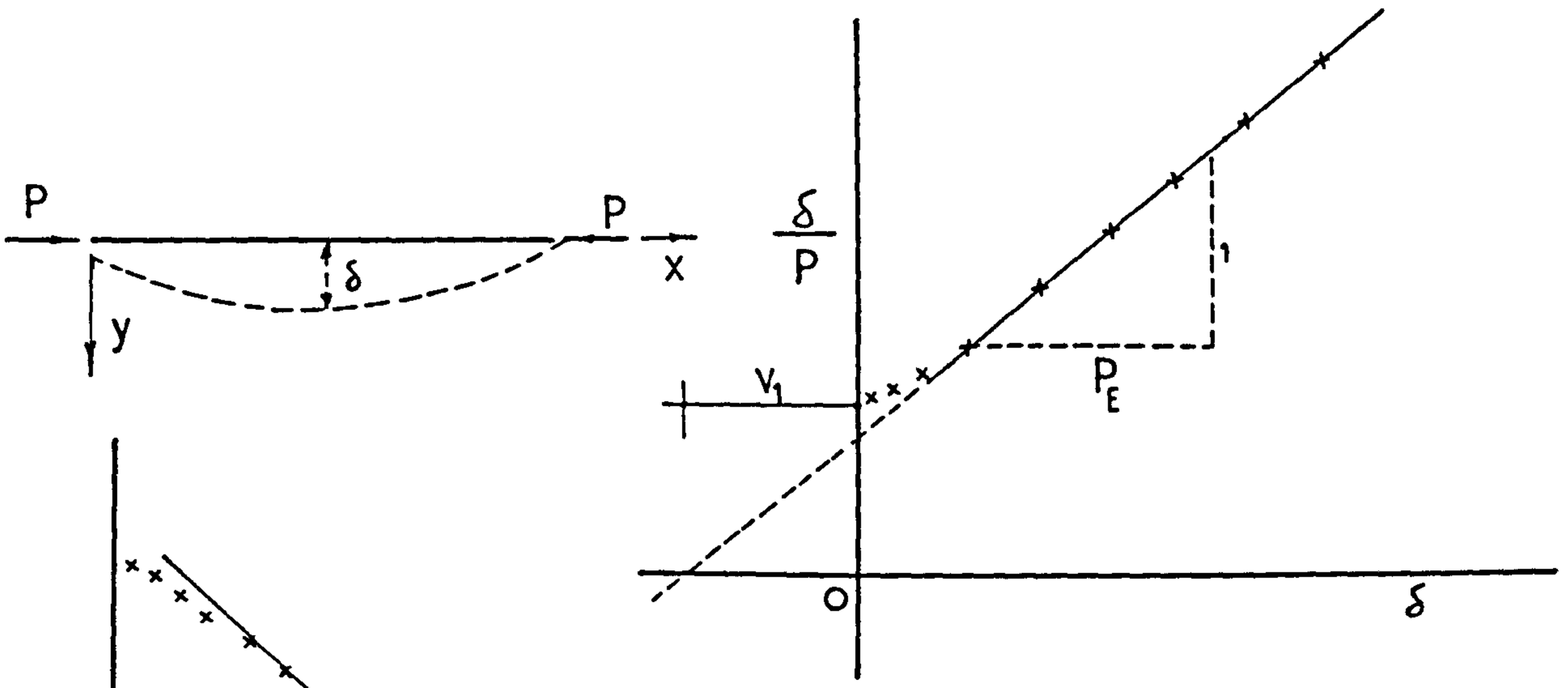

Fig.4.1 Standard Southwell Plot

Fig.4.2 Modified Southwell Plot

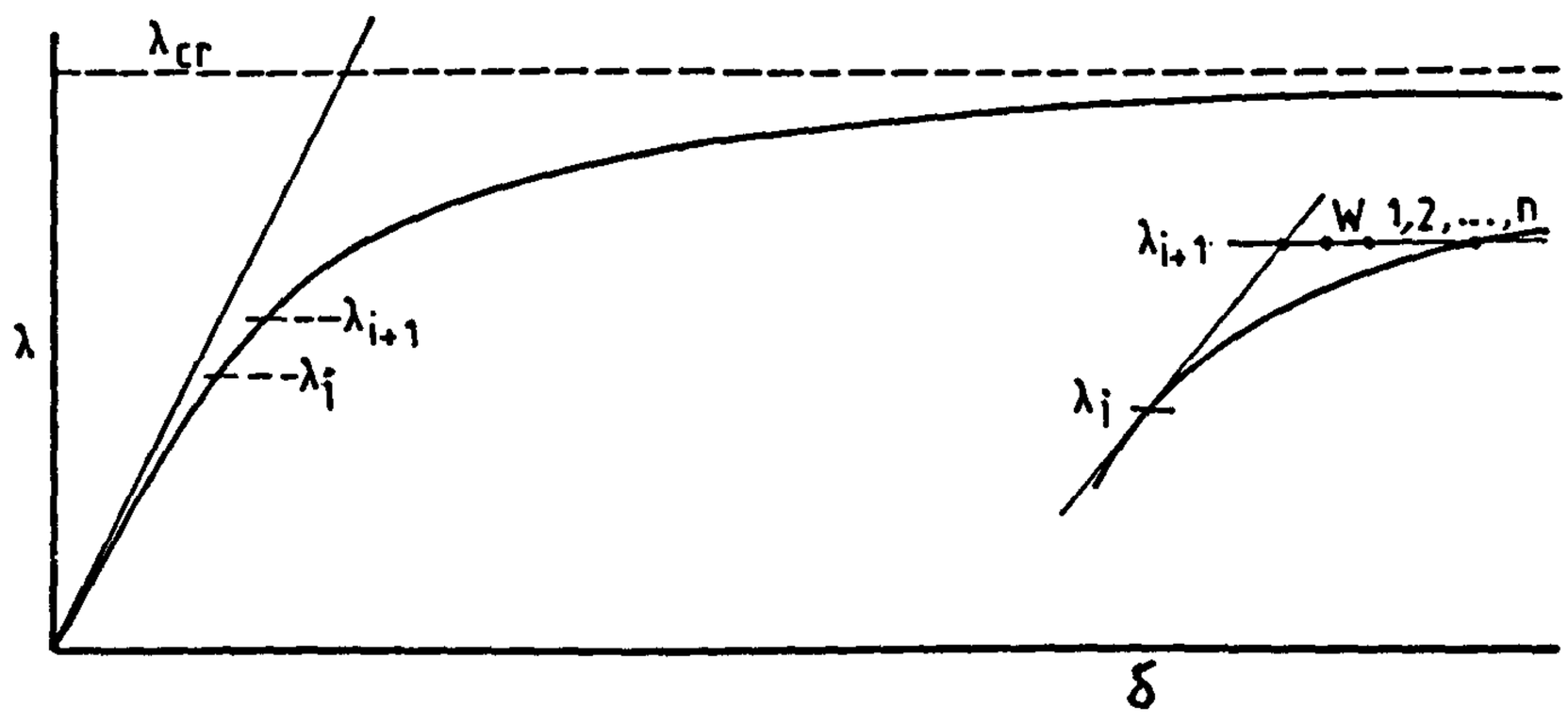

Fig.4.3 The Inner Iteration Procedure

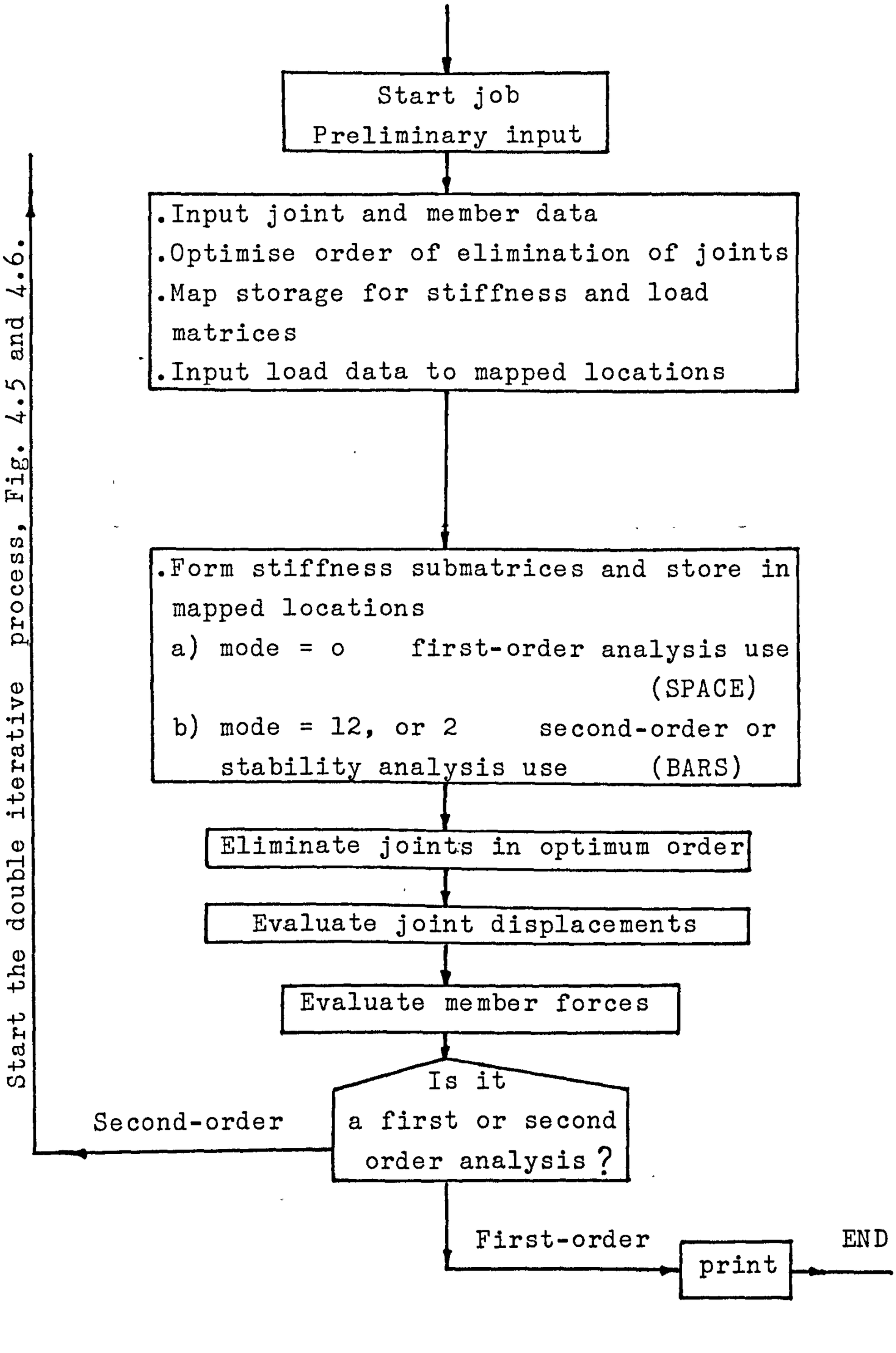

Fig. 4.4. - Flow diagram of the computer program.

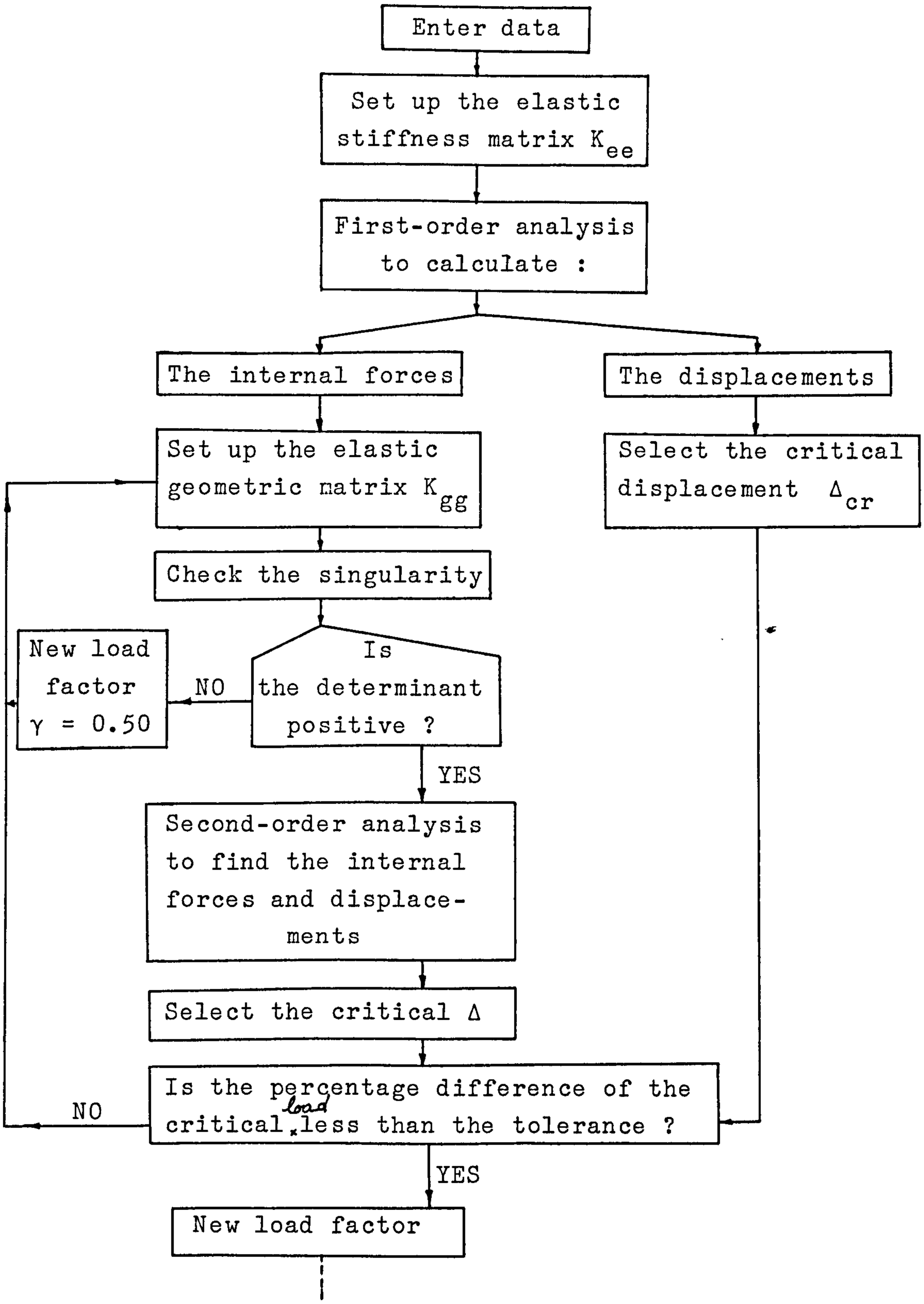

Fig. 4.5. - The flow chart of the computer operations to find the value of Δ_{cr} at a given load factor.

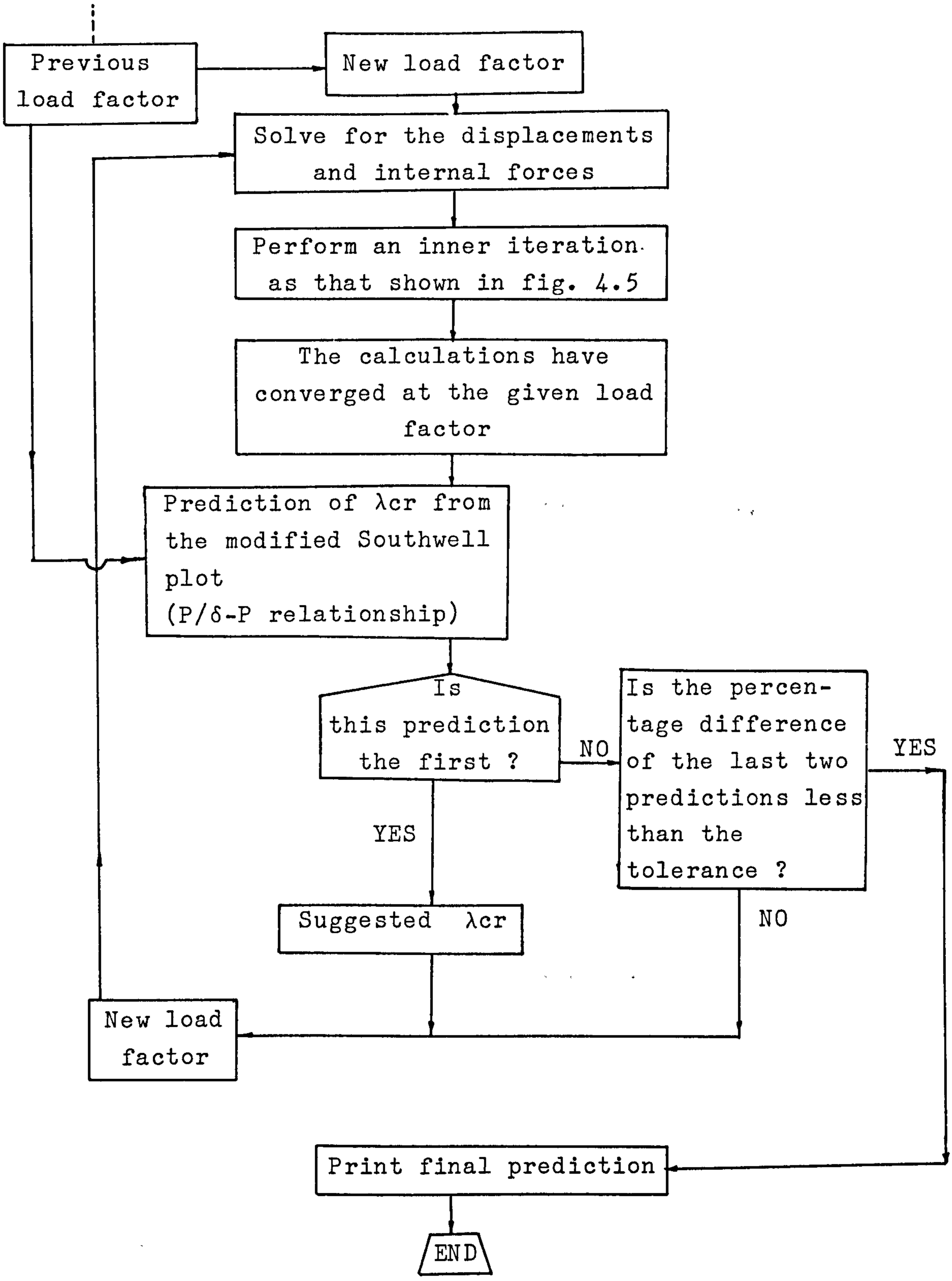

Fig. 4.6. - The flow chart of the prediction of λcr from the modified Southwell plot.

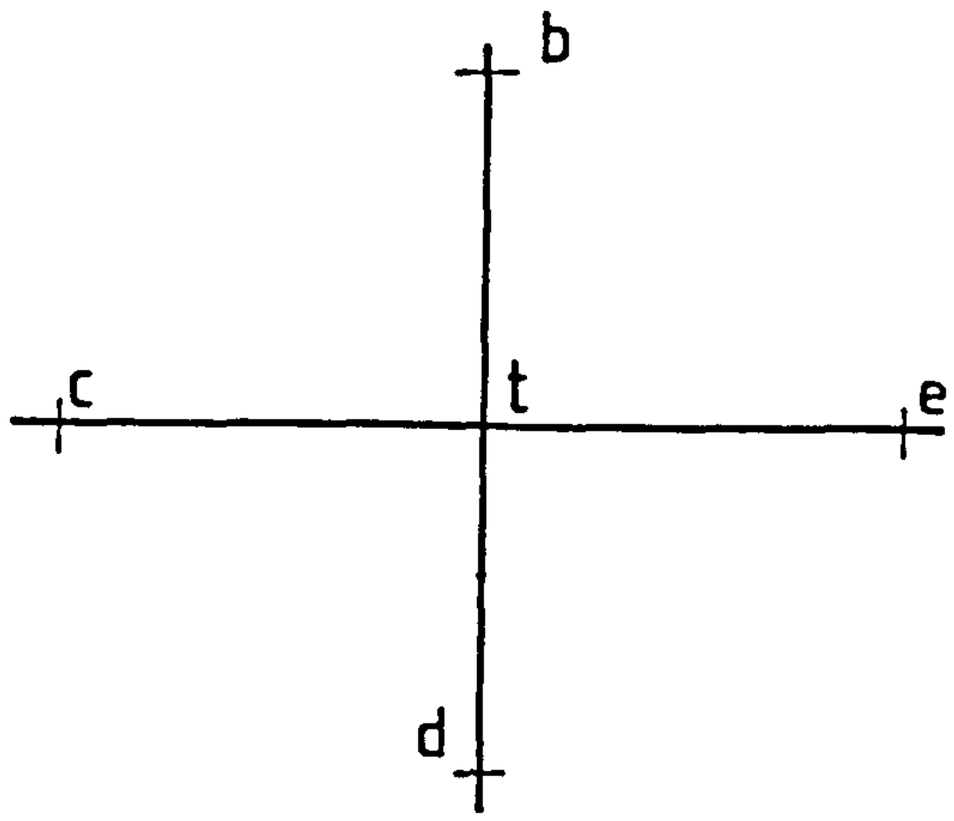

Fig.4.7 Joints Connecting Part Of The Structure

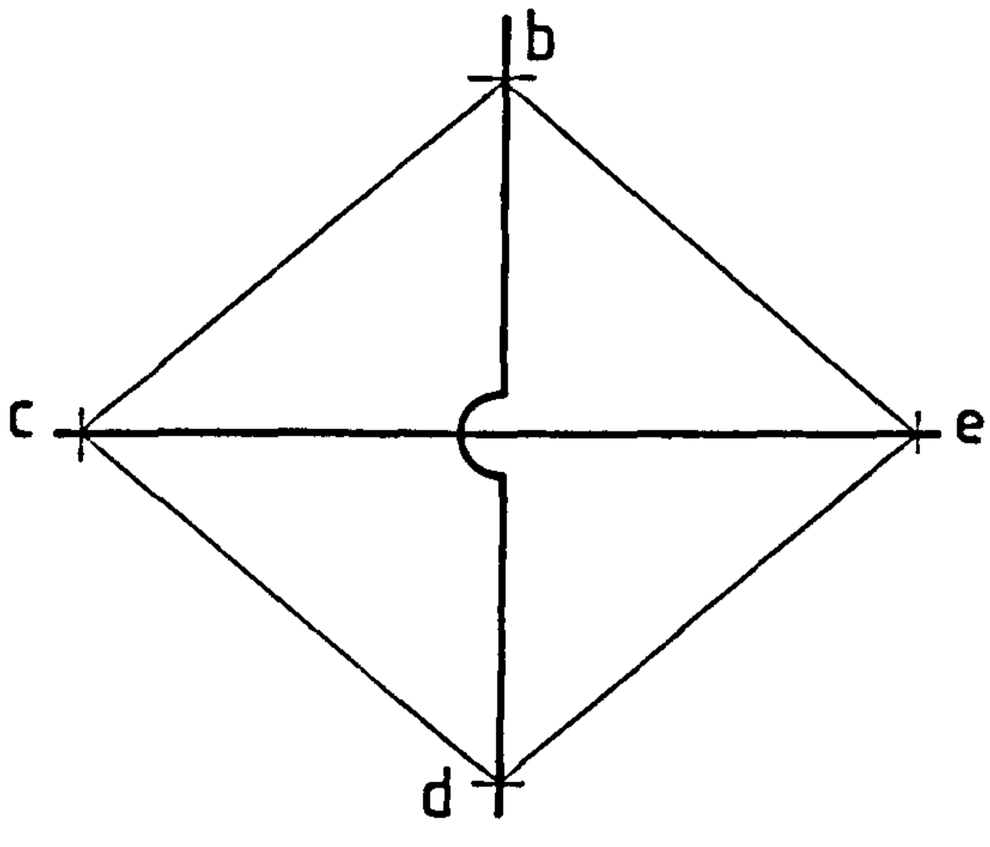

Fig.4.8 Imaginary Connections After Eliminating Joint t

CHAPTER FIVE

Bimoment Distribution in Thin-Walled Members

5.1. INTRODUCTION

The behaviour of thin-walled members subjected to either uniform or nonuniform torsion has become an important topic for investigation in recent years. The growing use of cold-formed light gauge members in the construction of steel frameworks has been the main reason behind the increasing number of studies reported in this subject.

A thin-walled member subjected to torsion has the tendency to warp. However, if such warping is restrainedat any cross section,longitudinal stresses and displacements will be developed in the member. The generalized force corresponding to these longitudinal stresses is called bi-moment. The stresses and deformation arising in a thin-walled member as a result of the bimoments are of great importance and could be a major factor in the design.

The fundamental theory of nonuniform torsion has been established and presented by many authors (1,2,3). Vlasov (1) was the first to introduce the term "bimoment" as the generalized force corresponding to the longitudinal stresses resulting from the nonuniform torsion. However, Vlasov's work was limited to single span beams with relatively simple cases of loading.

Black (79) presented a comprehensive experimental and theoretical study on the evaluation of longitudinal stresses in single-span cold formed channel beams subjected to combined bending and torsion. Black's theoretical analysis was based on simplifying the differential equation of torsion by neglecting the St. Venant torsional rigidity term. In order to examine the validity of the approximate theoretical procedure Black (79) compared the results with the corresponding closed form solutions. He proposed that the true value of the bi-moment can be calculated by multiplying the approximate value

by a correction factor. The correction factor depends on the value of $k\ell$, where $k = \sqrt{\frac{GJ}{EI_\omega}}$, the type of loading and the support conditions of the beam.

In another paper, Black and Semple (80) reported a comprehensive study concerning the behaviour of thin-walled continuous beams under nonuniform torsion. They presented the closed form solution for the case of a three-span continuous beam loaded with central concentrated torque. They also suggested the use of the bimoment-distribution method which is directly analogous to the Hardy-Cross moment distribution technique, and provided expressions for the distribution and carry-over factors. This method was used by Walker (81) in his study of the different techniques of calculating the bimoment distribution of three-span continuous beams. The procedure was later refined and made more general by Khan and Tottenham (82) and applied by Medwadowshi (83) to a number of practical problems.

A completely new approach to the problem of calculating the bimoments of continuous structures has recently been proposed by Davies (84). He suggested that, as the differential equation governing the torsional behaviour of thin-walled members is identical to the differential equation of second-order bending, the same technique of solution can be used. The method has proved to agree very well with the bimoment distribution method for a number of continuous beam problems previously presented by Walker (81), and Khan and Tottenham (82).

This chapter presents a study on the different methods which can be used to calculate the bimoment distribution caused by the nonuniform torsion of thin-walled beams. These methods include the finite element formulation of the general elastic stiffness matrix given in chapter three of this thesis. The validity and accuracy of the finite element formulation of the torsional behaviour has been checked by analysing a number of problems for which highly accurate solutions are available. An experimental study on the longitudinal stresses arising in simply supported Z-beams unrestrained at the supports against

warping and subjected to combined bending and torsion is also presented. The measured longitudinal stresses are compared to the corresponding theoretical values.

5.2. METHODS USED FOR CALCULATING THE BIMOMENTS

5.2.1. Single span beams

5.2.1.1. Closed-form solutions

The differential equation which describes the behaviour of a thin-walled beam subjected to nonuniform torsion is given by,

$$EI_\omega \frac{d^4\theta_x}{dx^4} - GJ \frac{d^2\theta_x}{dx^2} = m \qquad (5.1)$$

in which, m is the intensity of the external torsional couple per unit length.

Equation 5.1 can be rewritten in terms of the bimoment B as follows,

$$\frac{d^2B}{dx^2} - k^2B = -m \qquad (5.2)$$

where, $k = \sqrt{\frac{GJ}{EI_\omega}}$, and the bimoment B is given by,

$$B = EI_\omega \frac{d^2\theta_x}{dx^2} \qquad (5.3)$$

The general solution of eq. 5.2 as given by Vlasov (1) takes the form,

$$B = A_1 \cosh kx + A_2 \sinh kx + B_o \qquad (5.4)$$

in which, A_1 and A_2 are constants of integration depending on the boundary and loading conditions, and B_o is the particular solution.

For a simply supported beam with length ℓ and subjected to central concentrated torque T, the particular solution B_o in eq. 5.4 is equal to zero. Because of the symmetry, the general solution need only be found for half the span. The boundary conditions are,

$$\text{at } x = o : \quad \theta_x = o \ , \quad B = o \tag{5.5.a}$$

$$\text{and} \quad \text{at } x = \frac{\ell}{2} : \quad \frac{d\theta_x}{dx} = o \ , \quad \frac{dB}{dx} = \frac{T}{2} \tag{5.5.b}$$

The general solution of the bimoment B as given by Vlasov (1) is,

$$B = \frac{T \sinh kx}{2K. \cosh k\ell/2} \ , \quad o \leqslant x \leqslant \ell/2 \tag{5.6}$$

The angle of twist θ_x is given by,

$$\theta_x = - \frac{1}{EI_\omega} \frac{T \sinh kx}{2k^3 \cosh k\ell/2} + \frac{T}{2EI_\omega k^2} x \tag{5.7}$$

Similar forms of solution for B and θ_x can be obtained for other cases of loading and end conditions.

5.2.1.2. Simplified solutions

Black (79) suggested that if the torque component $GJ \frac{d^2\theta_x}{dx^2}$ due to St. Venant shear stresses is much smaller than that due to warping bending $EI_\omega \frac{d^4\theta_x}{dx^4}$, eq. 5.1 can be simplified to,

$$EI_\omega \frac{d^4\theta_x}{dx^4} = m \tag{5.8}$$

Equation 5.8 is similar in form to the equation of plane bending which relates the deflection v and the

intensity q_y of the applied load ($EI_z \frac{d^4v}{dx^4} = q_y$). Thus for a simply supported beam subjected to central concentrated torque T, the approximate value of the bimoment B at the middle cross section ($x = \frac{\ell}{2}$) is given by,

$$B_{app.} = \frac{T\ell}{4} \qquad \text{at } x = \frac{\ell}{2} \tag{5.9}$$

The approximate value of θ_x at the middle cross section ($x = \frac{\ell}{2}$) can then be given by,

$$\theta_{x\ app.} = \frac{T\ \ell^3}{48\ EI_\omega} \quad \text{at } x = \frac{\ell}{2} \tag{5.10}$$

The accuracy of the approximate solution depends on the value of $k\ell$ where $k = \sqrt{GJ/EI_\omega}$. The error in the approximate value of the bimoment can be evaluated by considering the ratio between the approximate and accurate values of the bimoment. Thus, for a simple beam with central concentrated torque T, the error is,

$$\frac{B_{app}}{B} = \frac{k\ell\ \cosh\ k\ell/2}{2\sinh\ k\ell/2}\ , \quad \text{at } x = \ell/2 \tag{5.11}$$

Walker (81) suggested that the value $B_{app/B}$ can be considered as a correction factor F to the approximate value of bimoment. He provided a number of graphs for the correction factor F for different values of the non-dimensional beam property $k\ell$. Under any case of torsional loading and boundary conditions, the accurate value of the bimoment at the middle cross section can then be calculated using the following equation,

$$B = F \cdot B_{app} \tag{5.12}$$

Walker (81) presented the graphs of the correction factor F for simply supported beams and fixed end beams subjected to either central concentrated or uniformly distributed torque. Such graphs can be used for design purposes.

5.2.2. Continuous Beams

5.2.2.1. Bimoment-distribution method

This method can be applied in an analogous manner to the well known moment distribution method used for solving plane bending problems. Black and Semple (80) presented the expressions of the carry-over factor and the bimoment distribution factors for equal span continuous beams. Khan and Tottenham (82) established the method in more general steps by defining the following coefficients needed for the calculations:

a) Warping stiffness of the beam ρ : which is defined as the bimoment required at one end of a simple beam to produce a unit warping at this end while the other end being fully fixed against warping.

b) Carry-over factor C : is the ratio between the carry-over bimoment, developed at the fixed far end due to a unit warping at the near end, and the warping stiffness of the beam.

c) Distribution factor D : is the ratio of the bimoment shared by a joining member to the balancing bimoment at the joint.

Khan and Tottenham (82) presented the expressions of ρ and C for three different cases of boundary conditions namely,

1. Beam fully restrained at the far end.
2. Beam with far end restrained against rotation θ_x only.
3. Beam with far end free.

The warping stiffness ρ and the carry-over factor C for each of these three cases are given in Appendix A.5.1.

After calculating both ρ and C for each span of the continuous beam the analysis can then be carried out in a similar manner as for the well known moment distribution method.

5.2.2.2. Analogy with second-order bending technique

This method has been proposed by Davies (84) who suggested that, as the differential equation describing the torsional behaviour is identical to that of the second-order bending, identical techniques of analysis can be used. The governing differential equation of a prismatic beam subjected to bending M_z and axial tension P is given by,

$$- EI_z \frac{d^4v}{dx^4} + P \frac{d^2v}{dx^2} = q_y \qquad (5.13)$$

in which, q_y is the intensity of the acting uniform load in y direction.

Equation 5.13 is similar, in form, to the governing differential equation of torsion (eq. 5.1). Thus the torsional behaviour of the beam can be treated as the second-order behaviour under combined bending and axial load. The solution can be given in the form of the modified stiffness matrix which includes the use of conventional stability functions (84). By replacing the bending terms by their corresponding torsional terms the load-displacement relationship becomes,

$$\begin{bmatrix} T_{w1} \\ B_1 \\ T_{w2} \\ B_2 \end{bmatrix} = \frac{EI_\omega}{\ell} \begin{bmatrix} \frac{1}{\ell^2}\phi_1 & & & \\ \frac{1}{\ell}\phi_2 & \phi_4 & \text{Symmetric} & \\ -\frac{1}{\ell^2}\phi_1 & -\frac{1}{\ell}\phi_2 & \frac{1}{\ell^2}\phi_1 & \\ \frac{1}{\ell}\phi_2 & \phi_3 & -\frac{1}{\ell}\phi_2 & \phi_3 \end{bmatrix} \begin{bmatrix} \theta_{x1} \\ \theta'_{x1} \\ \theta_{x2} \\ \theta'_{x2} \end{bmatrix} \qquad (5.14)$$

where, T_{w1}, T_{w2} are the values of the warping torque at end 1 and 2 of the element 1-2 of the beam respectively and B_1, B_2 are the bimoment values at the two ends respectively.

The functions ϕ_1, ϕ_2, ϕ_3, and ϕ_4 are similar to the stability functions of the second-order bending analysis. These functions are given in Appendix A.5.2.

A second-order plane frame computer program can then be used to carry out the analysis.

5.2.3. Finite element method

The elastic stiffness matrix presented in chapter three of this thesis can be used to analyse thin-walled structures under torsion. In order to examine the validity and accuracy of the finite element solutions of torsional problems, a number of examples, for which highly accurate solutions are available, were analysed using the computer program presented in chapter four of this thesis.

Fig. 5.1 shows the finite element calculations of the correction factors of the maximum bimoment of simply supported beams subjected to central concentrated torque T. The figure also shows the correction factors calculated by Walker (81) using eq. 5.6 as a ratio between the approximate solution (GJ = o) and the formal solution of the bimoment It can be seen that, up to a value of $k\ell$ equal to 4.0, the two-element solution agrees very well with the closed form solution. For values of $k\ell$ bigger than 4.0, the error in the two-element solution increases with the increase of $k\ell$. The four-element solution, however, agrees very well with the closed form solution for all the $k\ell$ values considered in the analysis. The same notations can be drawn from fig. 5.2 for the case of a fixed end beam loaded with central concentrated torque T.

The details of the three-span continuous beam studied by Walker (81) is shown in fig. 5.3. Walker presented three solutions *for* this problem, namely,

a) Approximate solution by neglecting the St. Venant torque component $GJ \frac{d^2\theta_x}{dx^2}$

b) The bimoment distribution method

c) The formal (closed-form) solution.

These solutions, together with the finite element solution, are shown in fig. 5.4. It can be seen that the approximate method gives overestimated and unacceptable values of the bimoment. The bimoment distribution method agree well with the closed form solution of the bimoment values at the interior supports and at mid-span of the beam. The finite element solution is much closer to the formal solution. The error in the finite element solution for the bimoment at mid-span is almost 1.8 per cent, while for the bimoment at the interior support it is almost 1.7 per cent only.

Fig. 5.5 shows the two-span continuous beam with overhanging end which was solved by Khan and Tottenham (82), using the bimoment distribution method. Davies (84) presented another solution to this problem by the analogy with second-order bending technique (eq. 5.14). This problem has also been solved using the finite element computer program presented in chapter four of this thesis. It can be seen that the three solutions are almost identical. The bimoment values along the beam are given in table 5.1. The error in the finite element values is confined to the span which is loaded with uniformly distributed torque, where in the finite element solution the load is replaced by concentrated torques at the joints.

It can be concluded that the finite element formulation of the elastic stiffness matrix can be used to predict with high accuracy the behaviour of beams subjected to torsional loads.

5.3. EXPERIMENTAL STUDY OF COLD FORMED Z-BEAMS SUBJECTED TO COMBINED BENDING AND TORSION

5.3.1. Object

The purpose of the tests described in this section

was to study the behaviour of cold-formed steel Z-beams subjected to combined bending and torsion. A simply supported Z-beam was tested under three different cases of combined loading. Longitudinal stresses were measured at two cross sections of the beam. The test results were compared with the corresponding theoretical stresses.

5.3.2. Test program

Details of the Z-beam cross section are shown in fig. 5.6. The span of the beam was taken equal to 3.0 m. The beam was symmetrically loaded with two equal vertical concentrated loads. The distance between the two loads was equal to 1.10 m. as shown in fig. 5.6.

The test program consisted of a series of three tests as shown in fig. 5.7. During the first test, static loads were applied to the top flange at a distance equal to 2.0 cm from the web (fig. 5.7.a). In the second test the vertical loads were applied to the web at a distance equal to 3.0 cm. above the level of the bottom flange (fig. 5.7.b). During the last test (Test 3) the load was applied to the bottom flange at a distance equal to 2.0 from the web (fig. 5.7.c).

5.3.3. Test rig

The test rig was designed to simulate the following end conditions for the beam ab shown in fig. 5.7:

Translational : u_a is fixed, and u_b is free

v_a, and v_b are fixed

w_a, and w_b are fixed

Rotational : θ_{xa}, and θ_{xb} are fixed

$\psi_a = (\frac{dv}{dx})_a$, and $\psi_b = (\frac{dv}{dx})_b$ are free

$\phi_a = (\frac{dw}{dx})_a$, and $\phi_b = (\frac{dw}{dx})_b$ are free

Warping : χ_1 and χ_2 are free

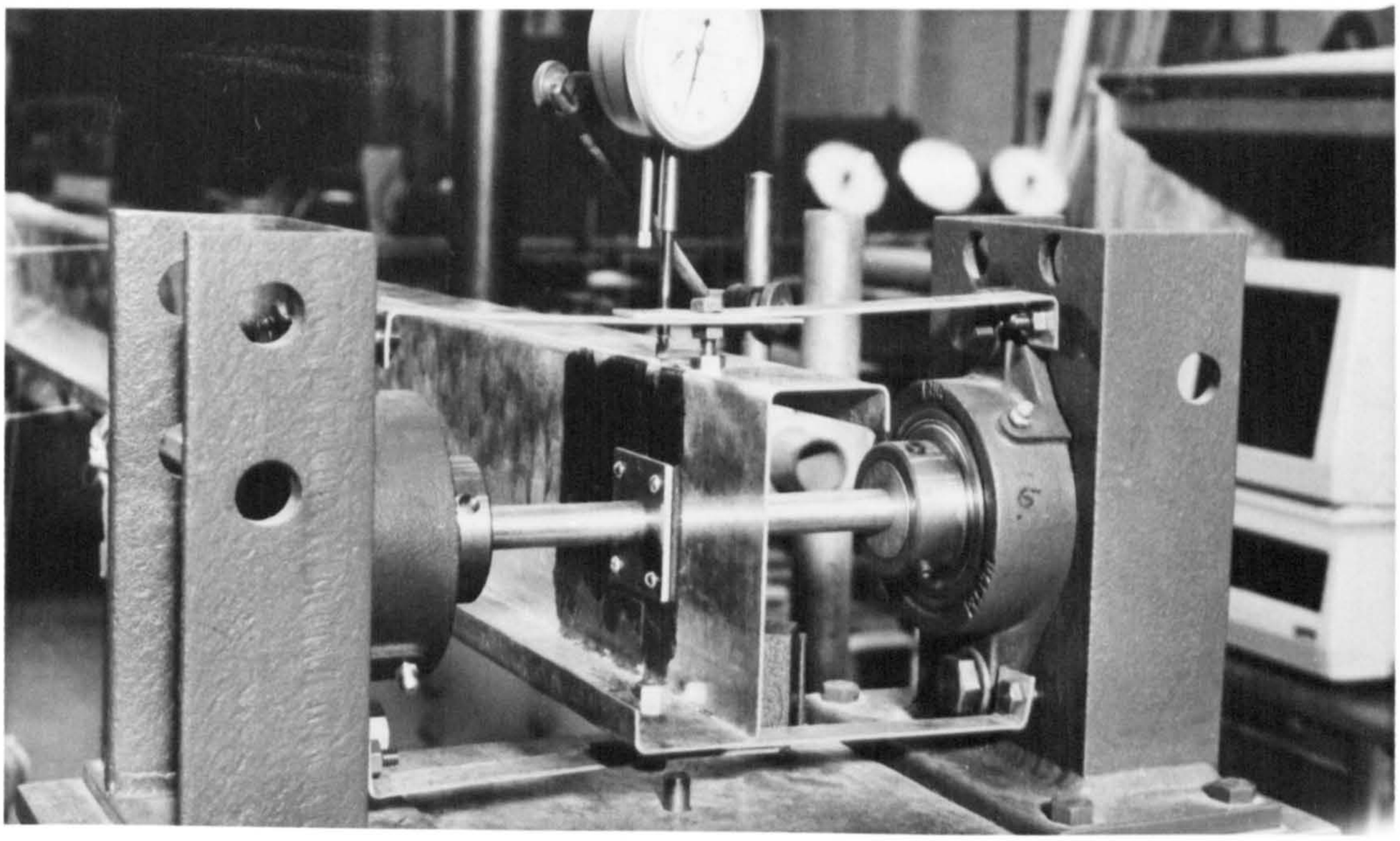

Plate 5.1 Restraining arrangements at the support

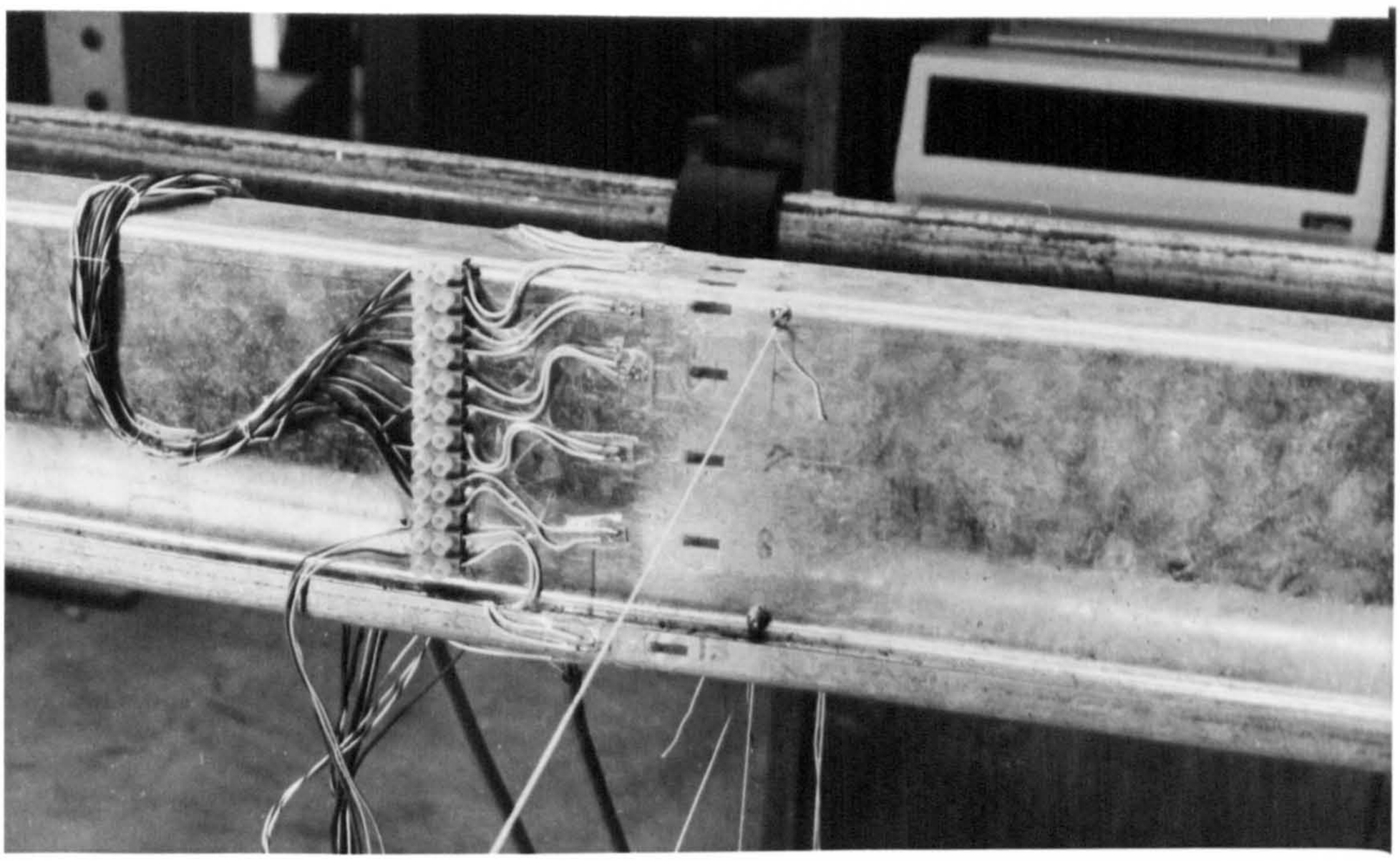

Plate 5.2 Strain gauges at cross-section I-I

The test rig consisted of end support frames as shown in fig. 5.8. In order to achieve translational freedom in x direction or. turntable was mounted on needle roller bearings.

In order to simulate the twisting and warping conditions, light gauge steel 'L' brackets were firmly attached between the upright members of the end support frames and each flange at the theoretical point of zero warping as shown in fig. 5.9. Reinforcement plates were bolted to each side of the web at each support in order to prevent the buckling of the web. The dimensions of these plates are shown in fig. 5.10. The restraining arrangements at the support are shown in plate 5.1.

In each of the first and third tests, the static loads were applied to the loaded flange by means of steel hangers passing through holes in the flange. In the second test, each hanger was passing through a hole in a bracket connected to the bottom of the web.

5.3.4. Instrumentation

In order to measure the longitudinal strains caused by the combined bending and torsion,two cross sections of the beam were provided with electrical resistance strain gauges. The locations of the two gauged cross-sections are shown in fig. 5.11.a. The locations of the strain gauges along the two cross-sections are shown in fig. 5.11.b and 5.11.c. Each cross-section was provided with 13 strain gauges; five were attached to the web, three for each flange, and one per lip. The strain gauges were connected to a Solartron Orion Delta data logger (plate 5.4). Each strain gauge formed the active arm of a wheatstone bridge while the other three arms were built into the logger. The measured strains were printed at each load increment.

5.3.5. Test results

Static loads were applied to the beam in ten increments 4.0 kg/hanger at each increment up to a load of 40.0 kg per

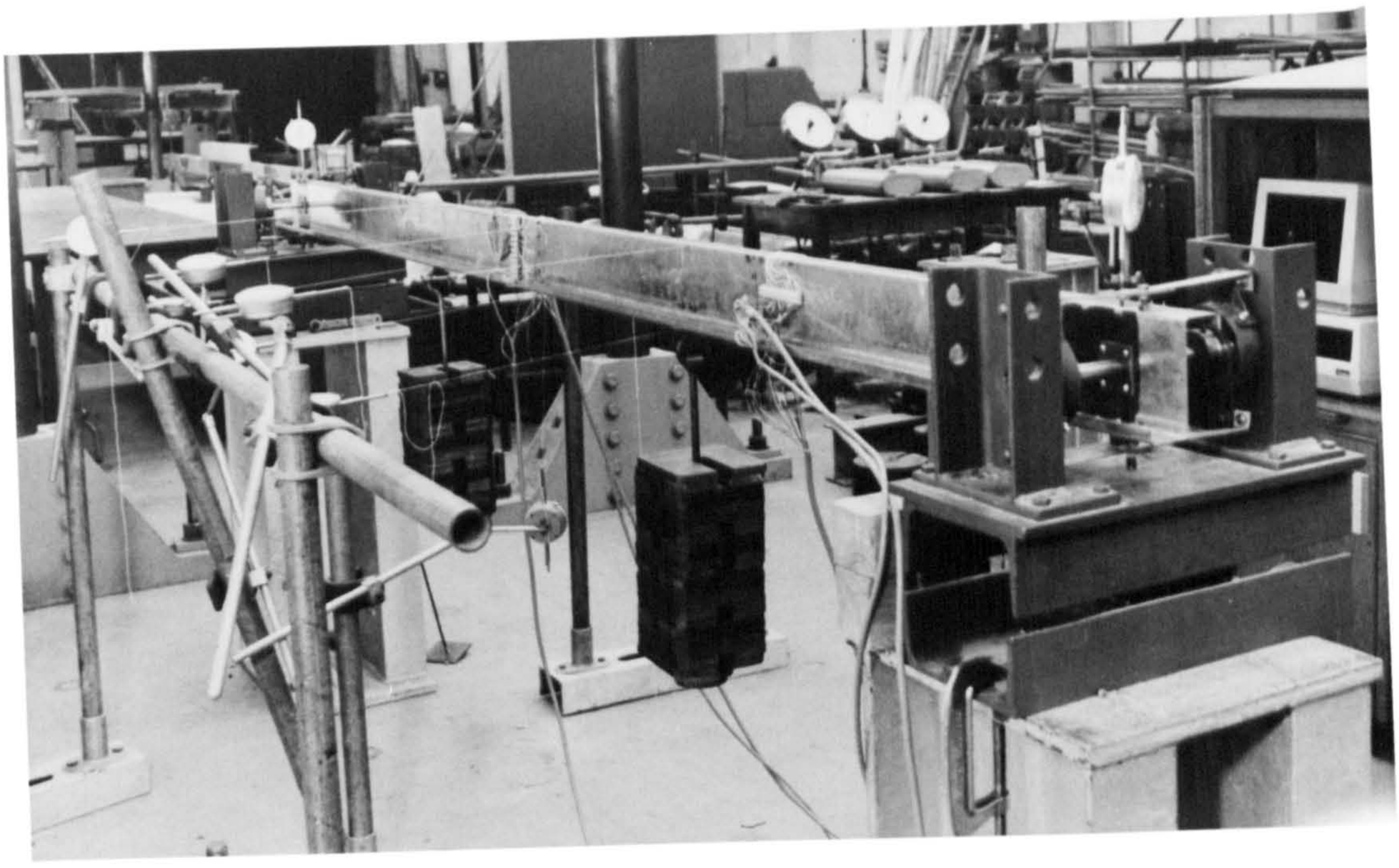

Plate 5.3 Loading of test 3

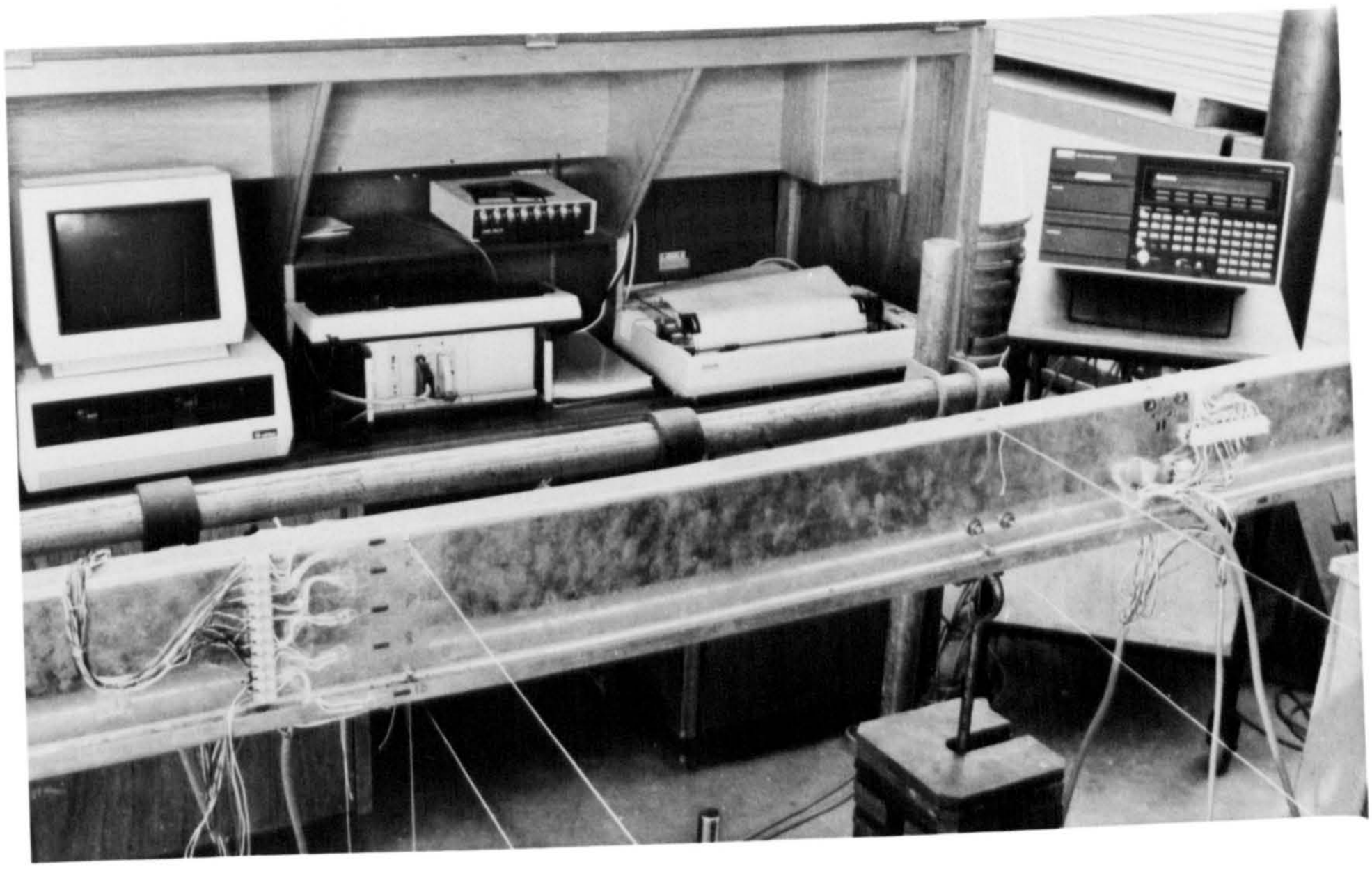

Plate 5.4 Longitudinal strain measurements during test 3

hanger. The load was kept at such a low value in order to avoid high geometric nonlinearity.

Fig. 5.12 shows the increase in the maximum compressive strain in the top flange, with the increase of the applied load. It can be seen that the most critical case is the first case of loading when the top flange is loaded (Test 1). The load-strain relationship of test 2 shows that the nonlinearity starts at a very low load level. In the third test where the load was applied to the bottom flange, the strain-load relationship is almost linear. In this case the torque caused by the eccentricity of the applied load works against the natural twist of the cross section, due to the load component in the direction of the major principal axis.

The value of E, the modulus of elasticity, and μ, Poisson's ratio, found for this beam were 190 kN/mm^2 and 0.30 respectively. The theoretical values of the longitudinal stresses were calculated using the equation given by Vlasov (1) for the combined bending and bimoment (eq. 3.10). The bending moment and the bimoment value were calculated using the finite element computer program presented in chapter four of this thesis. Two types of analysis have been considered, namely, a) linear analysis, and b) second-order analysis.

Fig. 5.13 shows the longitudinal strains of the cross section 1-1 of the beam under acting dead weight equal to 40.0 kg per each of the two hangers. It can be seen that the general level of agreement between the theoretical values of the longitudinal strain calculated from a second-order analysis and the corresponding experimental values, is very good. Furthermore, the linear analysis (first order) leads to inaccurate values of the strain even at such low load level.

Fig. 5.14 shows the longitudinal strains of cross-section 2-2 of the beam. Excellent agreement again is found between the theoretical longitudinal strains (from second-order calculations) and the corresponding measured values.

It can be concluded that the finite element method gives highly accurate predictions of the bimoments for this type of problems. Nevertheless, the accuracy of a second-order analysis of Z-beams subjected to combined bending and torsion is still questionable. The validity of the small-displacement theory which has been considered in the derivation of the finite element matrices will be discussed in chapter seven of this thesis. The effect of high geometric nonlinearity has been avoided here by keeping the maximum value of the applied load very low (40.0 kg/hanger).

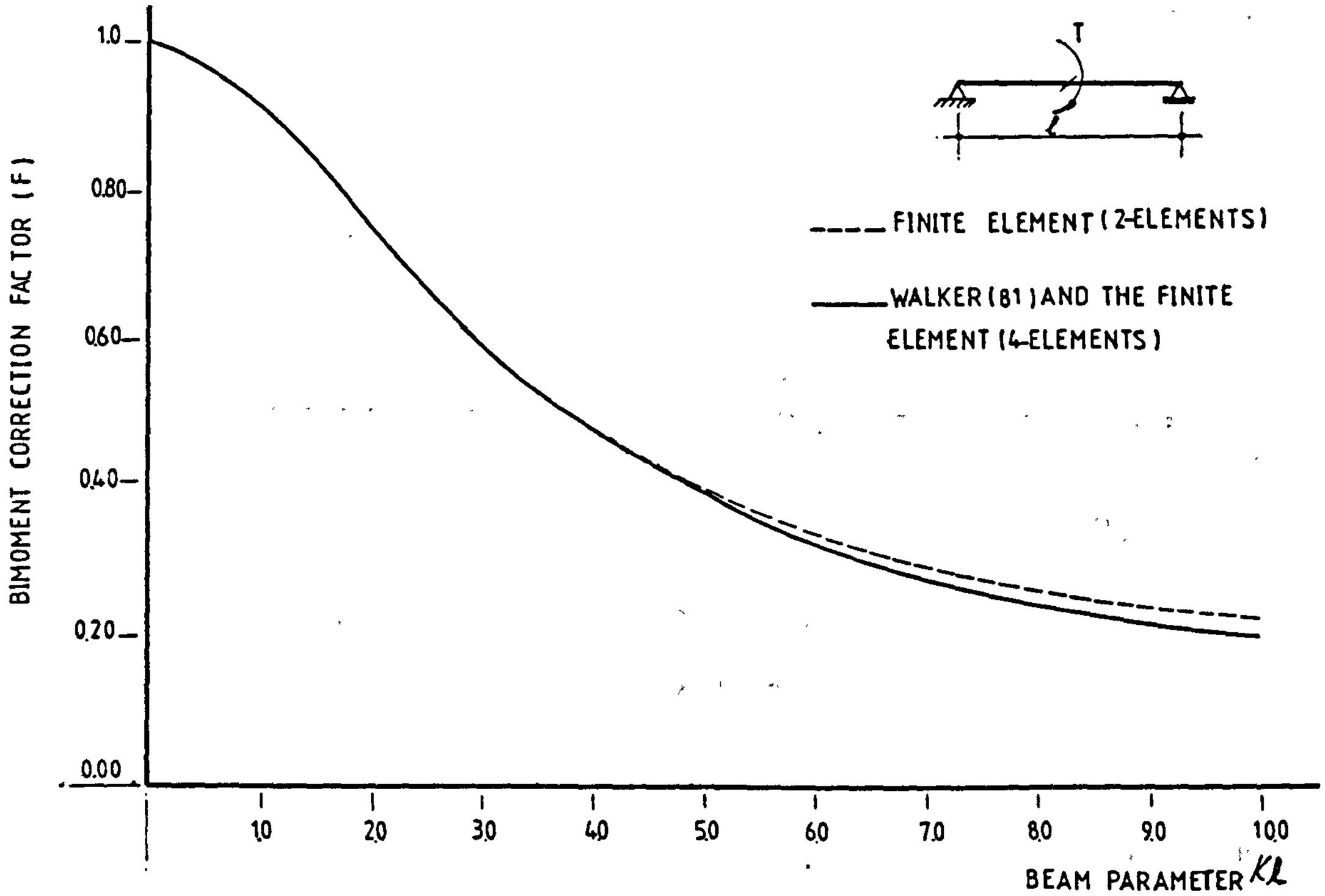

Fig. 5.1 Correction Factors F For Simply Supported Beams Subjected to Central Concentrated Torque

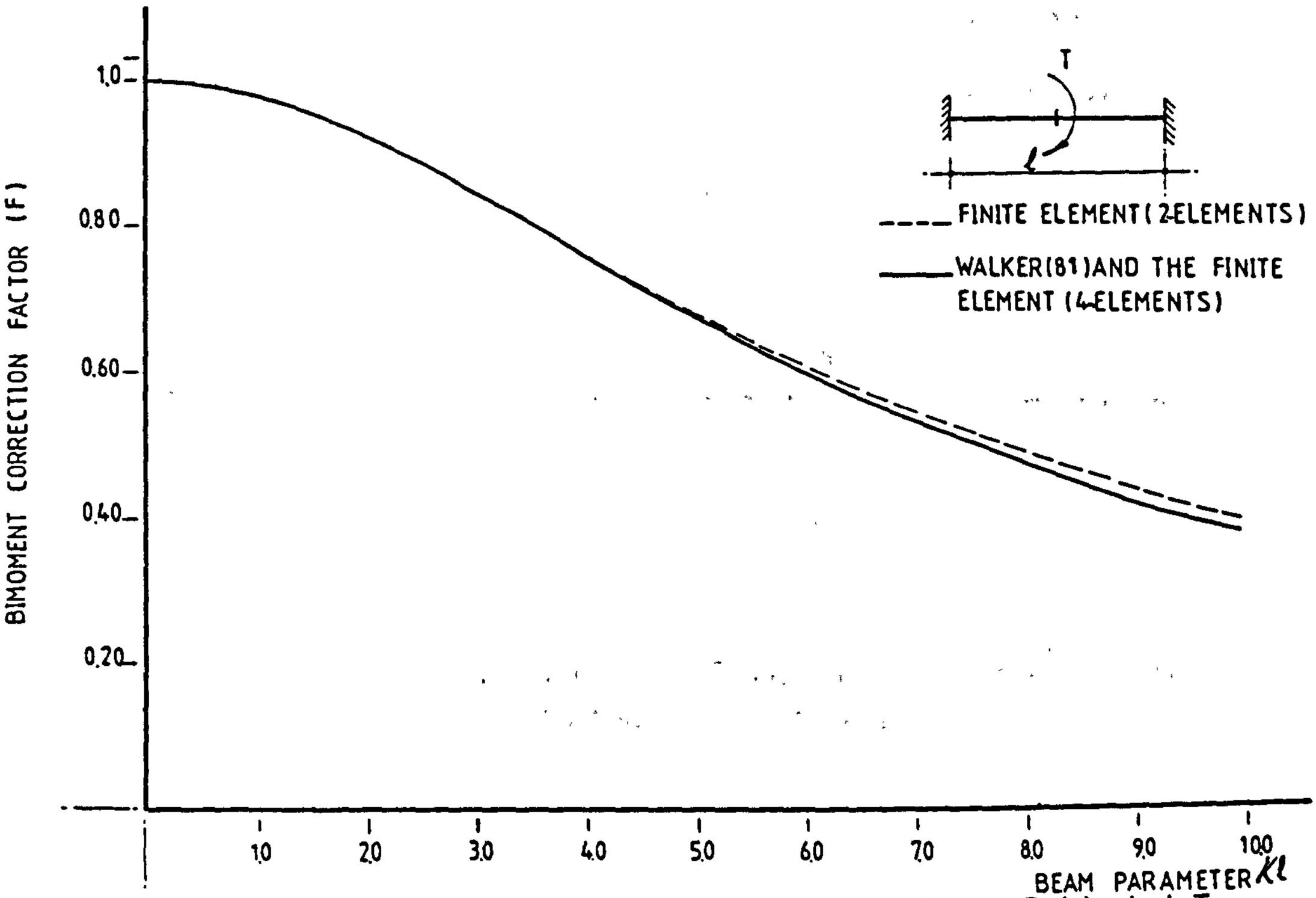

Fig 5.2 Correction Factors F For Fixed End Beams Subjected To Central Concentrated Torque

DIMS IN MM

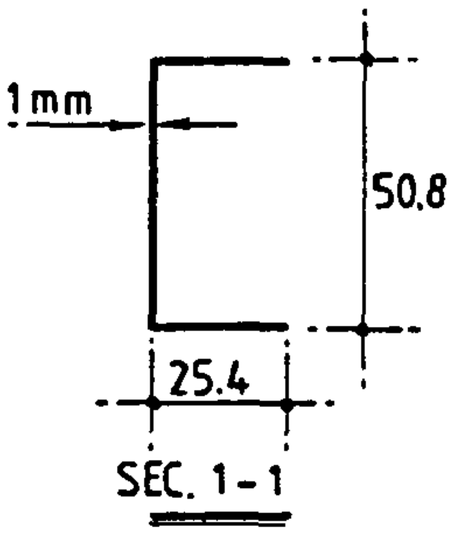

$I_\omega = 3.14 \times 10^6$ mm^6
$J = 35.46$ mm^4
$K = 0.0021$ mm^{-1}

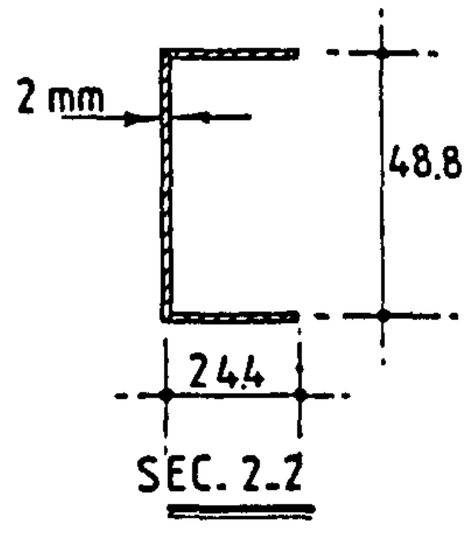

$I_\omega = 5.10 \times 10^6$ mm^6
$J = 273$ mm^4
$K = 0.0046$ mm^{-1}

$E = 200.0$ KN/mm^2 $G = 80.0$ KN/mm^2

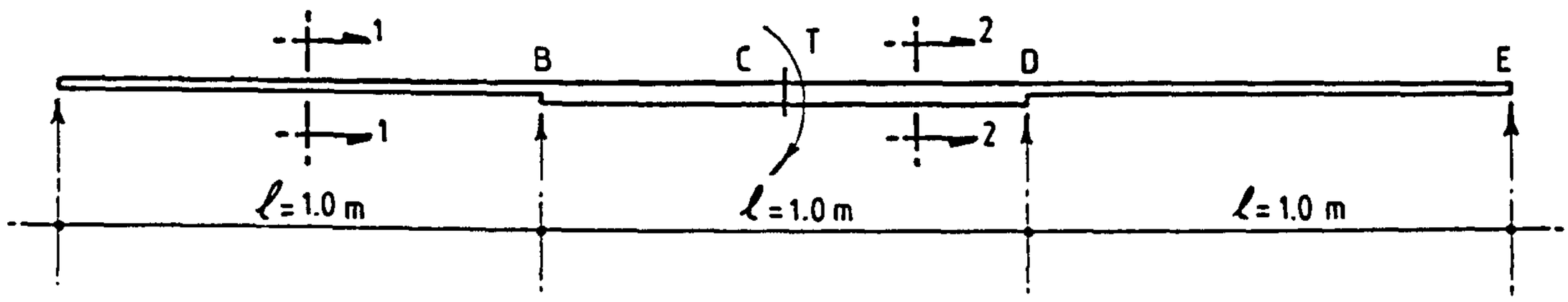

Fig.5.3 The Three-Span Continuous Beam Solved By Walker (81)

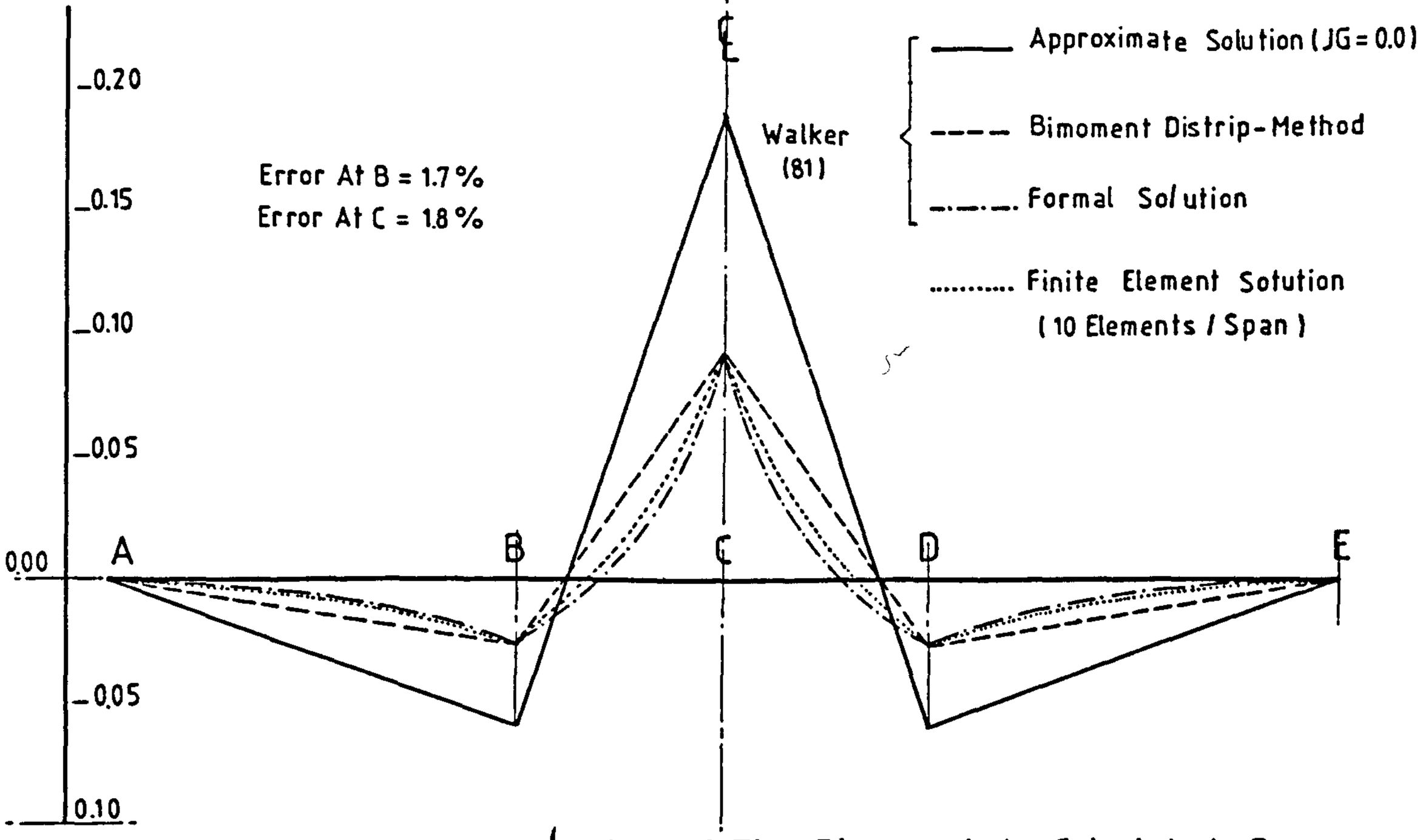

Fig.5.4 The Distribution Of The Bimoment As Calculated By Walker (81) And By The Finite Element Method

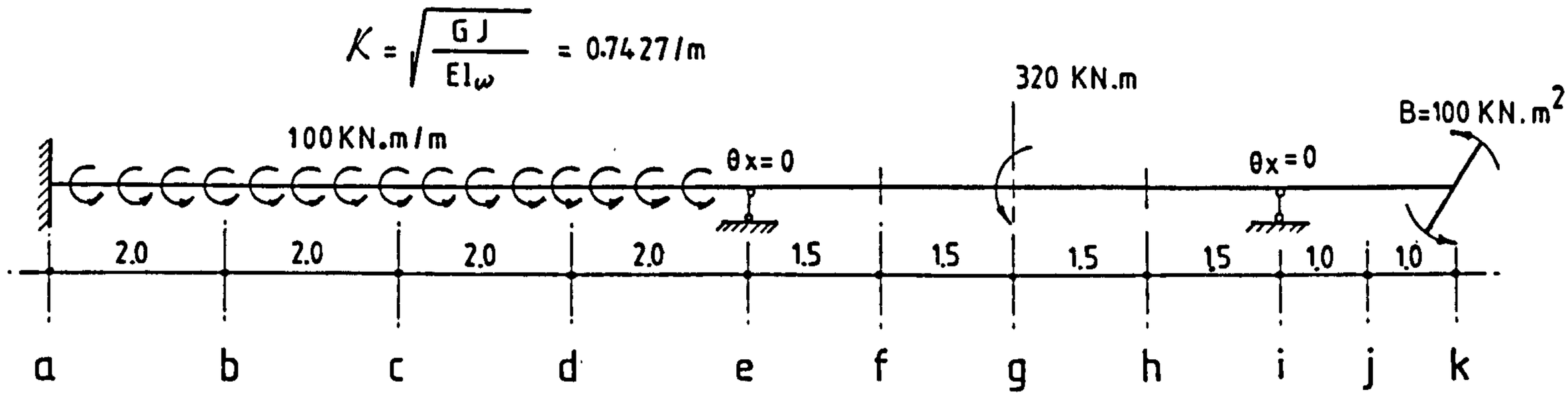

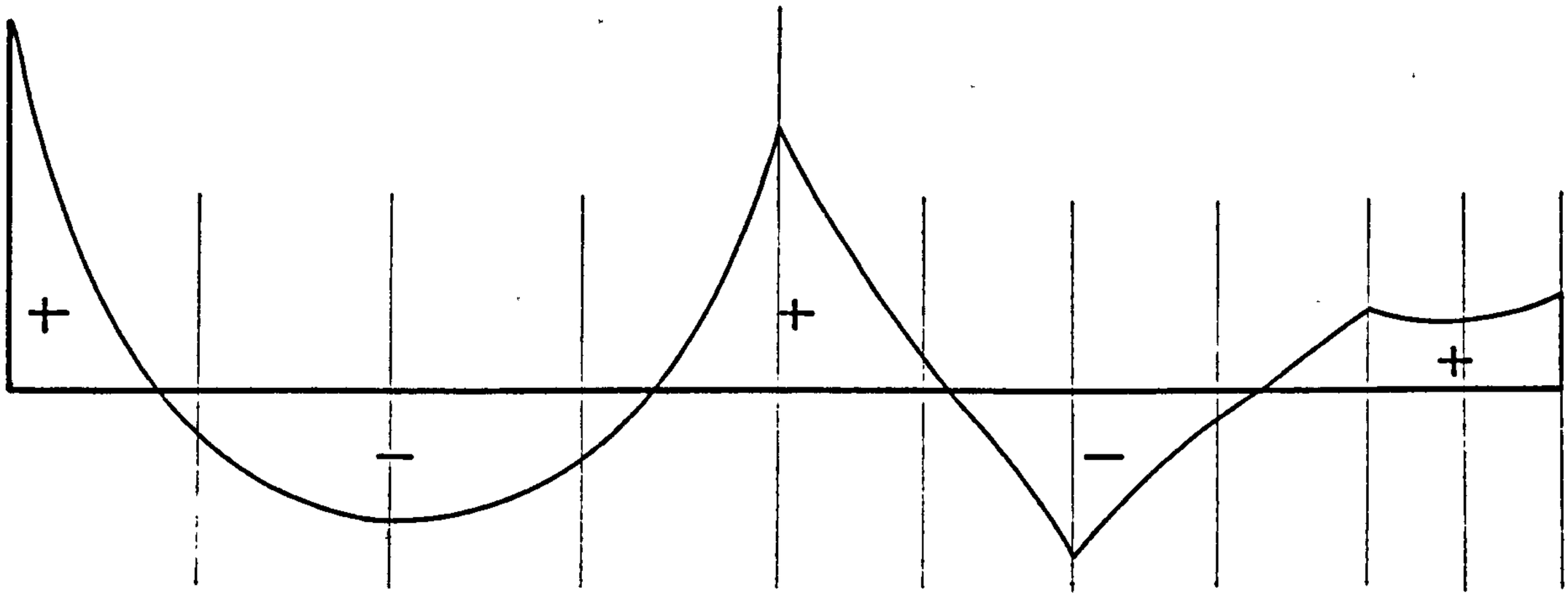

Fig.55 Bimoment Diagram Calculated By Three Methods Of Analysis,Namely, (a) The Bimoment Distribution (82),The Analogy With Second-Order Bending (84), And The Finite Element

SECTION / METHOD	a	b	c	d	e	f	g	h	i	j	k
Khan / Tottenham (82)	376.0	-48.9	-129.2	-70.0	279.4	32.0	-172.2	-25.6	85.4	71.7	100.0
Davies (84)	375.9	-50.1	-129.2	-70.8	279.5	32.0	-171.6	-25.5	85.5	72.0	100.0
Finite Element	383.6	-52.6	-131.4	-72.6	278.7	31.7	-171.7	-25.5	85.6	72.0	100.0

Table 5.1 Bimoment Values Of The Beam Shown Fig. 5.5

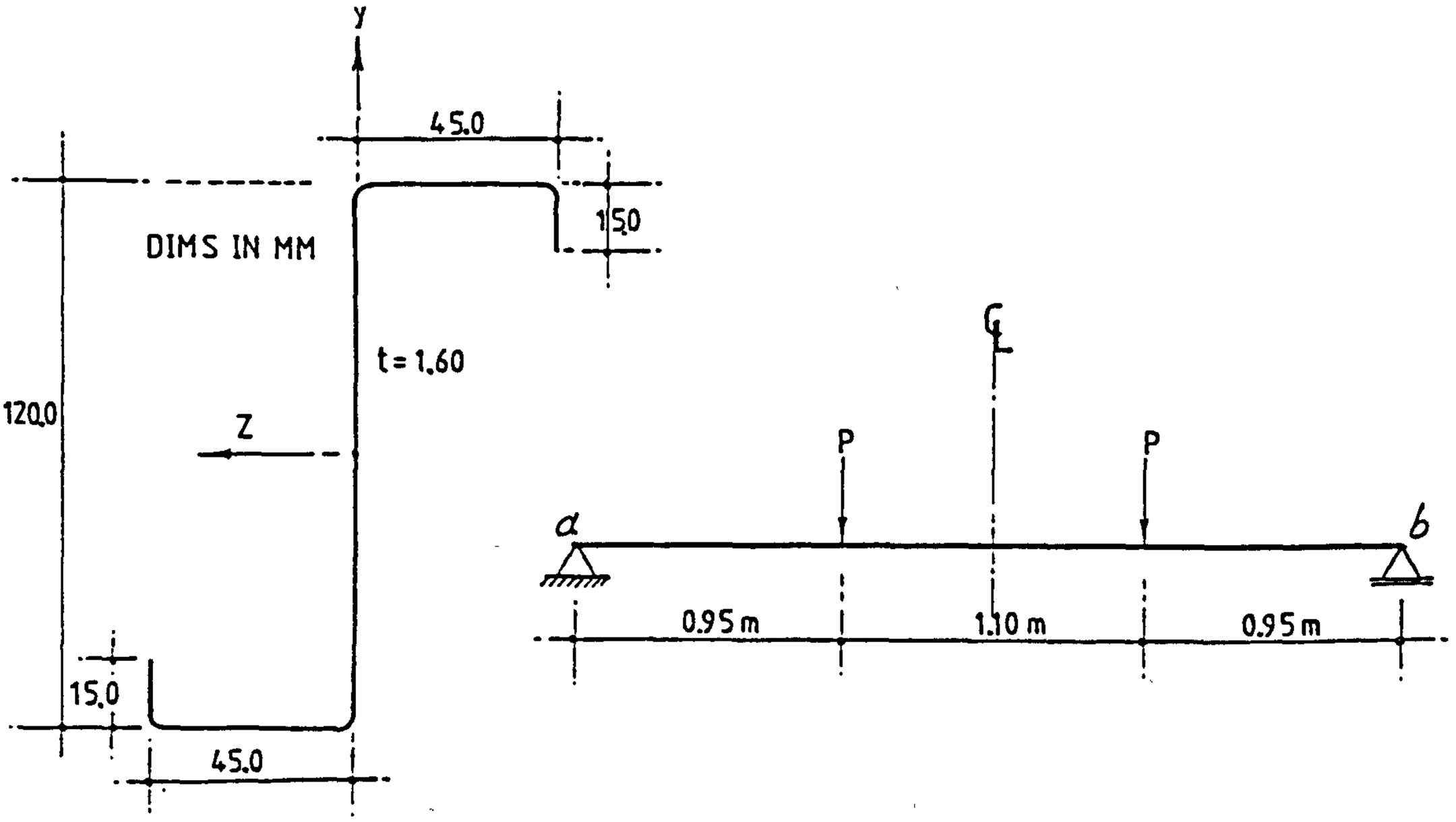

Fig.5.6 The Tested Beam And Its Cross Section

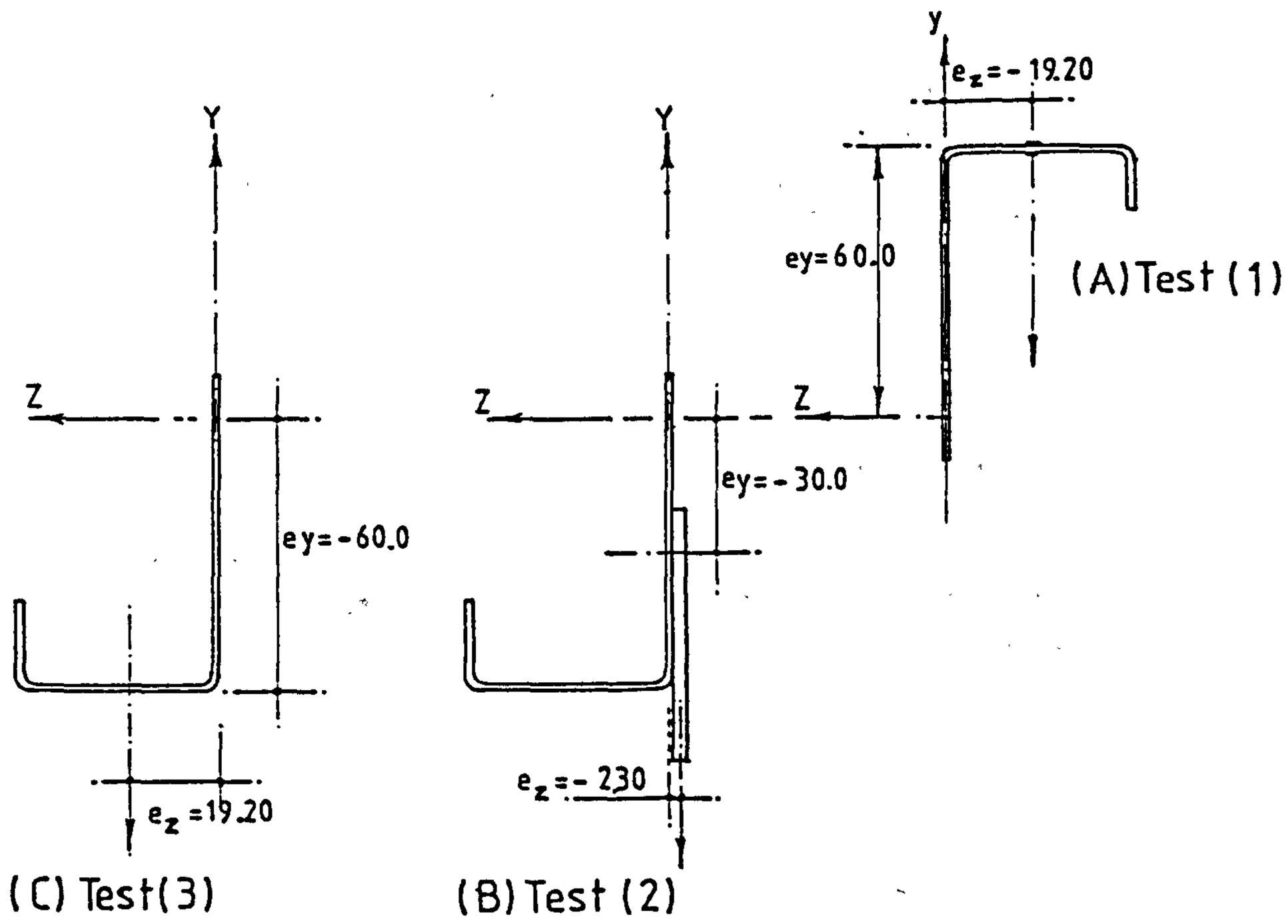

Fig.5.7 Positions Of The Applied Loads
In The Three Tests

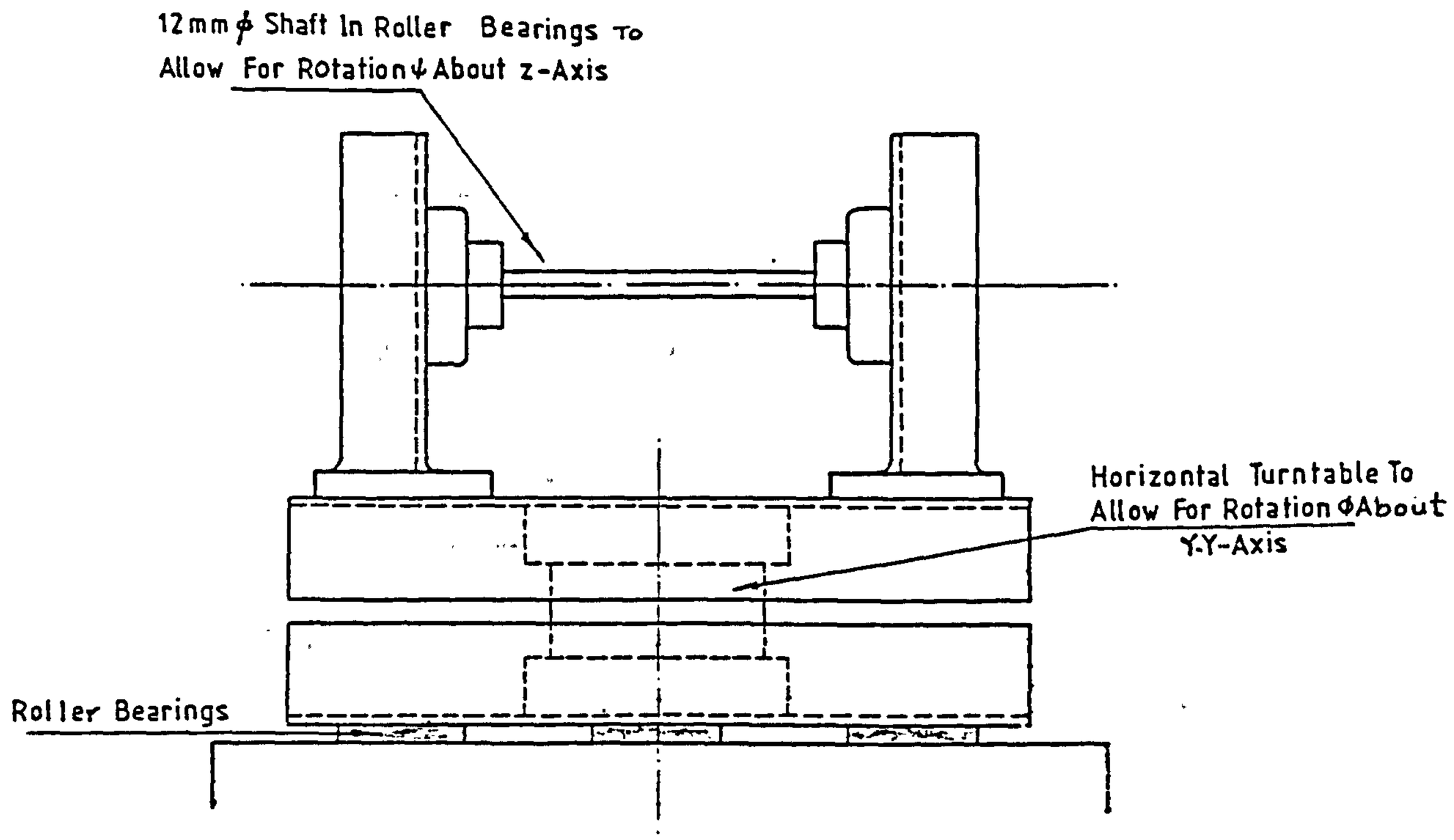

Fig.5.8 The End Support's Frame

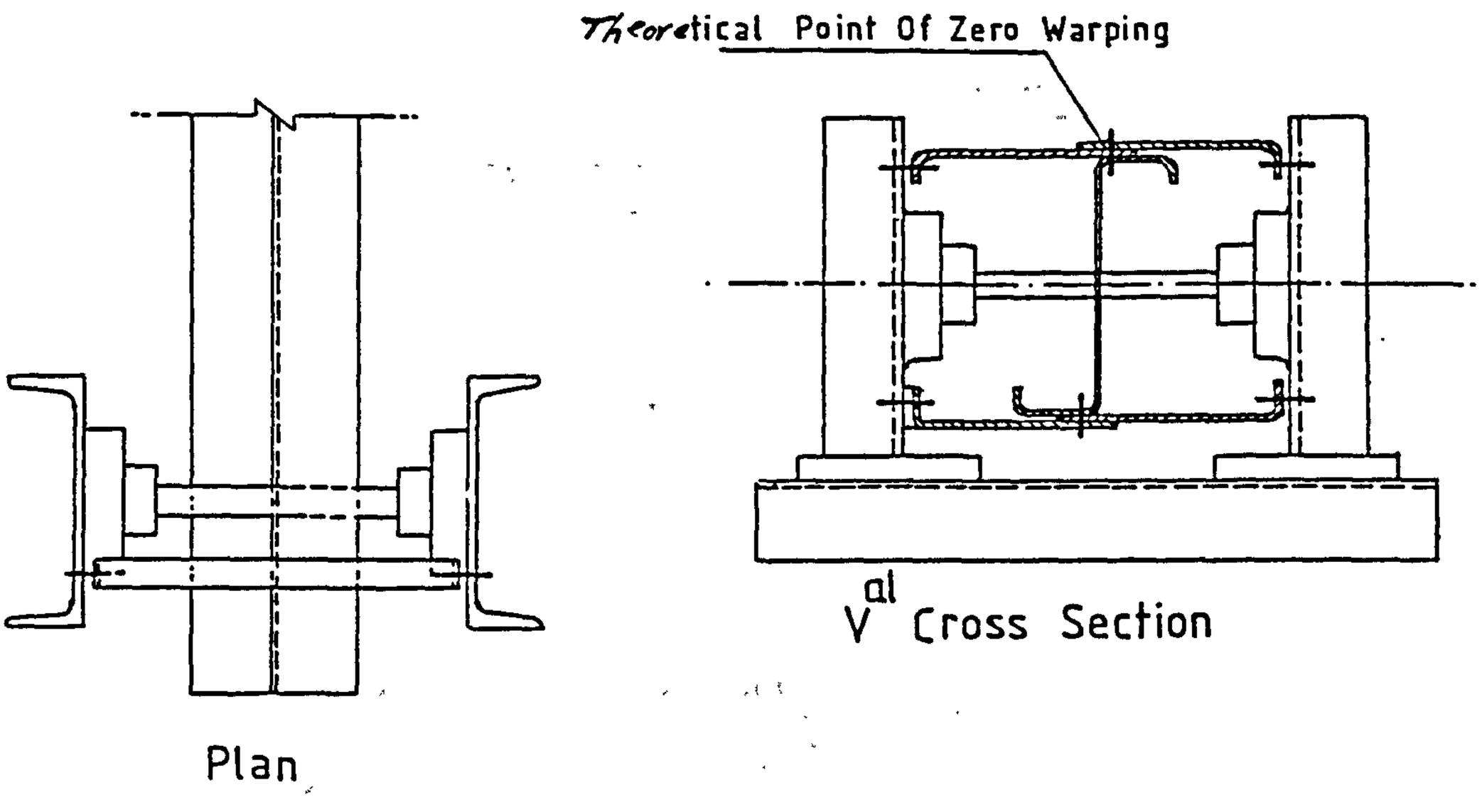

Fig.5.9 The Light Gauge Steel (L) Brackets Used To Simulate
The Torsional And Warping Conditions

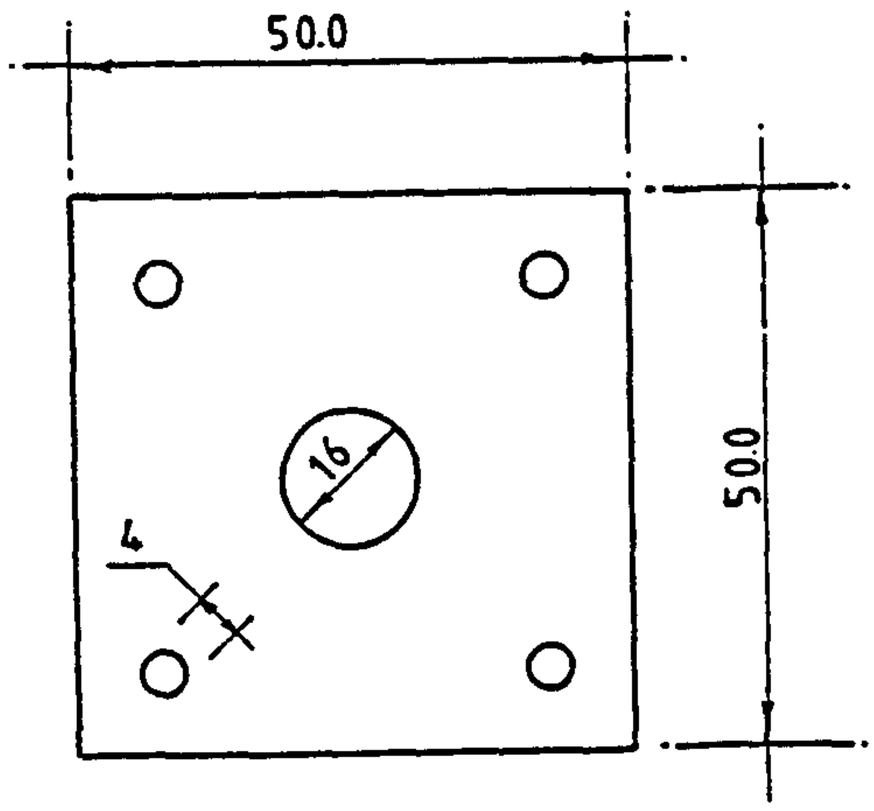

Fig.5.10 The Dimensions Of The Reinforcement Plate

DIMS IN MM

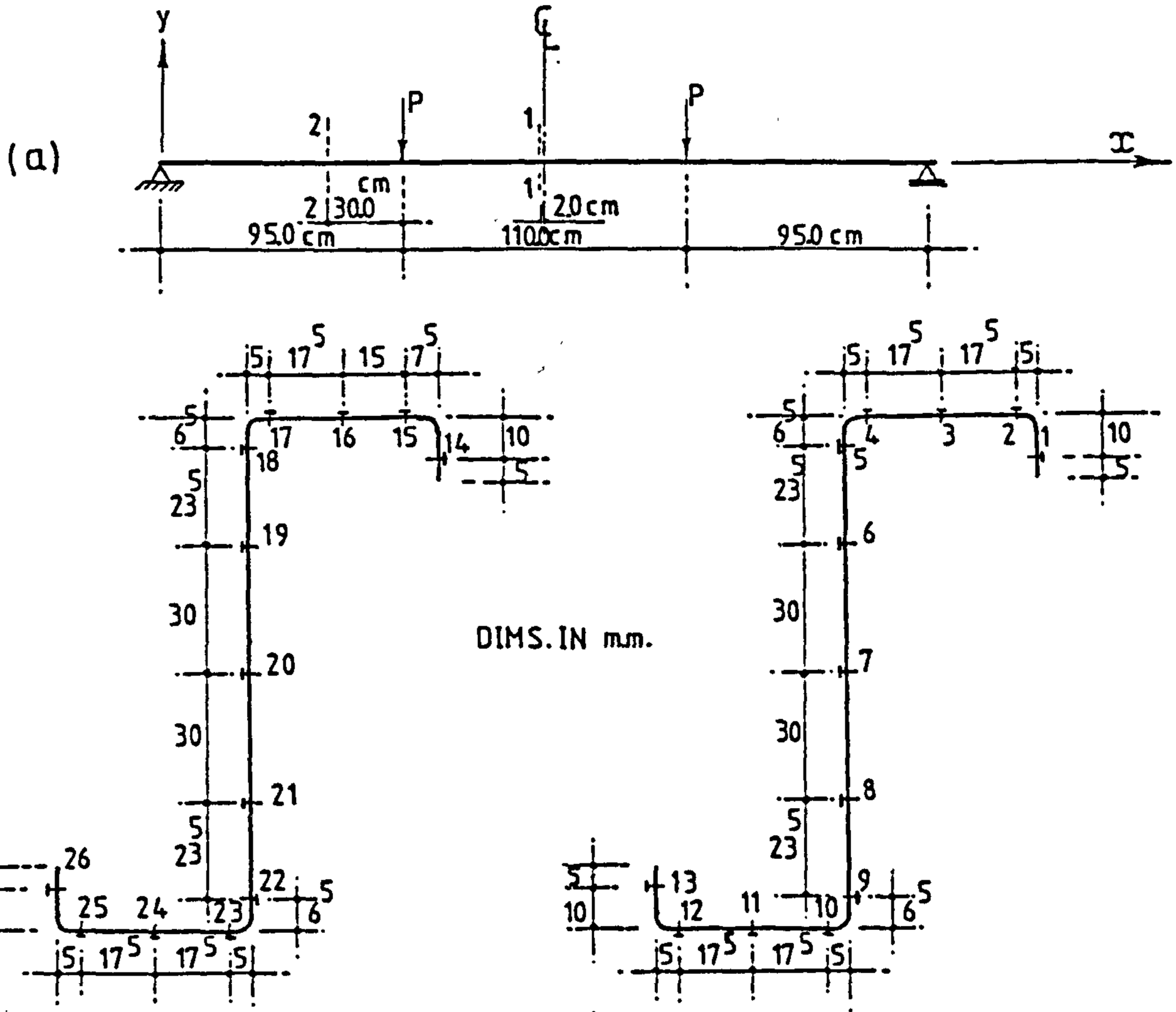

FIg.5.11 The Positions Of The Strain Gauges For Sec.1_1 And 2_2

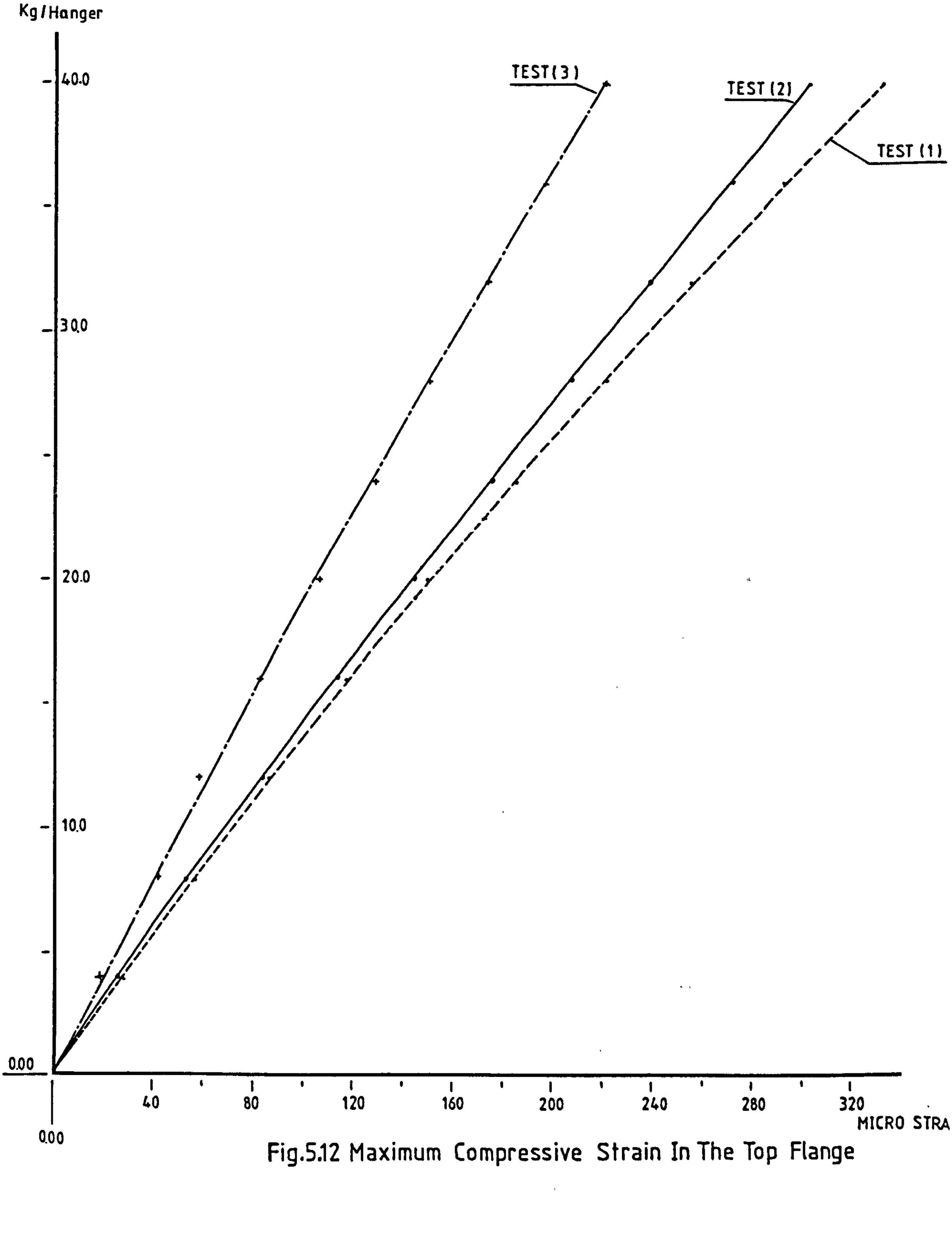

Fig.5.12 Maximum Compressive Strain In The Top Flange

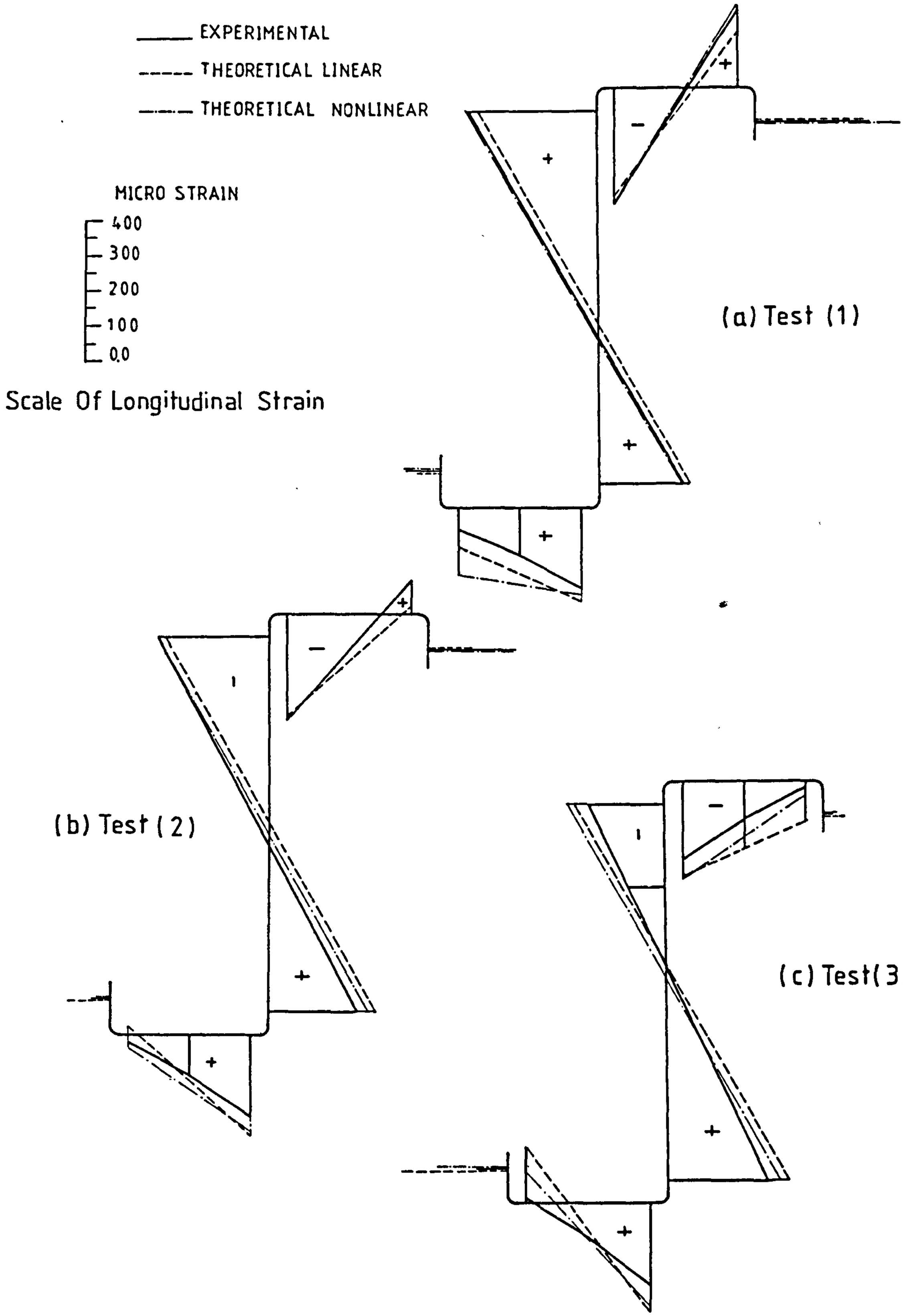

Fig.5.13 Longitudinal Strains At Cross Section 1_1
Under Static Load = 40 Kg/Hanger

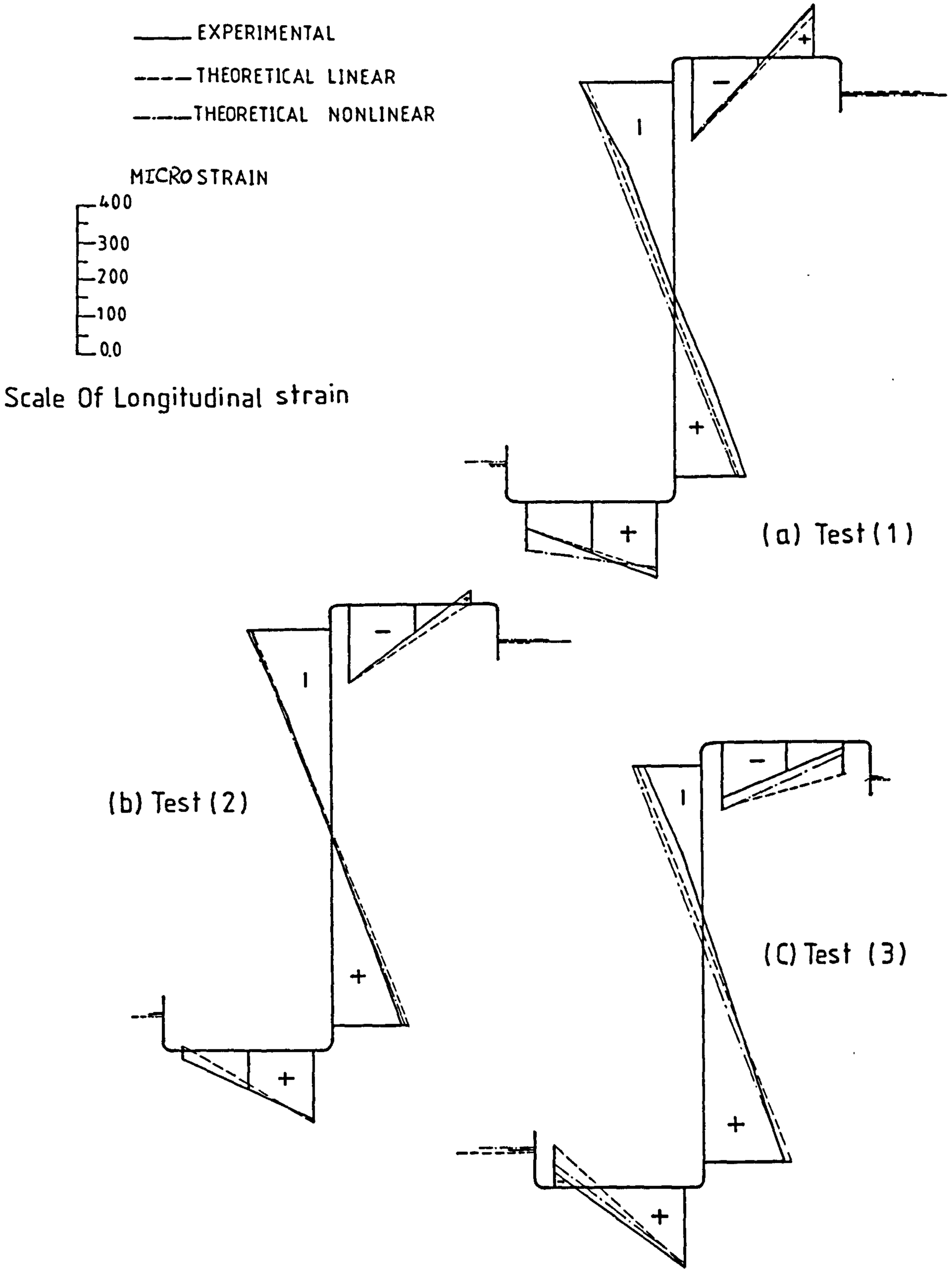

Fig.5.14 Longitudinal Strains AT Cross Section 2-2
Under Static Load = 40 Kg / hanger

CHAPTER SIX

Application of the Finite Element Method to Buckling Problems

6.1. GENERAL

The derivation of the new finite element formulation of the elastic torsional-flexural buckling of thin-walled structures has been given in chapter 3 where the main features of the elastic stiffness and geometric matrices have been discussed. It is the purpose of this chapter to demonstrate the validity and accuracy of the finite element formulation by presenting solutions for a variety of problems for which exact or highly accurate solutions by alternative means are available. The study reported herein is limited to problems with no torsional displacements in the prebuckling stage (no external bimoments). The finite element computer program described in chapter 4 was used to predict the buckling loads.

The chapter begins by presenting solutions to a number of conventional stability problems to illustrate the validity of the modified "Southwell technique" which is employed in the computer program for evaluating the critical buckling loads. It then proceeds to establish the accuracy of the formulation when used to analyse more complex problems as will be discussed in the following sections.

6.2. CONVENTIONAL STABILITY PROBLEMS

Four separate examples are discussed in this section. In each case the solution given by the finite element is presented as a ratio of the exact solution given by Timoshenko (2).

6.2.1. Pure torsional buckling

The pure torsional buckling of an axially loaded strut with a cruciform cross section is considered here. Under such loading the strut exhibits angular displacements only. The exact solution presented by Timoshenko (2) is given by,

$$P_{cr} = \frac{A}{I_o} \left(\frac{\pi^2 EI_\omega}{\ell^2} + GJ \right) \qquad (6.1)$$

Fig. 6.1 shows the distribution of the angle of twist θ_x just prior to buckling given by the two-element solution. It can be seen from the table given that the two-element solution has an excellent agreement with the exact solution. Fig. 6.2 shows the modified Southwell plot from which the buckling load of the eight-element case has been predicted. In this case the plot is a straight line.

6.2.2. Lateral buckling of a simple beam by uniform bending

Fig. 6.3 shows a simply supported I-beam with length ℓ = 400 cm loaded by uniform bending moment M_z. The exact solution of this case as given by Timoshenko (2) is,

$$M_{cr} = \frac{\pi}{\ell} \sqrt{EI_y \left(GJ + EI_\omega \frac{\pi^2}{\ell^2} \right)} \qquad (6.2)$$

It can be seen from fig. 6.3 that the two-element solution differs by only 0.66 per cent from the exact solution while for four and eight-element, the finite element solutions are 0.17 and 0.13 per cent in error, respectively. The modified Southwell plot for the eight-element solution is shown by fig. 6.4.

6.2.3. Lateral buckling of a simple beam by central concentrated load

Fig. 6.5 shows a simply supported I-beam with length ℓ = 400 cm loaded by central concentrated load P_y acting at the shear center. The exact solution given by Timoshenko (2) is,

$$M_{cr} = \gamma_1 \frac{\sqrt{EI_y \, GJ}}{\ell^2} \qquad (6.3)$$

in which, γ_1 is a dimensionless factor which depends upon the ratio $(\ell^2 . GJ/EI_\omega)$. Values of γ_1 are tabulated in reference 2.

The results of the finite element calculations are given in fig.6.5. It can be seen that there is an excellent agreement between the finite element solutions and the exact value of M_{cr}. The lateral displacement w of the middle cross section of the beam just prior to buckling is also shown in fig. 6.5, while fig. 6.6 shows the modified Southwell plot for the eight-element solutions.

6.2.4. Lateral buckling of a cantilever beam by concentrated load at the free end

The exact solution of this case was presented by Timoshenko (2), and is given by,

$$M_{cr} = \gamma_2 \frac{\sqrt{EI_y \, GJ}}{\ell^2} \qquad (6.4)$$

where, γ_2 is a dimensionless factor which depends on the ratio $(\ell^2 . GJ/EI_\omega)$. Values of γ_2 are tabulated in reference 2.

Fig. 6.7 shows the finite element solutions for this case. The finite element solutions give overestimated values for the buckling load. The error changes from 2.59 per cent for the two-element solution to 1.2 per cent for the eight-element solution. The lateral displacement w just prior to buckling is shown in fig. 6.7, while fig. 6.8 illustrates the three operations carried out by the computer program to predict the eight-element solution.

It can be seen from the previous examples that the accuracy of the finite element solutions, when compared to the exact solution, is excellent. The procedure followed to predict the buckling load, which is known as "the modified Southwell plot" has proved to be a very efficient and straight forward technique. One major advantage of the computer program used is that it calculates the displacement so that the general shape of the buckling mode can be observed.

6.3. ELASTIC LATERAL BUCKLING OF CONTINUOUS BEAMS

This section presents the results of a study carried out using the finite element computer program given in chapter 4 in order to examine the validity and accuracy of the method when used to analyse the torsional-flexural buckling of continuous beams.

The effect of the elastic-lateral bracing at the interior supports on the elastic-lateral buckling load of continuous beams has been investigated using the finite element method. Solutions have been obtained for the problems studied by Hartmann (54). The comparison between the finite element solutions and Hartmann's procedure is presented in the first part of this section.

The second part of this section deals with the elastic lateral buckling of continuous beams with all spans loaded where the spans interact during buckling. Finite element solutions for a series of continuous beams previously tested by Trahair (51) are given in the second part of this section.

6.3.1. Elastically restrained continuous beams

Hartmann (54) presented a theoretical study of the elastic buckling behaviour of continuous beams taking into account the effects of continuity and of lateral bracing stiffness on the critical load. Three types of lateral bracing stiffness, namely, a) axial stiffness, b) strong-axis flexural stiffness, and c) weak-axis flexural stiffness, were considered in the study. All loads were assumed to be acting through the shear center of the beam.

The analytical procedure given by Hartmann (54) was based on dividing the beam into a number of segments n, where any segment i is a straight part of the beam between the ith and the $(i+1)$th joints. Applied loads, reactions and elastic restraints occur at the specified joints connecting the segments. Hartmann (54) presented the differential equations which describe the buckling behaviour of segment i and the continuity equations at joints i and $(i+1)$ in terms of

the elastic stiffness of the lateral bracing at the joints. The solution of the differential equations was based on performing numerical integrations of the differential equations for a given set of boundary conditions and constructing the determinant of the resulting equations. This determinant is considered as the buckling criterion.

For representing the axial stiffness K_u of the lateral bracing, Hartmann (54) used the nondimensional coefficient γ suggested by Flint (45), where,

$$\gamma = \frac{K_u \cdot \ell^3}{48\ EI_y} \qquad (6.5)$$

and in which, K_u is the axial stiffness of the lateral bracing, ℓ is the length of the beam, and I_y is the least moment of inertia of the beam cross section.

The strong axis flexural stiffness S_x was also related to the torsional stiffness of the beam using the nondimensional coefficient δ where,

$$\delta = \frac{S_x \cdot \ell}{GJ} \qquad (6.6)$$

Fig. 6.9 shows the three types of continuous beam problems investigated by Hartmann (54). In order to present the finite element solutions for these cases the lateral bracing at the interior supports was simulated by beam members having an area A_{br} and strong axis moment of inertia I_{br}. For a given value of the nondimensional coefficient γ the cross sectional area of the bracing member A_{br} is given by,

$$A_{br} = \frac{48\ \gamma \cdot I_y \cdot \ell_{br}}{\ell^3} \qquad (6.7)$$

in which, ℓ_{br} is the length of the lateral bracing member.

For a given value of δ the moment of inertia of the assumed bracing member I_{br} becomes,

$$I_{br} = \frac{\delta \cdot GJ}{4E\ell} \ell_{br} \qquad (6.8)$$

The critical buckling load P_{cr} is given by,

$$P_{cr} = \frac{\alpha}{\ell^2} \sqrt{EI_y \cdot GJ} \qquad (6.9)$$

in which, α is the critical load parameter.

Hartmann (54) considered different values of the nondimensional beam property kℓ where $k = \sqrt{GJ/EI_\omega}$ ·He reported that for all the values of kℓ, using a value of γ equal to 11.0,the lateral displacement at the interior support was reduced to about 2 per cent of the maximum lateral displacement of the beam. Thus in each of the three types of problems considered in the study (fig. 6.9) the coefficient γ was taken equal to 11.0.

Table 6.1 presents the values of the critical load parameter α calculated by the finite element method (4 elements/ span) for the case shown in fig. 6.9.a, where one of the two spans of the continuous beam is loaded with central concentrated load P. The table also shows the values of α given by Hartmann (54) and the corresponding lower-bound values calculated using Salvadori's method (48). It can be seen that there is an excellent agreement between the values of α given by Hartmann (54) and the corresponding finite element values. The percentage difference of the finite element solutions compared to Hartmann's calculations for the case when kℓ = 2 and $S_x \cdot \ell / GJ = 370$ is shown in fig. 6.10. For the four-element solution the difference is about 0.19 per cent while increasing the number of elements to which each span is divided to eight elements results in 0.09 per cent difference only.

The effect of the strong axis flexural stiffness of the lateral bracing on the critical load parameter α is shown in fig. 6.11 for different values of $k\ell$. It can be seen that the general level of agreement between Hartmann's method and the finite element solutions is good. However, for low values of the nondimensional property $S_x \cdot \ell/GJ$ some differences between the two solutions can be noticed. The difference depends also on the value of $k\ell$. For example if the value of $S_x \cdot \ell/GJ$ is taken equal to 50 the percentage difference for a beam having $k\ell = \infty$ (narrow rectangular cross section) is almost zero, while for $k\ell = 2.0$ the percentage difference increases to 2.6 per cent. No details were given by Hartmann (54) about the approximate solution of the governing differential equation representing the torsional behaviour of the beam. However, Nethercot (36) showed that the accuracy of Hartmann's method is dependent on the value of $k\ell$.

Fig. 6.12 shows the comparison between the finite element solution of the critical load parameter α and the values of α given by Hartmann (54) for the case shown in fig. 6.9.b. when each of the two spans of the continuous beam is loaded with a central concentrated load P. For beams with narrow rectangular cross section ($k\ell = \infty$), Hartmann's method is in excellent agreement with the finite element method. For continuous beams with $k\ell$ value equal to 4.0, Hartmann's method gives overestimated values of the critical load parameter α.

Table 6.2 presents the values of the critical load parameter α for the case shown in fig. 6.9.c., where the central span of the three-span continuous beam is loaded at the middle with a transverse concentrated load P. It can be seen that, compared to the finite element solutions, for high values of the nondimensional coefficient $S_x \cdot \ell/GJ$, the accuracy of Hartmann's method is very good even for beams with high values of the warping rigidity.

6.3.2. Interaction buckling of continuous beams

Trahair presented a series of theoretical studies (6,49,50) concerning the effect of end restraints on the elastic torsional-flexural buckling of symmetrical beam elements. He showed that the buckling load of a continuous beam with only one span loaded can be calculated by considering the restraining effect of the unloaded adjacent spans on the loaded span.

For the two-span continuous beam shown in fig. 6.13 the major axis bending M_B is given by,

$$M_B = - \left(\frac{dv}{dx}\right)_B \cdot \frac{3EI_{z2}}{\ell_2} \qquad (6.10)$$

The effect of the major bending restraint on the bending moment M_B can be given by,

$$M_B = - \left(\frac{dv}{dx}\right)_B \cdot \frac{3EI_{z1}}{\ell_1} \; \frac{\beta_1}{1-\beta_1} \qquad (6.11)$$

in which, β_1 is the major axis bending end restrain parameter. The parameter β_1 is given by,

$$\beta_1 = \frac{1}{1 + S_{z1}/S_{z2}} \qquad (6.12)$$

where, $S_{z1} = \frac{I_{z1}}{\ell_1}$, and $S_{z2} = \frac{z2}{\ell_2}$ (6.13)

Following the same procedure, the minor axis flexural end restraint parameter β_2 and the end warping restraint parameter β_4 can be given by the two equations,

$$\beta_2 = \frac{1}{1 + S_{y1}/S_{y2}} \qquad (6.14)$$

and $$\beta_4 = \frac{1}{1 + h_1 \cdot S_{y1}/h_2 \cdot S_{y2}} \qquad (6.15)$$

where, $S_{y1} = \frac{I_{y1}}{\ell_1}$, $S_{y2} = \frac{I_{y2}}{\ell_2}$, (6.16)

and h_1, h_2 are the distances between the centroids of the flanges of the cross sections of span AB and BC respectively. If the same cross section is used for both spans then,

$$\beta_1 = \beta_2 = \beta_4 = \frac{1}{1 + \ell_2/\ell_1} \quad (6.17)$$

The critical buckling load P_{cr} is given by,

$$P_{cr} = \frac{\gamma}{\ell^2} \sqrt{EI_y\ GJ} \quad (6.18)$$

in which, γ is the critical load parameter.

Trahair (6) presented tables for the γ values for different load cases and different values of the end restraint parameters β_1, β_2, and β_4.

In another paper Trahair (50) discussed the case when all the spans of the continuous beam are loaded at the same time. In this case each span participates in the buckling behaviour of the beam by interacting with the adjacent spans. The critical buckling load of the continuous beam can then be evaluated by analysing the interaction behaviour of the individual spans. Fig. 6.14 shows a uniform two-span narrow rectangular continuous beam where the two spans are loaded with central concentrated loads P_1 and P_2 respectively. The beam is prevented from twisting and deflecting at the supports. The major axis flexural end restraint parameters of the two spans can be given by,

$$\beta_{11} = \frac{1 + P_2\ell_2^2/P_1\ell_1^2}{1 + \ell_2/\ell_1} \quad (6.19)$$

$$\beta_{12} = \frac{1 + P_1\ell_1^2/P_2\ell_2^2}{1 + \ell_1/\ell_2} \quad (6.20)$$

To satisfy the continuity condition at the interior support B in the lateral direction the minor axis end restraint parameters β_{21}, and β_{22}, must be related as follows:

$$\beta_{22} = \frac{-\beta_{21}\,\ell_2/\ell_1}{1 - \beta_{21}(1 + \ell_2/\ell_1)} \qquad (6.21)$$

The critical buckling loads P_{1cr} and P_{2cr} are given by,

$$P_{1cr} = \frac{\gamma_{21}}{\ell_1^2}\sqrt{EI_{y1}\,GJ}\,, \text{ and } P_{2cr} = \frac{\gamma_{22}}{\ell_2^2}\sqrt{EI_{y2}\,GJ} \qquad (6.22)$$

where, γ_{21} and γ_{22} are the critical load parameters.

For given values of the ratios ℓ_2/ℓ_1 and P_2/P_1 the major axis restraint parameters β_{11} and β_{12} can be calculated from eq. 6.19 and 6.20. By selecting the proper values of the minor axis restraint parameters β_{21} and β_{22}, the values of γ_{22} and γ_{21} can be evaluated from graphs given by Trahair (50).

Fig. 6.15 shows combinations of the critical load parameters for span ratio $\ell_2/\ell_1 = 5.0$, presented by Trahair (50). It can be noted that there are three significant combinations of the parameters γ_{22} and γ_{21} and these can be stated as follows:

(i) $P_1 > o$, and $P_2 = o$

in this case,

$$\gamma_{22}/\gamma_{21} = o\,,\ \beta_{11} = \frac{1}{1 + \ell_2/\ell_1}\,, \text{ and } \beta_{12} = \infty \qquad (6.23)$$

The minor axis restraint parameters are,

$$\beta_{21} = \frac{1}{1 + \ell_2/\ell_1}\,, \quad \beta_{22} = -\infty \qquad (6.24)$$

(ii) $P_2 > o$, and $P_1 = o$

in this case,

$$\gamma_{21}/\gamma_{22} = o \ , \ \beta_{11} = \infty \ , \text{ and } \beta_{12} = \frac{1}{1 + \ell_1/\ell_2} \qquad (6.25)$$

The minor axis restraint parameters are,

$$\beta_{21} = -\infty \ , \text{ and } \beta_{22} = \frac{1}{1 + \ell_1/\ell_2} \qquad (6.26)$$

(iii) Zero interaction

In this case the minor axis restraint parameters $\beta_{21} = \beta_{22} = o$ and there is no minor axis interaction between the two spans. The major axis end restraint parameters β_{11}, and β_{12} can be calculated from eq. 6.19 and 6.20. The critical load parameters γ_{21}, and γ_{22} can then be evaluated from the graphs given by Trahair (50).

The interaction diagram between these three significant combinations of the critical load has a curved shape as shown in fig. 6.15. Trahair (50) suggested that the interaction curve can sufficiently be approximated by linear relations between the three significant points as shown by the dotted lines in fig. 6.15. The comparison shown indicates that he was essentially correct.

In order to examine the validity and accuracy of the analytical procedure, Trahair (51) carried out a series of experiments on high strength aluminium I-section continuous beams under different combinations of central concentrated loads. Each beam was prevented from twisting and deflecting laterally at the supports. Experimental critical loads were evaluated from the load and deflection measurements using the modified Southwell plot method. Trahair (51) showed that, in general, the calculated values of the experimental critical loads were higher than the measured failure loads by almost 4.0 per cent.

Fig. 6.16 shows the three-span continuous beam (A-20.20.20.2) of reference (51) which have been analysed by the finite element method. The beam was prevented from twisting and deflecting laterally at the supports. Central transverse loads were applied to the beam at the level of the top flange. The two outer spans (right and left) were loaded with almost the same load P_1 while the middle span was loaded with load P_2.

In order to perform the finite element analysis, the additional effect of the load being applied at a distance $\frac{h}{2}$ above the shear center, where h is the height of the cross section, has to be considered. An additional term equal to Ph/2 corresponding to the degree of freedom θ_x at the loaded cross section of each span has been included in the geometric matrix.

Table 6.3 shows the comparison between the finite element solutions (4 elements/span) and the experimental values of the critical load given by Trahair (51), for the three-span continuous beam shown in fig. 6.16. It can be seen that in general the values of the buckling load calculated by the finite element method are less than the corresponding experimental values. However, as mentioned before, Trahair (51) has pointed out that the extrapolated experimental critical loads were generally higher than his predicted failure loads by almost 4.0 per cent.

Fig. 6.17 shows the percentage error of the finite element solutions for the seventh test in table 6.3. High accuracy can be achieved by dividing each span into four elements. In comparison to the experimental value of the critical load, the eight-element solution differs by -0.9 per cent only.

Fig. 6.18 shows the interaction curve for the three-span continuous beam shown in fig. 6.16, calculated by three techniques, which are:

(a) Extrapolating from the experimental measurements using the modified Southwell plot method.

(b) The finite element method using four elements per span.

(c) The approximate method given by Trahair (50), which is based on analysing the interaction effect between the individual spans.

It can be seen that the approximate method presented by Trahair (50) is in good agreement with the finite element method for the three major points of the interaction curve (when $P_1 = 0$, $P_2 > 0$, when $P_2 = 0$, $P_1 > 0$, and at zero interaction). For the rest of the interaction curve, the finite element is in close agreement with the experimental results while the approximate method given by Trahair (50) is more conservative.

Fig. 6.19 shows the distribution of the lateral displacement w at a near buckling stage for the case when the three spans of the beam are almost equally loaded. It can be seen that in this case buckling starts at the outer spans which are the most critical. The angle of twist θ_x has a similar distribution as shown in fig. 6.20.

Fig. 6.21 shows the four steps carried out by the computer program to evaluate the buckling load from the calculated values of the lateral displacement w at the middle cross section of one outer span and the corresponding values of the load factor.

6.4. ELASTIC LATERAL BUCKLING OF MONOSYMMETRIC BEAMS AND CANTILEVERS

6.4.1. The effect of monosymmetry

The differential equations of equilibrium which describe the buckling behaviour of a monosymmetric beam loaded with uniform bending moment M_z were presented by Timoshenko (2) as follows,

$$EI_y \frac{d^4w}{dx^4} - M_z \frac{d^4\theta_x}{dx^4} = o \qquad (6.27)$$

$$EI_\omega \frac{d^4\theta_x}{dx^4} - (GJ - M_z \cdot \beta_z) \frac{d^2\theta_x}{dx^2} - M_z \frac{d^2w}{dx^2} = o \qquad (6.28)$$

in which, β_z is the monosymmetric constant.

For the cross section shown in fig. 6.22 the constant β_z is given by the equation,

$$\beta_z = \frac{1}{I_z} \left(\int_A y^3 \, dA + \int_A z^2 \, y \, dA \right) - 2y_o \qquad (6.29)$$

The monosymmetric property β_z results from the effect of the bending stresses when acting on the buckled cross section. During buckling the bending compressive and tensile stresses acting on the slightly rotated cross section may form a resultant torque. For doubly symmetric I-beams the resultant torque caused by the bending stresses is equal to zero ($\beta_z = o$). In monosymmetric beams, however, there is *no* balance between the torque caused by the compressive bending stresses and that due to the bending tensile stresses ($\beta_z \neq o$). Such effect causes a change in the effective torsional stiffness of the cross section as can be seen in eq. 6.28. The effect of monosymmetry is such that the critical load is larger when the tensile bending stresses acts on the smaller of the two flanges of the cross section.

For a simply supported monosymmetric I-beam loaded with uniform bending moment M_z, the elastic buckling moment M_{cr} is given by (40),

$$M_{cr} = \frac{\pi \sqrt{EI_y \, GJ}}{\ell} \left[\frac{\pi\delta}{2} + \sqrt{1 + \bar{K}^2 + \left(\frac{\pi\delta}{2}\right)^2} \right] \qquad (6.30)$$

where, $$\bar{K} = \sqrt{\frac{\pi^2 \, EI_\omega}{GJ \cdot \ell^2}} \qquad (6.31)$$

and $$\delta = \frac{\beta_z}{\ell} \sqrt{\frac{EI_y}{GJ}} \qquad (6.32)$$

In 1972, Anderson and Trahair (40) presented a comprehensive theoretical and experimental study concerning the buckling behaviour of monosymmetric beams and cantilevers under different loading cases. The theoretical analysis was based on using the finite integral method to solve the governing differential equations which describe the torsional-flexural buckling behaviour of monosymmetric beams. For simply supported beams loaded with central concentrated load P, the critical value of the load P_{cr} is given by, (40)

$$P_{cr} = \frac{\gamma_2}{\ell^2} \sqrt{EI_y\ GJ} \qquad (6.33)$$

in which, γ_2 is the critical load parameter.

If the acting load is uniformly distributed with intensity u, the critical value of the load can be given by (40),

$$u_{cr} = \frac{\gamma_3}{\ell^3} \sqrt{EI_y\ GJ} \qquad (6.34)$$

where, γ_3 is the critical load parameter.

Anderson and Trahair (40) presented tables of γ_2 and γ_3 values for monosymmetric beams and cantilevers. In order to verify the theoretical method Anderson and Trahair (40) carried out an experimental investigation on the buckling behaviour of high strength aluminium cantilevers with mono-symmetric I-cross section. Each cantilever was loaded at the free end with transverse concentrated load at a distance $\bar{a}$ from the shear center.

The effect of moment gradient in a monosymmetric beam was not included in any of the previous studies which presented a finite element formulation for the elastic torsional-flexural buckling of thin-walled systems (24,26,28). The new geometric stiffness matrix presented in chapter 3 of this thesis includes, for the first time, the effect of

monosymmetry. This effect appears, in the geometric matrix, as a reduction in the effective torsional stiffness in terms of the acting bending stresses.

This section presents a study undertaken to examine the validity and accuracy of the finite element evaluation of the elastic lateral buckling loads of monosymmetric beams and cantilevers. Three types of problems have been studied, namely:

a) Lateral buckling of simply supported monosymmetric I-beams under uniform bending moment.

b) Lateral buckling of simply supported monosymmetric I-beams under central concentrated load.

c) Lateral buckling of monosymmetric I-cantilevers loaded at the free end with transverse concentrated load.

Two types of monosymmetric cross sections have been considered in this study and these are:

(i) A cross section with $\bar{K} = 0.10$ and $\delta = -0.10$

(ii) A cross section with $\bar{K} = 1.0$ and $\delta = -0.60$

where, K and δ are given by eq. 6.31 and 6.32 respectively.

The finite element solutions of cases a, b and c have been compared with the corresponding values of the buckling loads evaluated using the theoretical method given by Anderson and Trahair (40). The validity of the finite element formulation has also been checked by analysing two of the cantilever problems tested by Anderson and Trahair (40). The results of the finite element study will now be discussed.

6.4.2. Simply supported beams by uniform moment

Table 6.4.a. presents the finite element solutions for the simply supported monosymmetric beam with a cross section having $\bar{K} = 0.10$ and $\delta = -0.10$, as ratios of the critical bending moment evaluated using eq. 6.30. It can be seen that there is an excellent agreement between the

finite element solutions and the closed form solution of eq. 6.30. The two-element solution is in error by 0.44 per cent while the eight-element solution gives an error of 0.01 per cent only. The finite element solutions for the simply supported beam with cross section type (ii) are given in table 6.4.b. Again, the finite element agrees very well with the closed form solution of this beam.

6.4.3. Simply supported beams under central concentrated load

A closed form solution for this case is not available. The results of the finite element analysis are given as ratios of the critical buckling load calculated using eq. 6.33, where the load parameter γ_2 has been taken from the tables given by Anderson and Trahair (40).

Table 6.5.a. presents the finite element solutions for the beam with cross section type (i) ($\bar{k}$ = 0.10, δ = - 0.10) while table 6.5.b. presents the results of the cross section type (ii) ($\bar{k}$ = 1.0, δ = - 0.60). It can be seen that for both examples the agreement between the two methods is very good, nevertheless, the convergence of the finite element solutions is slightly slower for the second type of cross-sectional properties ($\bar{k}$ = 1.0, δ = - 0.60).

6.4.4. Cantilevers loaded with transverse concentrated load at the free end

Finite element solutions of this case are given in table 6.6.a. for the cantilever with a cross section type (i) and in table 6.6.b. for type (ii). The results are given as ratios of the critical buckling load calculated using the analytical procedure given by Anderson and Trahair (40). The level of agreement between the two methods is excellent as it can be seen from the tables.

6.4.5. Comparison between the finite element solutions and the experimental results

Anderson and Trahair (40) presented the results of an experimental study on the torsional-flexural buckling of

monosymmetric I-cantilevers. The study was undertaken to obtain a verification of the theoretical procedure given by the two authors (40) for calculating the elastic critical loads of monosymmetric beams and cantilevers.

Finite element solutions of two of the cantilevers tested by Anderson and Trahair are presented in table 6.7. Each of the two cantilevers had a length of 65.0 inches and a cross sectional property, $\bar{K}(\bar{K}^2 = \pi^2 EI_\omega/GJ\ \ell^2)$ equal to 0.475, while the values of $\delta(\delta = \beta_z \sqrt{EI_y/GJ})/\ell)$ for the two cantilevers were equal to + 0.18 and - 0.18 respectively. The concentrated load was applied to each cantilever along the y axis of cross section at the free end at a distance $\bar{a}$ from the shear center where $\bar{a}$ was taken equal to - 0.027 and - 0.22 inches respectively.

The results of the finite element analysis are given as ratios of the experimental buckling loads. The comparison given in table 6.7 shows an excellent correlation between the finite element method and the experimental values of the buckling load. It can also be seen from table 6.7 that the theoretical method given by Anderson and Trahair (40) is not at the same level of agreement with the experimental results. The error in their method increases with the absolute increase of the distance $\bar{a}$.

It can be concluded that the new finite element formulation given in chapter three of this thesis can be used to analyse the torsional-flexural buckling of mono-symmetric beams and cantilevers. Compared to closed form solutions, finite integral solutions and test results, the accuracy of the new finite element formulation has proved to be excellent.

6.5. TORSIONAL-FLEXURAL BUCKLING OF PLANE FRAMES

The study reported in this section was undertaken to examine the validity and accuracy of the finite element formulation presented in chapter 3 when used to carry out a three-dimensional stability analysis of plane frames. The computer program presented in chapter 4 was used to evaluate the critical loads of a number of plane frame problems for which experimental results are already available.

The first part of this section presents the finite element solutions for the lateral buckling loads of two elastically restrained, narrow rectangular plane frames. These two frames were tested by Hartmann (55) in order to obtain a verification to his theoretical method of analysis (53).

The interaction buckling of doubly symmetric I-plane frames loaded with in-plane concentrated transverse loads was investigated both experimentally and theoretically by Vacharajittiphan and Trahair (60). A comparison between the finite element solutions and the experimental and theoretical results given by Vacharajittiphan and Trahair (60) is presented in the second part of this section.

6.5.1. Torsional-flexural buckling of elastically restrained narrow rectangular plane frames

Hartmann (53) presented a theoretical method for the elastic lateral buckling analysis of elastically restrained single-story single-bay plane frames. The method has been based on performing numerical integrations of the governing differential equations which include the restraining effect of the lateral bracing.

In order to examine the accuracy of the theoretical procedure, Hartmann (55) conducted an experimental investigation on the elastic lateral buckling of narrow rectangular continuous beams and plane frames. Twenty rigid frame tests were carried out. The column bases of each frame were designed to be hinged in the plane of the frame and in the plane perpendicular to it, while the base rotation about the

longitudinal axis of the column was prevented. Each frame was loaded by sidesway loading applied to one of the knees of the frame at the mid-depth of the beam by means of a cable running over a pulley. There was a tendency for the bases to stick by friction at high loads.

In order to present the finite element solutions for the tested frames, the lateral bracing at the knees was simulated by beam members having a cross sectional area A_{br} and strong axis moment of inertia I_{br}. The cross sectional area A_{br} is given by,

$$A_{br} = \frac{48 \cdot \gamma_f \cdot I_y}{\ell_c^3} \ell_{br} \qquad (6.35)$$

where, ℓ_{br} is the length of the beam member representing the knee bracing and γ_f is the nondimensional coefficient used by Hartmann (55) to represent the axial stiffness K_u of the lateral bracing at the knees.

The nondimensional coefficient γ_f is given by,

$$\gamma_f = \frac{K_u \cdot \ell_c^3}{EI_y} \qquad (6.36)$$

in which, ℓ_c is the length of the column of the frame, and I_y is the least moment of inertia of the column's cross section.

The strong axis moment of inertia I_{br} of the beam member simulating the knee bracing is given by,

$$I_{br} = \frac{\delta \cdot GJ}{4 \cdot \ell_b} \ell_{br} \qquad (6.37)$$

where, δ is the nondimensional coefficient used by Hartmann (55) to represent the torsional restraining effect of the lateral bracing.

The nondimensional coefficient δ is given by,

$$\delta = \frac{S_x \cdot \ell_b}{GJ} \qquad (6.38)$$

in which, ℓ_b is the length of the beam and S_x is the strong axis flexural stiffness of the knee bracing.

During the first series of tests (10 tests) the strong axis flexural stiffness of the knee bracing S_x was set equal to zero, while the axial stiffness K_u was varied. For the first five tests in the series, the coefficient γ_f was held constant at a value of 20 while for the other five tests γ_f was taken equal to 760.

The effect of the axial stiffness of the lateral bracing K_u on the critical buckling loads of the frame is shown in fig. 6.23. As there was a tendency for the column bases to stick by friction, Hartmann (50) presented the corresponding theoretical values of the critical load for both hinged based frames and for fixed based frames. It can be seen from fig. 6.23 that there is excellent agreement between the finite element method and the theoretical method of Hartmann (53), and that both methods agree very well with the experimental results.

During the second series of tests, the nondimensional coefficient γ_f, which reflects the effect of the axial stiffness of the lateral bracing at the knee joints K_u in terms of the shear stiffness of the column, was held constant at a value equal to 760. The nondimensional coefficient δ, which represents the effect of the strong axis flexural stiffness of the lateral bracing S_x in terms of the torsional stiffness of the beam of the frame, was varied. For the first five tests in the series, δ_f was held constant at a value equal to 4.0, while for the last five tests δ_f was taken equal to 7.30.

Fig. 6.24 shows the effect of the strong axis flexural stiffness of the lateral bracing on the critical buckling load of the frame. The theoretical results are presented for the case when the bases of the frame are hinged and also for the case when these bases are fixed in the plane of the frame.

The level of agreement between the finite element solutions and the corresponding experimental buckling loads for the first five tests in the series ($\delta = 4.0$) is good. However, the results of the other five tests ($\delta = 7.30$) are higher than the corresponding values of the buckling given by the finite element method. Hartmann (55) reported that the results of these five tests were higher than expected due to the friction at the bases of the frame which changed the end conditions from hinged to partially fixed in the plane perpendicular to the plane of the frame. The comparison in fig. 6.24 also shows that, for values of δ between zero and 8, Hartmann's theoretical method seems to give overestimated values of the buckling load in comparison with the corresponding finite element solutions. This confirms what was previously found in section 6.3.1. when discussing the continuous beam problems (fig. 6.11 and 6.12).

6.5.2. Interaction buckling of doubly symmetric I-portal frames

In 1973, Vacharajittiphan and Trahair (60) proposed a theoretical method for analysing the elastic lateral buckling of doubly symmetric I-portal frames loaded with in-plane concentrated transverse loads. The method is based on using the finite integral technique to solve the governing differential equations which describe the buckling behaviour of the frame.

In order to obtain a verification of the theoretical procedure, Vacharajittphan and Trahair (60) carried out a series of tests on two small scale portal frames made of high strength aluminium I-section. The lower end of each column was fully fixed. The beam-to column joints were designed to transfer all the structural action except the bimoments. Rigid lateral supports were provided to prevent the lateral movements at the knee joints of each frame. Each frame was loaded with two equal concentrated loads P_1 each, applied vertically at the column tops, while the beam was loaded at the middle of the span with vertical load P_2.

Fig. 6.25 shows the dimensions of the first group of frames tested by Vacharajittphan and Trahair (60). The interaction curve for this group of frames is also shown in fig. 6.25. The level of agreement between the finite element calculations and the measured values of the buckling load is excellent. It can also be seen that the theoretical method given by Vacharajittphan and Trahair (60) seems to give underestimated values of the buckling load.

Fig. 6.26 presents the interaction buckling curve of the second group of frames which had a column-to beam length ratio equal to 2.0. Again the finite element solutions of this case agree very well with the corresponding test results.

6.6. THREE-DIMENSIONAL BUCKLING ANALYSIS OF SPACE FRAMES

The problem of analysing the elastic buckling behaviour of space frames has been for many years a topic for investigation by many research workers. The comprehensive study presented by Renton (9) formed a good attempt toward establishing an analytical procedure to deal with such problems. However, the procedure is limited to space frames loaded at the corner joints only. The method has been previously discussed in chapter 2 of this thesis.

In 1980, Razzaq and Naim (11) presented a theoretical study on the elastic instability behaviour of rigid-jointed unbraced single-story single-bay space frames subjected to equal or unequal concentrated column top loads. The study was based on applying the modified elastic stiffness matrix proposed by Renton (9) to carry out a second-order elastic analysis of the space frames. By selecting the proper buckling mode in each loading case, the value of the load at which the load-displacement curve became relatively flat, was taken as the critical load.

The study reported herein was undertaken to examine the validity and accuracy of the finite element solutions of the three-dimensional buckling analysis of space frames. Finite element solutions of the space frame problems considered by Razzaq and Naim (11) are presented in table 6.8.

Fig. 6.27 shows the dimensions and the loading system of the rigid jointed space frame studied by Razzaq and Naim (11). Static vertical concentrated loads P_1, P_2, P_3 and P_4 were applied at the column tops. These loads can be defined in terms of a load parameter Q as,

$$P_i = \lambda_i \cdot Q \quad , \quad \text{and} \quad i = 1,2,3,4 \qquad (6.39)$$

where, λ_i is a constant load multiplication factor.

Table 6.8 shows the comparison between the finite element calculations of the buckling loads and the corresponding values given by Razzaq and Naim (11). For the first case (case a), when the four columns of the frame are equally loaded, the finite element method gives only 0.03 per cent more than the buckling load given by Razzaq and Naim (11). The convergence of the finite element solutions for this case of loading is shown in table 6.9. The agreement between the two methods for the second case of loading (case b), when the four columns of the frame are all loaded but not equally, is excellent. The finite element solution differs by 0.04 per cent only from the value of the buckling load given by Razzaq and Naim (11).

In case 'c' of loading, where only one column is loaded, the finite element method gives a value of the buckling load almost 10.0 per cent less than the corresponding value given by Razzaq and Naim (11). No detailed information has been given in reference (11) about this case. However, this difference may be due to the buckling mode considered by Razzaq and Naim (11) not being the critical one. The analytical procedure given by Razzaq and Naim (11) gives correct predictions of the buckling load as long as the critical joint is one of the corner joints of the frame. However, in this case of loading, the critical joint lies on the longest beam near the loaded joint. Thus, the procedure followed by Razzaq and Naim (11) may, in some cases, lead to overestimated buckling loads.

The level of agreement between the two methods for the rest of the loading cases is good. While the difference in the results in cases 'd' and 'f' is almost 2.0 per cent, the difference in case 'e' decreases to 1.5 per cent only.

6.7. SUMMARY AND CONCLUSIONS

The applicability of the finite element method has been demonstrated by analysing a variety of torsional-flexural buckling problems using the computer program presented in chapter 4 of this thesis. In all cases, good convergence and excellent accuracy have been obtained by using few elements. The results of the cases considered can be summarised in the following points:

(a) Four types of conventional buckling problems were investigated, namely,

1. pure torsional buckling of an axially loaded strut;
2. lateral buckling of a simply supported beam by uniform bending;
3. lateral buckling of a simply supported beam by central concentrated load;
4. lateral buckling of a cantilever beam by a concentrated load at the free end.

Finite element solutions of these problems were compared with closed-form solutions (2). The comparison showed a good convergence of the finite element solutions and excellent agreement with the closed-form solutions.

(b) The following types of continuous beam problems were analysed:

1. elastically restrained continuous beams;
2. interaction buckling of continuous beams.

The first part (1) was devoted to the effect of lateral bracing stiffness on the buckling behaviour of continuous beam. Solutions have been presented for the problems analysed theoretically by Hartmann (54).
The accuracy of Hartmann's method is dependent on the warping

rigidity of the beam cross-section. For beams with narrow rectangular cross-section, the accuracy of Hartmann's method is very good. The accuracy decreases with the increase of the warping rigidity EI_ω of the beam.

The interaction behaviour between the adjacent spans of a continuous beam has been investigated using the finite element method. The comparison with test results, previously given by Trahair (51), showed good correlation and excellent accuracy of the finite element solutions.

(c) The new geometric matrix presented in chapter 3 of this thesis contains new terms corresponding to the effect of monosymmetry. In order to examine the validity and accuracy of the new terms, the following types of problems have been investigated:

1. lateral buckling of simply supported monosymmetric I-beams by uniform moment;
2. lateral buckling of simply supported monosymmetric I-beams subjected to central concentrated load;
3. lateral buckling of monosymmetric cantilevers under concentrated load at the free end.

The comparison with closed form, finite integral solutions (40), and test results (40) showed a good convergence and excellent accuracy of the finite element solutions in all cases.

(d) Finite element solutions of the three-dimensional buckling behaviour of plane frames, were obtained. The comparison was made with previous test results for two types of problems, namely,

1. buckling of elastically restrained narrow rectangular plane frames under sidesway loading (53);
2. Interaction buckling of doubly symmetric I-portal frames subjected to transverse vertical loads (60).

In both cases, good agreement has been observed between the finite element solutions and the corresponding test results, using four elements per each frame member.

(e) The validity and accuracy of the finite element analysis of the three-dimensional buckling behaviour of space frames have been examined. Finite element solutions were obtained for the cases investigated theoretically by Razzaq and Naim (11), using the second-order matrix method proposed by Renton (9). The comparison showed good agreement between the finite element solutions, using 4 elements per member, and the corresponding values of buckling load given by Razzaq and Naim (11). However, the study showed that the procedure followed by Razzaq and Naim (11) to predict the buckling load from the load-displacement relationship may, in some cases, lead to overestimated buckling loads.

1_Pure Torsional Buckling

CRUCIFORM SECTION 200X200X10 mm

MODULUS OF ELASTICITY E= 200.0 KN/mm^2

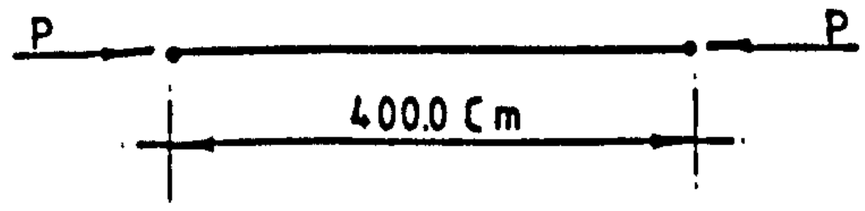

NO OF ELEMENTS	PREDICTION
2	1.00002
4	1.00002
8	1.00083

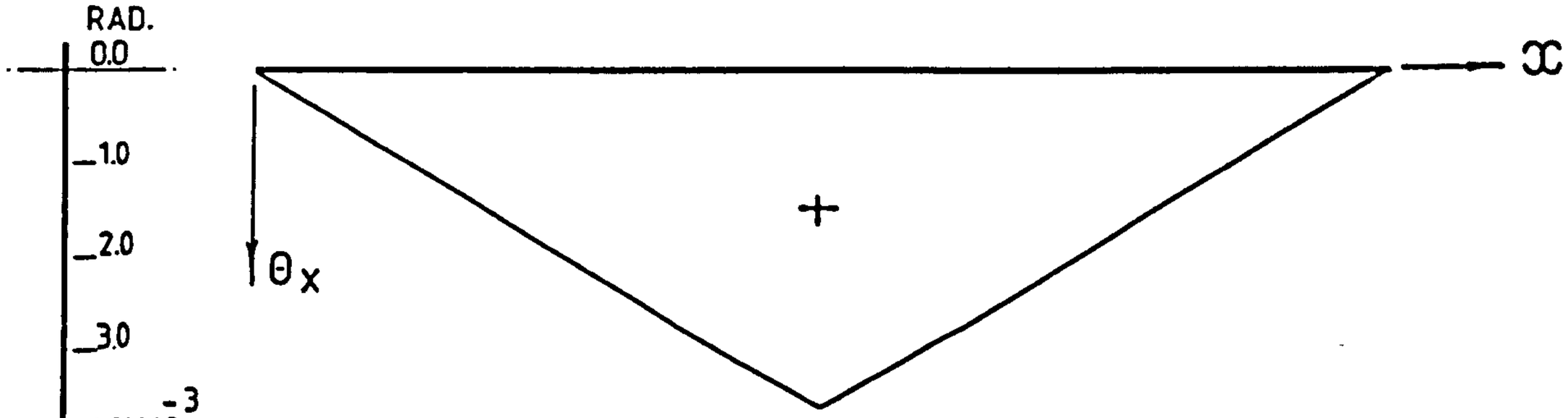

Fig.6.1 Distribution Of The Angle Of Twist Θx

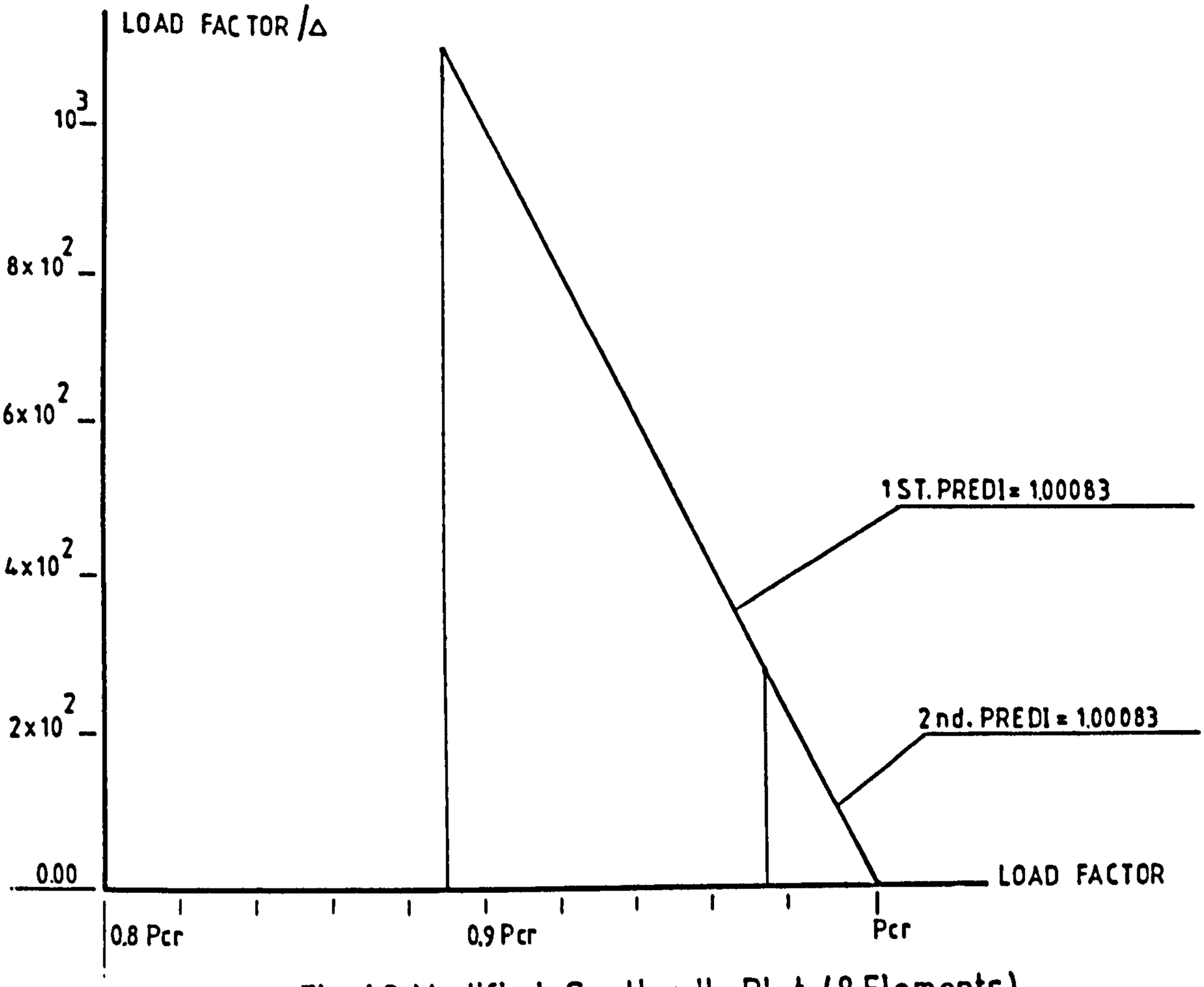

Fig.6.2 Modified Southwell Plot (8-Elements)

2_ Lateral Buckling By Uniform Bending

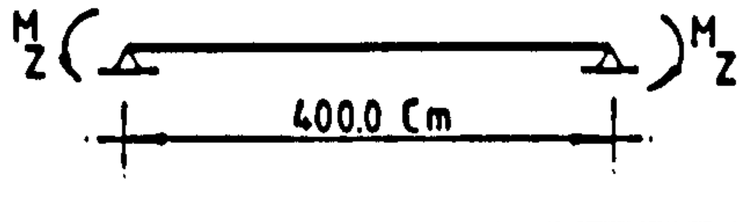

1-CROSS SECTION

$E = 200.0\ KN/mm^2$

PROPERTIES OF SECTION:

$A = 20.0\ Cm^2$

$I_y = 180.0\ Cm^4$

$JG = 1000.0\ KN\ Cm^2$

$I_\omega = 500.0\ Cm^6$

NO OF ELEMENTS	PREDICTION
2	1.00655
4	1.00165
8	1.00131

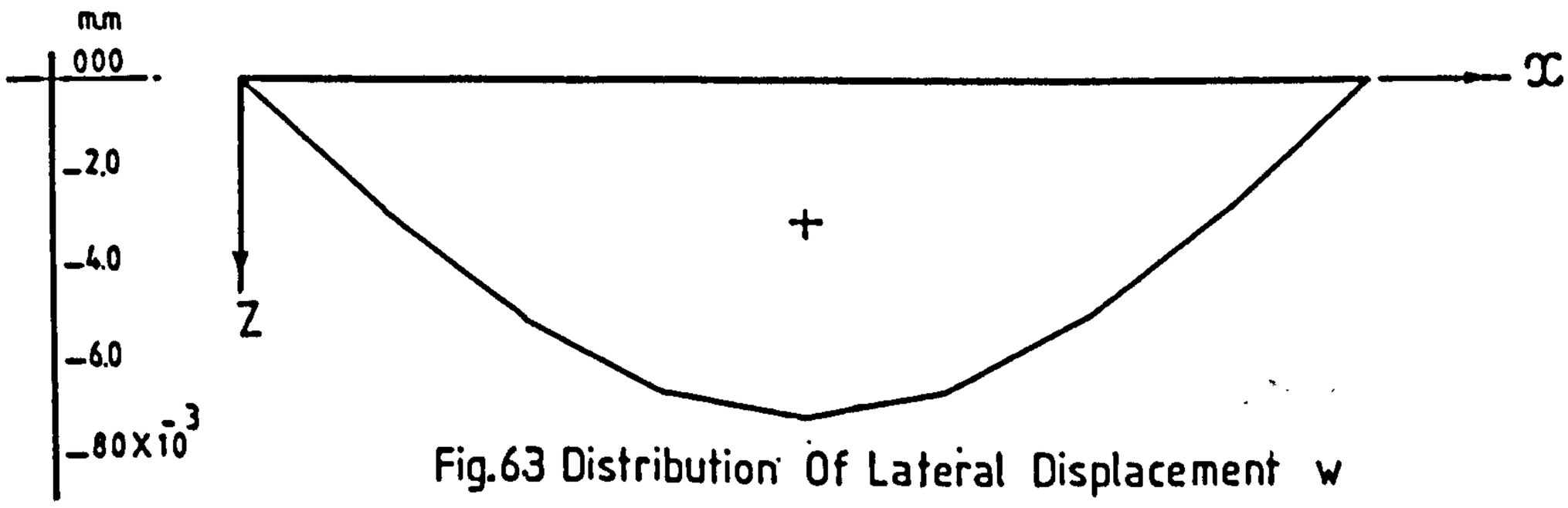

Fig.63 Distribution Of Lateral Displacement w

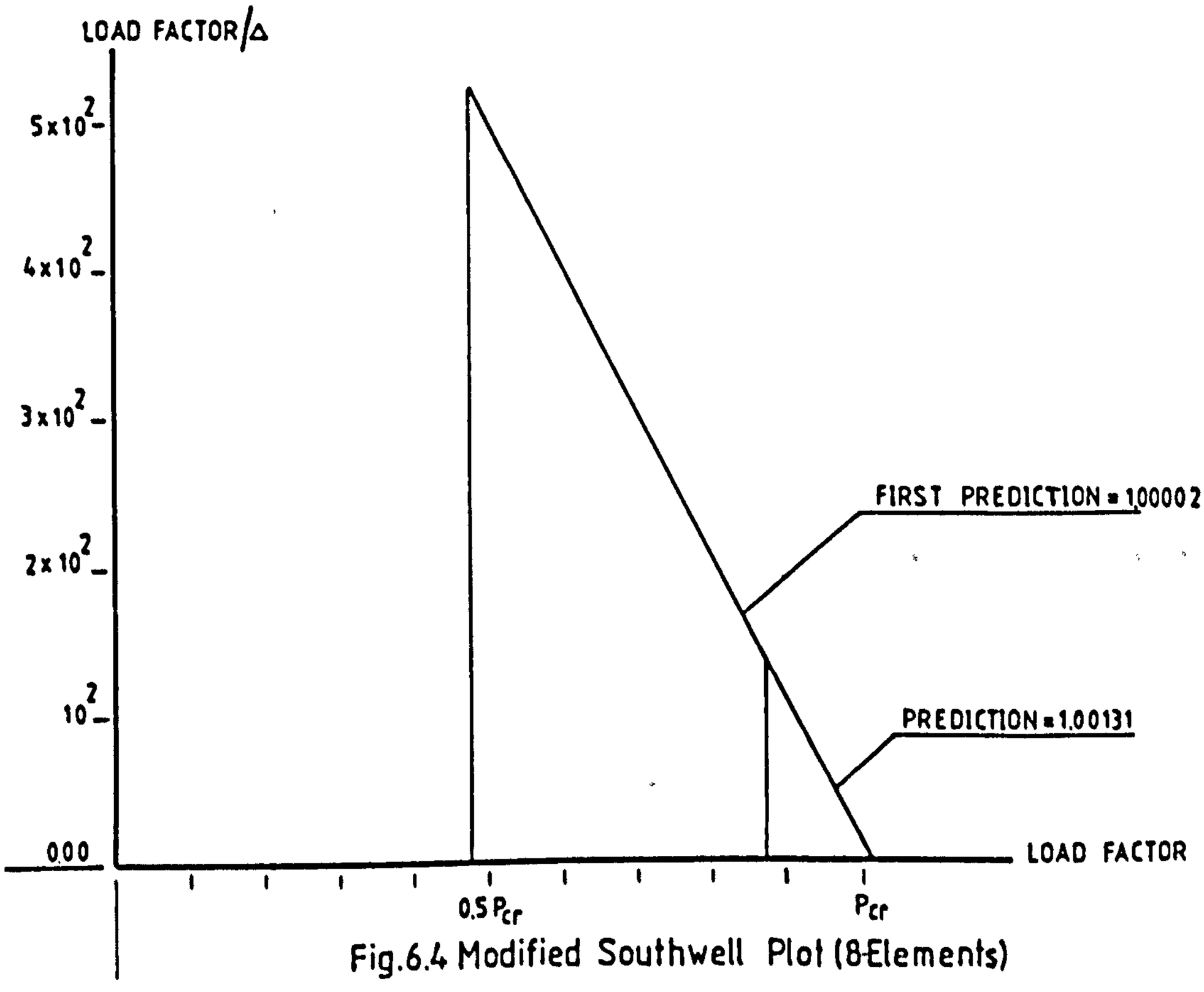

Fig.6.4 Modified Southwell Plot (8-Elements)

3_LATERAL BUCKLING BY CONCENTRATED LOAD

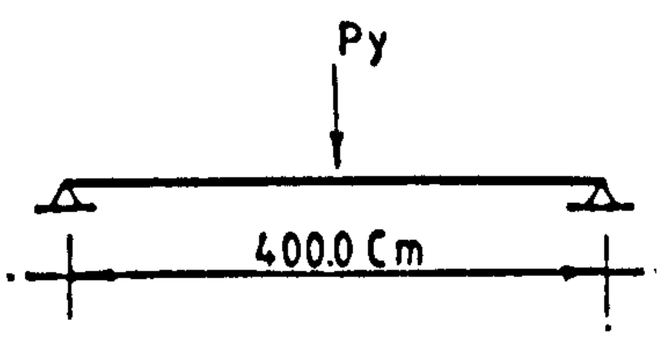

1_CROSS SECTION

$E = 200.0\ KN/mm^2$

PROPERTIES OF SECTION =

$A = 20.0\ Cm^2$

$I_y = 180.0\ Cm^4$

$JG = 1000.0\ KN\ CM^2$

$I_\omega = 500.0\ Cm^6$

NO OF ELEMENTS	PREDICTION
2	1.00480
4	0.999457
8	0.998775

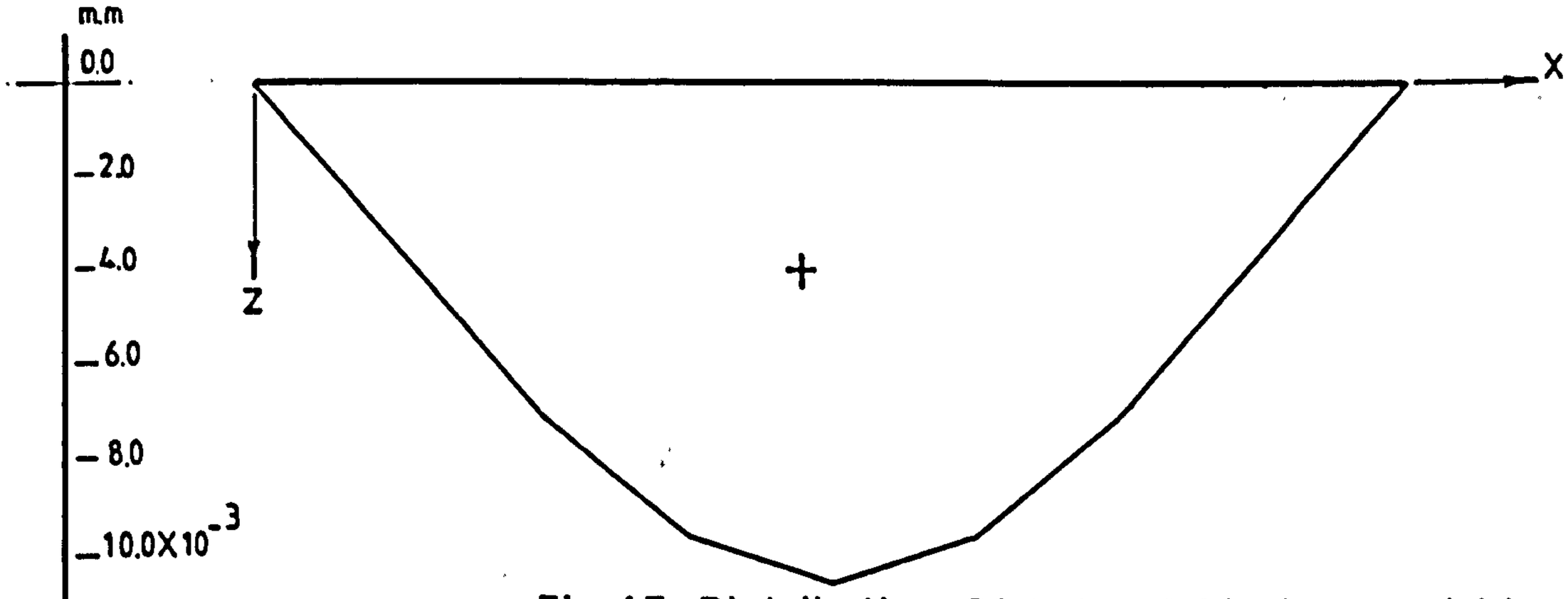

Fig.65 Distribution Of Lateral Displacement W

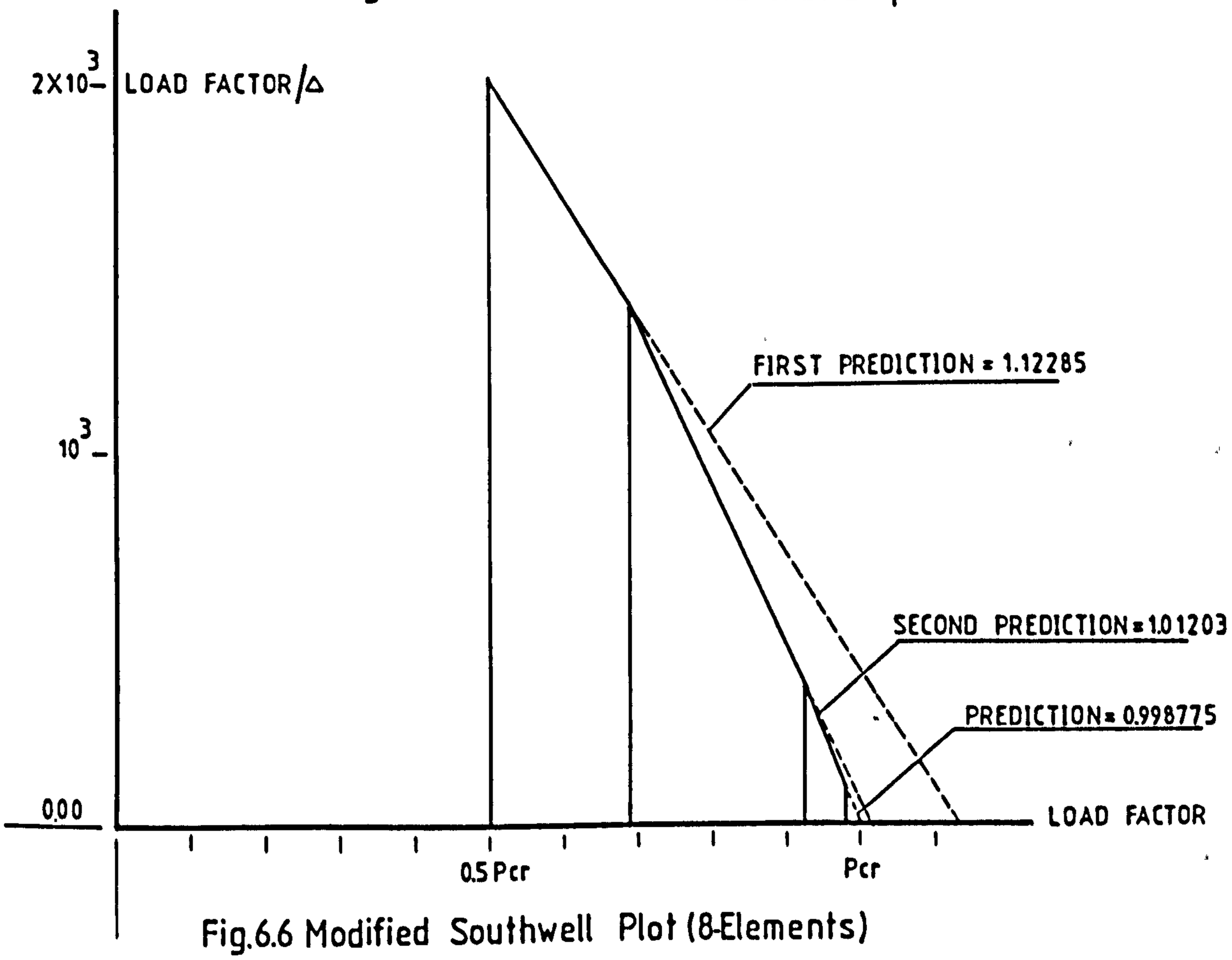

Fig.6.6 Modified Southwell Plot (8-Elements)

4·Lateral Buckling Of Cantilever By Concentrated Load

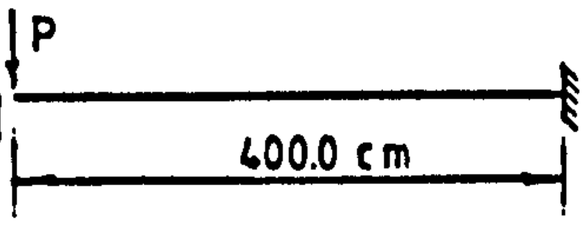

1.CROSS SECTION

$E=2000\ KN/mm^2$

PROPERTIES OF SECTION

$A=20.0\ Cm^2$

$I_y=180.0\ Cm^4$

$G_J=1000.0\ KN\ Cm^2$

$I_\omega=500.0\ Cm^6$

NO OF ELEMENTS	PREDICTION
2	1.02588
4	1.01342
8	1.01228

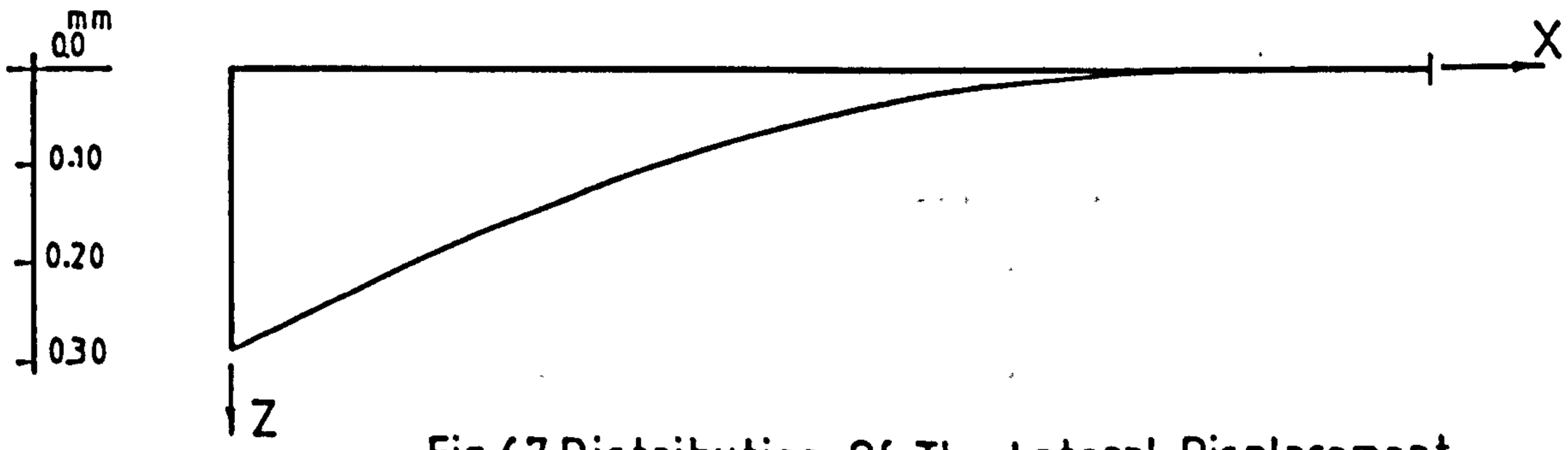

Fig.6.7 Distribution Of The Lateral Displacement

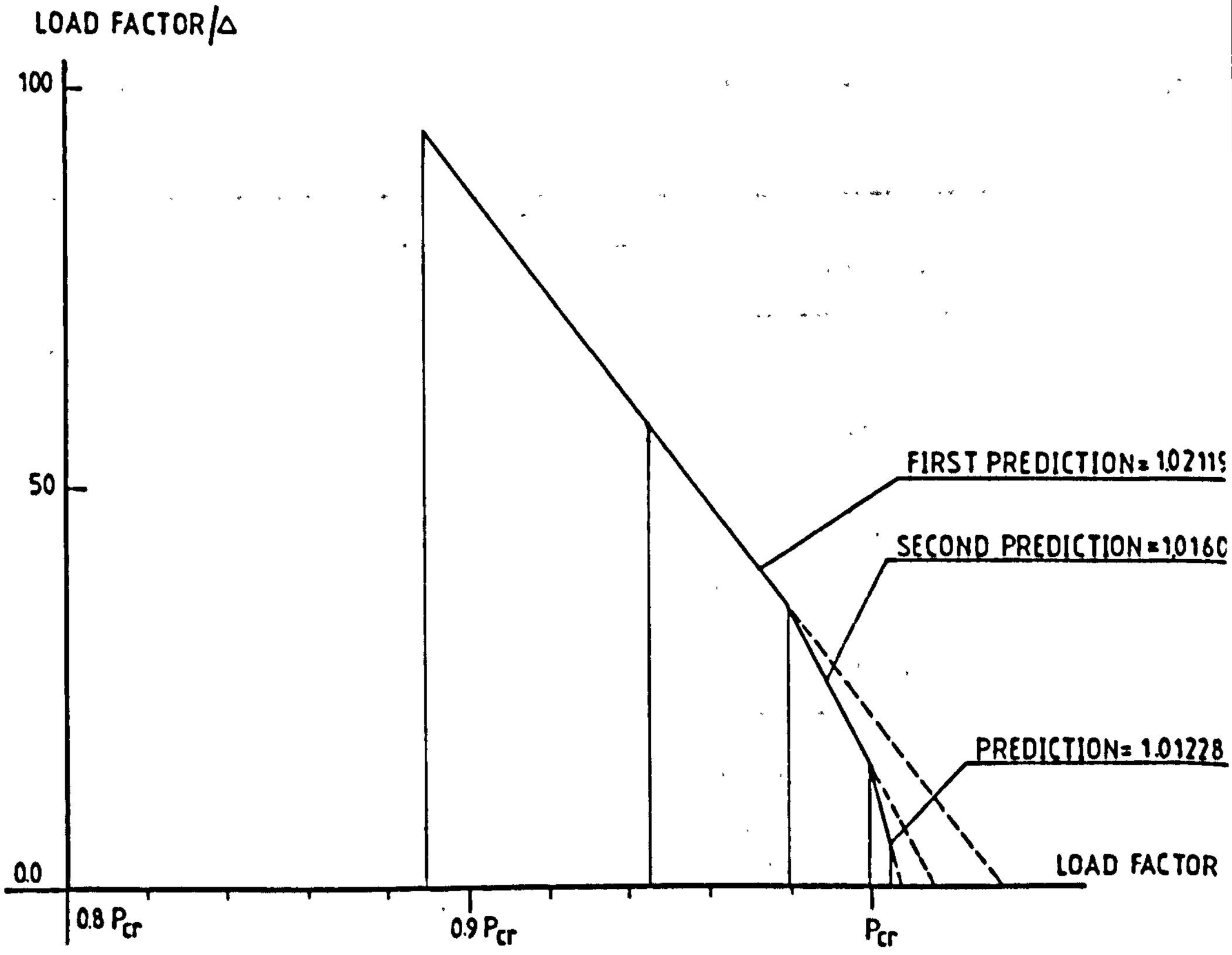

Fig.6.8 Modified Southwell Plot (8 Elements Load Applied $= P_{cr}$)

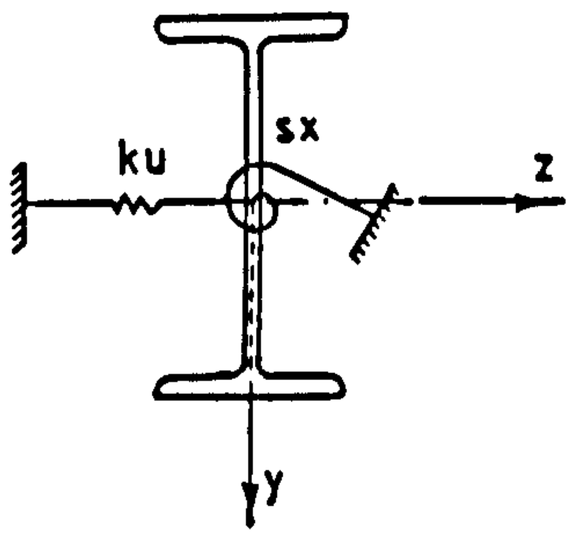

DETAILS OF CROSS SECTION a-a
AT INTERIOR SUPPORT

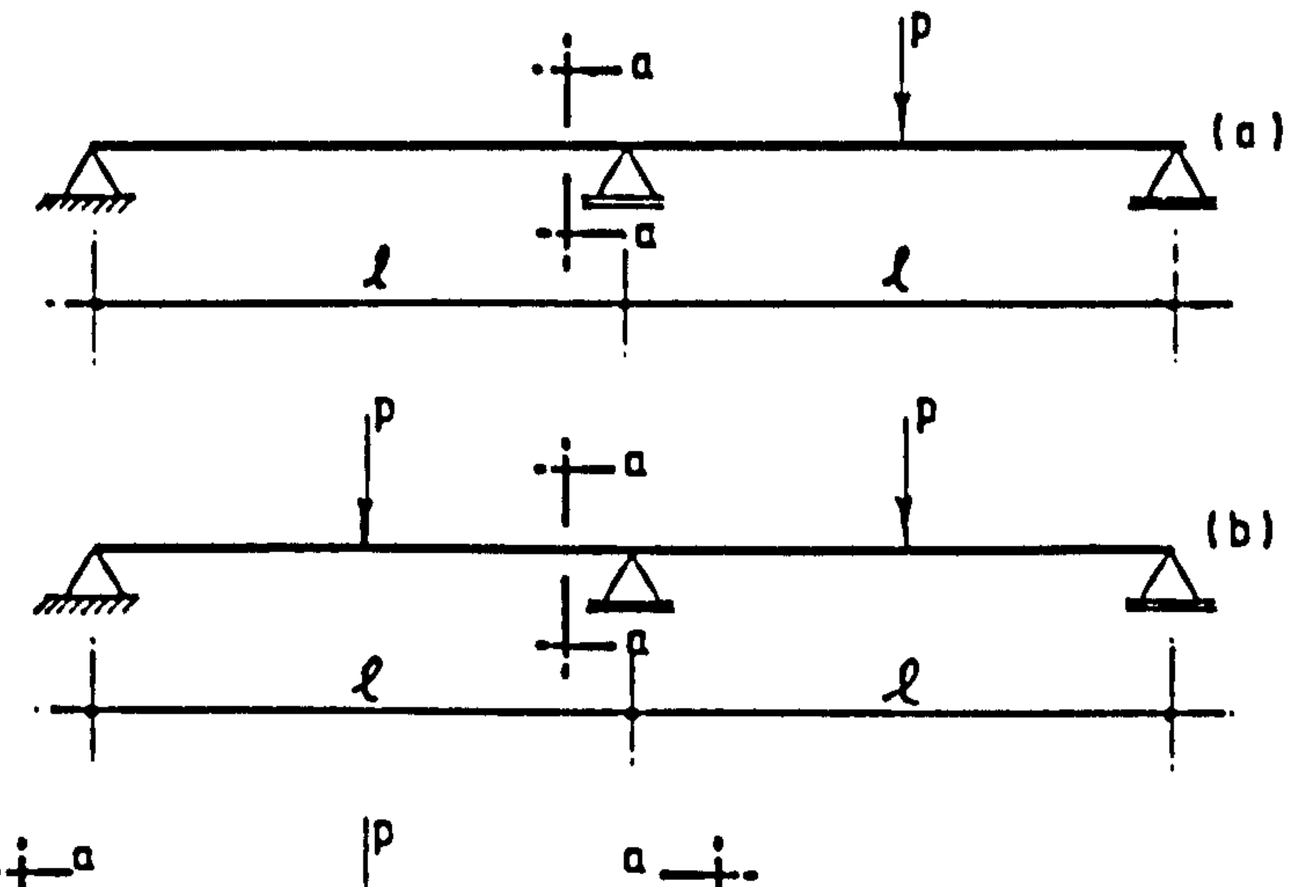

Fig. 6.9 Continuous Beams Studied By Hartmann (54)

Examples Taken For Comparison

ℓ = Span = 4.0 ms E = 20000.0 KN/Cm^2

Section Properties = A = 30.0 Cm^2 Iy = 400.0 Cm^4 GJ = 500 Kn. Cm^2, I_ω To Be Calculated

$K\ell$	$\frac{KU.\ell^3}{48EI_y}$	$\frac{Sx.\ell}{GJ}$	CRITICAL LOAD PARAMETER (α)		
			LOWER BOUND SALVADORI (48)	HARTMANN (54)	FINITE ELEMENT*
2.0	11.0	370	41.70	52.90	53.0
4.0	11.0	190	28.40	34.40	34.54
6.0	11.0	180	25.20	29.60	29.64
8.0	11.0	110	23.90	27.30	27.25
∞	11.0	50	22.0	23.30	23.66

Table 6.1 Critical Load Parameter (α) For Two Span Continuous Beam - One Span Is Loaded At The Middle (Case a)

* Number Of Elements Taken = 4 / Span

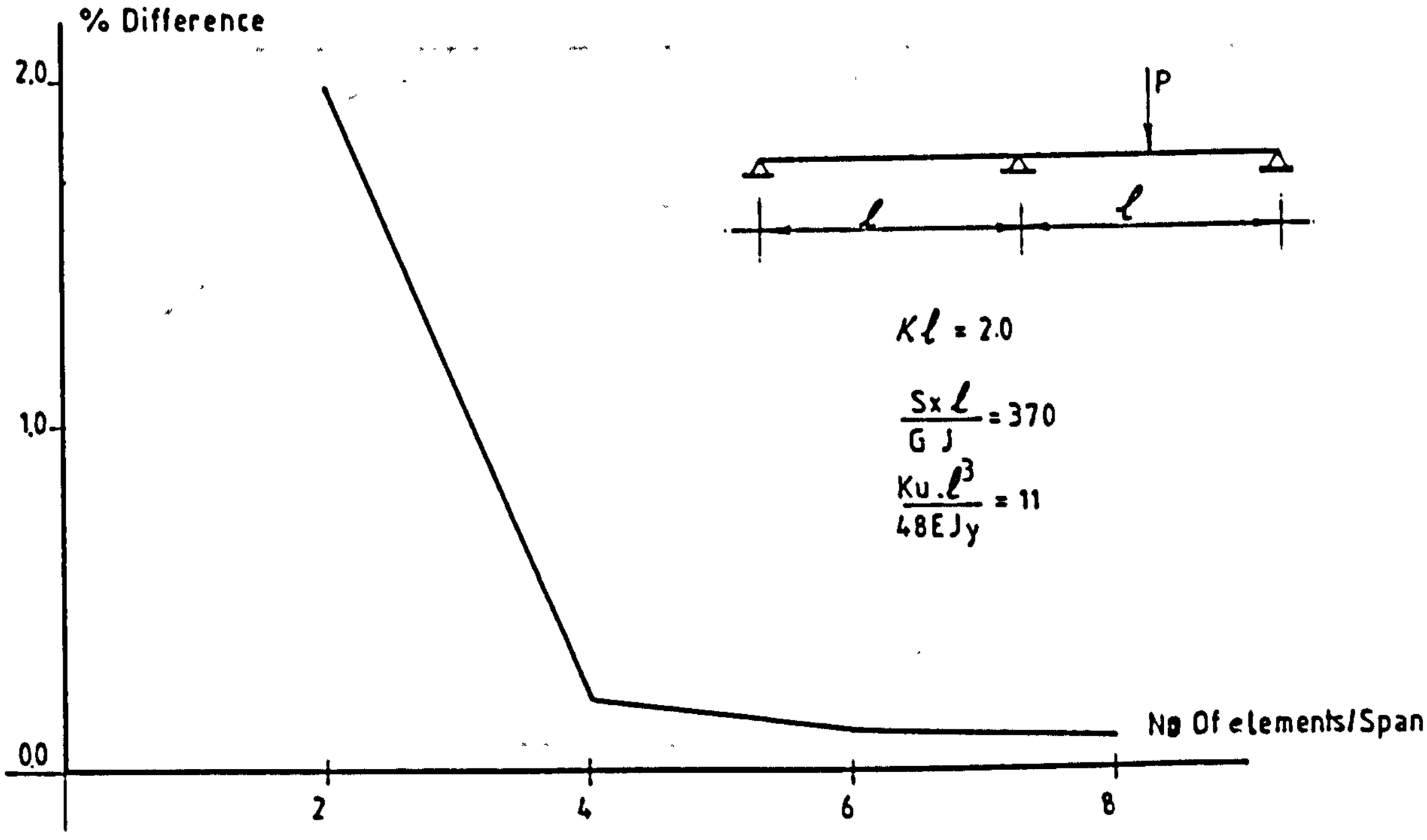

Fig.6.10 Convergence Of Finite Element Solutions
Two Span Continuous Beam (Case a)

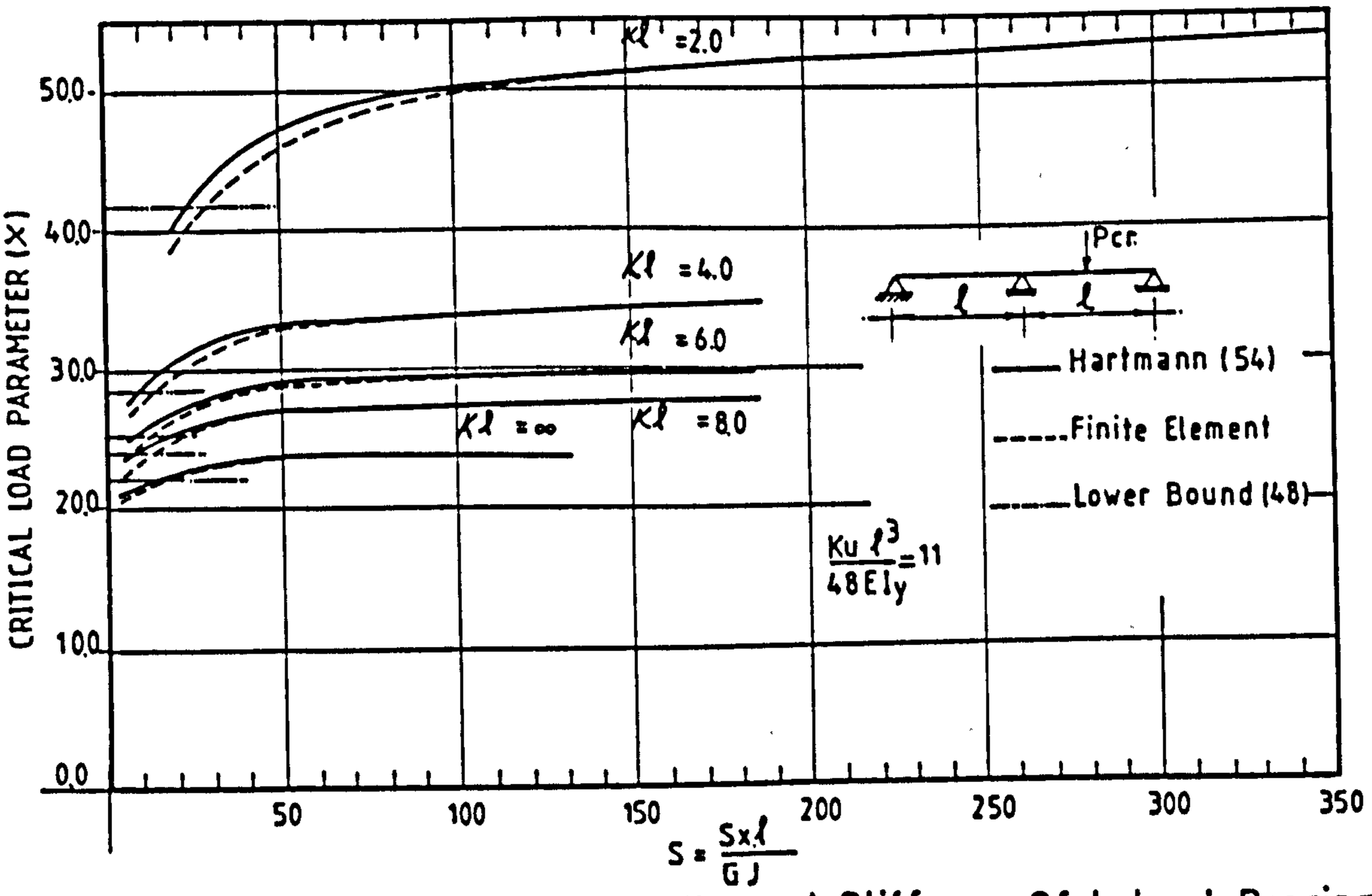

Fig.6.11.Effect Of Strong-Axis Flexural Stiffness Of Lateral Bracing
On The Critical Load Of Two Span Beam (Case a)

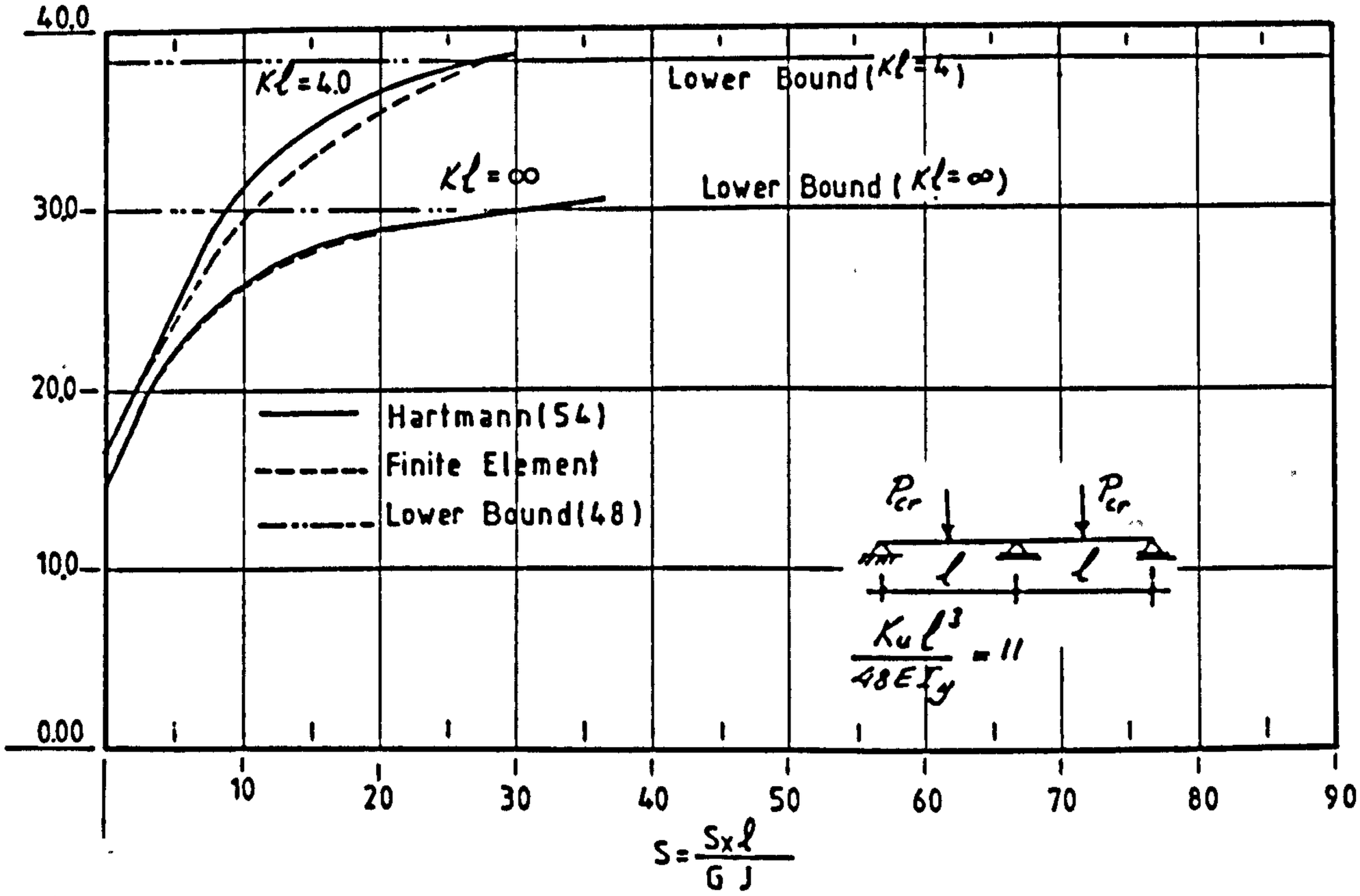

Fig.6.12 Effect Of Strong-Axis FLexural Stiffness Of Lateral Bracing On Critical Load Of Two Span Beam-The Two Spans Are Loaded (Case b)

$K\ell$	$\frac{Ku.\ell^3}{48 E I_Y}$	$\frac{Sx\ell}{GJ}$	Critical Load Parameter (α)		
			LOWER BOUND SALVADOR(54)	HARTMANN (48)	FINITE ELEMENT
2.0	11	477	51.6	8 2.0	81.53
4.0	11	374	35.10	51.40	51.86
6.0	11	112	31.20	41.50	41.56
∞	11	47	27.2	29.80	30.50

Table 6_2 Critical Load Parameter (α) For Three Span Continuous Beam-Central Span Is Loaded At The Middle (Case c)

• Numer Of Elements Taken = 4/Span

span l_1 : I_{z1}, I_{y1}
span l_2 : I_{z2}, I_{y2}

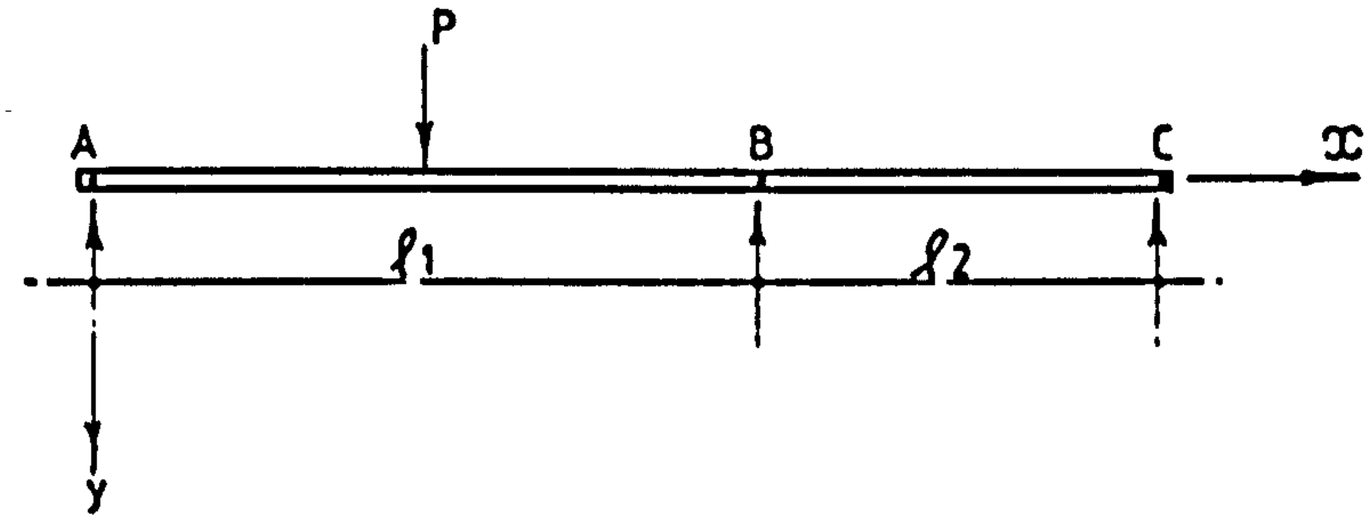

Fig.6 13 Two Span Continuous Beam With Only One Span Loaded

span l_1 : I_{z1}, I_{y1}
span l_2 : I_{z2}, I_{y2}

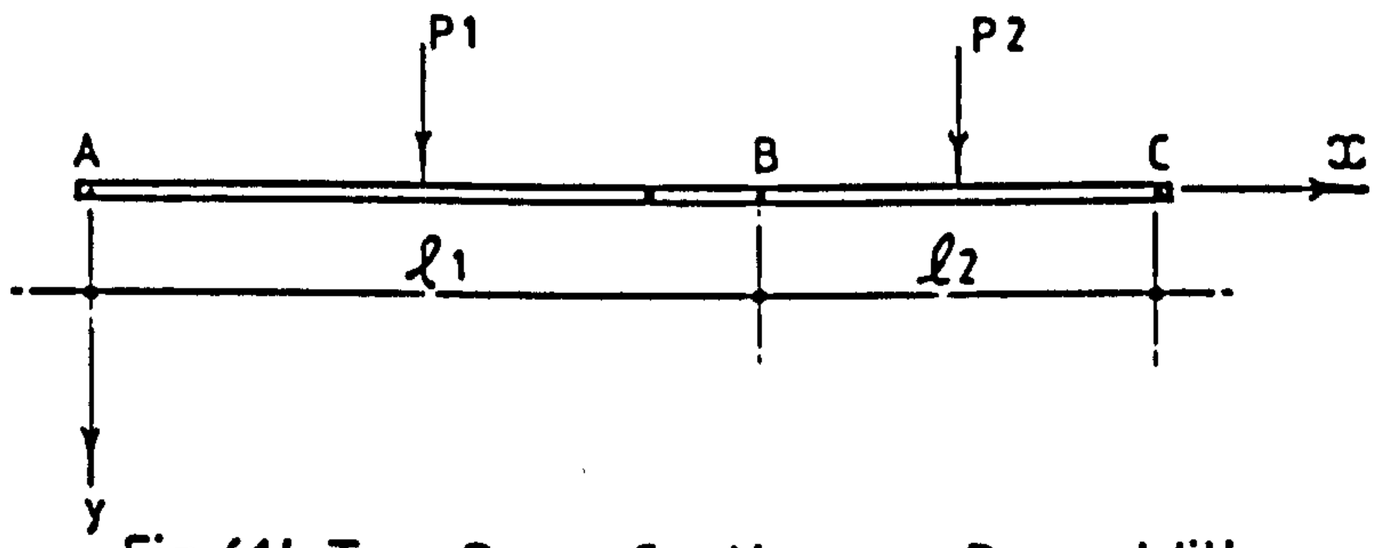

Fig.6.14 Two Span Continuous Beam With Two Spans Loaded

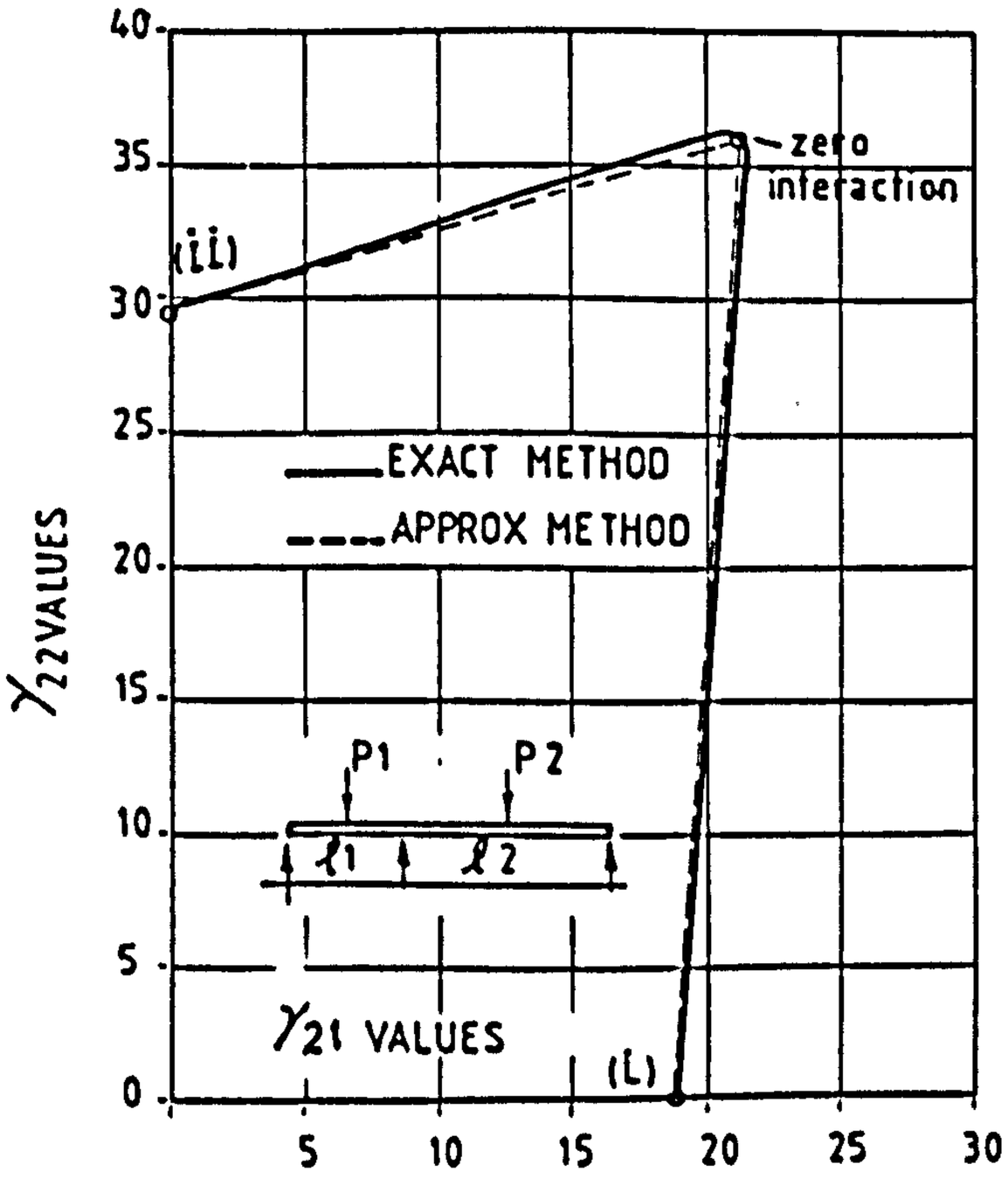

Fig.6.15 Critical Load Parameters For Two Span Beam With $l_2 / l_1 = 5.0$ (ref. 50)

$E I_y = 1.92$ KIP. In^2

$GJ = 0.241$ KIP. In^2

$E I_\omega = 0.154$ KIP. In^4

1 KIP = 4.45 KN 1 INCH = 25.40 mm

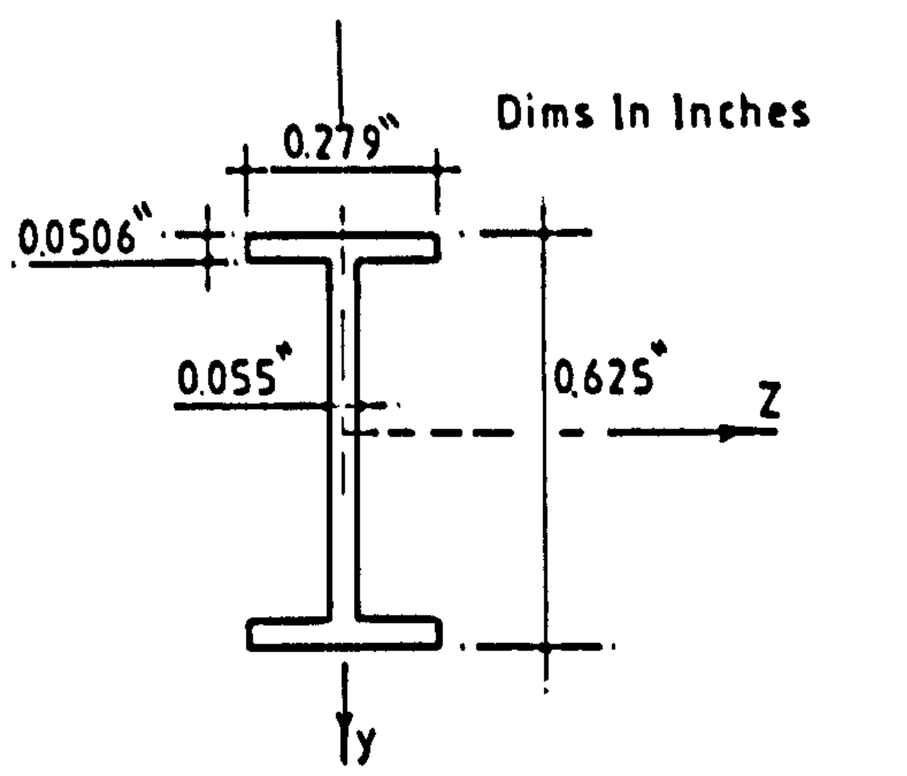

CROSS SECTION OF BEAM A.20.20.20_2

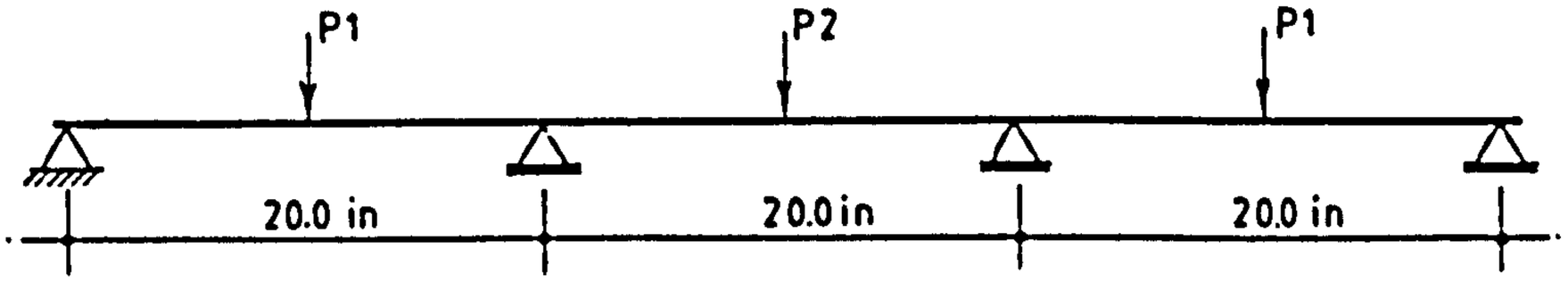

Fig.6.16. The Continuous Beam A.20.20.20_2
Presented In Ref. (51)

TEST NUMBER	LOAD P_1 (LH) IN POUNDS	LOAD P_2 IN POUNDS	LOAD P_1 (RH) IN POUNDS	FINITE ELEMENT CRITICAL LOAD FACTOR
1	44.8	45.0	44.8	0.9534
2	37.4	10.0	37.4	0.9894
3	39.6	20.0	40.2	09672
4	42.0	31.5	41.0	0.9681
5	10.0	51.8	10.0	0.9974
6	20.0	57.0	20.0	0.9885
7	32.0	60.4	31.8	1.0007
8	46.8	63.8	47.2	0.9369
9	—	49.8	—	0.9540
10	36.0	—	35.8	0.9786

Table 6.3 Comparison Between The Experimental Critical Loads And The Finite Element Results (4Elements/Span) For Beam A.20.20.20.2

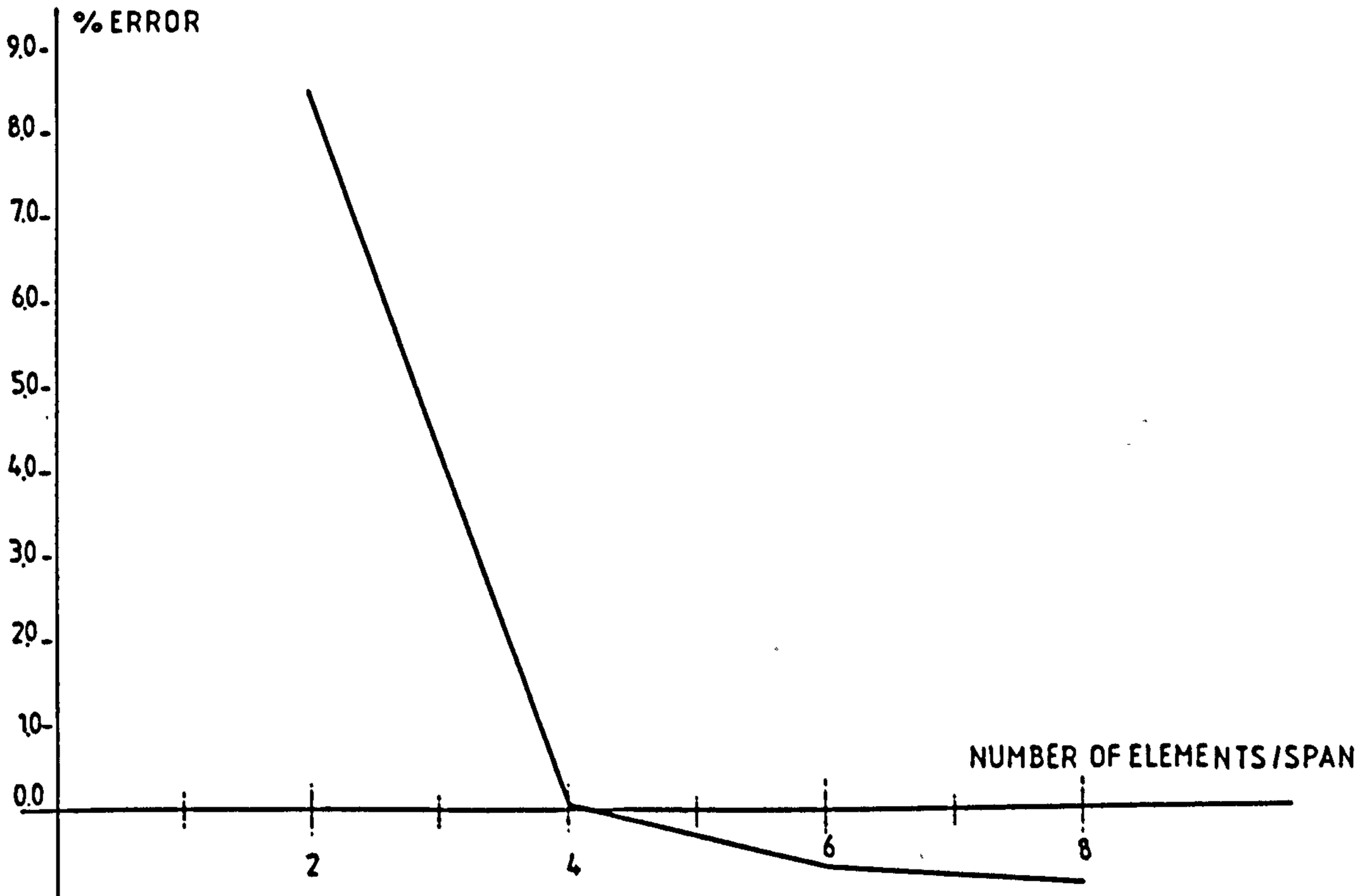

Fig.6.17 Convergence Of Finite Element Solutions For Test 7 (Ref. 51)

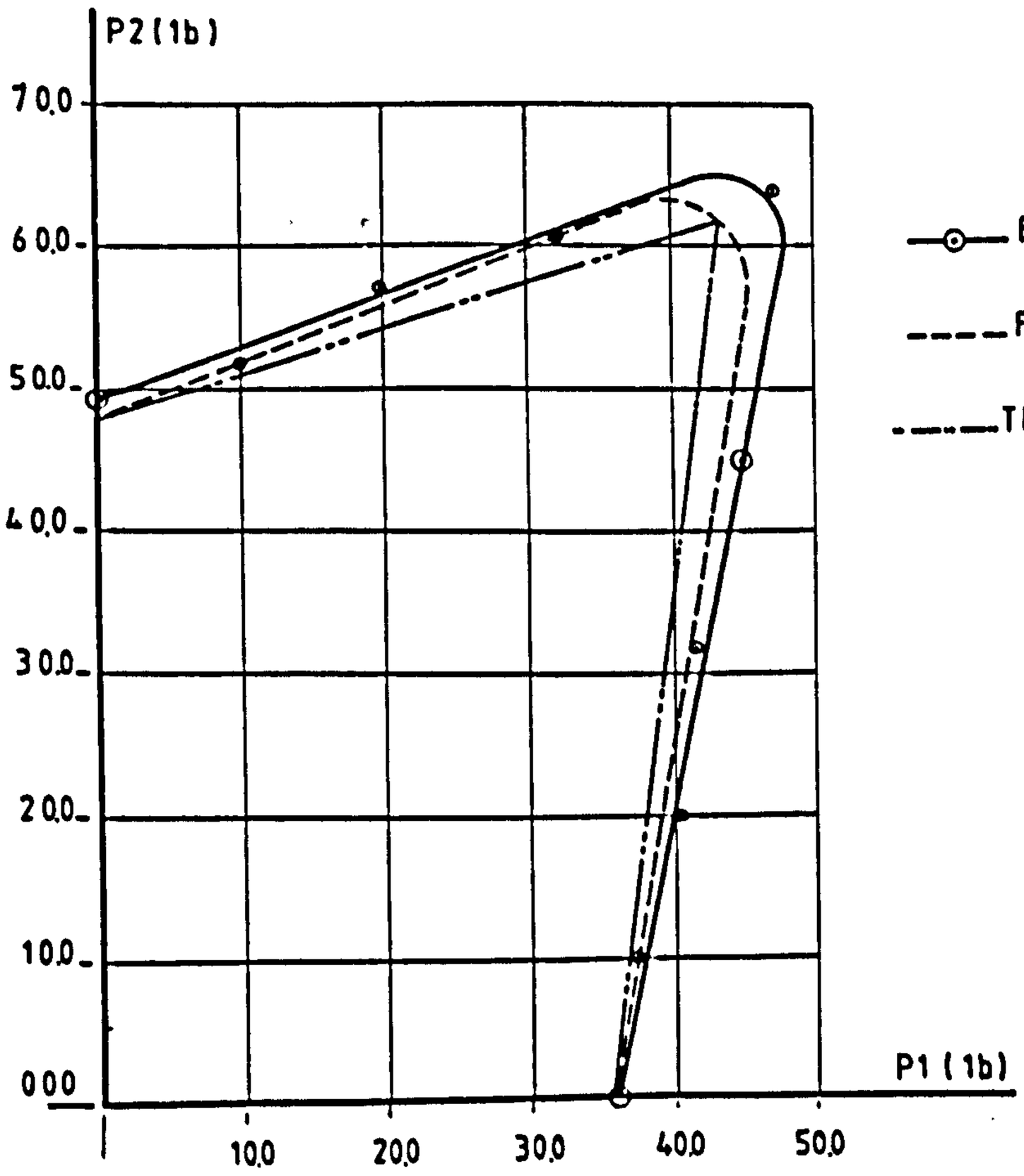

Fig.6.18 Critical Loads Of Beam A20_20_20_2 (Ref.51)

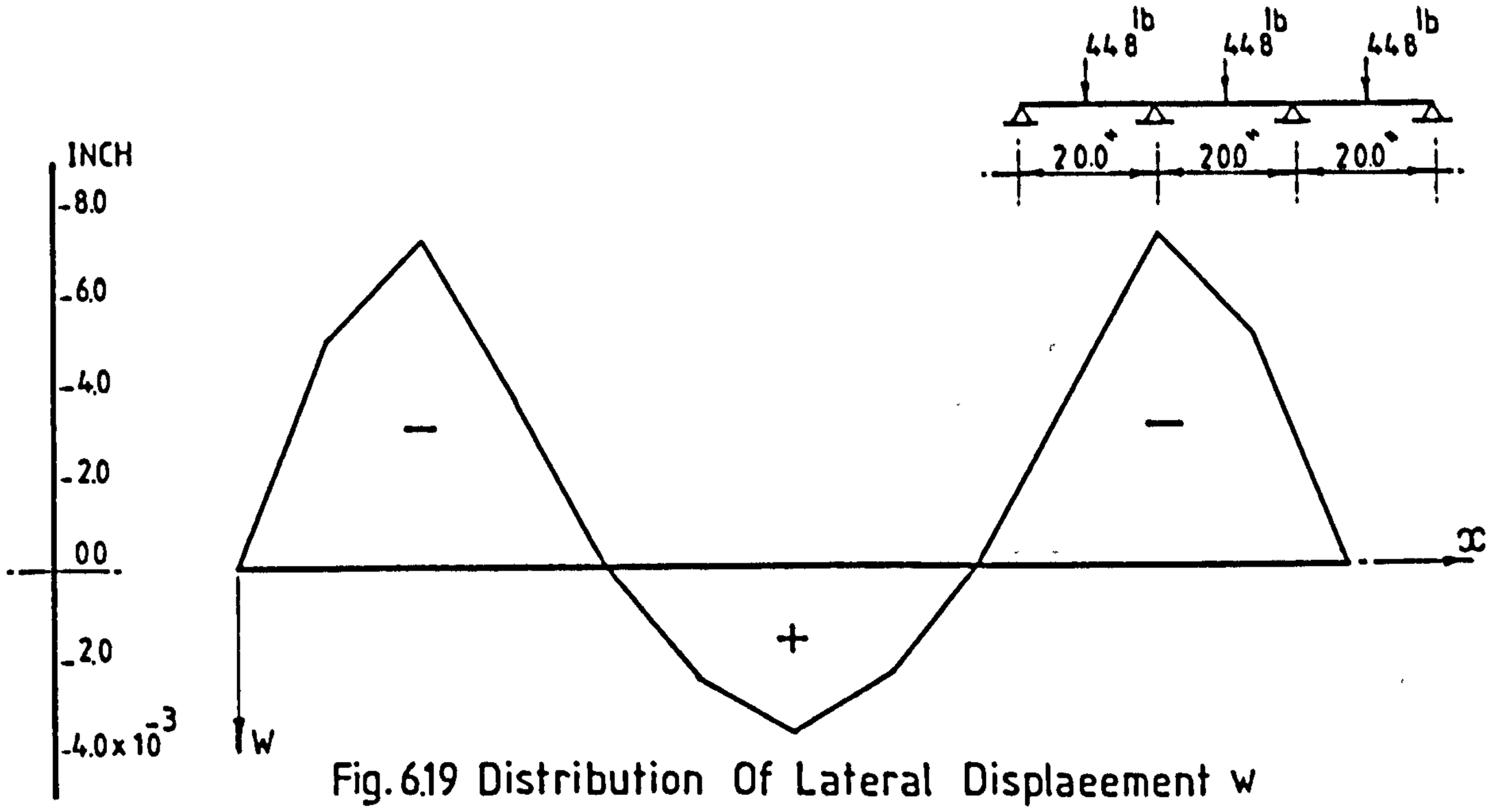

Fig. 6.19 Distribution Of Lateral Displaeement w

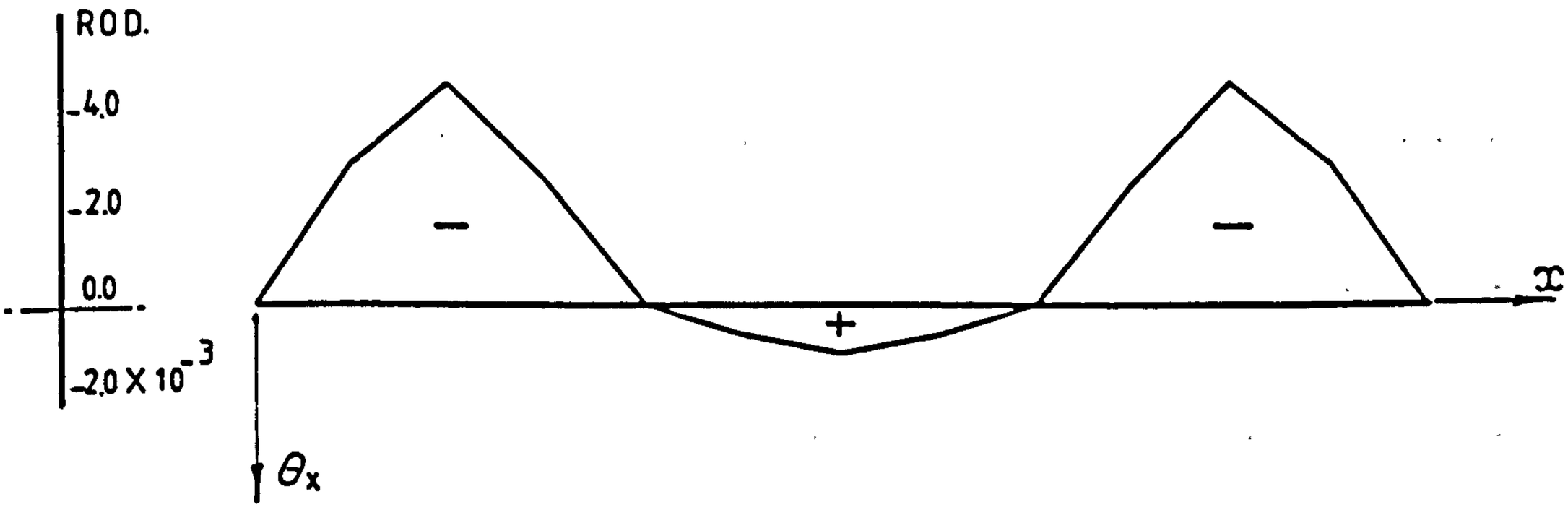

Fig. 620 Distribution Of The Angle Of Twist θ_x

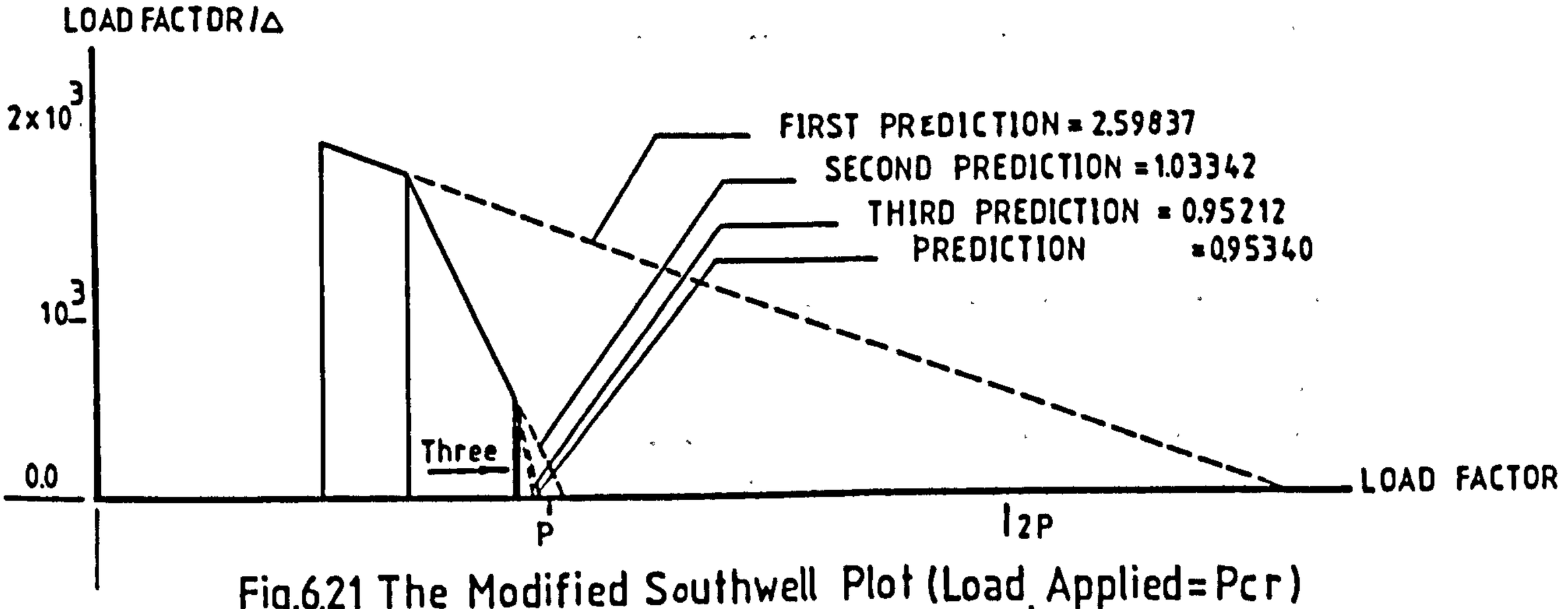

Fig. 6.21 The Modified Southwell Plot (Load Applied = Pcr)
For Test 1 (4 Elements / Span)

$$\beta_z = \frac{1}{I_z}\left(\int_A y^3 dA + \int_A Z^2 y dA\right) - 2y_o$$

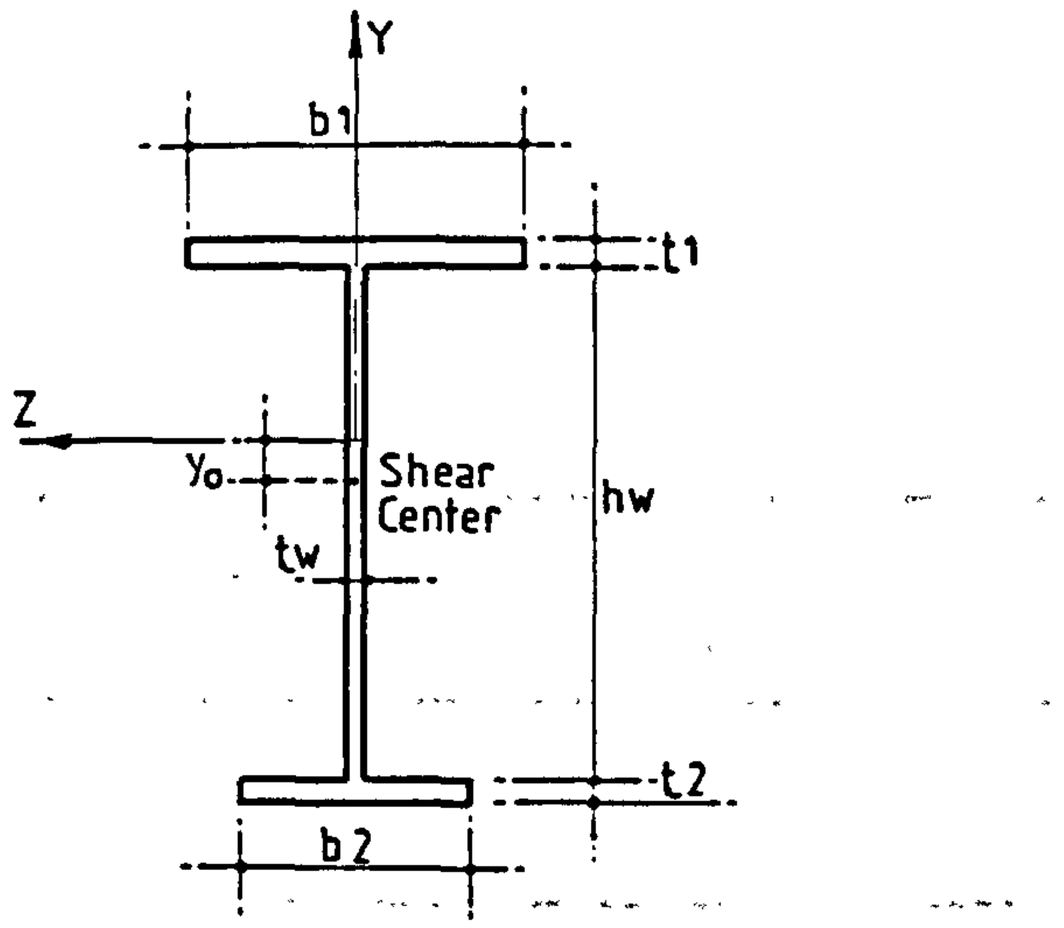

Fig.6.22 Monosymmetric I.Cross Section

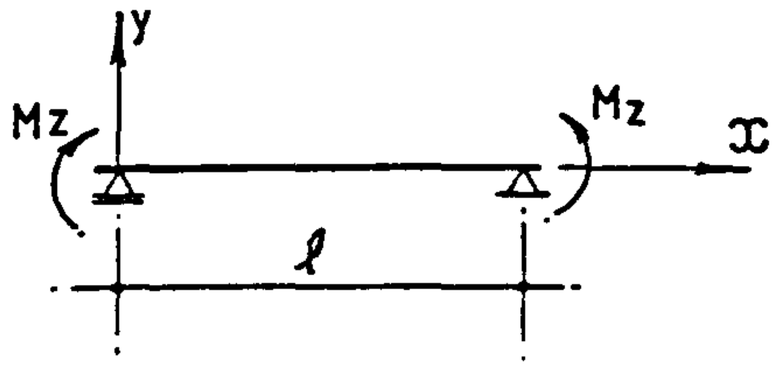

(a) $\bar{K}$=0.10,And δ =-0.10

2ELEMENTS	4ELEMENTS	6 ELEM.	8 ELEM.
1.0045	1.0004	0.9995	1,0001

(b) $\bar{K}$=1.0,And δ =-0.60

2ELEMENTS	4 ELEM.	6 ELEM	8 ELEM.
1.0007	1.0005	0.9971	1.0001

Table 6.4.Finite Element Solutions For Monosymmetric Simply Supported Beams Under Uniform Moment

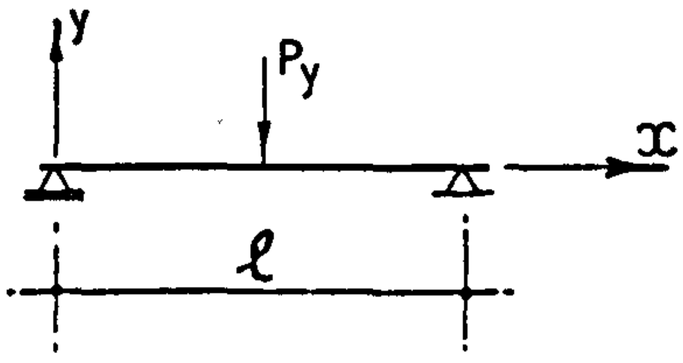

(a) $\bar{K}$=0.10,And δ =-0.10

2 ELEM	4 ELEM	6 ELEM	8 ELEM
1.0352	1.0033	1.0032	1.0032

(b) $\bar{K}$=1.0,And δ =-0.60

2 ELEM	4 ELEM	6 ELEM	8 ELEM
1.1863	1.0348	1.0181	1.0108

Table 6.5. Finite Element Solutions For Monosymmetric Simply Supported Beams Under Central Load P_y

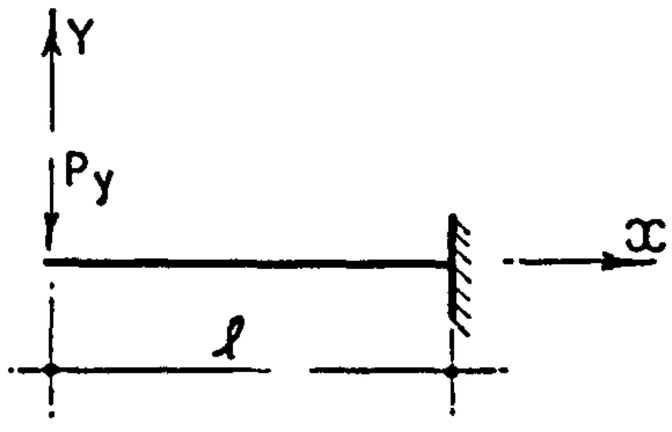

(a) $\bar{K}$= 0.10 And δ = 0.10

2 ELEM	4 ELEM	6 ELEM	8 ELEM
1.0810	1.0149	1.0078	1.0064

(b) $\bar{K}$= 1.0 And δ = 0.60

2 ELEM	4 ELEM	6 ELEM	8 ELEM
1.0356	1.0029	1.0028	0.9987

Table 6.6 Finite Element Solutions Of Monosymmetric Cantilevers Loaded With P_y At The Free End

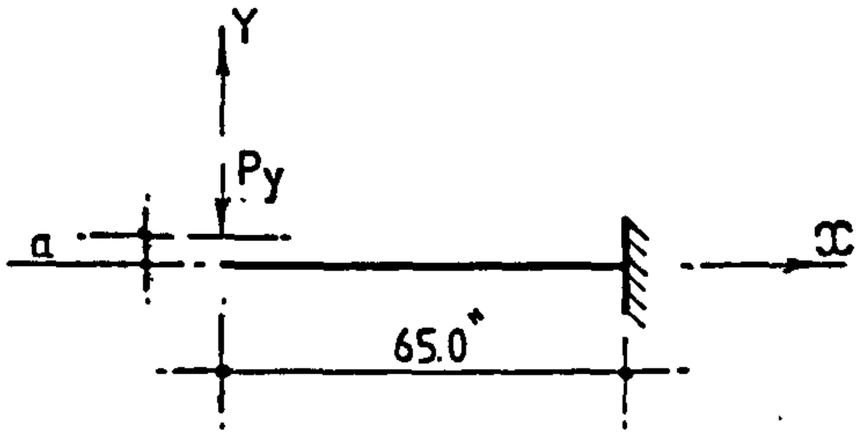

(a) δ=0.18 And a = 0.027

2 ELEM	4 ELEM	6 ELEM	8 ELEM
1.0471	1.0082	1.0005	0.9965

R = 1.0052

R = Ratio Between Theoretical Result Given In Ref-40 And The Experimental Value Of The Critical Load

(b) δ = -0.18 And a = -0.22

2 ELEM	4 ELEM	6 ELEM	8 ELEM
1.0457	1.0017	1.0012	1.0013

R = 1.0265

Table 6.7. Finite Element Solutions Of The Monosymmetric CantileversTested By Anderson And Trahair (40)

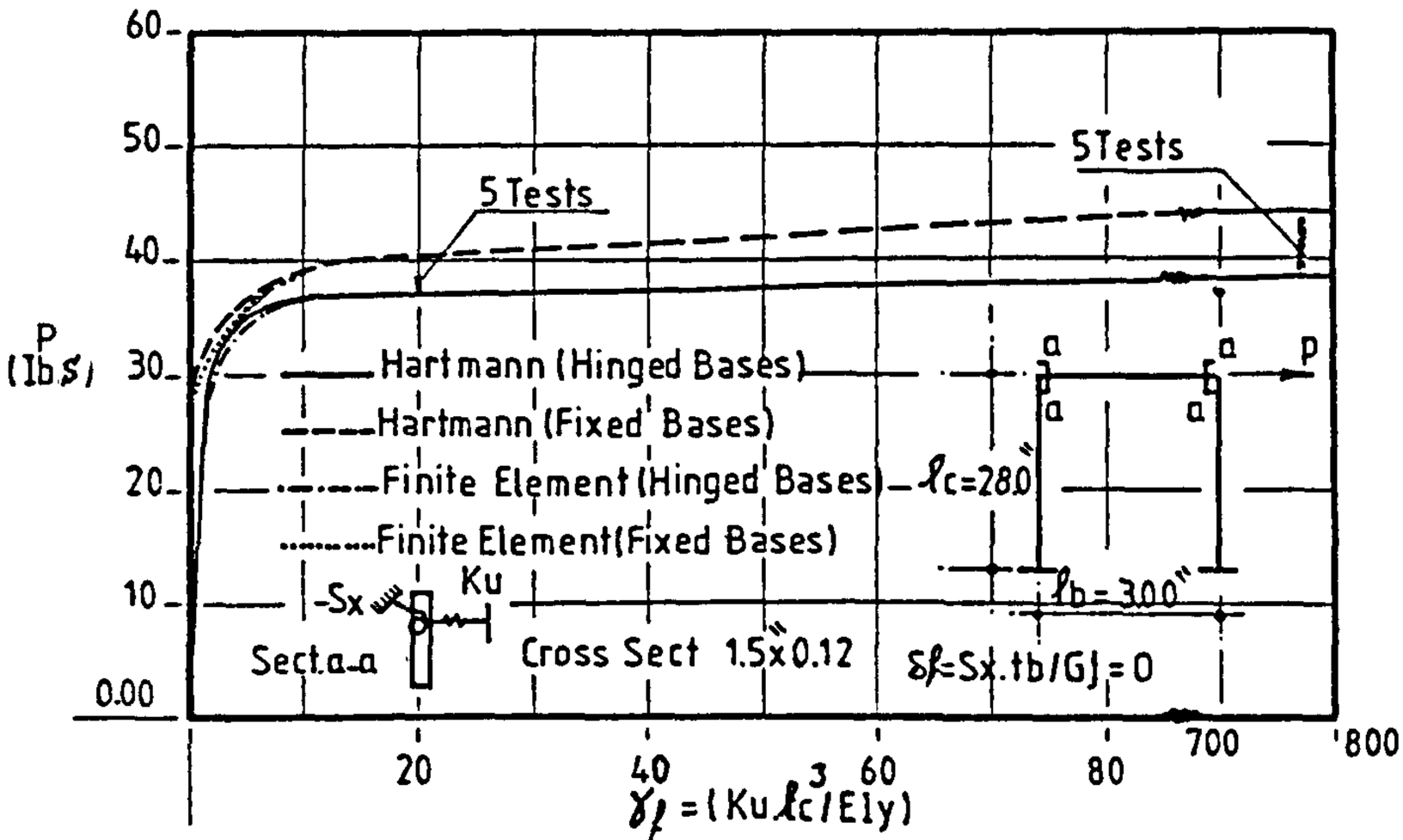

Fig.6.23 Effect Of Axial Stiffness Of Knee Bracing On Buckling Load Of Frame (Comparsion Between The Finite Element And Ref. 55)
No Of Elements Taken = 12

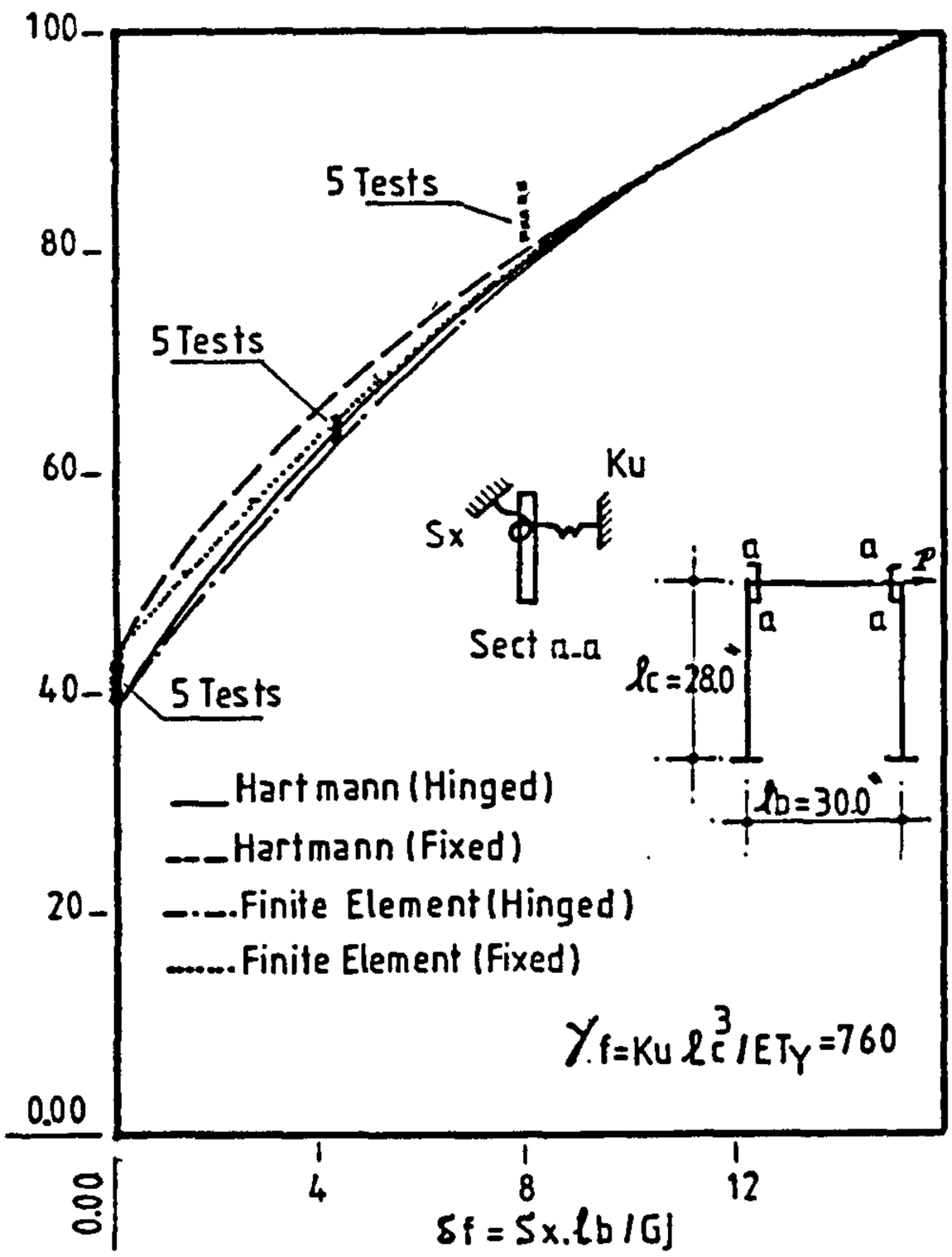

Fig.6.24 Effect Of Torsional Stiffness Of Knee Bracing On The Buck.Load
(Comparison Between The Finite Element And Ref.55)
No Of Elements Taken = 12

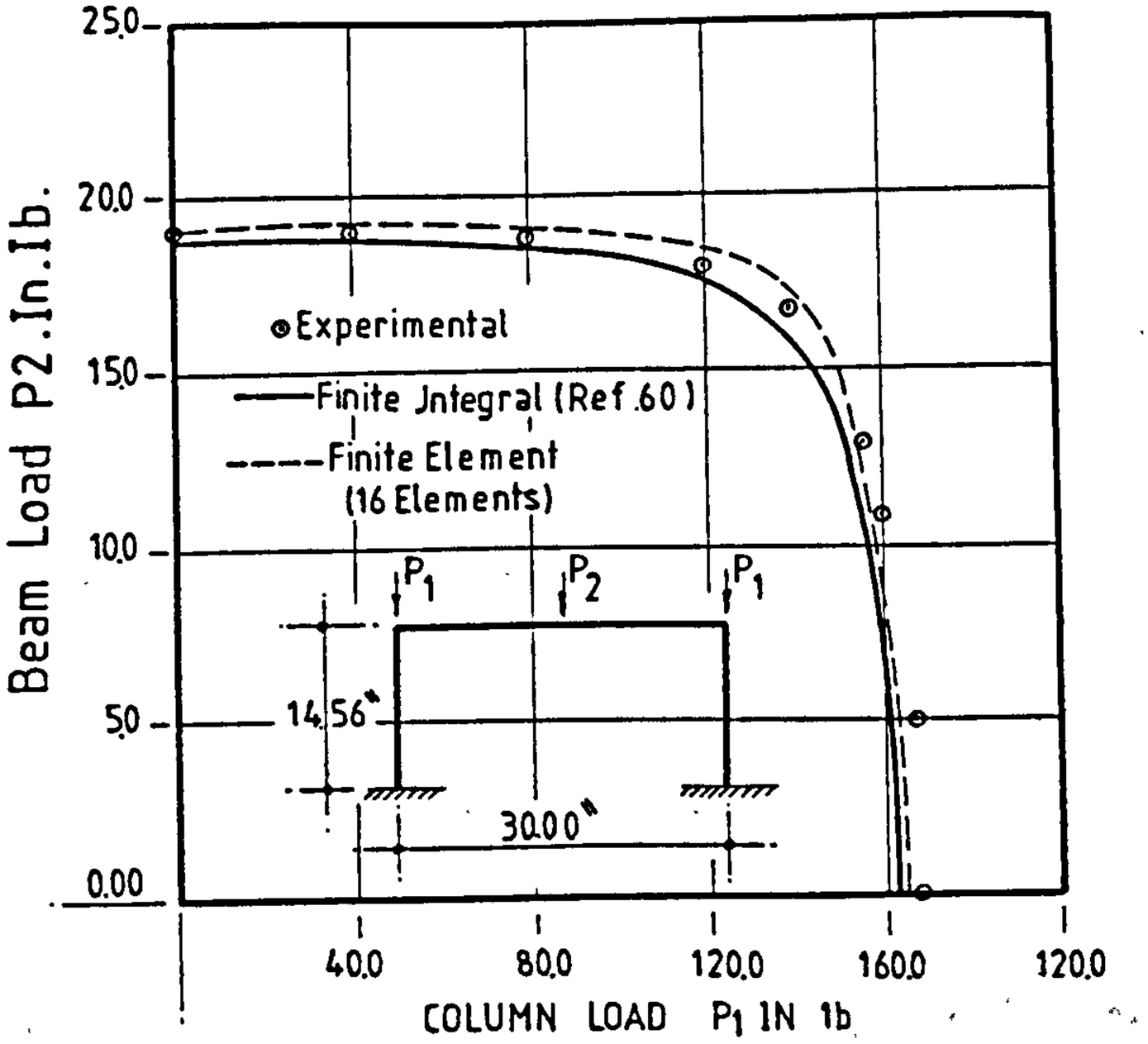

Fig.6.25 Interaction Buckling For Frame 1
In Ref 60

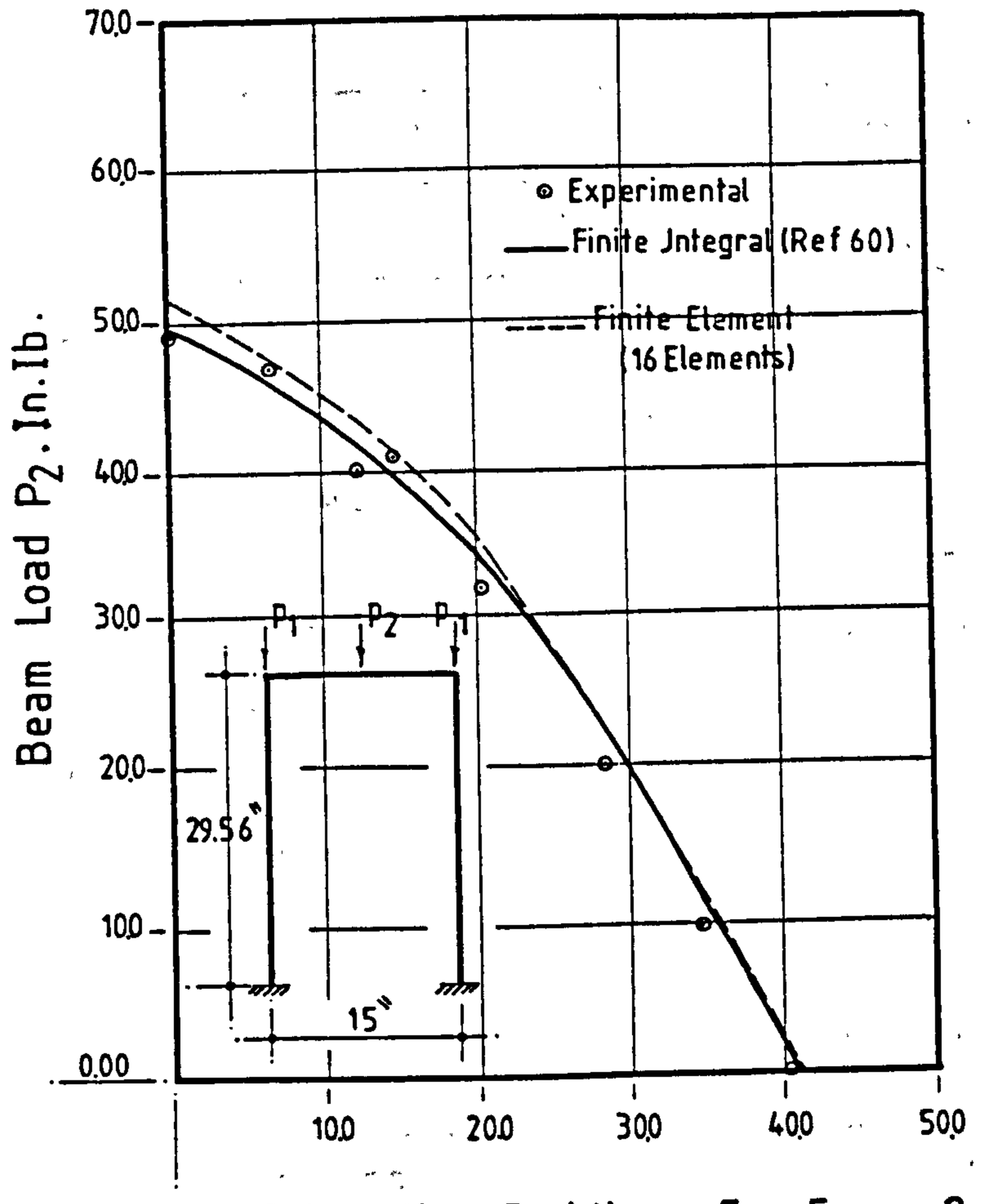

Fig.6.26 Interaction Buckling For Frame 2
In Ref 60

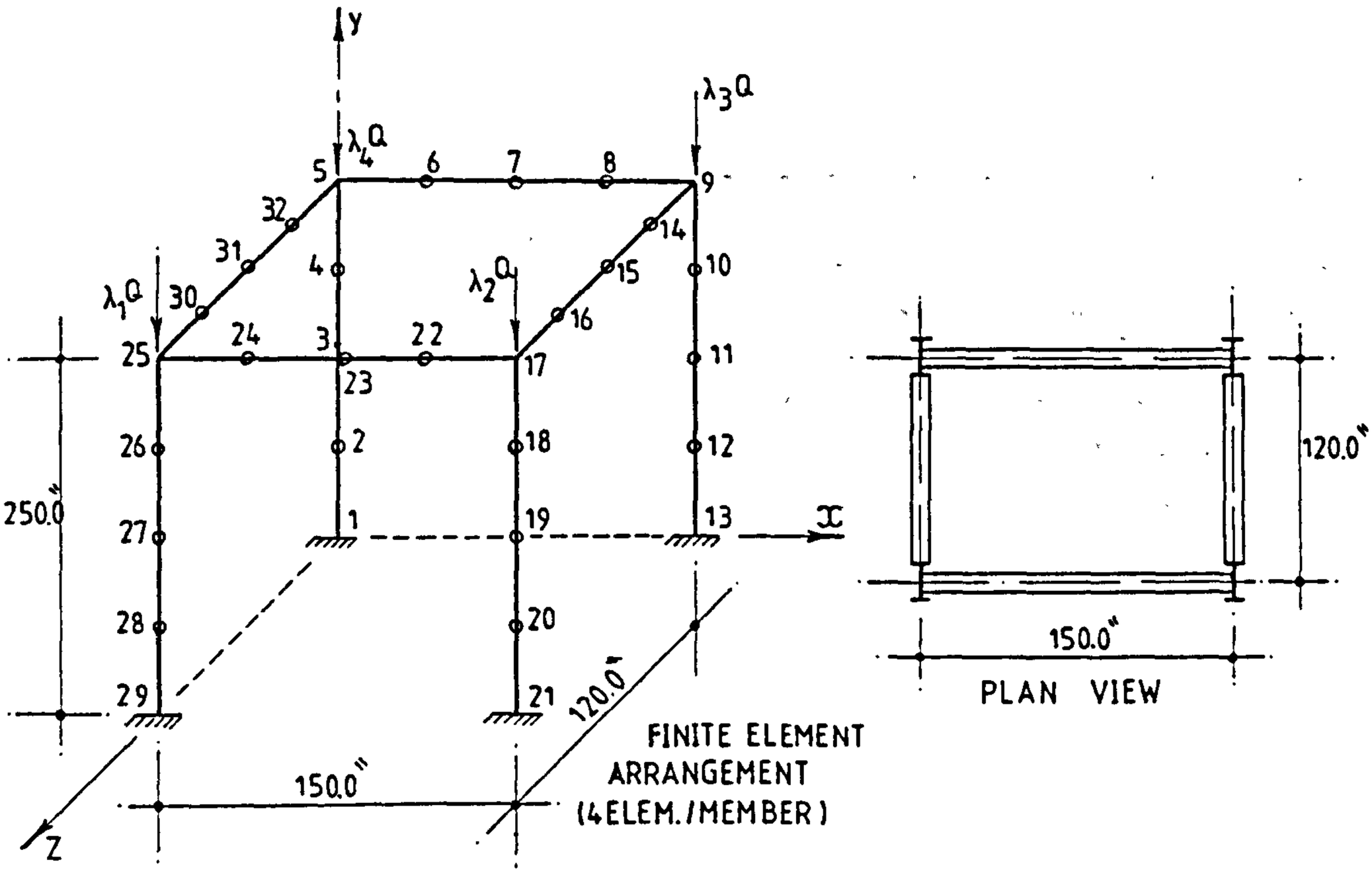

Fig.6.27 The Dimensions And Loading System Of The Frames Studied By Razzaq And Naim (11)

LOADING CASE	$\sum P$ IN KIPS REF-(11)	LOAD MULTIPLIC. FACTORS				FINITE ELEMENT SOLUTIONS		
		λ_1	λ_2	λ_3	λ_4	CRITICAL JOINT	CRITICAL Deg.Of Free	Critical Load Factor
A	601.0	1.0	1.005	1.0	1.0	16	U	1.0003
B	590.0	2.0	4.0	2.0	1.0	10	U	1.0004
C	520.0	1.0	0.005	—	—	24	W	0.9012
D	576.0	—	1.0	1.0	—	30	U	1.0190
E	590.0	1.0	0.005	1.005	—	18	U	1.0149
F	591.0	1.0	1.0	1.0	—	32	U	0.9824

Table.6.8 Finite Element Solutions For The Space Frames Studied By Razzaq And Naim (11)

NU OF ELEMEN PER MEMBER	1	2	3	4
FINITE ELEMENT SOLUTIONS	1.0160	1.008	1.0036	1.0003

Table.6.9 Convergence Of The Finite Element Solutions For The Space Frame Loaded With Case (a) Of Loading.

CHAPTER SEVEN

Second-Order Torsional-Flexural Behaviour of Z-Beams

7.1. INTRODUCTION

The validity and accuracy of the new finite element formulation of the second-order torsional-flexural behaviour of thin-walled members presented in this study has been examined by analysing a number of different stability problems as has been illustrated in chapter 6. However, the comparisons were limited to structures loaded with in-plane flexural loading only, where prebuckling deformations can be neglected. In each of the problems considered the cross-section of the structure members had at least one axis of symmetry.

The derivation of the stiffness and geometric matrices was based on the small deflection theory where the prebuckling deformations are ignored. In Z-beams, however, a transverse vertical load will have a lateral component in the plane of the maximum rigidity. This load component causes a comparatively large displacement component before buckling starts.

The geometric (stability) matrix, presented in chapter 3 contains new terms representing the effect of sectorial monosymmetry for cross-sections with no axis of symmetry. This effect results from the longitudinal stresses caused by the warping moments (bimoments) and is given in terms of the sectorial cross-sectional property β_ω. This coefficient can be calculate using equation 3.32.

The study reported in this chapter was undertaken to obtain quantitative information on the second-order and stability behaviour of Z-beams under combined bending and torsion. A test program was undertaken and the results are compared with the finite element solutions. Two types of theoretical analyses were performed. The effect of sectorial monosymmetry was not included in the first solution, while this effect was considered in the second analysis.

7.2. TEST PROGRAM

The test program consisted of a series of five tests. The tested beams were of the same type and cross-sectional dimensions as the simply supported Z-beams used for the bimoment tests reported in chapter 5. The details of the cross-section are shown in fig. 5.6.

The first two beams had a span of 3.0 m, while in the other three tests, the span was equal to 2.0 m. Each beam was loaded with two equal point loads applied to the beam at the quarter and three quarter points by means of hangers. Loading arrangements in each of the five tests are shown in fig. 7.1.

The test rig shown in fig. 5.8 and 5.9 was used to simulate the required end conditions of the tested beams. These end conditions were identical to those of the tests reported in chapter 5. A full description of these end conditions is given in section 5.3.3.

Static loads were applied incrementally to the beam while the horizontal displacements of the flanges of the beam were measured at the quarter, half, and three-quarter points. At each cross-section, the angle of twist was calculated from the difference of the lateral displacements between the top and bottom ends of the web. Vertical deflections were measured at the mid-span cross-section. Locations of the 26 dial gauges used for the displacement measurements are shown in fig. 7.2.

7.3. TESTING PROCEDURE

During the first test (B - 1) dead weights were applied to the top flange of the beam by means of two hangers. Load increments were kept small. The support movements were measured after each load increment.

The test rig was designed to simulate the end conditions of free warping and fully restrained twist. During the test, however, it was noticed that the 'L' brackets, which were connected to the flanges at the theoretical point

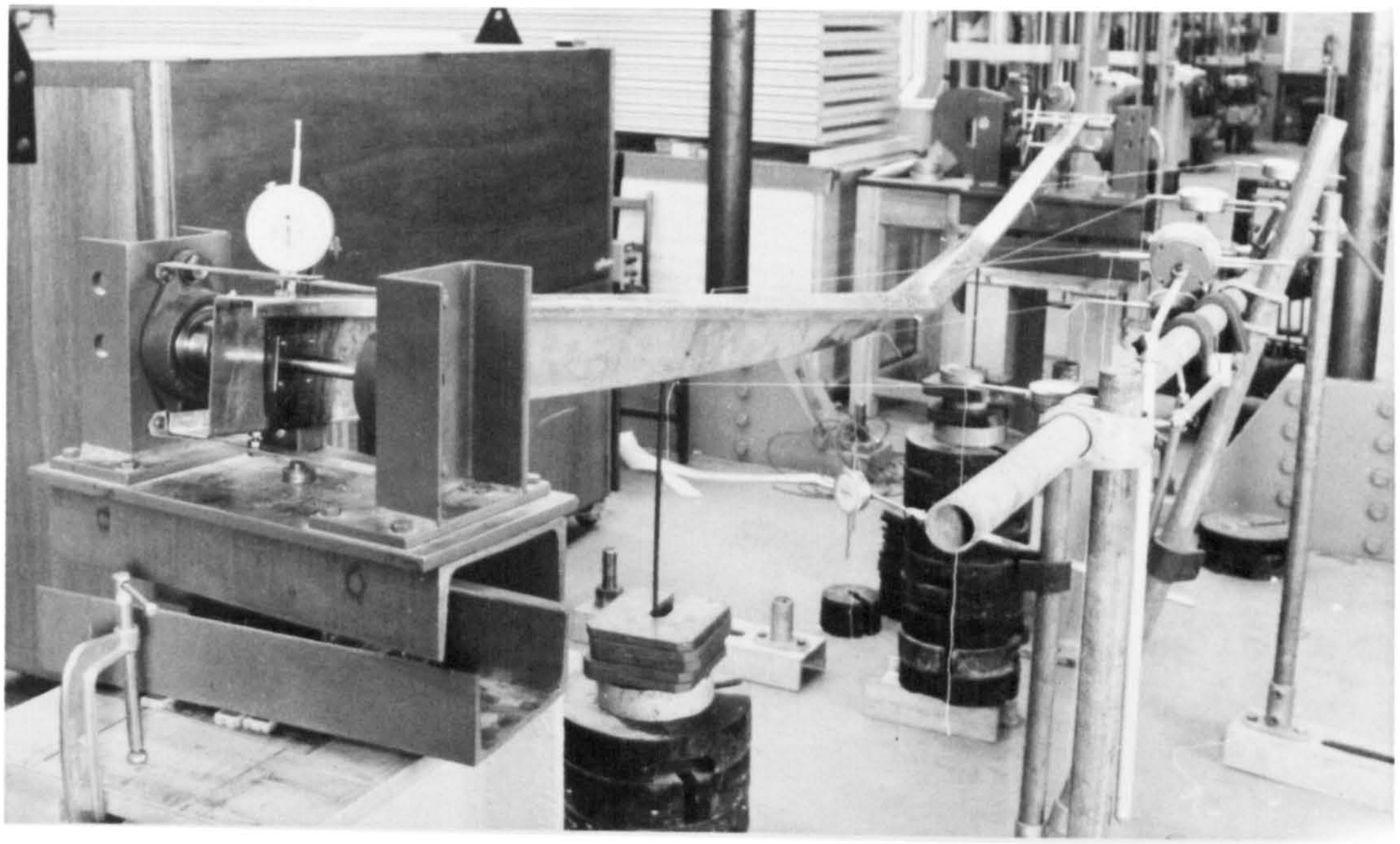

Plate 7.I Beam B-2 at the moment of failure

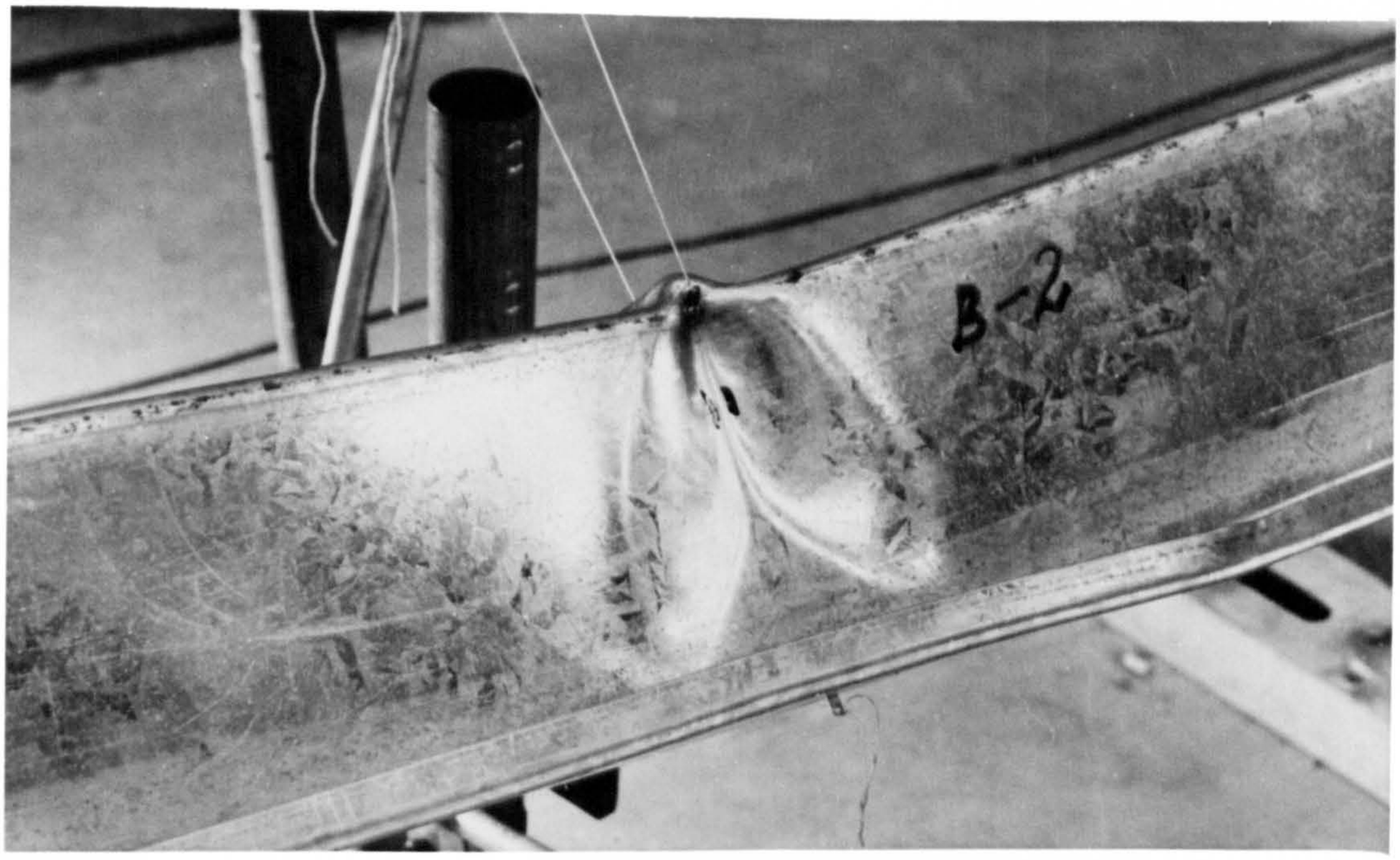

Plate 7.2 Web and flange failure of beam B-2

of zero warping (fig. 5.9), were loose allowing for slight twisting at the supports. In order to prevent this twisting, the connections of the 'L' brackets with the flanges of the Z-beam were made sufficiently stiff by using two nuts for each flange to L-bracket connection and carefully tightening these nuts. The check showed that these arrangements successfully prevented the web from twisting. Nevertheless, these stiffening arrangements imposed a noticeable restraint for the warping of the flanges. It was then decided to continue the test program with the same rig and to compare the results with the theoretical solutions of the two limiting conditions, namely, a) end warping free, and b) end warping restrained.

All beams were tested up to failure. In each of the five conducted tests, overall buckling started first followed by a complete collapse of the mid-span cross-section. Failure shapes of beams B - 2 and B - 3 are shown in plates 7.1 - 7.4.

7.4. DISCUSSION OF THE RESULTS

After each load increment, the deflection at each dial gauge was recorded. The vertical and horizontal displacements of the web were resolved into components in the directions of the two principal axes of the Z-cross-section. Horizontal movements at the top and bottom ends of the web were used to evaluate the angle of twist at the corresponding cross-section. Experimental displacements are compared with the corresponding theoretical values. As previously mentioned, the theoretical analysis was done twice, firstly by neglecting the effect of the bimoment. The calculations were repeated taking into account the new geometric matrix terms which reflect the effect of the longitudinal stresses caused by the bimoment.

The study presented in chapter 5 of this thesis has proved that the accuracy of the finite element calculation of the bimoments is excellent. For calculating the potential energy of the bimoment, the integration of eq. 3.46 was carried out numerically using the subroutine BIMOM which is given in appendix A.3.1. Values of the coefficients resulting

from the integration, K_{b1}, K_{b2}, ... , and K_{t4}, depend on the ratio $k\ell$, where $k = \sqrt{GJ/EI_\omega}$ and ℓ is the span of the beam.

Fig. 7.3, 7.4, and 7.5 show the comparison of the displacements for beam B - 1. In comparison to the theoretical results, the experimental values of the displacements lay between the results of the free end warping model and those of the fully restrained end warping model. However, the value of the horizontal displacement of the shear center are closer to the results of the fully restrained warping model. Including the effect of bimoment did not affect the results of the fully restrained end warping model. The bimoment stresses, however, increase the displacements calculated using the free end warping model.

The theoretical and experimental results of beam B - 2 are given in fig. 7.6, 7.7, and 7.8. In this loading case the effect of bimoment stresses is very small and does not change the values of the calculated displacements. Fig. 7.8 shows the comparison of the angle of twist. It can be seen that up to a load of 0.75 kN per hanger, the theoretical results of the angle of twist θ_x, calculated using the free end warping model, are very close to the test values. With increasing load the angle of twist θ_x starts to change direction and the difference between the theoretical and experimental results begins to increase. This difference could be due to the large displacements exhibited by the beam at high load levels which makes the small deflection theory insufficient to deal with this type of problems.

In the other three tests (B - 3, 4, 5) loads were applied at the bottom flange level. The $k\ell$ value of these beams is equal to 1.04 which is almost 2/3 of the $k\ell$ value of the 3.0 m span beam (B - 1, 2). Thus the coefficient K_{b1}, K_{b2}, ..., K_{t4} have bigger values in comparison with the coefficients of the 3.0 m span beams.

The results of tests B - 3, B - 4 and B - 5 are shown in fig. 7.9 - 7.17. It can be seen that the effect of

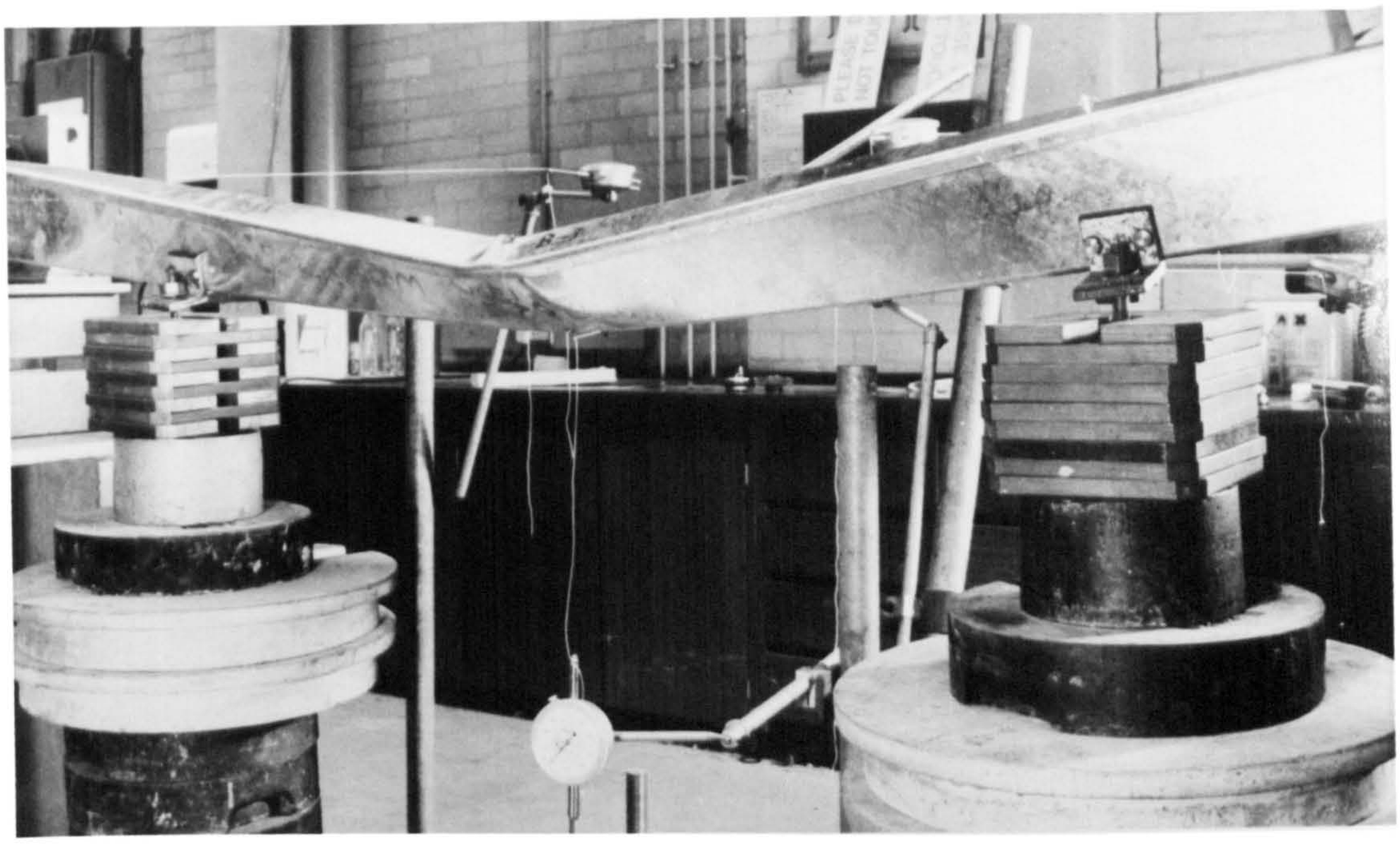

Plate 7.3 Beam B-3 at the moment of failure

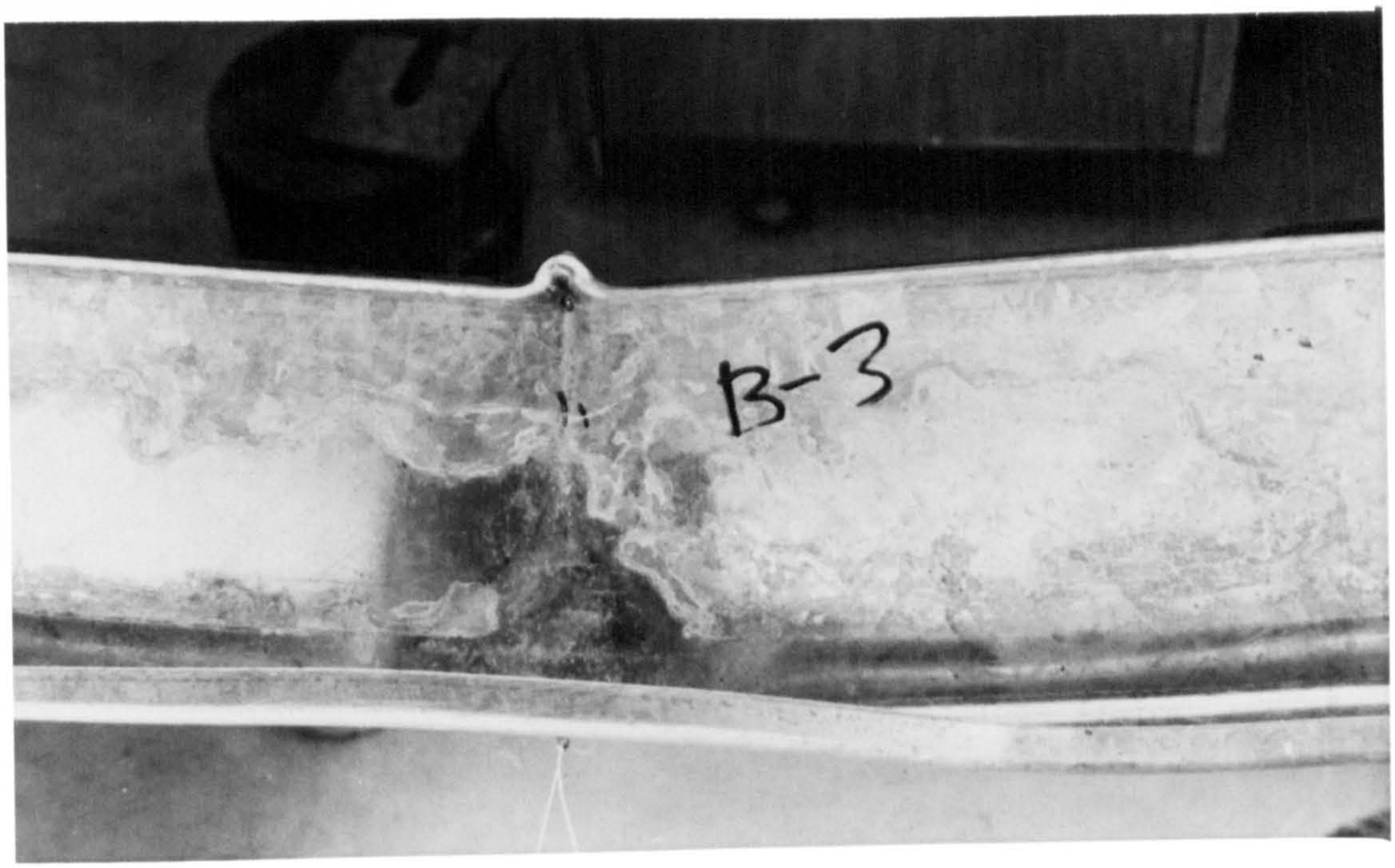

Plate 7.4 Web and flange failure of beam B-3

bimoment stresses is greater in these three tests in comparison with the previous two tests. Nevertheless, this effect is limited to the results of the free end warping model.

Fig. 7.17 shows the comparison of the angle of twist θ_x for beam B - 5 . The agreement between the theoretical and test results is good up to a load of 0.50 kN per hanger. At load levels higher than 0.50 kN, the theoretical model gives underestimated values for the angle of twist θ_x. The difference between the theoretical and test results increases with the increase of the applied load. Again, this difference may be due to the large displacements exhibited by the beam at high load levels which makes the small deflection theory insufficient to solve this problem.

Table 7.1 presents the comparison between the theoretical predictions of overall buckling loads and the actual failure loads of beams B - 1 —— B - 5. For the first two beams, B - 1 and B - 2, the theoretical buckling loads of the free end warping model are close to the actual failure loads. The theoretical loads are higher by almost 6.0 per cent for beam B - 1 and by almost 22.0 per cent for beam B - 2. For the rest of the beams the theoretical models give highly overestimated values of the buckling load. That may be due to the large displacements which took place in the prebuckling stage.

7.5. CONCLUSIONS

A number of important conclusions can be drawn from the discussion in section 7.4:

1. The effect of the bimoment stresses is dependent on the beam property $k\ell$, where $k = \sqrt{GJ/EI_\omega}$. For the two values of $k\ell$ considered in the study ($k\ell$ = 1.56, 1.04) the effect of the bimoment stresses has been confined to the case of free warping at the supports. If the ends of the beam are fully restrained against warping, the effect of the bimoment stresses is very small and can be neglected.

2. The calculations of the buckling load have shown that the small displacement theory is not always sufficient to

deal with Z-beams subjected to combined bending and torsion. Under such loading the beam exhibits large displacements before it tends to buckle in a torsional-flexural mode.

3. The test rig was designed to simulate the boundary conditions of free end warping and full restraint against end twist. The warping conditions were not accurately simulated. The connection between the L-bracket and the flange of the beam slightly prevented the longitudinal movement of the flange changing the conditions of the supports to semi-restrained warping.

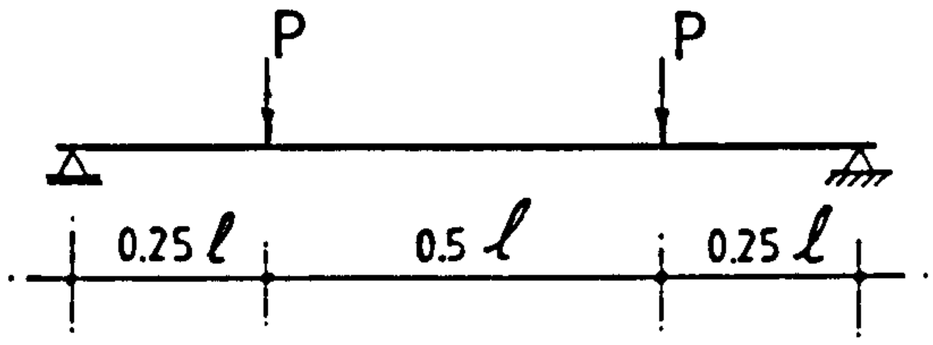

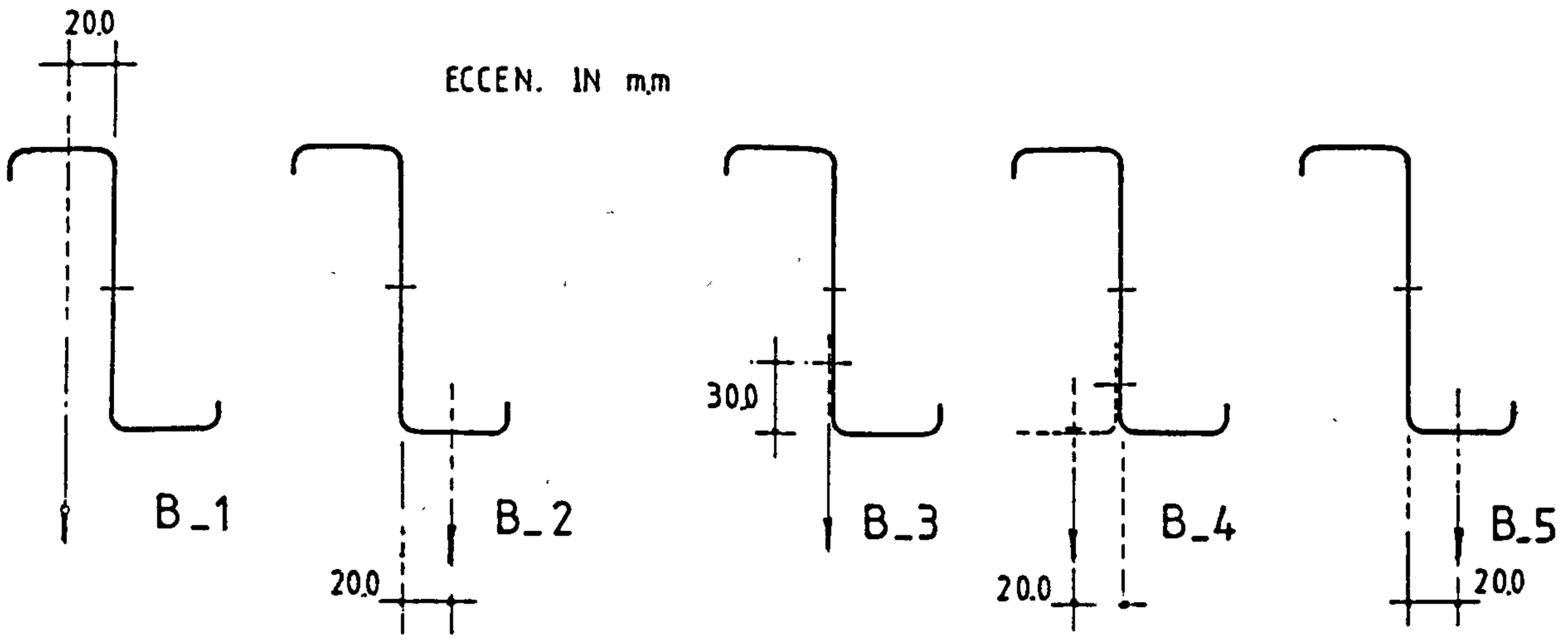

Fig.7.1 Loading Cases Of The Tested Beams

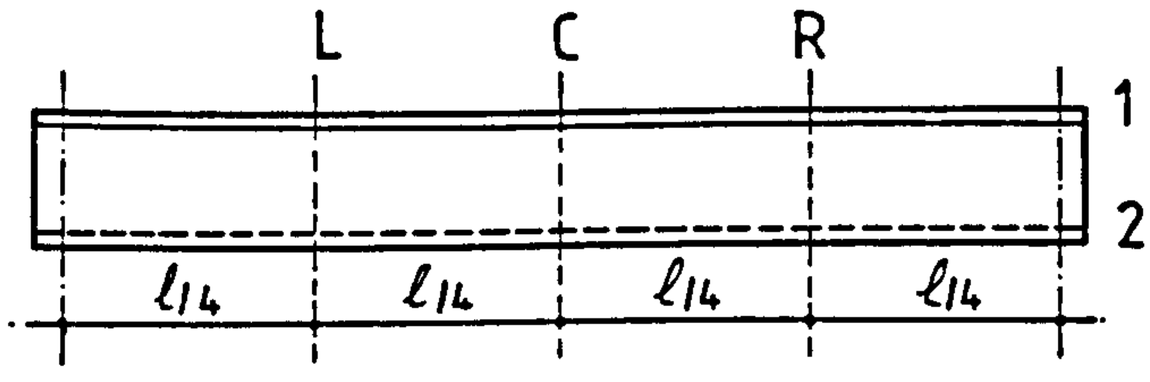

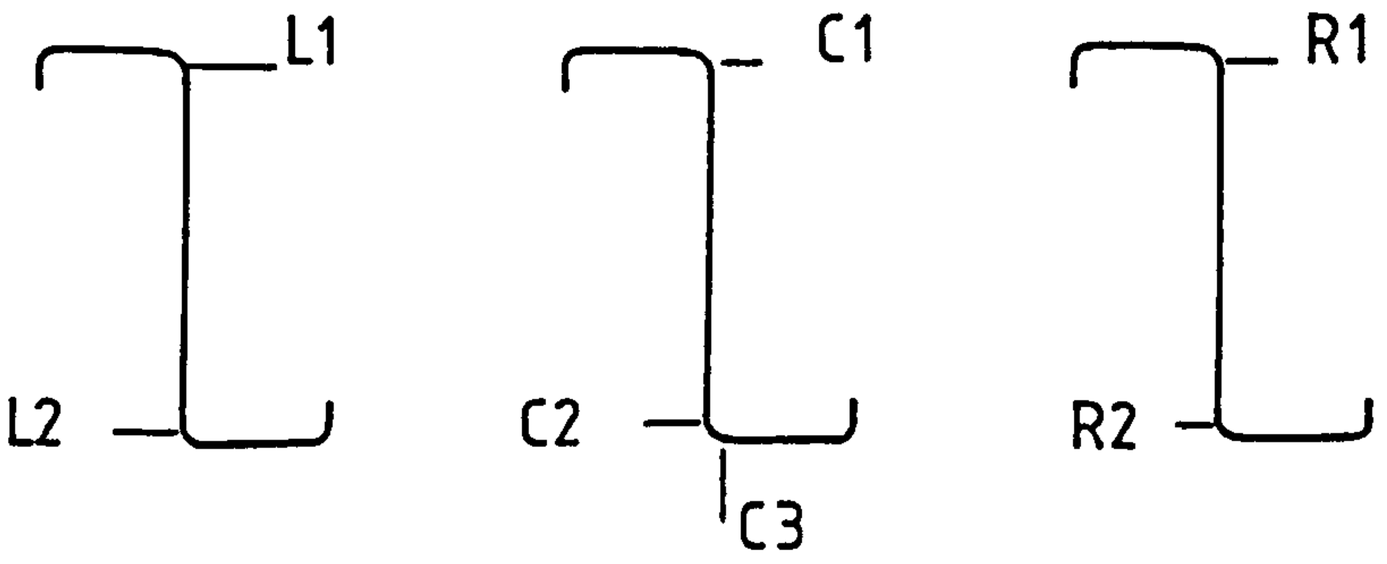

Fig.7.2 Locations Of The Dial Gauges

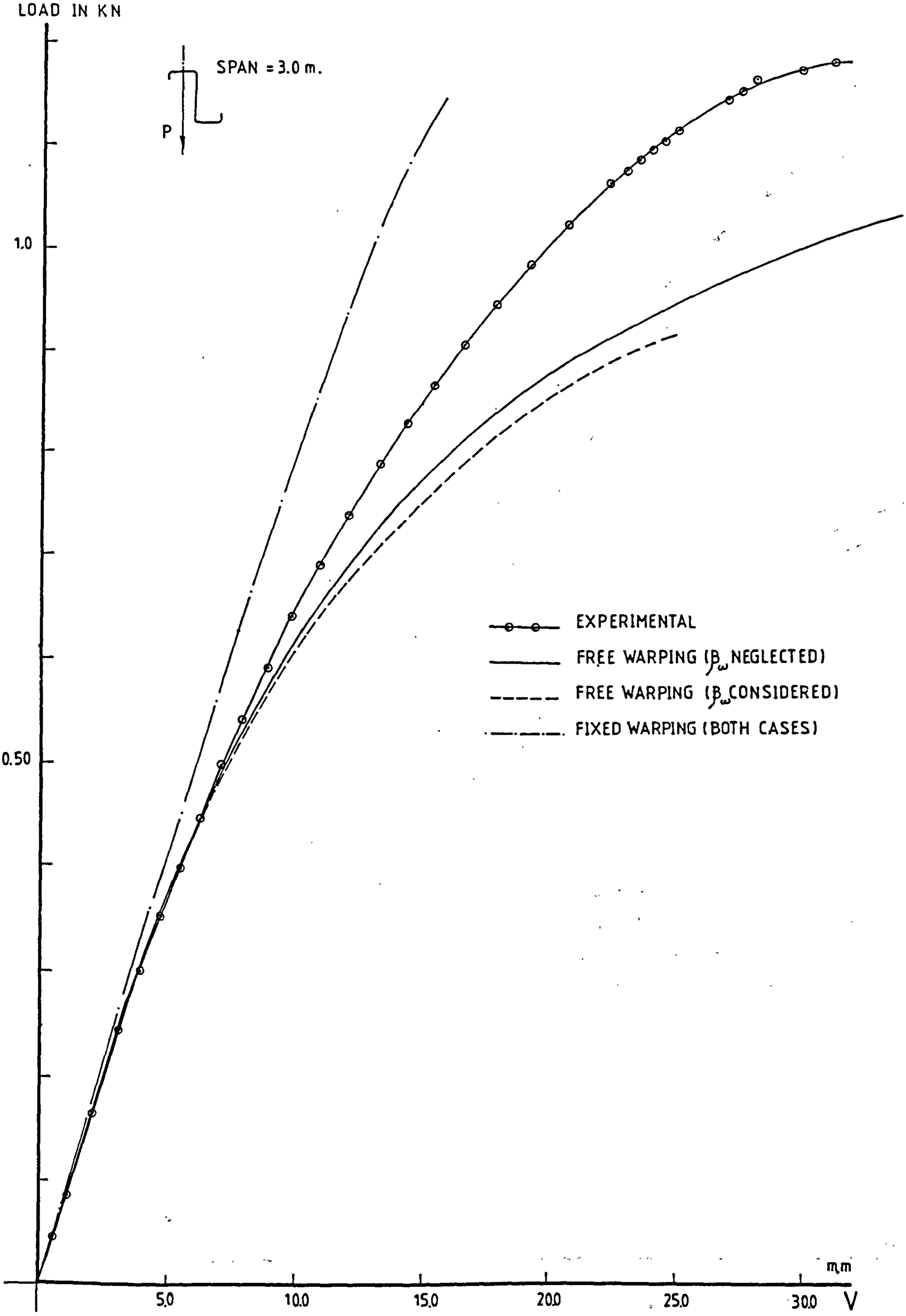

Fig.7.3 Test B_1 Vertical Deflection At Mid_Span

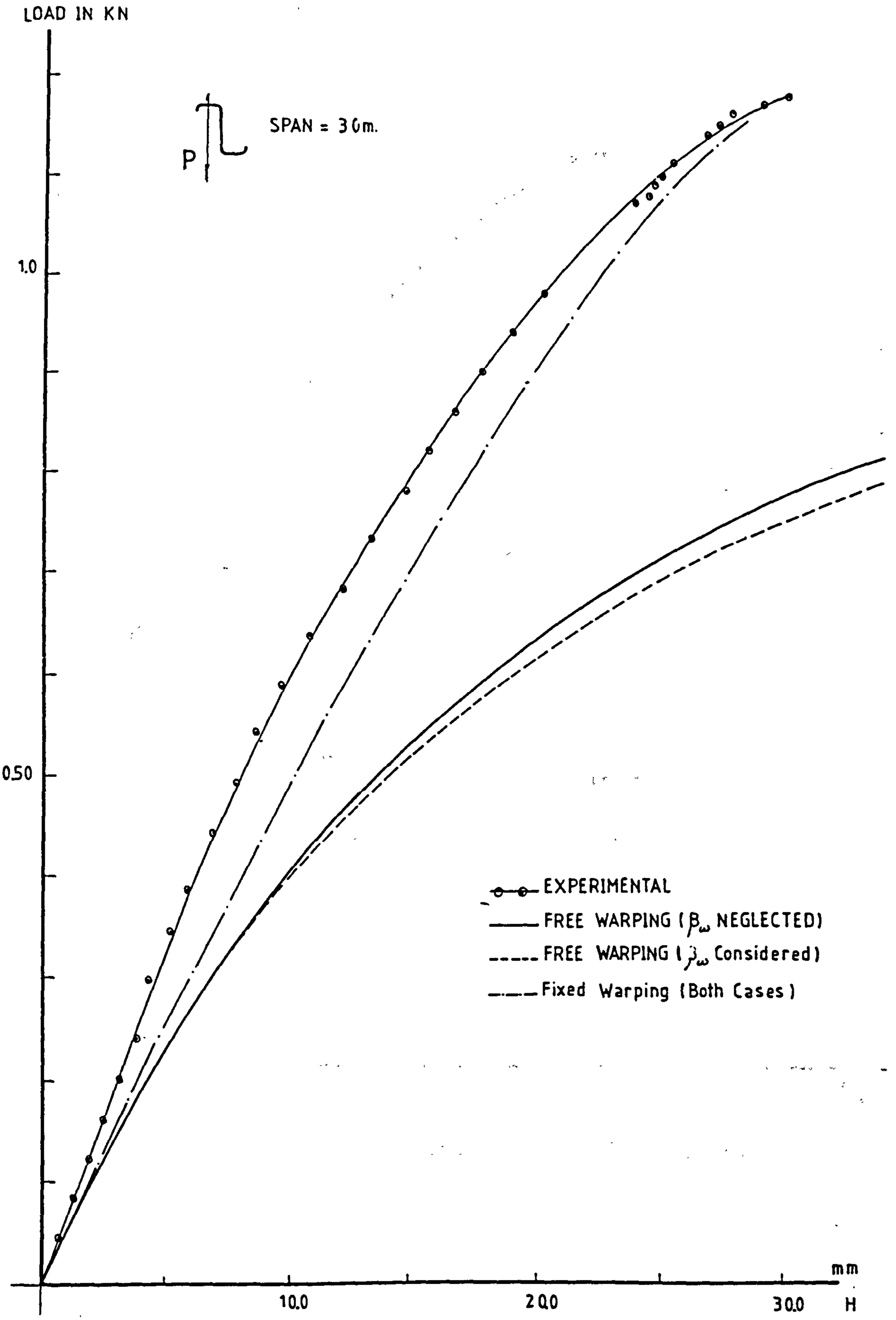

Fig. 7.4 Test B_1 Horizontal Movement At Mid_Span

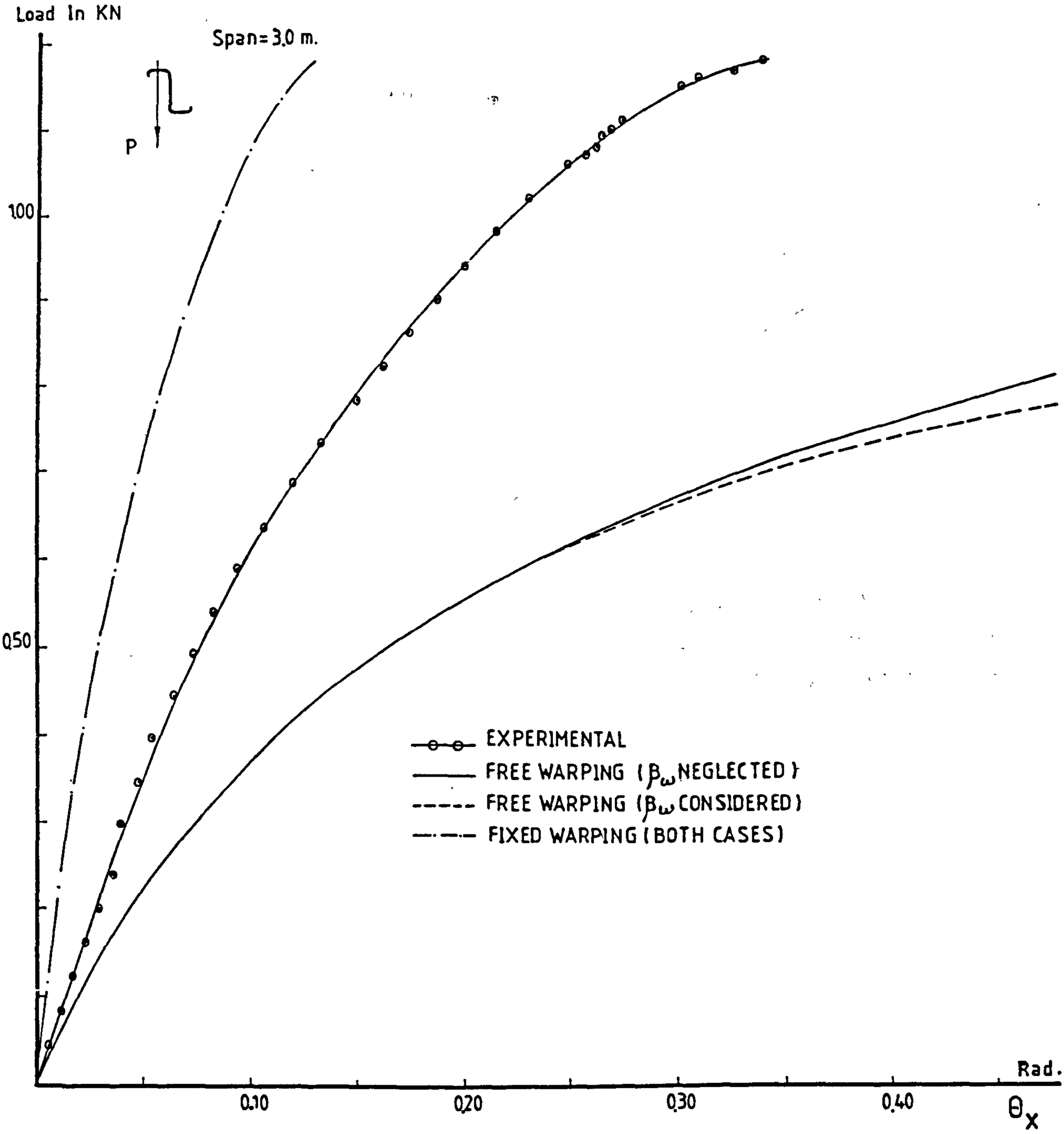

Fig. 7.5 Test B_1 Angle Of Twist At Mid-Span

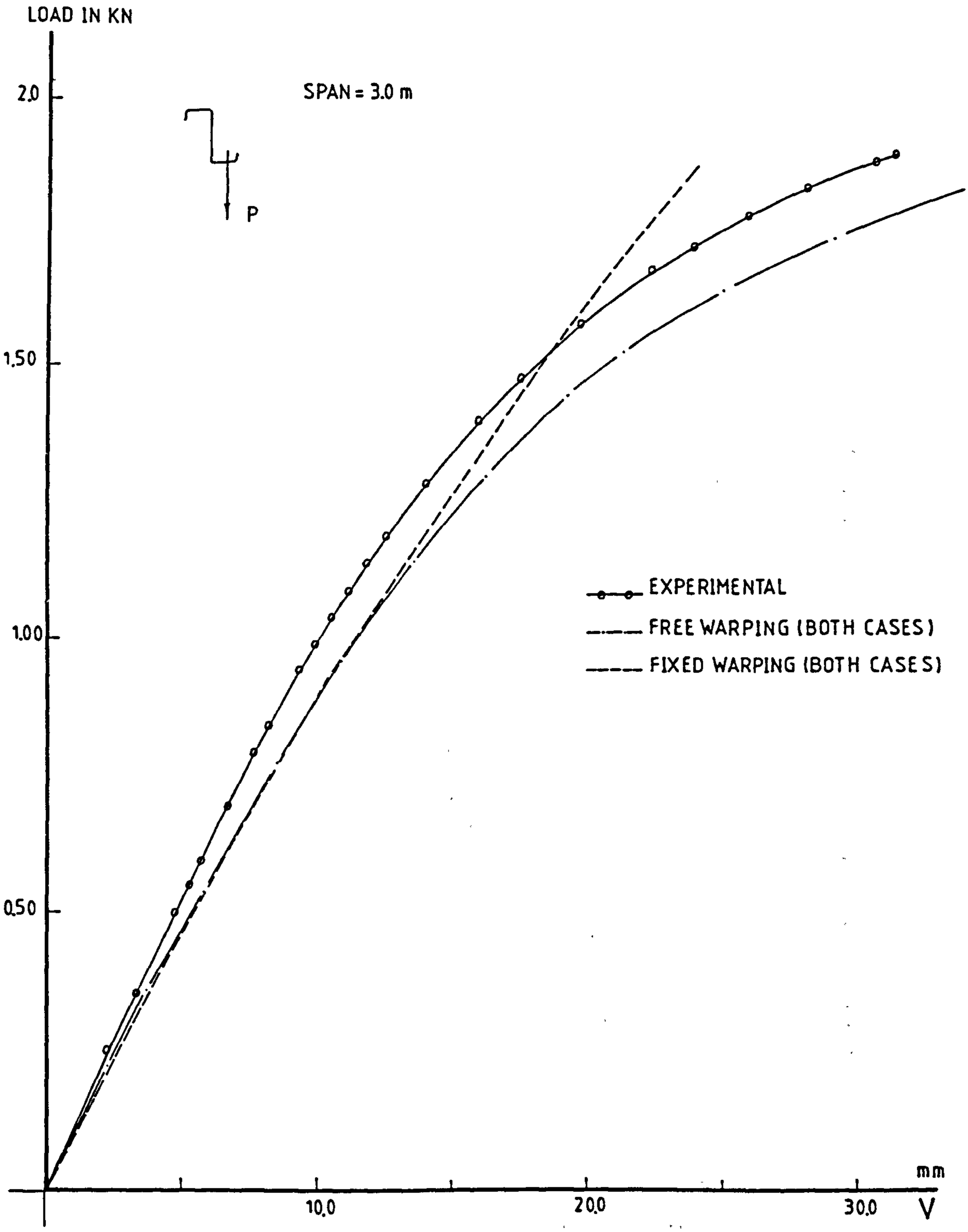

Fig. 7.6 Test B.2 Vertical Deflection AT Mid_Span

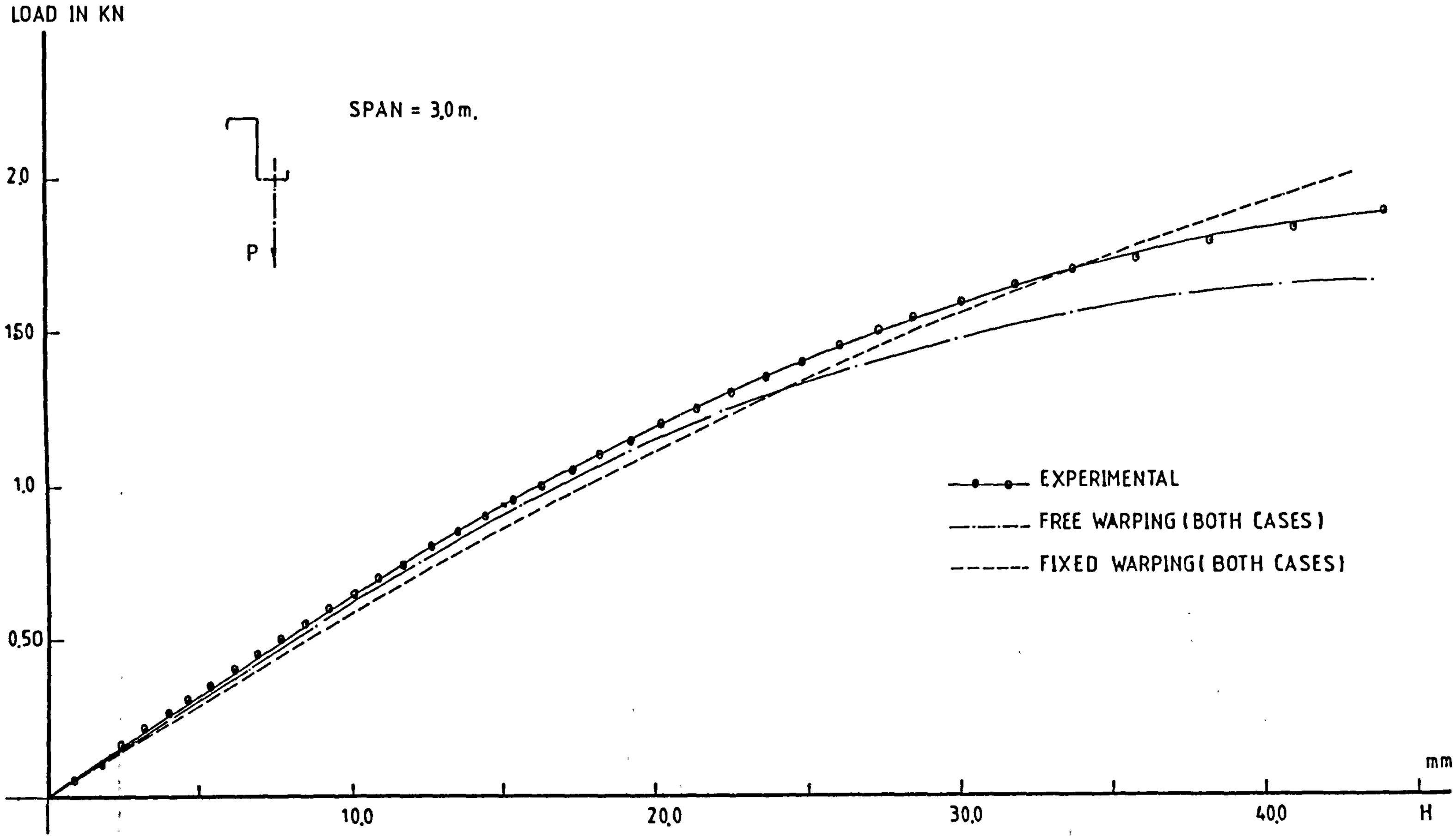

Fig. 7.7 Test B.2 Horizontal Movement At Mid-Span

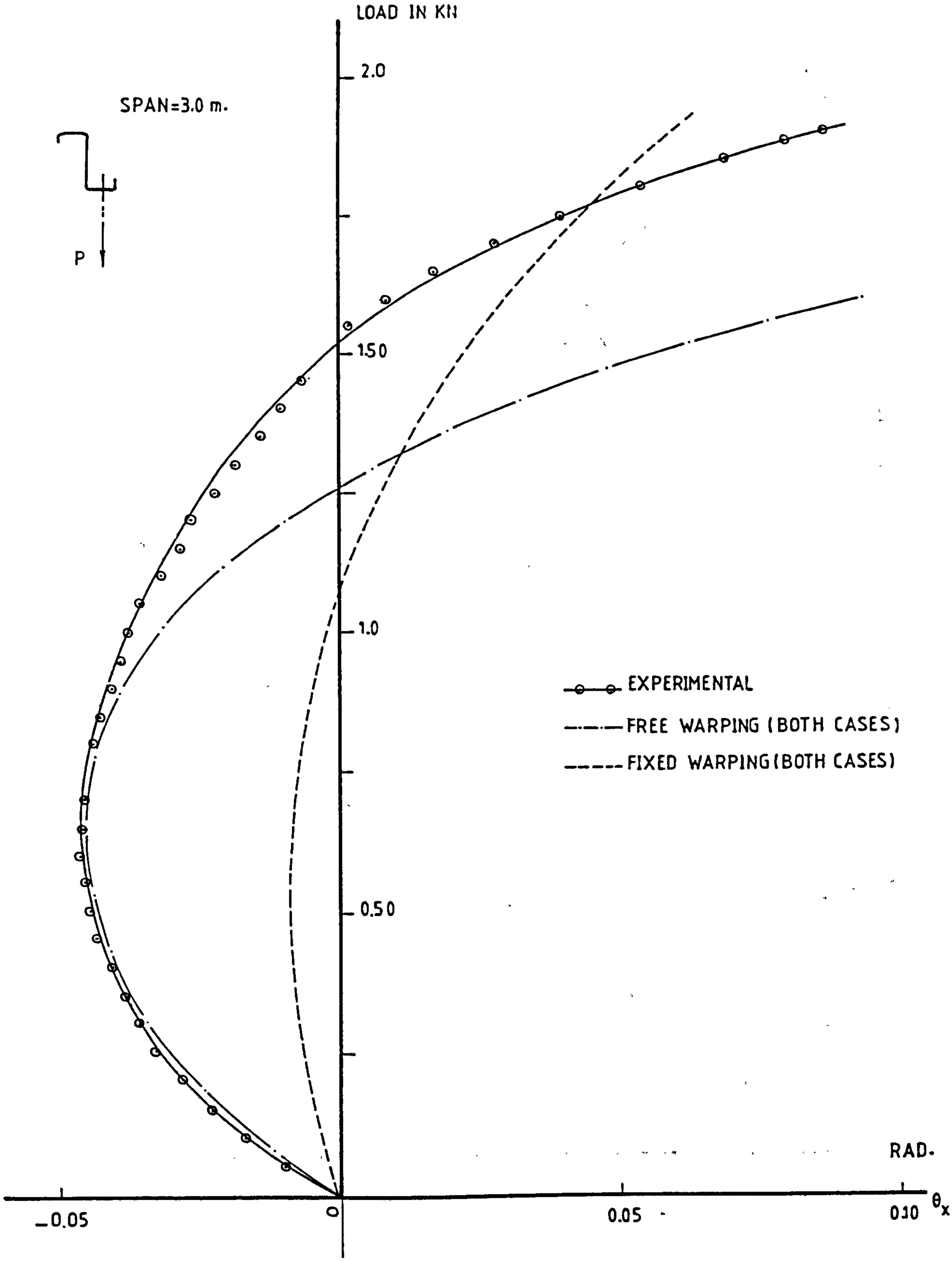

Fig.7.8 Test B_2 Angle Of Twist At Mid_Span

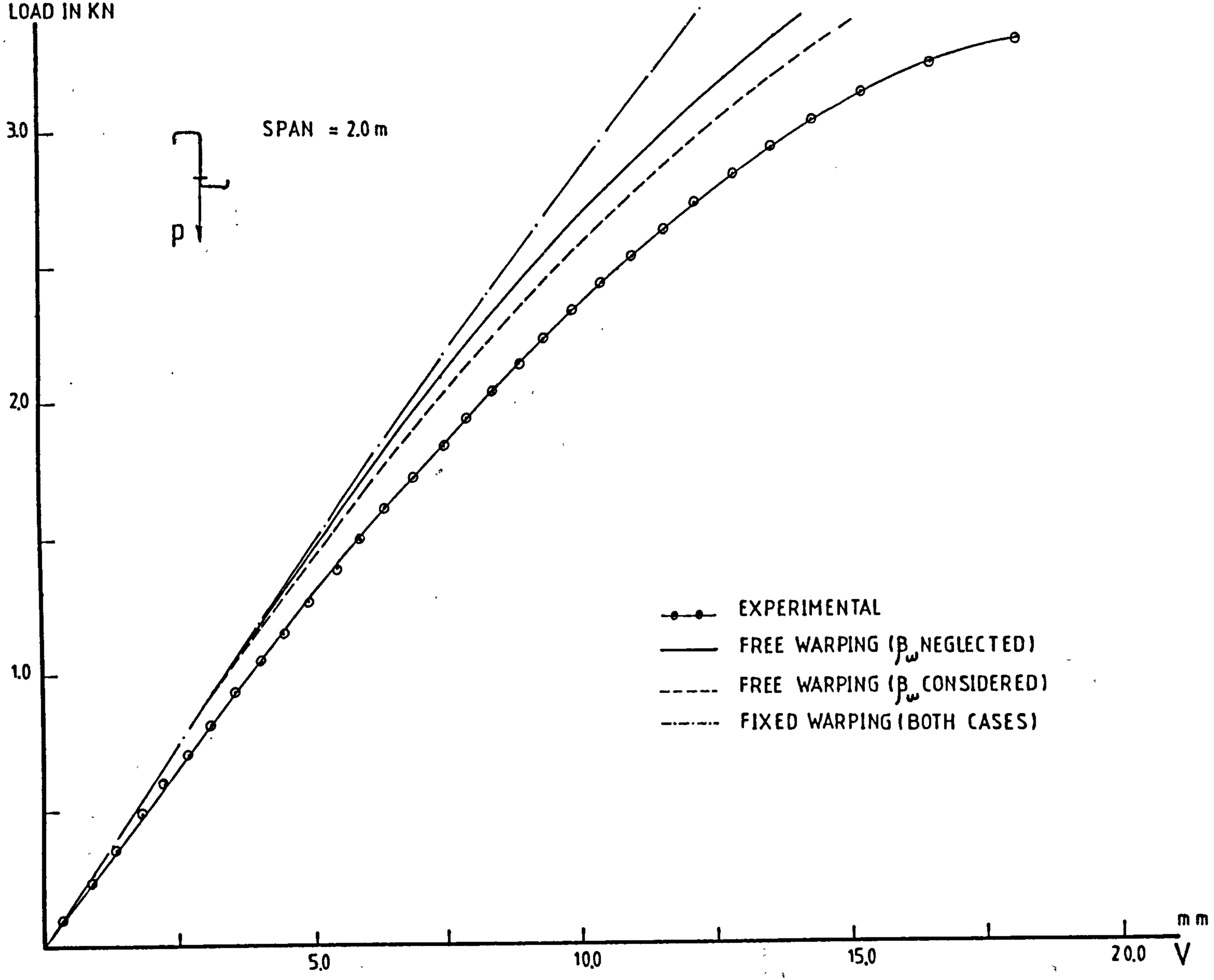

Fig. 7.9 Test B-3 Vertical Deflection At Mid-Span

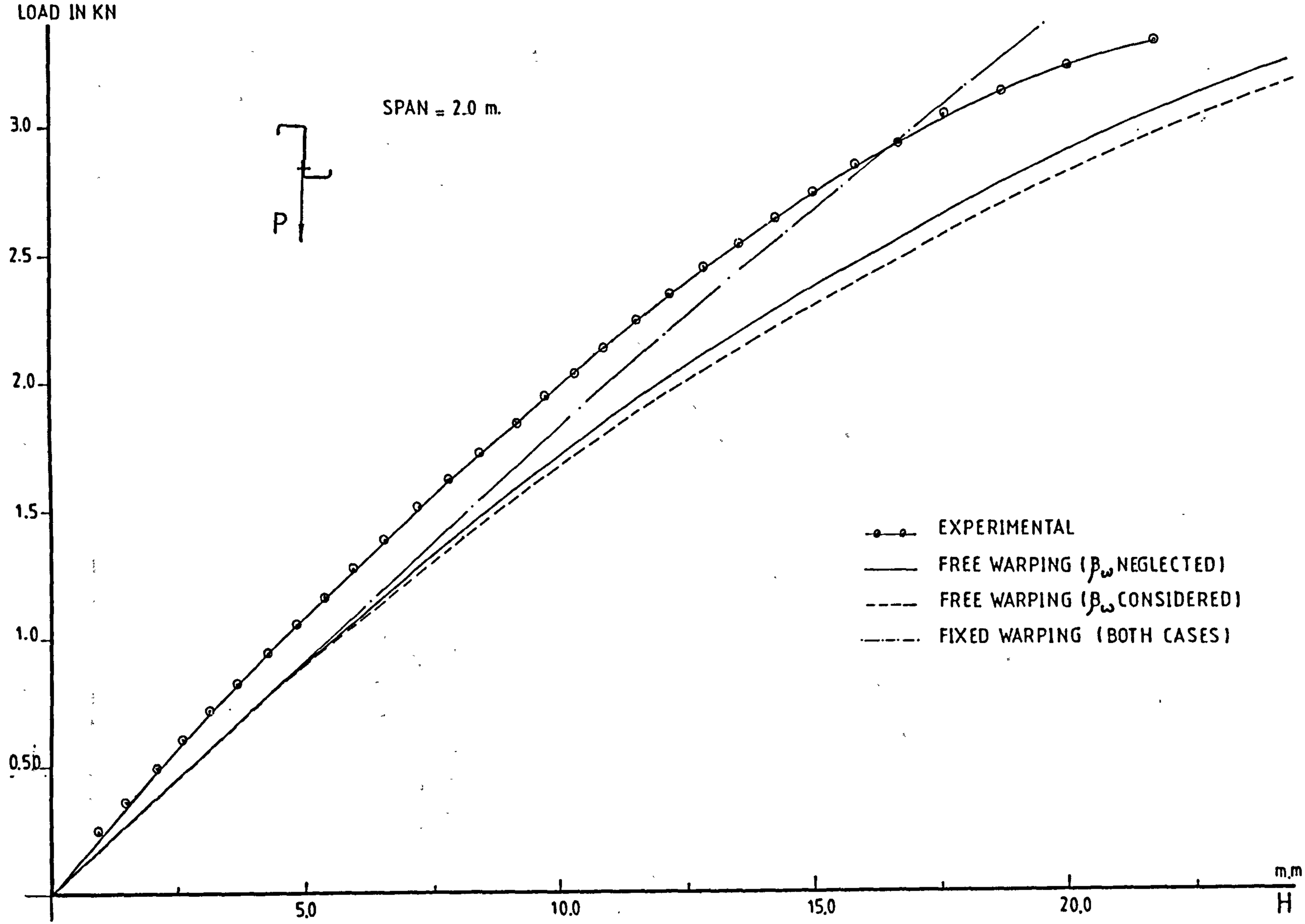

Fig. 7.10 Test B.3 Horizontal Movement At Mid-Span

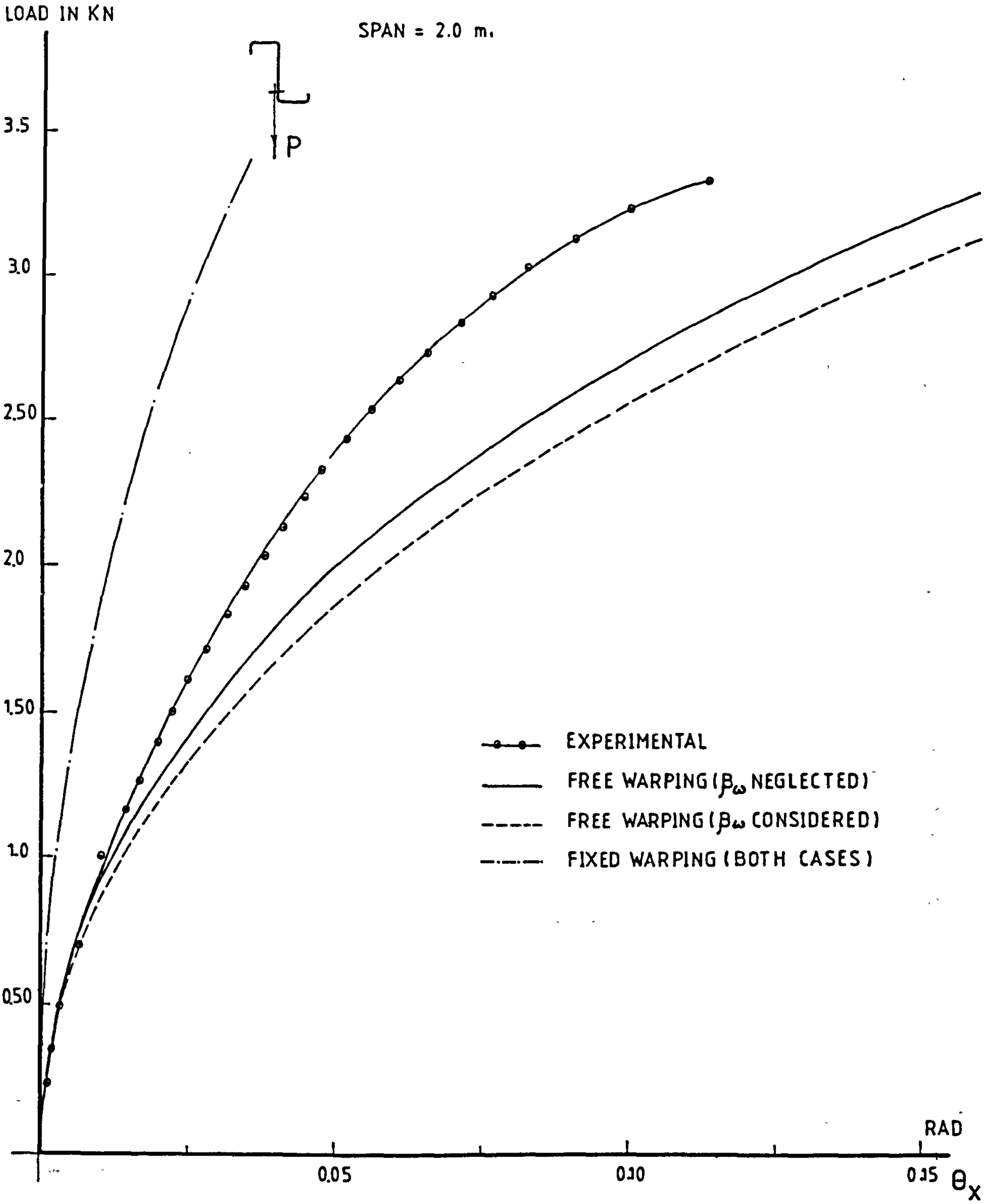

Fig. 7.11 Test B-3 Angle Of Twist At Mid-Span

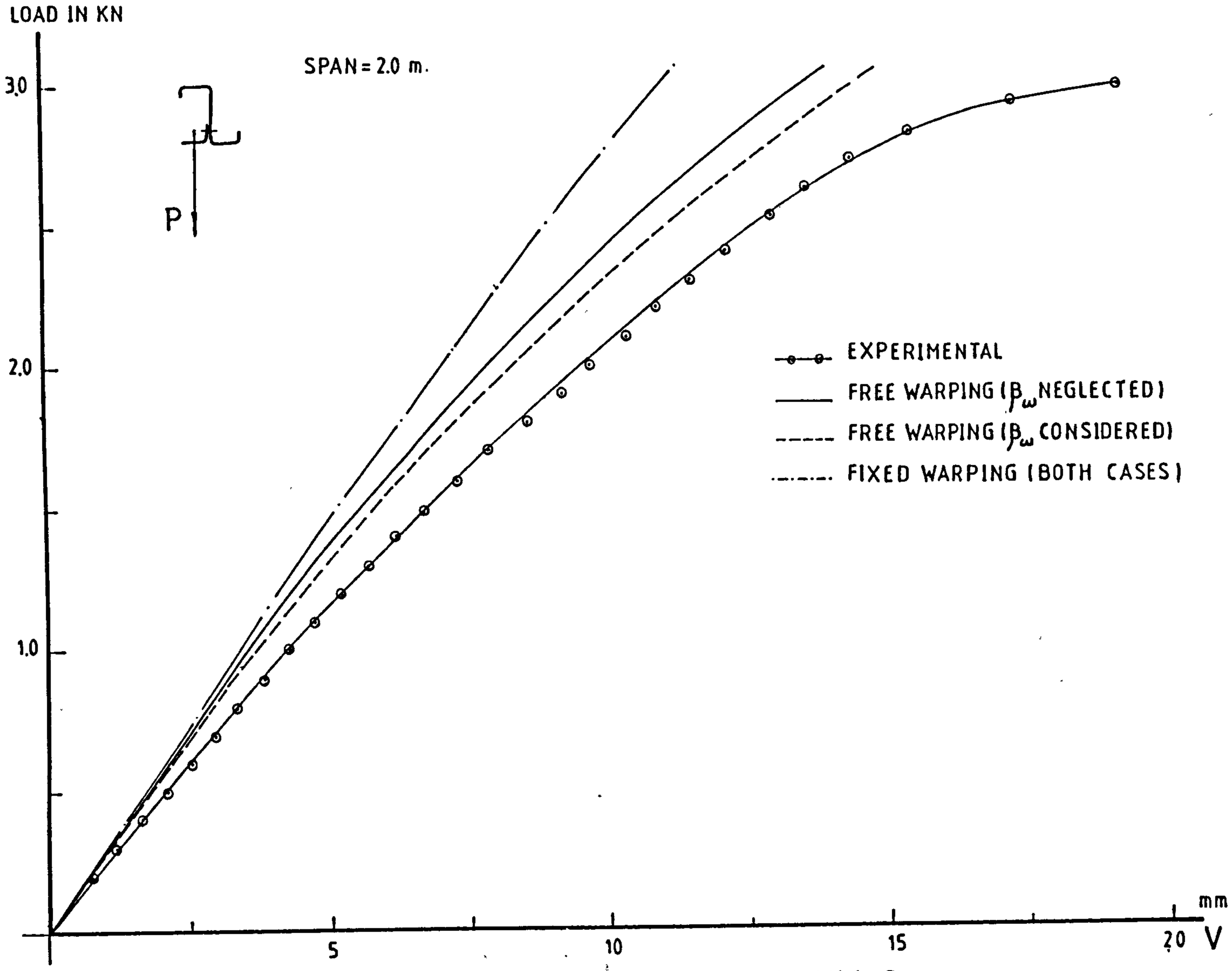

Fig. 7.12 Test B-4 Vertical Deflection At Mid-Span

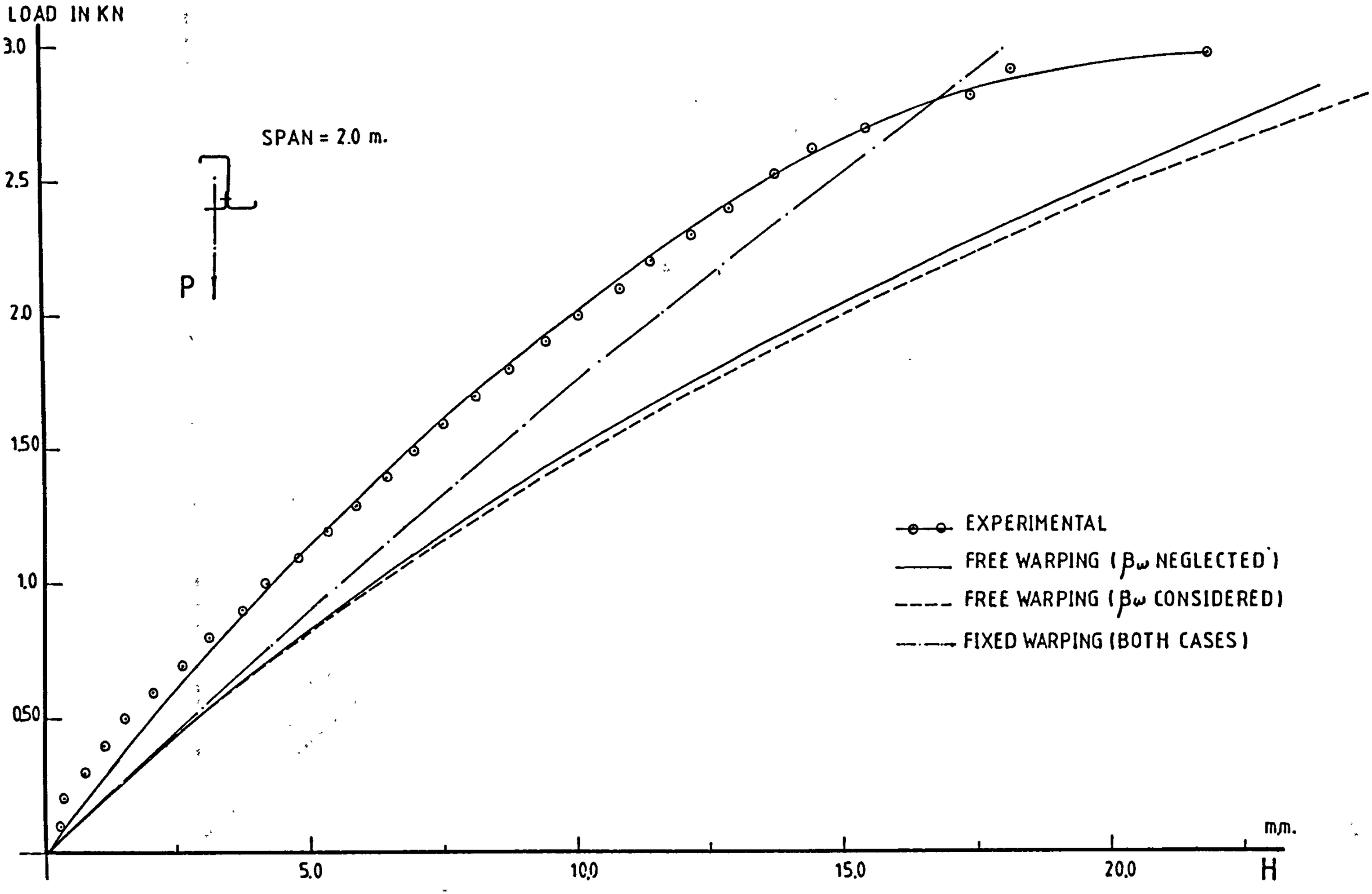

Fig.7.13 Test B-4 Horizontal Movement At Mid-Span

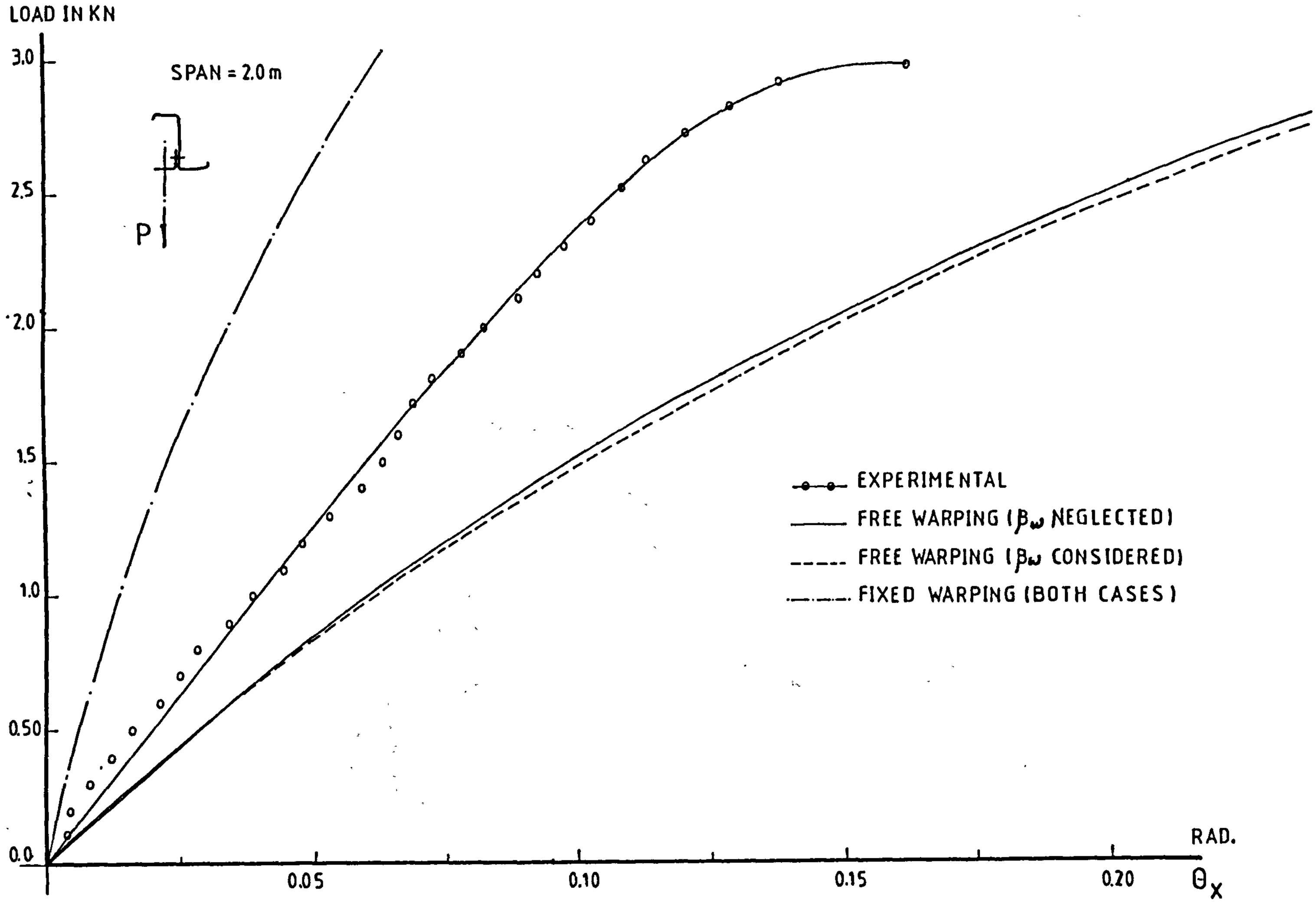

Fig. 7.14 Test B-4 Angle Of Twist At Mid Span

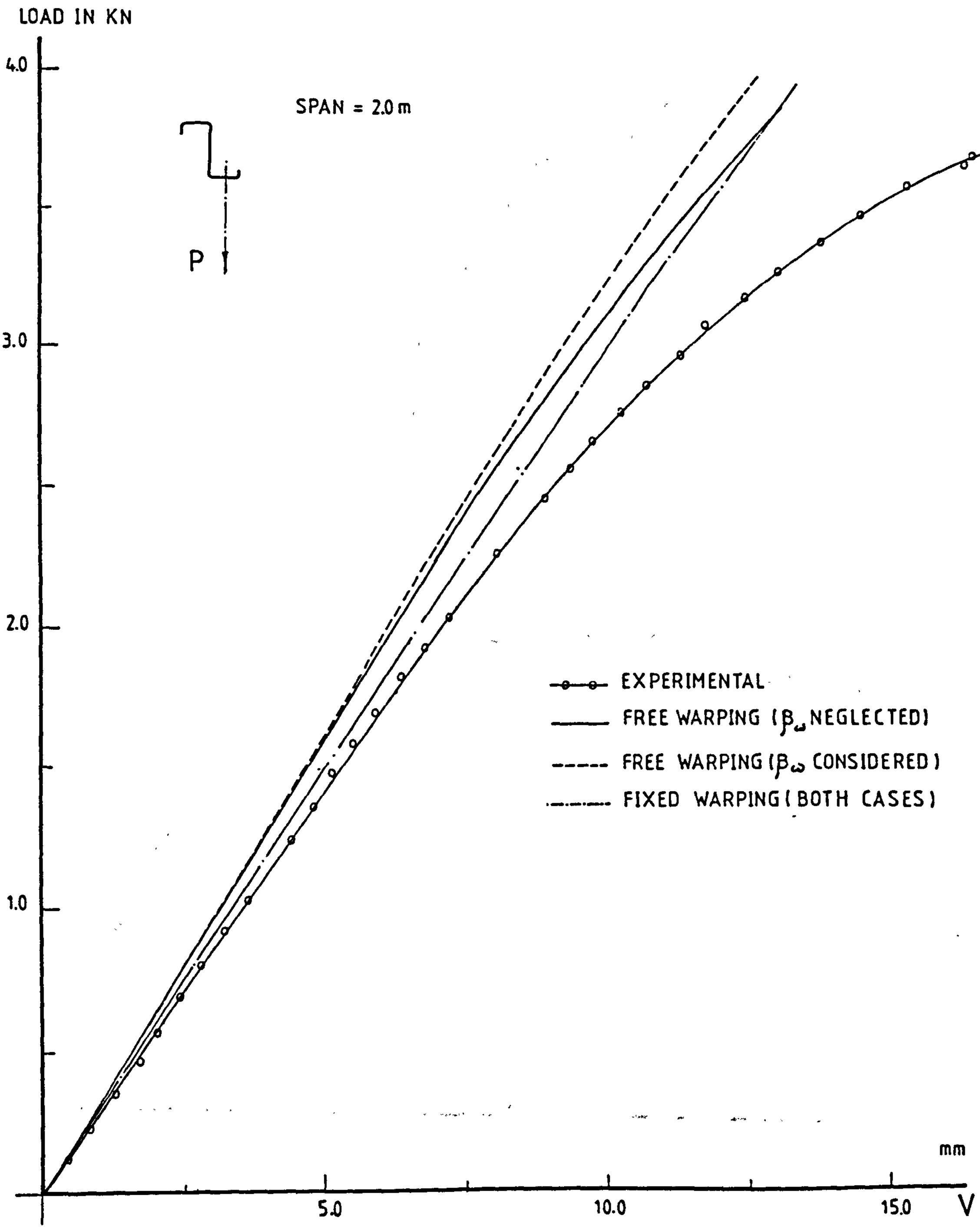

Fig. 7.15 Test B-5 Vertical Deflection At Mid-Span

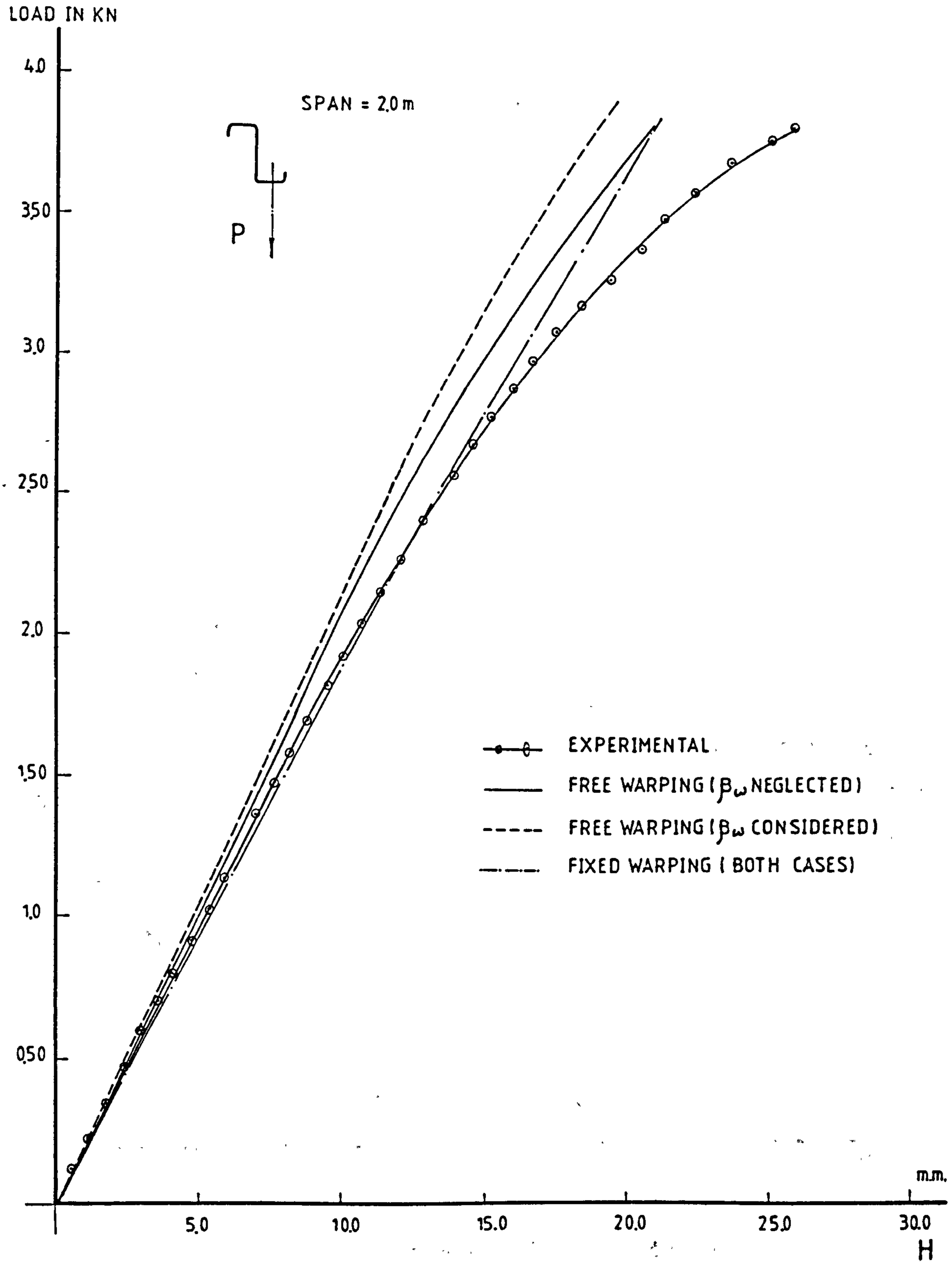

Fig. 7.16 Test B_5 Horizontal Movement At Mid-Span

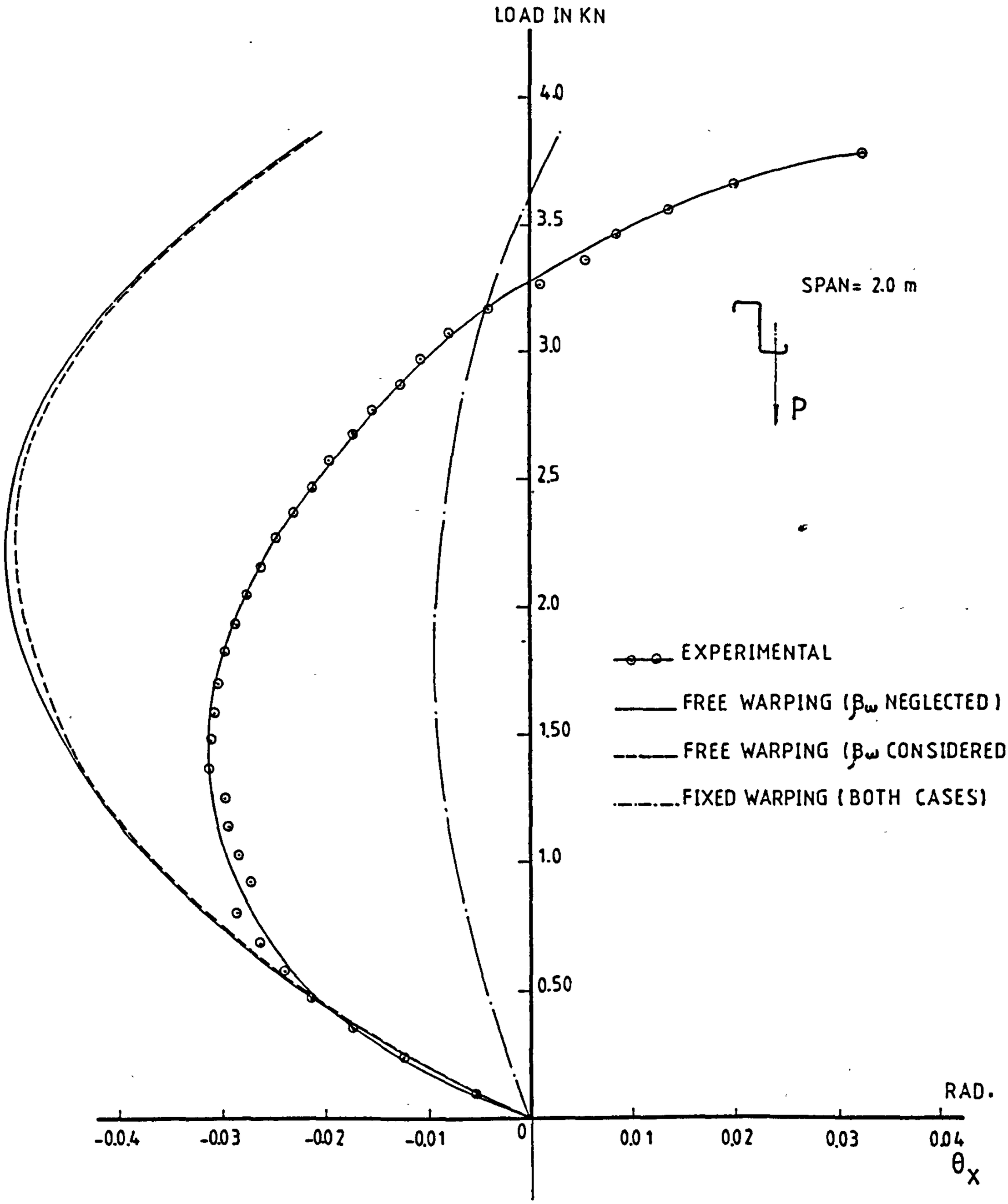

Fig.7.17 Test B_5 Angle Of Twist At Mid-Span

Test	Experimental failure load kN/hanger	Theoretical buckling load	
		warping free	warping restr.
B - 1	1.245	1.318	3.012
B - 2	1.920	2.350	3.968
B - 3	3.333	6.550	12.545
B - 4	2.963	6.014	11.805
B - 5	3.755	7.626	13.212

Table 7.1. Finite element solutions of the buckling loads in comparison with experimental failure loads.

CHAPTER EIGHT

CONCLUSION

The object of the work presented in the first part (Part I) of this thesis has been to develop a general finite element formulation for the torsional and lateral instability analysis of thin-walled structures. The new formulation is based on the theory of thin-walled structures presented by Vlasov (1).

The validity and accuracy of the new formulation were examined by presenting solutions for a number of instability problems which already have exact or highly accurate solutions derived by alternative means. The general level of agreement between the finite element solutions and the existing solutions of these problems was excellent.

A test program was carried out in order to obtain information on the behaviour of Z-beams subjected to combined bending and torsion and the validity of the finite element analysis of such beams. The first part of this test program was devoted to the evaluation of the longitudinal stresses caused by the bimoment and the accuracy of the finite element calculations of the bimoment values. The second part was performed in order to examine the accuracy of the finite element analysis of the second-order and buckling behaviour of Z-beams.

8.1. PRINCIPAL CONCLUSIONS

8.1.1.

The derivation of the stiffness and geometric matrices has been based on the assumption that at the instant of buckling the structure passes from a torsional-flexural displacement shape to another torsional-flexural shape. This means that the bimoment stresses are included in the analysis.

8.1.2.

Compared to the previously presented forms of the geometric (stability) matrix, 22,23,24,26,28), the geometric matrix derived in this thesis contains new terms allowing for more types of buckling problems to be analysed. The study undertaken to examine the validity of the new finite element formulation results in the following conclusions:

(i) The geometric matrix can be used to predict, with excellent accuracy, the torsional-flexural behaviour of monosymmetric beams and cantilevers loaded with in-plane transverse forces. The matrix includes the geometric characteristics β_y and β_z which reflect the effect of monosymmetry on the buckling behaviour of the beam. The new terms of the geometric matrix, corresponding to the effect of monosymmetry, have not been presented in any previous study.

(ii) In comparison with the previous studies, (24,28), the signs of the forces M_{z1}, M_{z2}, Q_{y1}, and Q_{y2}, in the geometric matrix, have been corrected according to the sign conventions of the shape functions used to represent the displacement v. In order to carry out a three-dimensional instability analysis of frames, a new transformation matrix has been developed. The method has successfully been applied to torsional-flexural buckling problems of plane and space frames. Excellent agreement was demonstrated between the finite element solutions and the available experimental or highly accurate solutions of these problems.

8.1.3.

By including the bimoment stresses as the fourth term in the equation of normal stresses, and by performing a numerical integration of the potential energy of the bimoment, new terms appear in the geometric matrix. Each of these terms is function of a cross-sectional property, β_ω, called the coefficient of sectorial monosymmetry. This coefficient is valid only for cross sections with no axis of symmetry.

8.1.4.

The test program was performed in two separate parts. The first part was devoted to the evaluation of the longitudinal stresses caused by the bimoment. The second part was conducted to study the second-order behaviour of Z-beams. Conclusions drawn from the comparison between the experimental and theoretical results were that:

(i) The elastic stiffness matrix, presented in chapter 3 of this thesis, can be used to predict, with excellent accuracy, the bimoment in thin-walled structures subjected to nonuniform torsion.

(ii) The effect of the bimoment on the second-order behaviour of Z-beams depends on the beam property $k\ell$ and on the end conditions of the beam. For beams with ends fully restrained against warping, the effect of bimoment stresses is very small and can be neglected.

(iii) The small deflection theory is not always sufficient to deal with Z-beams subjected to combined bending and torsion. This is due to the large displacements that often take place before the beam tends to buckle.

8.1.5.

A finite element computer program was used to carry out the theoretical calculations. The program was already available before the start of this project but it had to be modified according to the new finite element formulation. The method used to predict the buckling load from the load-displacement results is the modified Southwell plot technique. The method has proved to be applicable to all buckling problems presented in this study.

8.2. SUGGESTED FURTHER WORK

8.2.1.

The application of the new formulation to three-dimensional problems of plane and space frames was carried out assuming that the joints are sufficiently stiff for

warping to be neglected. The study reported by Vacharajittiphan, and Trahair (64), showed that this assumption is not always the correct one. The results of their study is rather difficult to incorporate in the analysis. With the growing use of cold-formed steel members to construct portal and space frames the warping behaviour of the joints, which are not always sufficiently rigid, plays an important role in the behaviour of the frame. There is a need to present information about the actual warping behaviour of the frame joints.

8.2.2.

A finite element formulation based on large displacement theory is needed to allow for the analysis of cross-sections with no axis of symmetry. The Z-beam tests have shown that the existing technique which is restricted to small deformations is not sufficient and leads to overestimated values of the buckling load.

P A R T (II)

CHAPTER NINE

Diaphragm Action in Truncated Pyramid Structures with Folded Plate Roofs.

9.1. INTRODUCTION

Safety and economy are always the two major criterions of structural design. Achieving a safe but lighter and more economical structure has always been the main motivation for any development in structural engineering.

The improved utilisation of the mechanical properties of structural materials has led to a better shaping of elements with economical distributions of the material. It has also helped in creating more advanced structural concepts, and new methods of analysis to achieve an optimal use of material capabilities.

It has been realised, through experimental investigations, that the classical way of analysing the structure as main and secondary systems and going consecutively from secondary to main is not always the right approach to describe the proper behaviour of the structure. In fact, each component part has its own contribution to the whole stiffness of the structure. In many cases the structure should be treated as one system with different types of element, each with its own function.

The contribution of the steel skin to the stiffness of a steel framed building can result in a substantial decrease in the traditionally calculated stresses and displacements. Theories to explain the steel skin action have led to new low-cost structures in which the in-plane strength of the sheeting plays a dominant role in the structure behaviour.

In 1974, at Mytchett near Camberly, Surrey, a full size low-cost skin building was tested (1,2) in accordance with BS449 Appendix A(3). The building was one of the units developed by the Metropolitan Architects Consortium for Education (MACE) to be used as nursery schools. The roof of

the building had the shape of a truncated pyramid with light cold formed framing members and covered by corrugated steel sheeting of trapezoidal profile. Later in 1980 a similar test was carried out, in the Department of Civil Engineering of the University of Salford, to study the behaviour of a two-bay Pyradome structure prefabricated by Oldroyd Brothers Ltd.(4). There was no precise method to analyse such structures, thus it was necessary to test a typical unit to satisfy the requirements of BS449(3).

The stability of both, the MACE unit and the two-bay Pyradome structure,depends on the diaphragm action of the roof sheeting. Apart from the approximate calculations given in references 1 and 2 for the MACE building no precise method,to the knowledge of the writer, has been presented to analyse such structures. The study reported in this chapter was undertaken to establish a theoretical method for predicting the elastic behaviour of the truncated pyramid structures, particularly under asymmetrical loading.

Initially, a single trapezoidal panel of the roof was studied under in-plan cases of loading using three methods of analysis, the finite element, full frame simulation, and simple truss modeling. The results have shown that the simple truss modeling is sufficient to explain the displacement configurations of the trapezoidal panel and to predict the fastener forces. The MACE unit has then been simulated with a space frame model having truss members to represent the in-plane shear flexibility of the roof sheeting. The two-bay Pyradome structure has also been analysed using the same procedure.

Because it was not possible to simulate precisely the degree of fixity of the connections between the frame members forming the skeleton of the structure, two limit bounds have been considered, namely: a) hinged connections, and b) fully rigid connections.

A full comparison between the calculated displacements and those recorded during the test is presented at the end of

this chapter. This comparison has shown that the proposed method can be used to predict the deflections of such structures with sufficient accuracy. The resulting forces in the sheet to frame member fasteners predicted from the space frame model of the MACE unit are also presented and discussed in section 11.5.2.

9.2. STRESSED SKIN DIAPHRAGM ACTION

9.2.1. General

The term diaphragm denotes a planar system with a thickness that is very small compared with the overall dimensions. Such a system possesses substantial rigidity in its own plane while it remains very flexible in the transverse direction. This property makes the diaphragm enormously capable of resisting in-plane shear forces.

Steel sheeting, properly fastened to the supporting elements of a steel framework, acts as a series of shear diaphragms. Such diaphragms may be used either in a secondary sense to support the structure against sway or in a primary sense in the case of shell-type structures and folded plates.

9.2.2. Historical background

As indicated by Nilson (5), the first attempt to study the diaphragm action was carried out in California in 1947 by C.B. Johnson and F.J. Converse, where a full-scale building was tested under the effect of lateral loads.

In 1960, Nilson (5), presented the results of some experimental investigations carried out in the University of Cornell to study the factors that influence the behaviour of shear diaphragms. He then suggested the so called "Cantilever test" as an experimental technique to evaluate the shear flexibility of diaphragms.

Ammar and Nilson (6) studied the behaviour of shear panels using different types of corrugated and orthotropic sheet. They pointed out the need for theoretical methods to predict the shear flexibility, and proposed a finite element

model to describe the distribution of internal forces in the diaphragm.

In 1973, after a research program lasting almost 20 years, Bryan (8) published the first book in the stressed skin action. This book represents the first comprehensive guide to the use of the shear diaphragm action in the design of steel frames. To make use of such action, he suggested that the flexibility of a complete diaphragm can be obtained by calculating each of the component flexibilities and summing them.

Davies and Lawson (9,10) showed that the expression given by Bryan (8) for the distortional flexibility of the corrugated profile ($C_{1.1}$) is not always valid, and can lead to wrong estimate of the deflections. They described an energy technique to calculate $C_{1.1}$, checked it with tests and finite element results, and provided tables for practical applications. Later, Davies (11) improved the method, proposing a more accurate representation for the distortional shape of the corrugated profile.

Finite element modeling has been adopted as the most appropriate method to study, in detail, the distribution of internal forces and deflections. Nevertheless, the amount of data and the special type computer program required make it difficult to be used. Davies (12) suggested a simplified method of analysis whereby the diaphragm components can be simulated by a plane frame with different types of element. The analysis can then be carried out using a conventional plane frame computer program. The method showed an excellent agreement with the finite element modeling.

So far, the most comprehensive study concerning the stressed skin diaphragm action is the book published by Davies and Bryan (13) in 1982. The book deals with every aspect in the subject and discusses, in detail, many techniques to incorporate the diaphragm action in the design of steel structures.

9.2.3. Diaphragm action

Fig. 9.1 shows a pitched roof portal frame clad with corrugated steel sheeting. Under the effect of the vertical load, shown by the arrows at the top of the frames, the apexes tend to move downwards while the eaves tend to move outwards. This movement is accompanied by in-plane distortion of the roof sheeting. The sheeting, with its enormous in-plane stiffness, tends to resist this movement by acting as the web of a deep plate girder. The two outermost purlins, at the eave and apex, form the flanges of this girder, and carry the axial forces due to bending. The end gables should be capable of carrying the reactions of the deep plate girder to the foundation (8,13).

Another important application of the shear diaphragm action is to be used to prevent sway of the flat-roofed structures. In the structure shown by fig. 9.2, side loads at eaves level, are applied directly in the plane of the sheeting. The deep plate girder composed of the sheeting and the two outermost purlins, at the eaves, carries the lateral load back to the end gables. Such gables may transfer the lateral load to the foundation by diagonal bracing or the gable may act as a vertical diaphragm if it is sheeted. Vertical loads are taken by the main system which can be designed as a simple beam and column structure. The horizontal wind bracing, in the plane of the roof, can be omitted (7,13).

Fig. 9.3 shows a low-cost building with folded plate roof. Such buildings rely entirely on the diaphragm action of the roof sheeting to carry lateral and vertical loads to the end supports. Uniformly distributed load on the roof is transferred by the sheeting to the fold lines. Line loads on the fold lines resolve themselves into in-plane loads acting in the two plate elements which meet at a given fold line. Each plate element with its two fold line members forms a deep plate girder system with a span equal to the length of the structure. The load is carried by the deep girders to the stiff end gables and then to the foundations (13).

9.2.4. Diaphragm arrangements and components

9.2.4.1. Basic arrangements

Fig. 9.4. shows the two basic arrangements of shear diaphragms. The span of the profiled sheeting may be directed either perpendicular to the span of the diaphragm (fig. 9.4.a) or parallel to it (fig. 9.4.b).

The design unit of a diaphragm is defined as the area of sheeting enclosed by two consecutive rafters and by the edge members. The diaphragm may be fastened either on all four sides (direct shear transfer) or on two sides to the perpendicular members only (indirect shear transfer), (13).

9.2.4.2. Components of a diaphragm panel

a) Individual lengths of profiled sheeting.
b) Perpendicular members. The sheeting must be firmly fastened to these members.
c) Parallel members.
d) Seam fasteners: connect longitudinal edges of adjacent sheet widths.
e) Sheet to perpendicular member fasteners.
f) Sheet to parallel member fasteners: If the parallel and perpendicular members are at the same level, the sheeting can directly be connected to the parallel members.
g) Shear connectors: If the perpendicular members pass over the parallel members shear connectors, with depth equal to the difference in level, can be used to connect the sheeting to the parallel members.
h) Connections between perpendicular and parallel members: If the sheeting is fastened on four sides these connections have no importance in the diaphragm action (13).

9.2.4.3. Failure modes

The possible failure modes of the diaphragm are:

a) Seam failure.

b) Failure in shear connectors (if used) at the panel ends.
c) Failure in the fasteners connecting the sheet to perpendicular members.
d) Failure due to buckling of the sheeting.
e) Failure of the outermost perpendicular members due to axial forces.

The diaphragm is most likely to fail by one of the first three modes (12).

9.2.5. Structural behaviour of hipped roof structures

A somewhat different example of a structure stability by diaphragm action is the MACE building shown in fig. 9.5. Under uniformly distributed vertical load the lower horizontal frame members act as a tension ring supported by the corner columns and the roof sheeting. The upper horizontal frame members form a compression ring which is supported mainly by the hip members. The upper horizontal members carry their line loads back to the apex joints by bending action. At a given apex joint the resulting load can be resolved into axial components in the three framing members meeting at this joint. Thus the frame member forces are statically determinate and can be calculated without considering the stressed skin action which is of a secondary nature in this loading case.

The bending of the frame members is restrained by the stressed skin action in the plane of the roof. This restraining effect results in a significant reduction of the bending and deflection of the hip members in particular (2,13).

Under asymmetric loading, however, the stability of the structure depends mainly on the stressed skin action of the trapezoidal panels of the roof. The axial forces in the frame members meeting at the apex joints no longer balance and a complex three-dimensional behaviour of the structure results. The behaviour of hipped roof structures under asymmetrical loading could only be predicted by testing a full-scale unit (13).

The theoretical method proposed in this chapter to analyse the hipped roof structures will be shown to be in good

agreement with the experimental results of: a) the test carried out on the MACE building which was constructed on site and, b) the prefabricated two-bay Pyradome structure.

9.3. LOADING TESTS ON THE MACE UNIT AND THE PYRADOME STRUCTURE

9.3.1. The MACE unit

Fig. 9.5 shows a typical MACE type 30 unit building constructed by the Metropolitan Architects Consortium for Education and tested in accordance with BS449. The roof was square in plan and had a truncated pyramid shape. Framing members, following the changes in slope, were constructed from cold formed steel. Details of the cross sections of these members are given in fig. 9.5.

Intermediate supports were provided by cladding panels to allow the lower square members to span 10.80 m between the columns. At each of the four corners, two bracing members were used to support the column and they were designed to resist lateral wind loads.

The top square members were designed to support a roof light on top of the roof. In the test, this light panel was replaced by a timber deck through which the load from the roof light was applied (1,2).

The roof sheeting had a trapezoidal profile with 80 mm depth and a net thickness of 0.67 mm. It was fastened to the supporting frame members, on all four sides, with 6.1 mm diameter self-drilling self-tapping screws through the troughs of alternate corrugations. Seam fasteners were self-drilling self-tapping screws with 4.1 mm diameter and placed at 250 mm centers.

9.3.2. The MACE unit loading tests

As it was not possible, at the time the structure was designed to make a reliable prediction of the behaviour of the structure particularly under asymmetrical loading, a full-scale unit had to be tested to satisfy the requirements of

BS449 (3). The test program was divided into two parts: a) stiffness tests, and b) strength tests.

a) Stiffness tests

Three different tests were carried out to satisfy the stiffness requirements:

Test 1. Load = Dead load + 1.5 x imposed load over the whole area.

Test 2. Load = Dead load + 2 x wind load (horizontal at eaves level).

Test 3. Load = Dead load + 1.5 x imposed load over half the area of the roof (asymmetric loading).

In each of the first two tests the load was maintained for 24 hours, then released and the recoveries were evaluated. In the third test, after recording the deflections, the load was kept on the roof to carry out the strength tests.

b) Strength tests

Test 4. Load = Self wt + 2 x (dead + imposed load) covering the entire roof.

Test 5. Load = load in test 4 + 2 x wind load (horizontal at eaves level).

In test 5 the load was maintained for 24 hours then the structure was unloaded and the recoveries were measured.

As this was a test on an actual structure which was required for later use, no tests to failure were undertaken.

Vertical loads were applied directly to the roof sheeting using sand bags weighing 56 lb each. Plywood sheets were used to distribute the load of the bags. Lateral loads, simulating the wind effect, were applied by a system of pulleys and wires at eaves level; wind test was carried out in two steps:

a) Lateral load of 2.46 kN/m applied to one side of the structure.
b) Lateral load of 1.23 kN/m applied to two opposite sides.

In each test the load was applied in four or five increments while deflection readings were recorded using dial gauges supported on scaffolding. The recorded deflections are presented and discussed in section (9.5.2.1) together with the corresponding theoretical results.

9.3.3. The two-bay Pyradome structure

Fig. 9.37 shows the two-bay Pyradome structure constructed by Oldroyd Brothers Ltd., and tested in the Department of Civil Engineering of the University of Salford (4). The structure took the shape of two MACE units connected together along one eave. The trapezoidal units forming the roof were prefabricated industrially and bolted together on site to form the shape of two truncated pyramids. Details of the framing members are given in fig. 11.37.

The sheeting used had a trapezoidal profile with 60 mm depth and 0.7 mm thickness. It was fastened to the supporting members on all four sides through every corrugation trough using Teks code 3.2 self-drilling self-tapping screws. Similar fasteners were used and placed at 200mm centers to connect longitudinal edges of adjacent sheet widths (4).

9.3.4. Loading tests on the two-bay Pyradome

The test program included three main vertical load tests and five side loading tests (4). The vertical loading tests were:

Test 1: Load taken up to working load (0.8 kN/m^2) applied uniformly over the entire area of the roof.

Test 2: Load taken up to acceptance test load (1.19 kN/m^2) applied uniformly over the entire area of the roof.

Test 3: Initially the load was applied over the whole area of the roof up to 0.4 kN/m^2. The load was then increased over area 'A' only (fig. 9.39) up to full working load (asymmetrical loading). After deflection reading had been recorded the load was increased over area 'B' (fig. 9.39) up to full

working load. The load was then increased over the entire area of the roof up to prototype test load (1.48 kN/m^2). Vertical loads were applied using sand bags each weighing 25 kg.

To carry out the side loading tests the two columns at 'o' and 'S' (fig. 9.39) were lifted above the anchor bolts of the bases and supported on skates prior to loading. Side loads were applied as concentrated loads at the base level using hydraulic jacks. These tests are explained in detail in reference '4'.

During vertical and side loading tests the vertical and horizontal movements were recorded after every load increment at sixteen locations using dial gauges. The recorded displacements of the working load test (test 1) and the asymmetric loading test (test 3) are considered in section (9.5.3) together with the corresponding theoretical results.

9.4. THE BEHAVIOUR OF THE PLANE TRAPEZOIDAL PANEL

9.4.1. General

The roof of the MACE unit, shown by fig. 9.5, is composed of four plane trapezoidal diaphragms supported by the four corner columns. Each diaphragm acts as a deep plate girder with variable depth. Frame members represent the two flanges while the roof sheeting acts as the web of the deep girder.

Under uniformly distributed vertical loading the stressed skin action of the sheeting is of secondary nature. Under asymmetrical loading, however, the stability of the structure depends mainly on the diaphragm action of the trapezoidal panels.

A comprehensive analysis of the behaviour of the trapezoidal panel, under in-plane cases of loading, is described herein. The analysis was carried out using three different techniques to simulate the shear flexibility of the diaphragm. A full comparison of the results is presented later.

The three techniques used are:

1. Finite element modeling
2. Plane frame simulation
3. Simple truss analysis.

The four in-plane cases of loading considered in the analysis are:

Case 1 : Uniformly distributed load of 2.6 kN/m acting upward along the bottom chord of the trapezoidal panel (the component of 2.46 kN/m horizontal wind load along one of the eaves).

Case 2 : Two vertical concentrated loads of 10.0 kN each acting downward at the two top corners of the trapezoidal panel.

Case 3 : One vertical load of 10.0 kN acting downward at a top corner of the trapezoidal.

Case 4 : One horizontal load (parallel to the chords) of 10.0 kN acting at a top corner of the trapezoidal.

The analysis was carried out for two different types of connections at the junctions of the framing member, namely a) hinged connections, and b) fully rigid connections.

9.4.2. Finite element modeling

The finite element modeling of regular shear diaphragms was first proposed by Ammar and Nilson (6). Davies and others (2) used the method to analyse the trapezoidal panel of the MACE unit under the action of uniform wind load, considering hinged corner joints.

Fig. 9.7 shows the finite element model described in reference 2 and used in the present analysis. Five types of elements have been used to simulate the components of the trapezoidal diaphragm. These types are:

1. Orthotropic rectangular plate elements
2. Orthotropic triangular plate elements
3. Beam elements

4. Spring elements for sheet to frame fasteners
5. Spring elements for seam fasteners.

Each of these element types will now be considered in turn.

9.4.2.1. Design of rectangular plate elements

The steel corrugated sheeting can be represented by two-dimensional orthotropic rectangular elements with two degrees of freedom at each node. To derive the 8 x 8 stiffness matrix of the element Ammar and Nilson (6) developed the elasticity matrix D where,

$$D = \frac{1}{1 - \gamma_{xy}\,\gamma_{yx}} \begin{bmatrix} E_x & \gamma_{xy}\,E_x & 0 \\ \gamma_{yx}\,E_y & E_y & 0 \\ 0 & 0 & (1-\gamma_{xy}\,\gamma_{yx})G_{eff} \end{bmatrix} \quad (9.1)$$

in which, E_y and E_x are the effective moduli of elasticity along the two axes of orthotropy, y and x, γ_{yx} and γ_{xy} are the corresponding values of Poisson's ratio and G_{eff} is the effective shear modulus. The two moduli of elasticity can be calculated from the expressions given by Ammar and Nilson (6) as follows:

$$E_y = \frac{\ell_o}{d}\, E_o \quad (9.2)$$

$$\text{and} \quad E_x = \frac{I_o}{I}\, E_o \quad (9.3)$$

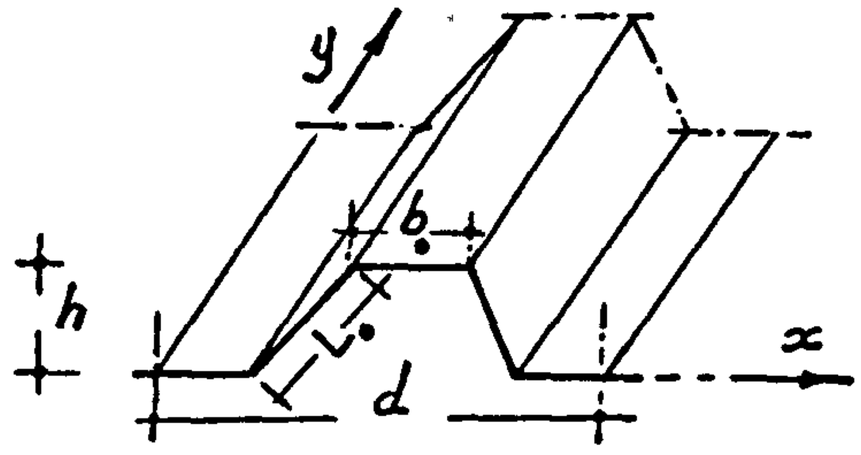

Fig. 9.6. Profile dimensions.

in which, ℓ_o = the developed length of one corrugation, E_o = the modulus of elasticity of the material, I_o and I are given by,

$$I_o = \frac{dt^3}{12} \quad (9.4)$$

$$\text{and} \quad I = t(b_o h^2 + \frac{2}{3} L_o^3) \quad (9.5)$$

where, the notations are given in fig. 9.6.

The two values of Poisson's ratio, γ_{yx} and γ_{xy}, can be calculated from the following relations:

$$\gamma_{yx} = \gamma_o \tag{9.6}$$

$$\text{and} \quad \gamma_{xy}.E_x = \gamma_{yx}.E_y \tag{9.7}$$

where γ_o is the value of Poisson's ratio for the material.

An expression for the effective shear modulus G_{eff} can be deriven from the total shear deformations of the sheeting (14). This expression takes the form:

$$G_{eff} = E_o \Big/ \left[\frac{d^{2.5}\,\bar{K}}{t^{1.5}\,b} + 2(1+\gamma_o)(1+\frac{2h}{d})\right] \tag{9.8}$$

in which b = the depth of the diaphragm, parallel to the corrugations, and $\bar{K}$ = the profile constant which is function of the profile dimensions and the arrangement of sheet to frame fasteners (13).

9.4.2.2. Orthotropic triangular elements

It is strongly recommended to avoid the use of such elements in the diaphragm analysis as far as possible (13). However, they have been used in the present analysis as infil pieces at the inclined edges of the diaphragm. The elastic properties, previously mentioned for rectangular elements, have been used to derive the 6 x 6 stiffness matrix of the orthotropic triangular element.

9.4.2.3. Beam elements

Beam elements have three degrees of freedom at each node, to represent the frame members of the diaphragm.

9.4.2.4. Spring elements for sheet to frame fasteners

Fig. 9.9 shows the spring element with zero size used to simulate the sheet to frame members fasteners and the seam

fasteners. Each spring has equal stiffness, K_x and K_y in the two orthogonal directions, x and y. Each frame to sheet fastener has been simulated individually since they tend to have different values of force and displacement.

9.4.2.5. Spring elements for seam fasteners

In a given seam line the fasteners have similar values of force. Instead of modeling each seam fastener individually they have been replaced by a small number of equivalent spring elements placed along the seam line at the nodes of the rectangular elements.

The flexibility of both the sheet to frame member fasteners and the seam fasteners has been taken as 0.15 *mm/KN* in the two orthogonal directions.

The finite element computer program used to carry out the analysis is that used by Davies and others (2).

9.4.3. Plane frame simulation

This method was first proposed by Davies (12) who applied it to regular diaphragms and to diaphragms with openings and showed that it agrees well with the finite element analysis of these types of diaphragms.

The method is based on representing the diaphragm assembly by a number of prismatic members forming an in-plane frame. The analysis can then be carried out using a conventional plane frame computer program.

The analysis of a rectangular diaphragm can always be simplified by eliminating the x-component of the displacement at each joint (12). Hence, spring elements having only axial stiffness in Y-direction K_y can be used to simulate the sheet to frame member fasteners. In the trapezoidal diaphragm, however, the x-component of the strain produced by the axial force of the inclined member has to be included in the analysis.

The model used to simulate the shear flexibility of the trapezoidal diaphragm is shown in fig. 9.8. The joints were allowed to move in x-direction. An additional type of

spring element has been provided beside those used for rectangular diaphragm analysis (12). Such elements simulate the flexibility of the sheet to frame fasteners, in x-direction. Types of elements used in the model will now be considered.

9.4.3.1. Beam elements

Conventional beam elements with three degrees of freedom at each node have been used to represent the frame members.

9.4.3.2. Diagonal truss members representing the sheeting

Each diagonal member has been used to simulate the shear flexibility of a sheet width p, where p is the pitch of sheet to frame fasteners. By equating the shear displacement of a width p of the sheeting to that of the equivalent diagonal member, the cross sectional area A of that diagonal takes the value,

$$A = \frac{b \cdot t \cdot G_{eff} \, \ell^3}{p \cdot E \cdot h^2} \qquad (9.9)$$

where:

b = depth of diaphragm panel represented by the diagonal member,

E = the elasticity modulus of the material,

ℓ = length of the diagonal member,

G_{eff} = effective shear modulus of sheeting, given by equation 9.8,

h and t are the depth and thickness of the sheeting profile.

9.4.3.3. Vertical truss members

These members have been used to satisfy the compatibility condition at the joints connected to the diagonal member. They have been chosen with sufficient stiffness for strain to be neglected. The vertical member has been given a cross sectional area equal to $2\ell_o t$, where ℓ_o is the developed length of one corrugation.

9.4.3.4. Prismatic members representing the seam fasteners

The total flexibility of the seam fasteners in a given seam has been simulated by a prismatic member having axial stiffness. The cross sectional area A of such member takes the value,

$$A = \frac{\ell}{n \cdot E \cdot f_s} \qquad (9.10)$$

in which, ℓ = length of the member, E = elasticity modulus, n = number of fasteners in the given seam, and f_s = flexibility of a seam fastener (taken 0.15 mm/kN).

9.4.3.5. Spring elements for sheet to frame fasteners

As mentioned before, it is necessary to model sheet to frame member fasteners precisely. In the present analysis spring elements with finite length have been used to represent these fasteners. The y-component of flexibility has been simulated by vertical springs with 1.0 mm length. Inclined springs have been provided to simulate the x-component of flexibility. Details of these springs are shown in figs. 9.10 and 9.11.

9.4.4. Simple truss analysis

This method is an extension to the approximate method of regular diaphragms analysis proposed by Bryan (8) and later modified by Davies (11,14). As illustrated by fig. 9.12, the trapezoidal diaphragm is simulated by a plane truss system. Diagonal members have been designed for the overall shear flexibility of the diaphragm. Edge members are allowed to carry in-plane bending. Vertical members have enough stiffness for their axial strain to be neglected.

The overall flexibility of the diaphragm assembly can be evaluated by considering each component flexibilities and adding them together. These flexibilities are:

a. $C_{1.1}$: due to distortion of the sheeting profile

b. $C_{1.2}$: due to shear strain in the sheeting

c. $C_{2.1}$: due to movement at the sheet to perpendicular member fasteners

d. $C_{2.2}$: due to movement in the seam fasteners

e. C_3 : due to axial strain in the edge frame members.

The expressions used to calculate these flexibilities are presented in appendix A.9.1. The overall shear flexibility C of the diaphragm assembly takes the form:

$$C = C_{1.1} + C_{1.2} + C_{2.1} + C_{2.2} + C_3 \qquad (9.11)$$

The cross sectional area A_d of the diagonal member used to simulate overall shear flexibility of a diaphragm width can be calculated from:

$$A_d = \frac{\ell_d}{E \cdot C \cdot \cos^2\theta} \qquad (9.12)$$

in which, ℓ_d = length of the diagonal, and θ = angle of inclination of the diagonal with respect to the direction perpendicular to the corrugations.

The derivation of equ. 9.12 is presented in appendix A.9.1.

9.4.5. Comparison between the results of the three methods

A full comparison between the results of the three methods used to study the behaviour of the trapezoidal diaphragm is given in figs. 9.13 up to 9.29. Four different cases of in-plane loading have been considered in the analysis. The comparison of the deflections has shown that the full frame simulation and the simple truss model both agree well with the more accurate finite element method.

The sheet to frame member fastener forces have been calculated from the internal forces given by the simple truss

model by making use of the distribution of fastener forces given by the finite element method. The procedure is given in appendix A.9.1. The same procedure can be applied using the distribution of fastener forces given by the full frame simulation of the trapezoidal diaphragm. However, the local fastener forces can be calculated directly from the internal forces of the simple truss model by considering only the fasteners at the joint. This may lead to overestimated values for the fastener forces as will be explained in the following discussion.

The comparison of the fastener forces calculated by the three methods of analysis used in the study is given in fig. 9.29 and table 9.1.

The following observations can be drawn from the comparison:

1. As illustrated by the figs. 9.21 - 9.28, under asymmetric load, either vertical (case 3) or horizontal (case 4), the deflections of the bottom and top flanges take asymmetric shapes. The figures show an excellent agreement between the results of the three methods. The largest error in the simple truss method in comparison to the finite element method is about 3% (figs. 9.21 and 9.25). Nevertheless,it is obvious that the method results in almost identical shapes of deflection under asymmetric load.

2. Under symmetrical vertical load acting at the top flange (case 2), the full frame simulation and the finite element method give almost identical values for the deflection of the top and bottom flanges (figs. 9.17 - 9.21). Considering hinged corner joints, the error in the simple truss method is about 9.5%, (figs. 9.17 and 9.19). For rigid joints, however, the results are almost identical to that of the other two methods (figs. 9.18 and 9.20).

3. The comparison of the deflections under uniform wind load is shown by figs. 9.13, 9.14, 9.15 and 9.16. Compared to the finite element, the largest error in the full frame simulation is about 5% (fig. 9..13). The error in the

simple truss method is almost 8.7% for the maximum deflection, and about 11% at mid-span (fig. 9.13). The difference between the two limit bounds considered in the analysis is significant in this loading case. The maximum deflection of the rigid corners model, (fig. 11.14), is about 66% of that calculated with hinged corners model, (fig. 9.13). The ratio is about 37% for the mid-span deflection.

4. Fig. 9.29 shows the distribution of fastener forces and the axial forces in the frame members under wind action (case 1) for the diaphragm with hinged corners. It should be noted that high local fastener forces occur at the apex joint and directly opposite to it in the bottom flange. This shows the need to strengthen the sheet to frame member connection at those locations by adding more fasteners.

5. Table 9.1 shows the comparison of the forces in the critical fasteners, calculated by the three methods used to analyse the trapezoidal diaphragm. Under symmetrical loading acting at the top flange (case 2) the acting shear produces very small fastener forces. In cases 1, 3 and 4 fasteners at the apex joints are the most critical. In case 1, where the load is distributed uniformly along the bottom flange, the maximum fastener force calculated by the finite element is 2.42 kN. For the same fastener the full frame simulation gives a value of 2.71 kN, which is higher by almost 11%, while the simple truss method gives a value of 2.52 kN, which is higher than the finite element result by 4% only. Considering only the local fasteners at the joint, the internal forces given by the simple truss model give a value of 3.25 kN for the same fastener. This is higher than the finite element result by almost 34%. Under asymmetrical loading, the maximum fastener force calculated by the full frame simulation is higher than the finite element value by almost 17%, while the simple truss method again gives 4% higher than the finite element method.

It can be concluded that the simple truss method can be used to predict the deflections of the trapezoidal diaphragm with sufficient accuracy. The method has also shown an excellent agreement with the finite element method in calculating the fastener forces. The full frame simulation agrees well with the finite element method in calculating both the displacements and the fastener forces. Moreover, the method has the advantage that it can be applied using a conventional plane frame computer program.

9.5. ANALYSIS OF THE MACE UNIT AND THE TWO-BAY PYRADOME

9.5.1. The model used in the analysis

Fig. 9.30 shows a plan view of the space frame model used to analyse the MACE structure. The overall shear flexibility of the trapezoidal panels forming the roof has been simulated by in-plane truss elements. The four cases of loading considered in the study are shown in fig. 9.31. The model has been solved for two types of end conditions:

a) Considering hinged connections between the frame members.

b) Considering that such connections are fully rigid.

The model used to study the two-bay Pyradome structure is presented in fig. 9.38. Two cases of uniform load have been considered in the analysis. They are shown in fig. 9.39.

A more simplified model has been proposed. This model can be used to offer approximate and easily calculated values of the deflection. In this model, the overall shear flexibility of the trapezoidal panel has been simulated by two diagonal members forming an x-truss panel. The results of using this model are given in tables 9.4 and 9.5, and in fig. 11.32.

The analysis has been carried out using the computer program described in chapter (4) and the SAP4 program (15).

9.5.2. Comparison and discussion of the results

9.5.2.1. The MACE unit deflections

a. Uniformly distributed load over the entire roof

Table 9.2 presents the comparison between the theoretical and experimental value of the displacements for this loading case. The increase in the experimental value of the deflection of the apex joint (joint 1) compared to the corresponding theoretical value was probably due to movement of the bolted connection during the test. Such movement at the apex joint may also be the reason for the increase in the value of the experimental deflection at the mid point of the apex member, in comparison to the theoretical value. However, such increase is much smaller as the apex member is restrained by the stressed skin action of the sheeting. The experimental value of the vertical deflection at the mid point of the hip member lies in between the two limits of the corresponding theoretical deflection. The deflection at this point is mainly due to the bending action of the hip member. Such bending is restrained by the stressed skin action of the adjacent sheeting.

It should be noted that the measured deflections are in most cases quite small and certainly sufficiently small for the influence of movement in bolted joints to be significant. Bearing this in mind, the general level of agreement between the test results and the corresponding theoretical values of the deflection, given by the simple truss model, is good.

Table 9.4 shows the comparison between the experimental values of the deflection and the corresponding theoretical values calculated with the x-diagonals model. It can be seen that this alternative simulation of the shear flexibility of the diaphragms results in a stiffer model which gives underestimated values of the deflection.

b. Horizontal wind load (cases c, and d)

Table 9.3 presents the comparison between the experimental and theoretical deflections in the two wind cases considered in the analysis. Apart from some high experimental results,

which will now be discussed, the general pattern of agreement between the analysis and the test results is good.

In case 'd' of loading, where the load is acting at the level of two opposite eave beams, the calculated value of the two horizontal displacements 3-x and 9-x at the mid point of the two opposite apex members are equal. The two corresponding experimental values are, however, not equal. The difference between them is almost 9.5% which is an indication of the variability of the experimental results. On the other hand, the difference between the two experimental values of the horizontal displacement at the mid point of the two opposite eave beams, which may again be expected to be equal, is about 26%. In case 'c' of loading, where the total load of case 'd' is applied to only one eave, the experimental value of the horizontal displacements at the mid point of the two apex members are close to the corresponding theoretical values. However, the experimental value of the horizontal displacement at the mid point of the loaded eave joints is about 60% greater than the corresponding theoretical value and drops to 40% increase in the experimental displacement at the mid point of the unloaded eave. The high increase of the measured displacements at the mid point of the two eave beams is probably because of three factors:

a) The previous analysis of the trapezoidal diaphragm has shown that, under uniform load acting along the bottom flange (wind load), the simple truss model has given about 11% less than the more accurate finite element method for the mid-span deflection.

b) The difference in the level of disagreement for the loaded and unloaded eaves in case 'c' of loading may indicate some local effect of the concentrated load.

c) For the relatively small displacements involved there is always likely to be a significant increase in the displacement due to movement in bolted joints.

The comparison between the experimental deflections and the corresponding theoretical values, given by the x-diagonal model, is presented in table 9.5. Again the

comparison reflects the increase in the stiffness of the model compared to the simple truss model.

c. Asymmetric load

Fig. 9.32 shows the comparison of the deflections under the action of the asymmetric load. The comparatively large deflections obtained in the case has shown that the asymmetric load represents the most critical loading condition for this structure. It can be seen, from the comparison, that the displacements measured during the test lie in between the two limits of the corresponding theoretical values. The experimental value of the displacement at a given location in the loaded half of the roof is close to the mean value of the two limit bounds. However, in the unloaded half of the roof the experimental displacement at a given location is much closer to the lower limit of the corresponding theoretical displacement. This could be because the bolts of the unloaded apex joint tended to stick by friction under the high internal forces produced in this case.

Fig. 9.32 also shows the results of the x-diagonals model. The pattern of agreement is similar to that discussed above for the simple truss model. However, as in the other cases of loading, the model shows more stiffness than the simple truss model.

9.5.2.2. Critical fastener forces calculated from the model of the MACE unit

The failure modes of a diaphragm assembly have been explained in section 9.2.4.3; however, the most likely modes are those involving fasteners. Thus to check the safety of the structure it is essential to calculate the fastener forces.

It has been shown in the analysis of the trapezoidal panel (section 9.4.5) that the simple truss method agrees well with finite element method for calculating the fastener forces. The individual fastener forces of the MACE unit roof have been calculated from the internal force distribution given by the

space frame model by making use of the distribution shape of fastener forces given by the finite element analysis of the trapezoidal panel.

Fig. 9.33 shows the forces in the fasteners at the apex joints and opposite to them when the structure is loaded by uniformly distributed load of 0.81 kN/m^2. It can be seen that under such loading the stressed skin action is of a secondary nature.

Fig. 9.34 shows the fastener forces when the roof is loaded asymmetrically. It is obvious that under this load the stability of the structure is dependent on the stressed skin action of the roof sheeting. It can be seen that high local forces occur in the fasteners at the apex joints. The value of the force in the most critical fastener is between 4.23 kN (hinged corners model) and 0.70 kN (rigid corners model). The ultimate capacity of an individual fastener is approximately 4.0 kN. However, the comparison of the displacements under asymmetrical loading (fig. 9.32) has shown that experimental displacements are closer to the corresponding theoretical values given by the rigid corners model than to the values given by the hinged corners model. Nevertheless these high local fastener forces show the need to strengthen the sheet to frame member connection by increasing the fasteners to every corrugation in the critical regions.

The critical fastener forces under horizontal wind loading are shown in figs. 9.35 and 9.36. It can be seen that the stressed skin action is confined to the loaded panels. In case 'c' of loading, when the horizontal wind load is acting along one eave beam, the force in the most critical fastener is between 3.22 kN (hinged corners model) and 2.36 kN (rigid corners model). The critical fasteners are thus safe but nevertheless they represent a potential weakness and again it is recommended to increase the fasteners to every corrugation in the critical locations.

9.5.3. The two-bay Pyradome deflections

Table 9.6 presents the comparison between the experimental deflections and the corresponding theoretical values, for the two cases of loading considered in the analysis. Apart from the high experimental deflections of the valley beam, the pattern of agreement between the experimental and theoretical deflections is good. The increase of the experimental deflection of the valley beam was probably due to movement of the bolts which were connecting the two beams of the valley member. The fastener forces can be calculated following the same procedure used for the MACE building.

9.6. CONCLUSIONS

1. The objective of the work reported in this chapter has been to present a theoretical model capable of describing the behaviour of the hipped roof structures under vertical and lateral loads. Under certain cases of loading, the stability of such structures depends entirely on the stressed skin action of the trapezoidal sheet panels which form the roof.

2. Three methods of analysis have been used to study the behaviour of the trapezoidal diaphragm under different cases of in-plane loading. The full frame simulation has proved to be in excellent agreement with the finite element method in predicting the displacements. However, the method slightly overestimated the fastener forces. On the other hand,the simple truss method has shown a good agreement with the finite element method in predicting both the displacements and the fastener forces.

3. The MACE structure has been modeled using simple truss panels to simulate the overall shear flexibility of the trapezoidal panels of the roof. The comparison between the theoretical and experimental deflections has shown that the simple truss model can be used to express the behaviour of the hipped roof structures with sufficient accuracy.

4. The critical fastener forces have been calculated using the internal forces given by the space frame model of

the MACE building. The procedure of calculation is based on using the distribution shape of fastener forces given by the finite element analysis of the trapezoidal panel of the hipped roof (Appendix A.9.2). The calculated fastener forces when the structure is loaded asymmetrically shows the need to strengthen the sheet to frame member connections in the highly stressed regions by increasing the fasteners to every corrugation .

5. A similar study has been carried out on the two-bay Pyradome structure. The theoretical deflections calculated with the proposed model have again shown adequate agreement with the corresponding experimental values.

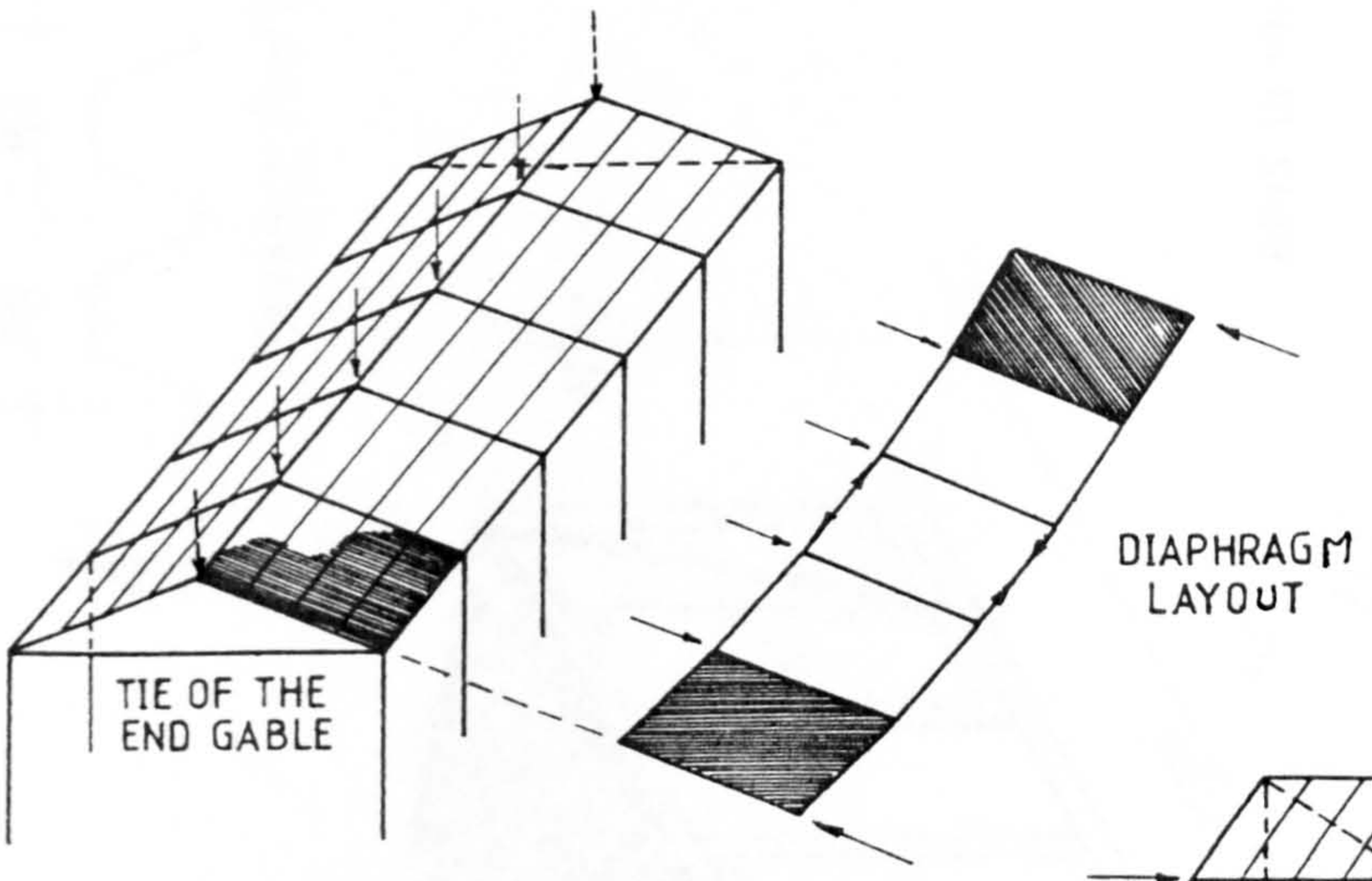

Fig.9.1 Diaphragm Action
In Pitched Roof Portal Frame Under
Vertical Load

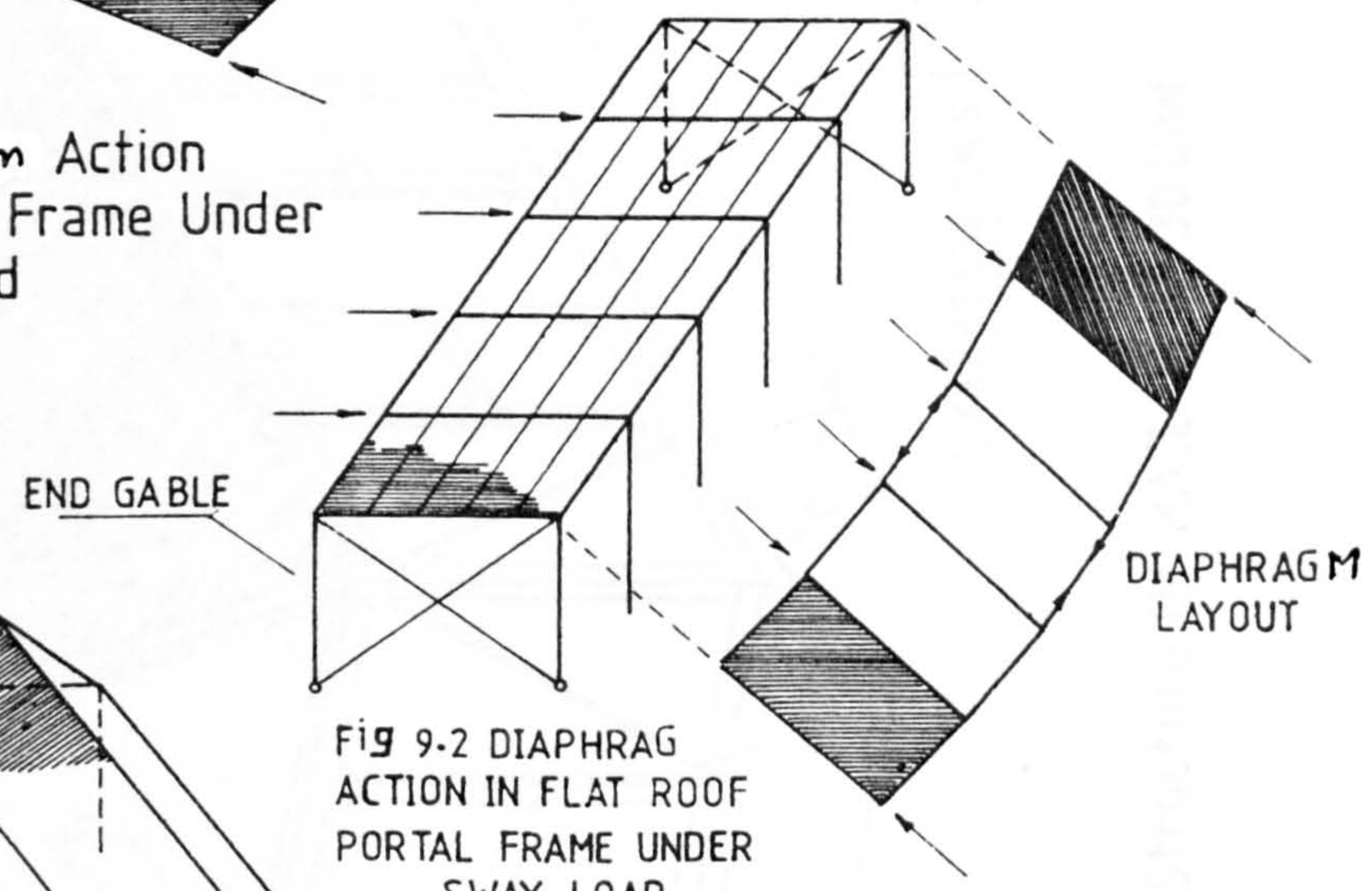

Fig 9.2 DIAPHRAG
ACTION IN FLAT ROOF
PORTAL FRAME UNDER
SWAY LOAD

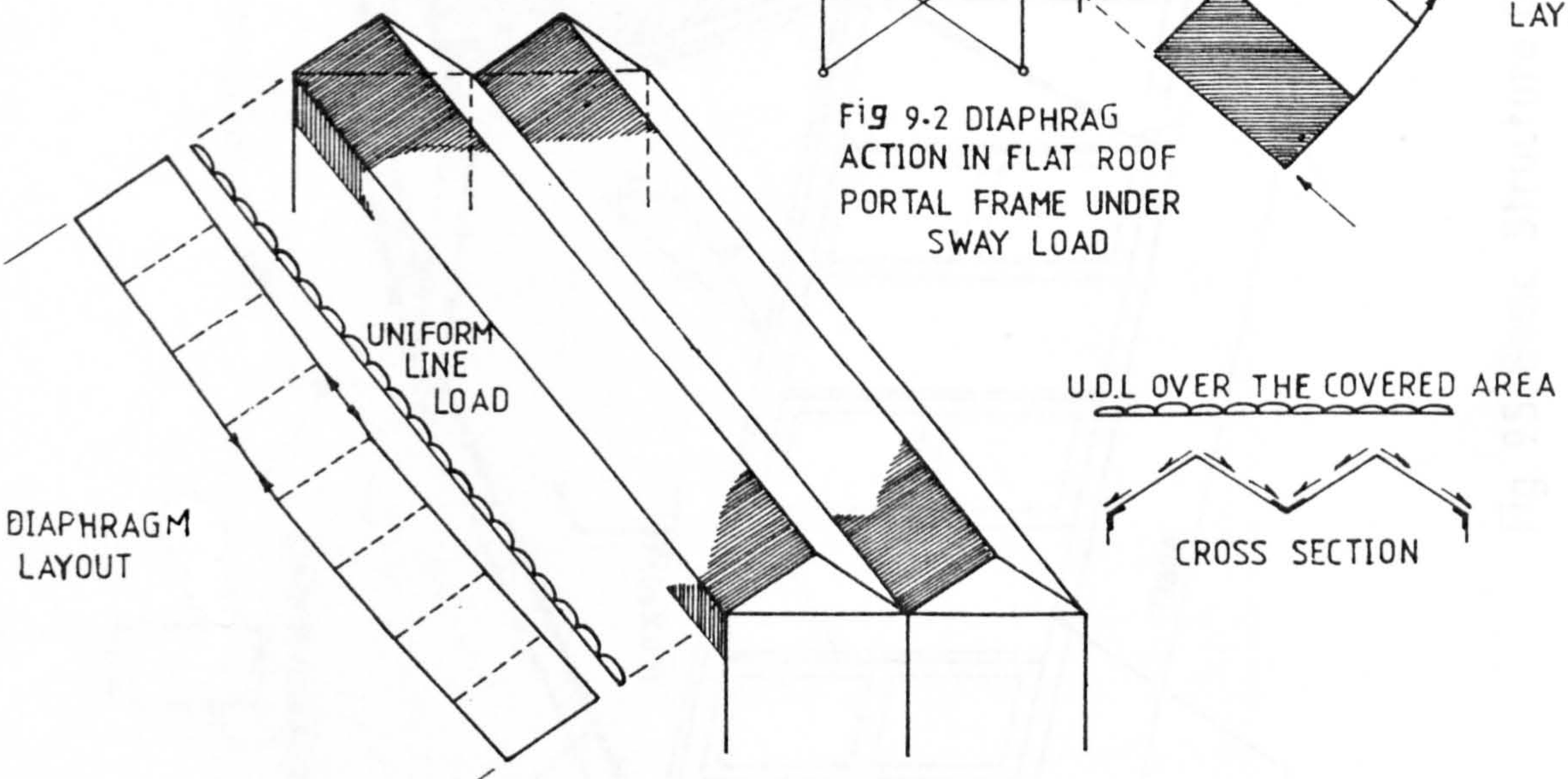

Fig 9.3 Diaphragm Action in Folded Plate Roof

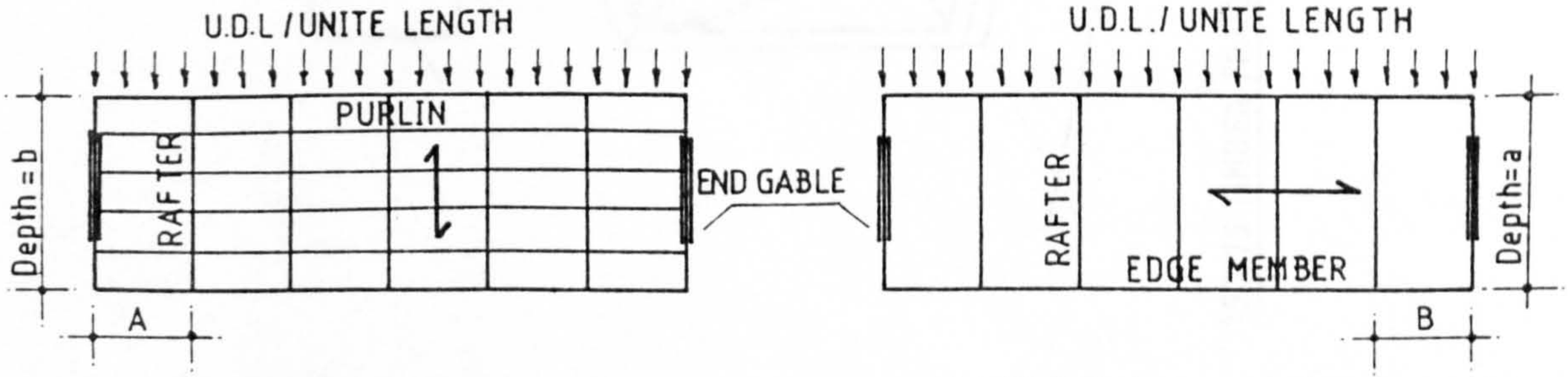

(A) SHEETING SPANNING PERPENDICULAR TO SPAN

(B) SHEETING SPANNING PARLLEL TO SPAN

Fig 9.4 Basic Diaphragm Arrangaments

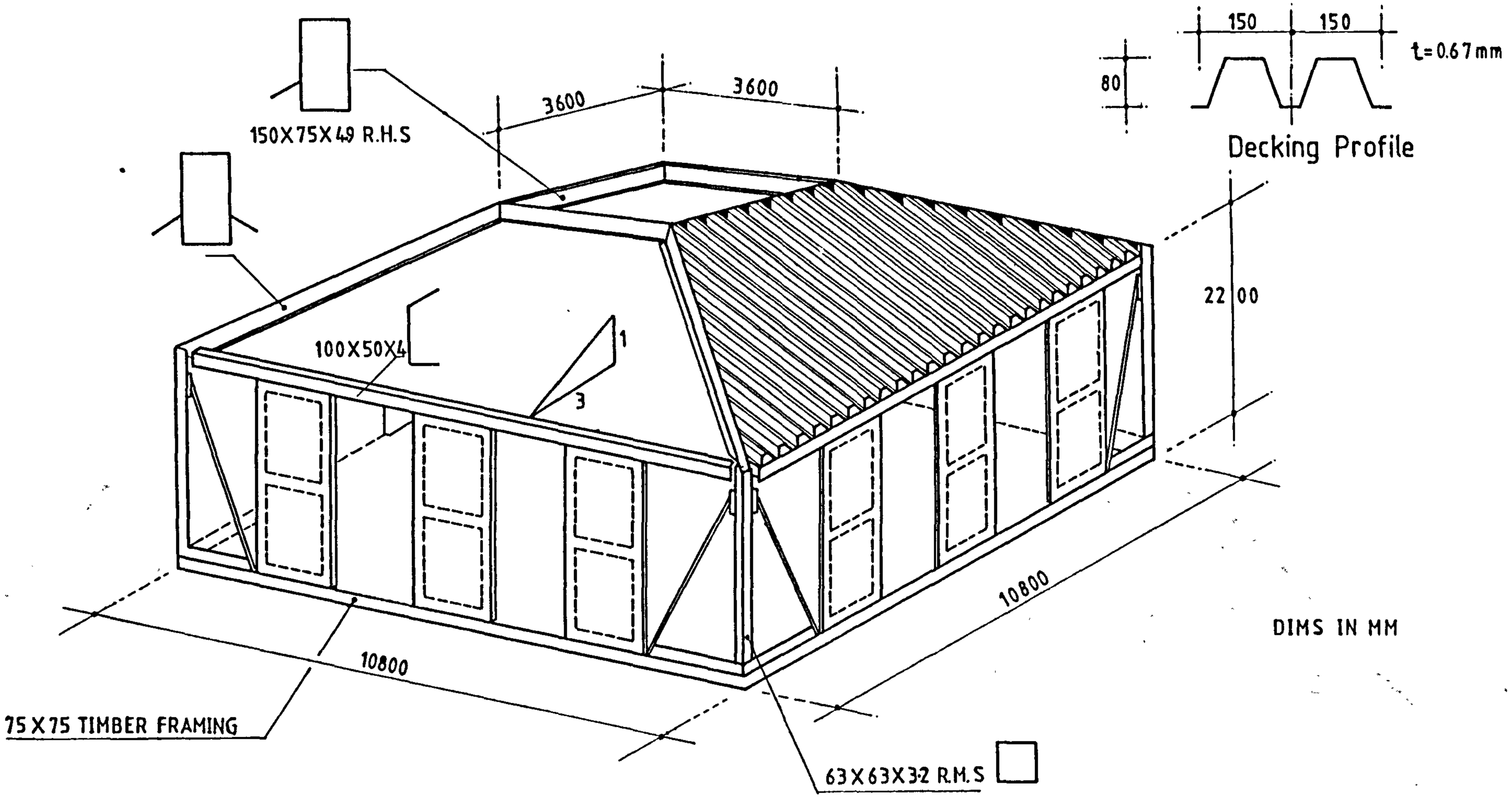

Fig. 9.5 Basic Structure Of MACE Type 30 Unit

FINITE ELEMENTS

- Rectangular Plate Elements Representing Sheeting
- Triangular Plate Elements Representing Sheeting
- Beam Elements
- Spring Elements For Sheet To Frame Fasteners
- Spring Elements Representing Lumped Seam Fasteners

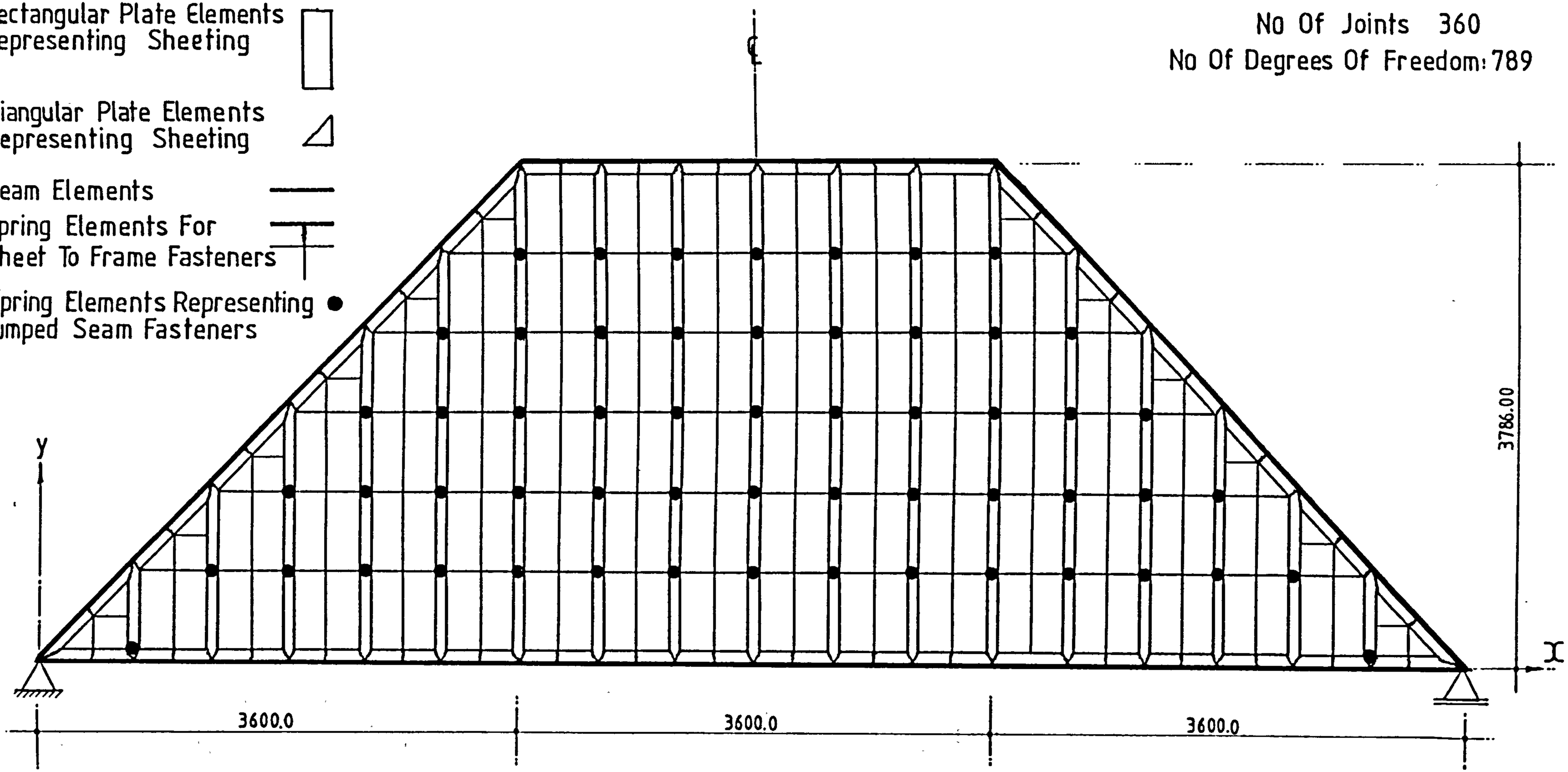

Fig 9.7 Finite Element Model For The Trapezoidal Diaphragm

Dims In MMS

Key To Frame Model

1. BEAM ELEMENT REPRESENTS FRAME MEMBER
2. DIAGONAL MEMBER REPRESENTS THE SHEAR STIFFNESS OF SHEETING
3. VERTICAL MEMBERS
4. PRISMATIC MEMBER REPRESENTS THE TOTAL NUMBER OF FASTENERS IN A SEAM
5. REPRESENTS THE HORIZONTAL STIFFNESS OF SHEET TO FRAME FASTENERS
6. REPRESENTS THE VERTICAL STIFFNESS OF SHEET TO FRAME FASTENERS

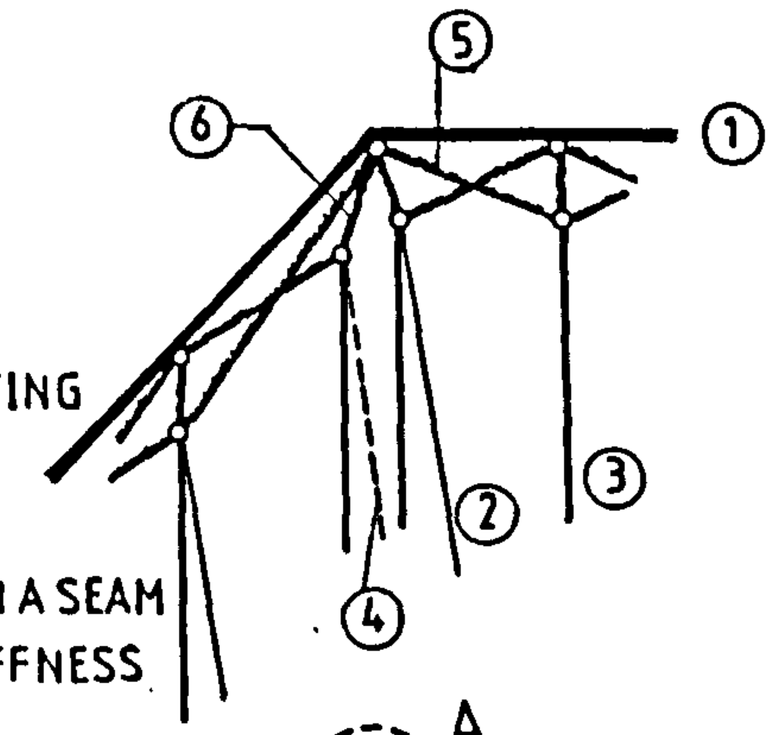

Detail (A)

NO OF JOINTS 178

NO OF DEGREES OF FREEDOM : 425

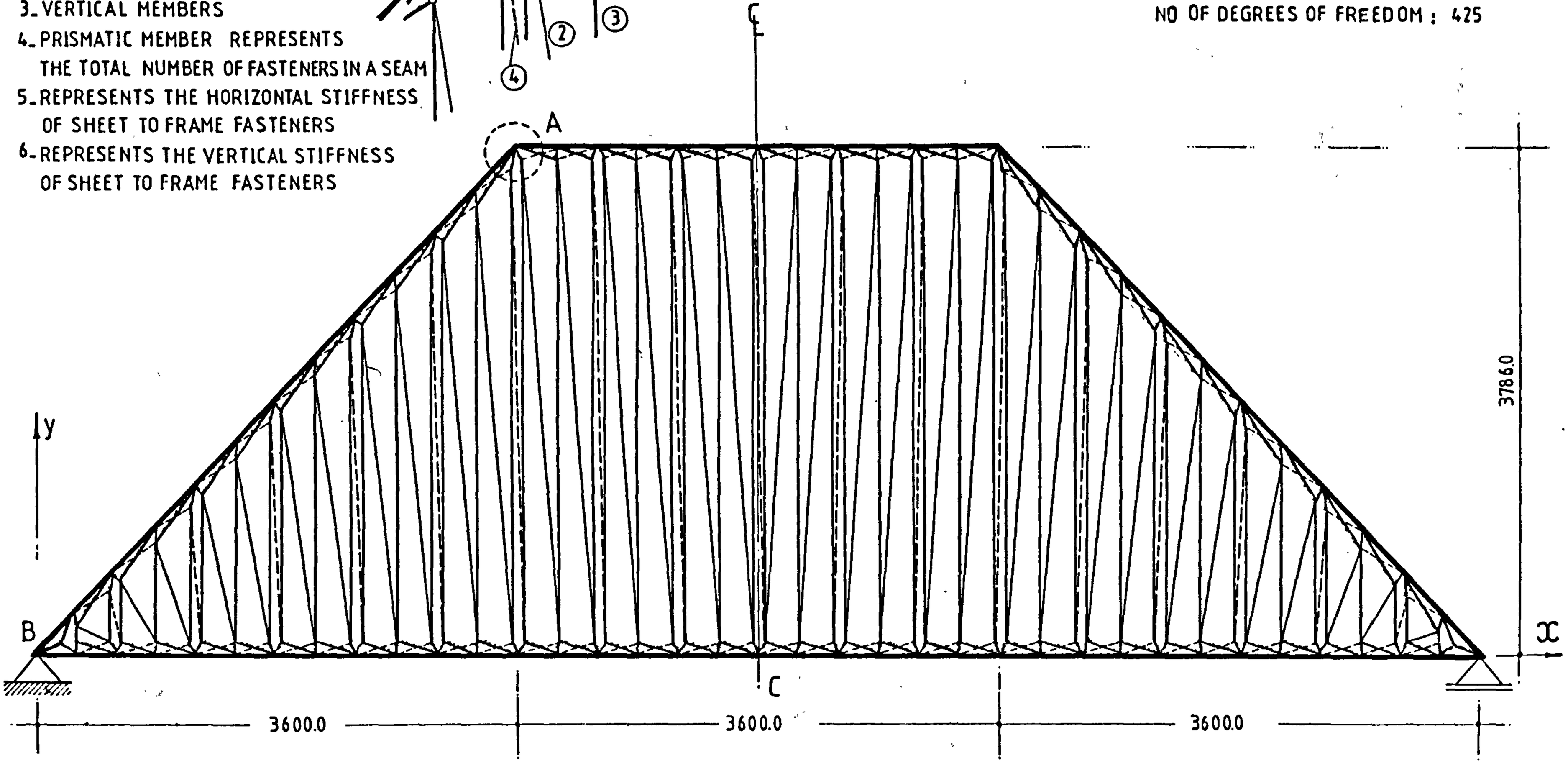

Fig.9.8 Full Frame Simulation Of The Diaphragm

DIMS IN MMS

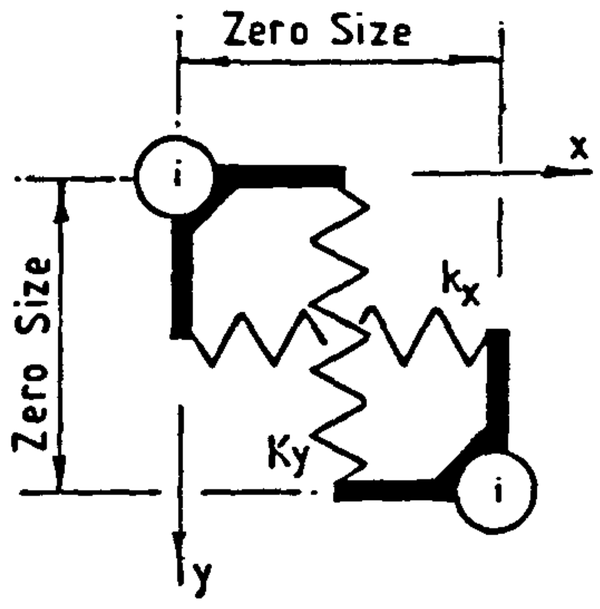

Fig.9.9 Finite Element Simulation Of Fastener

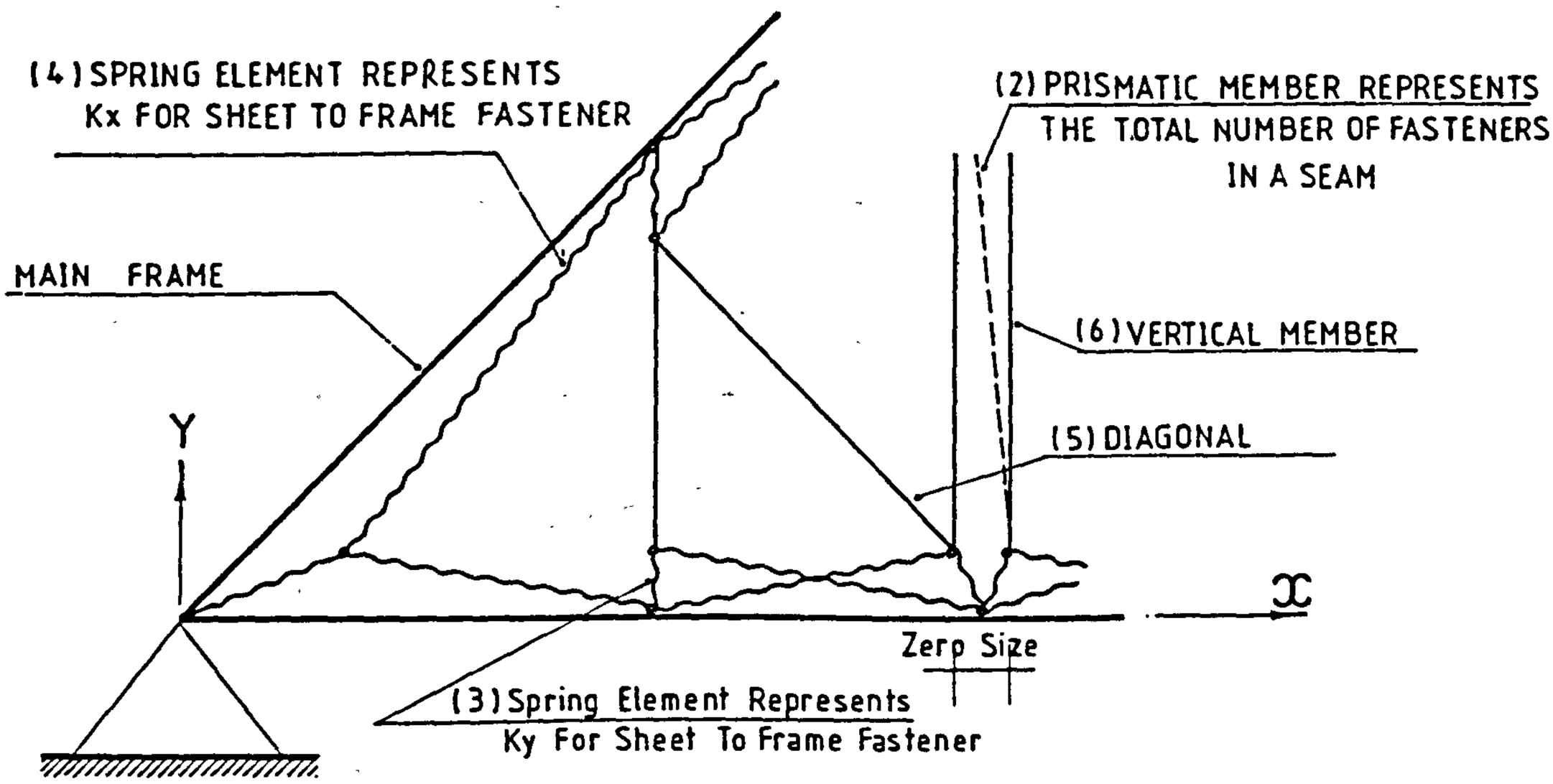

Fig.9.10 Details Of Joint (B)

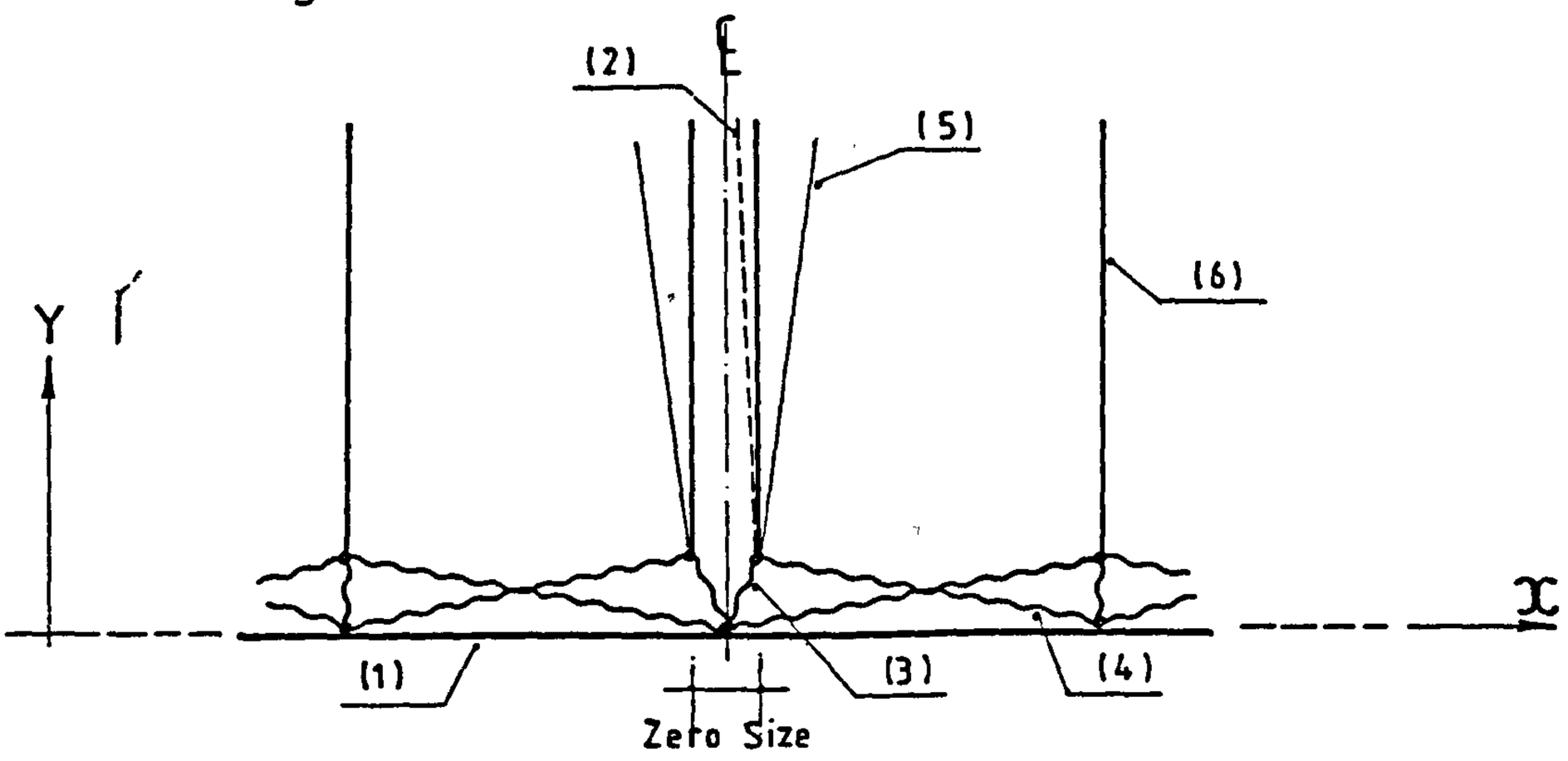

Fig.9.11 Details Of Joint (C)

Elements Of Model

1_Beam Element Represents Frame Members

2_Diagonal And Vertical Members Represent Sheeting

No Of Joints = 24

No Of Degrees Of Freedom = 69

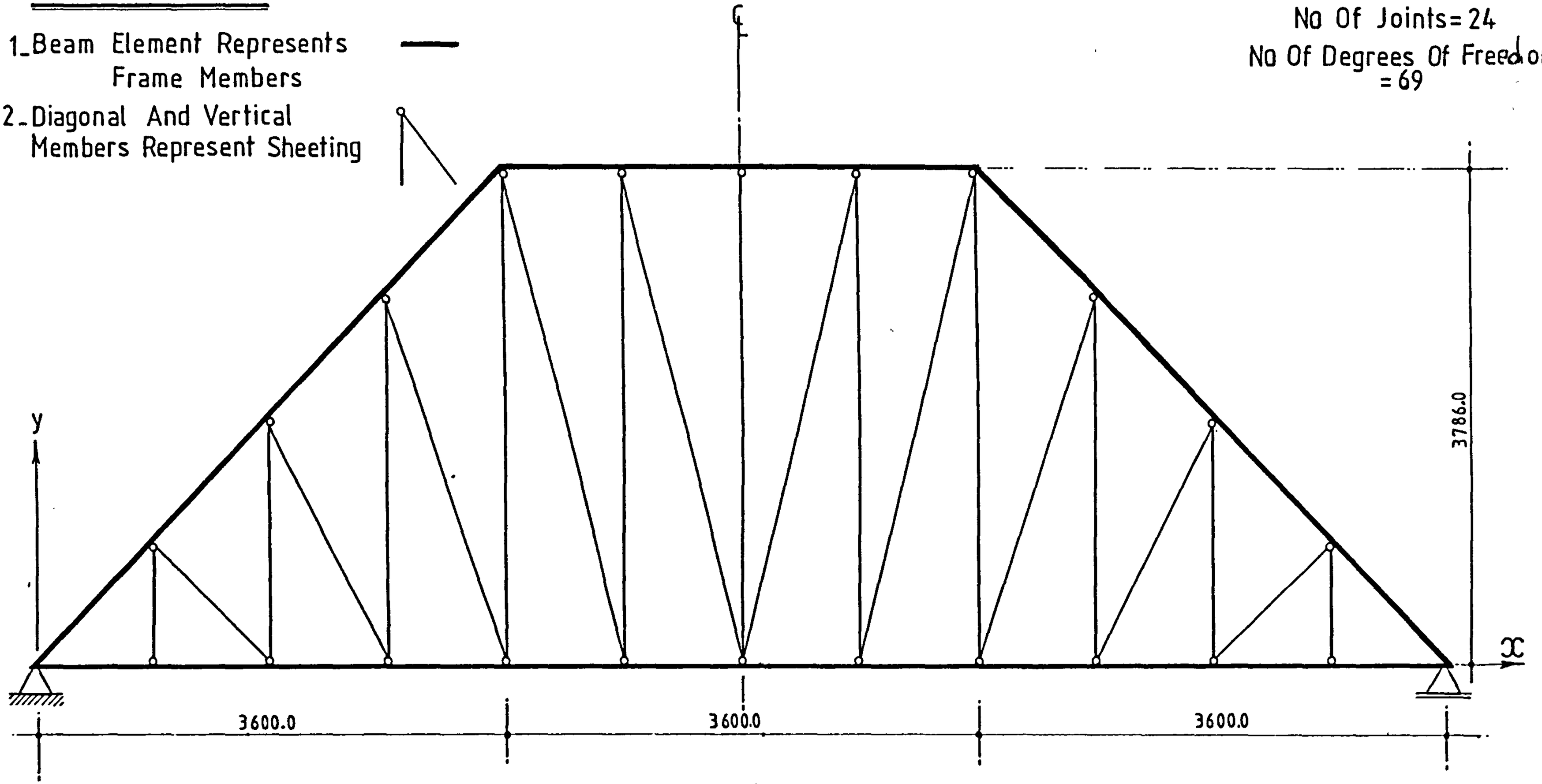

Fig.9.12 Simplified Truss For The Analysis Of The Diaphragm

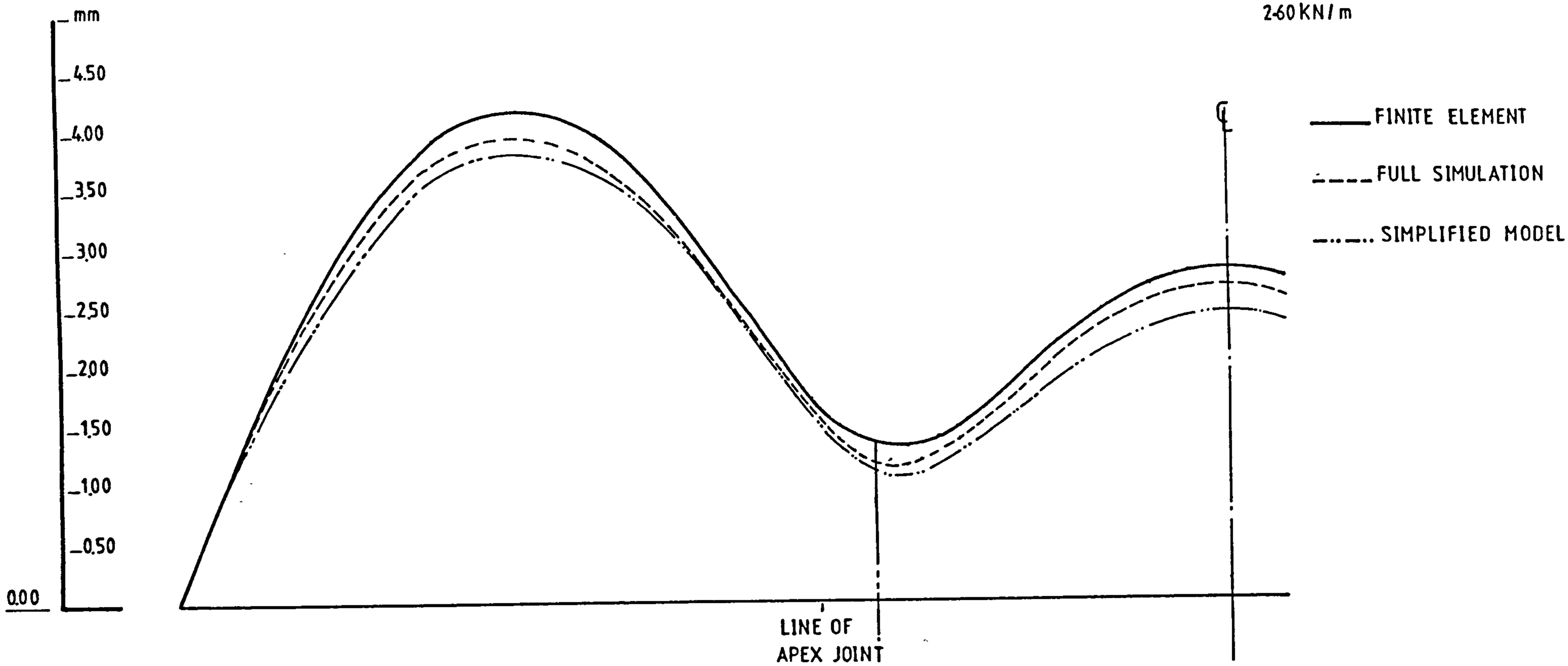

Fig. 9.13 Wind Load Case, In-Plane Displacements Of Bottom Flange
(Corner Joints Are Hinged)

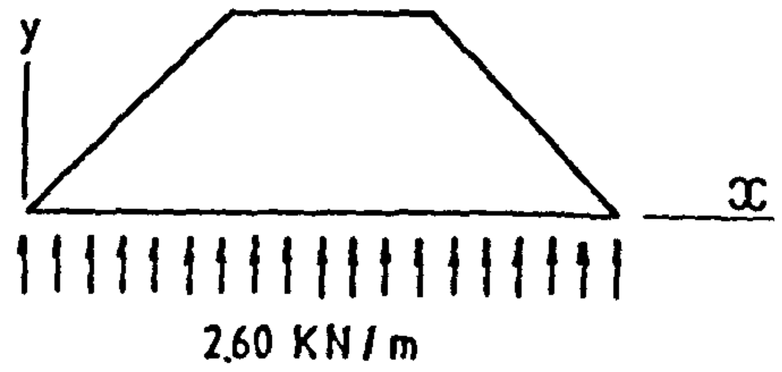

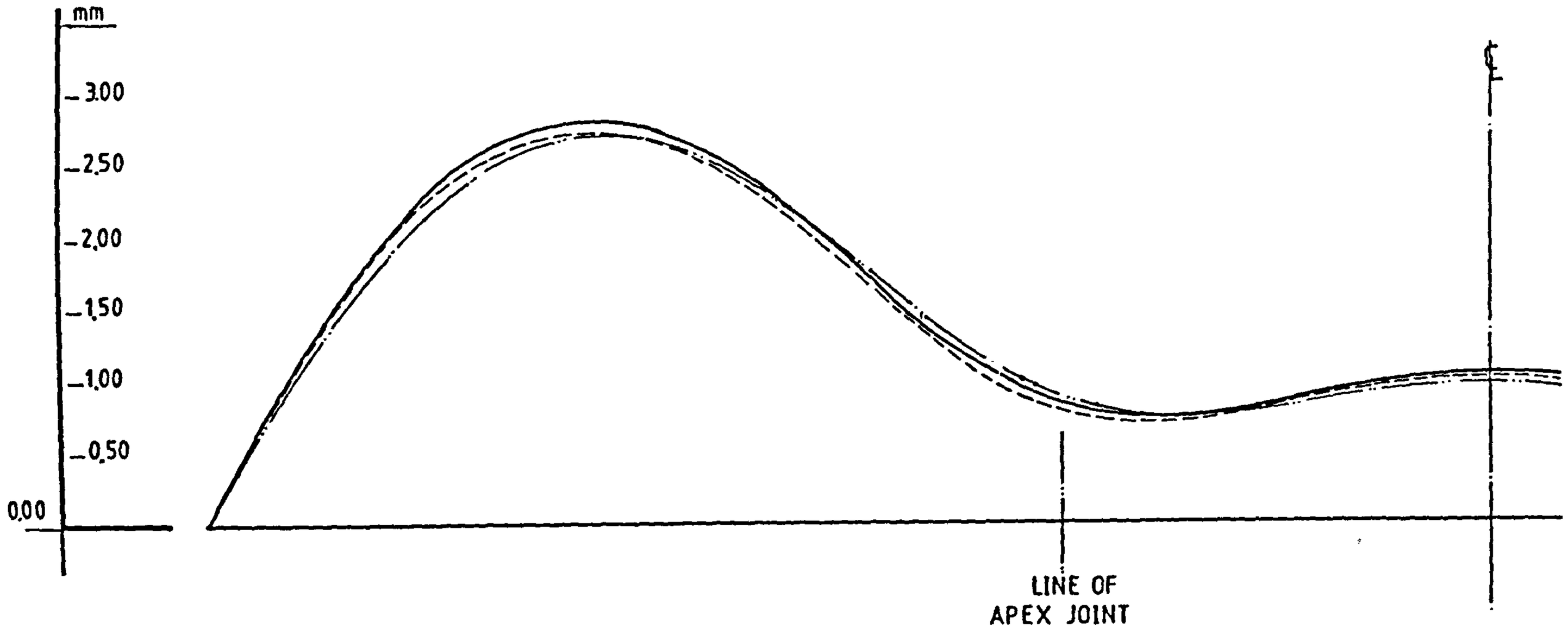

Fig. 9.14 Wind Load Case, In-Plane Displacements Of Bottom Flange
(Corner Joints Are Fixed)

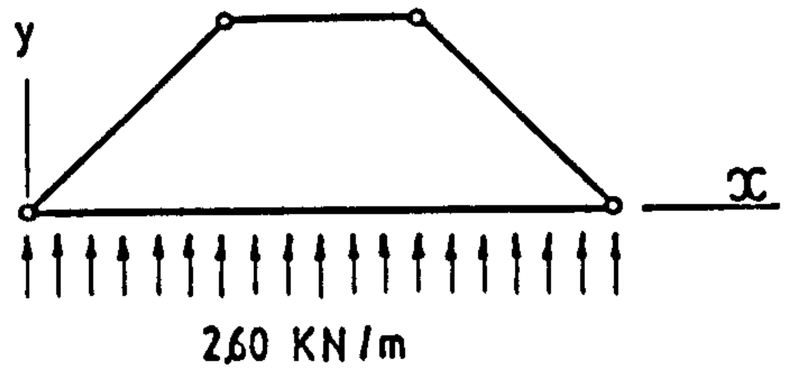

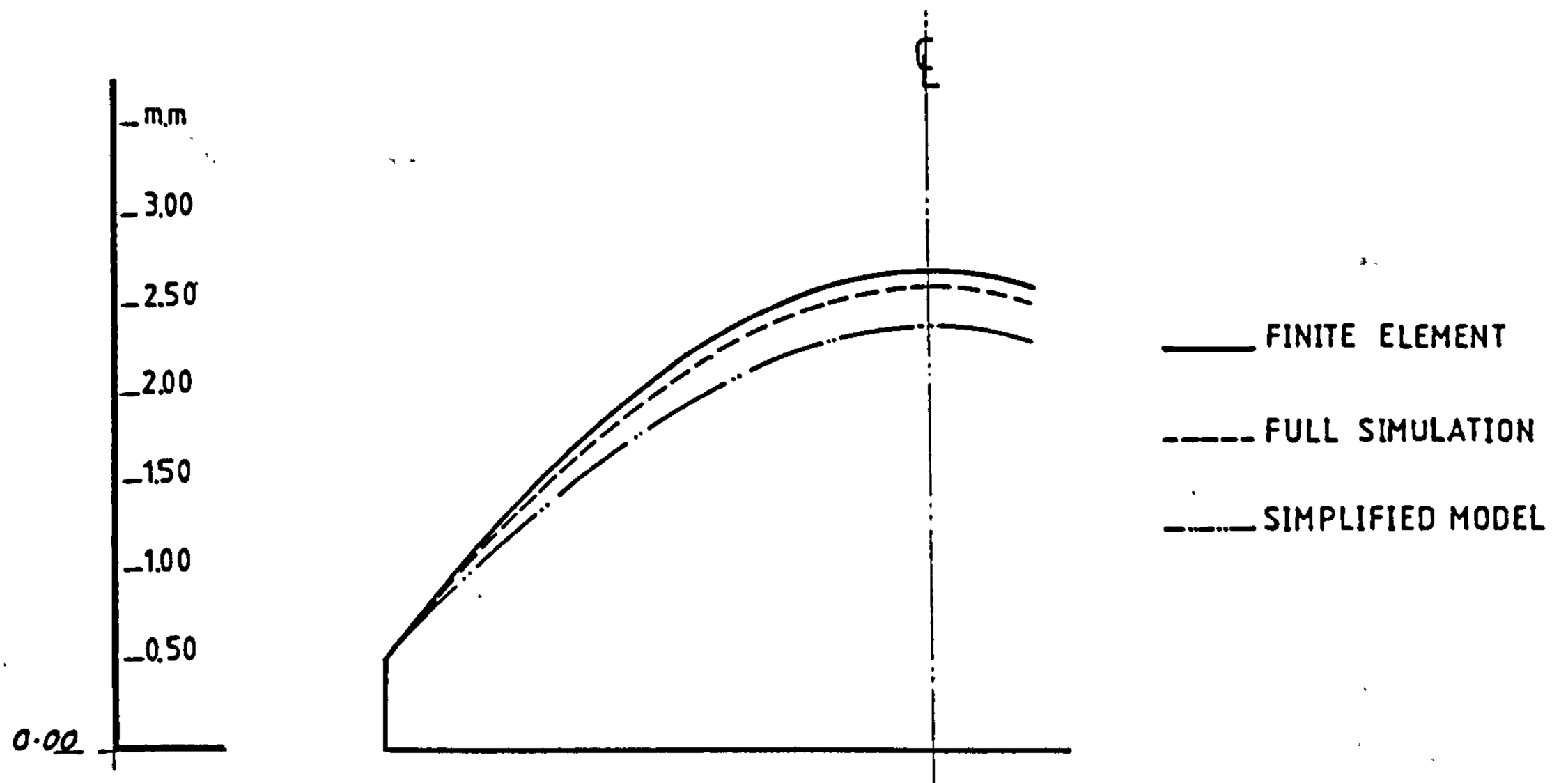

Fig. 9.15 Wind Load Case, In-Plane Displacements Of Top Flange
(Corner Joints Are Hinged)

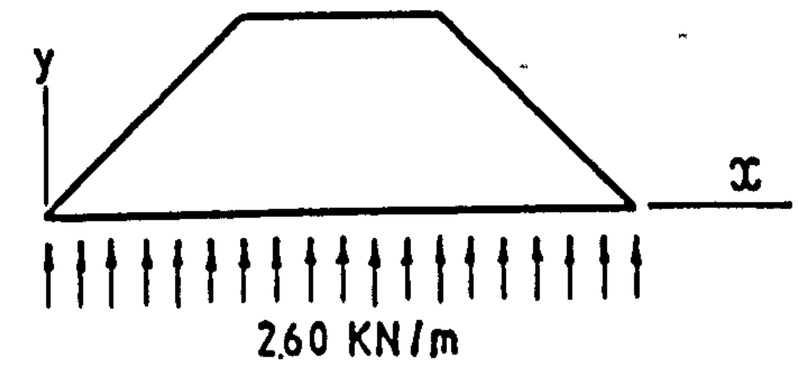

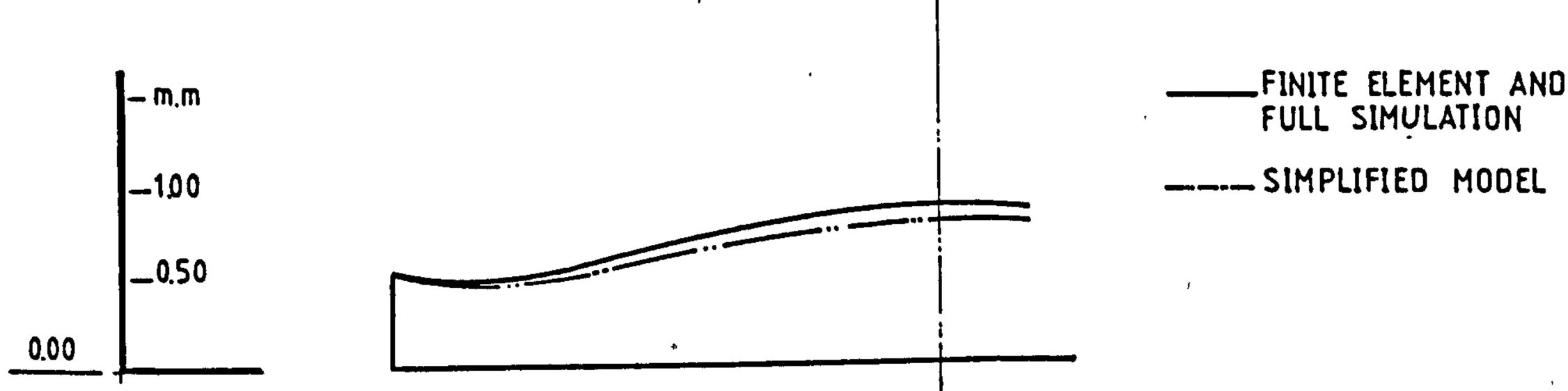

Fig. 9.16 Wind Load Case, In-Plane Displacements Of Top Flange
(Corner Joints Are Hinged)

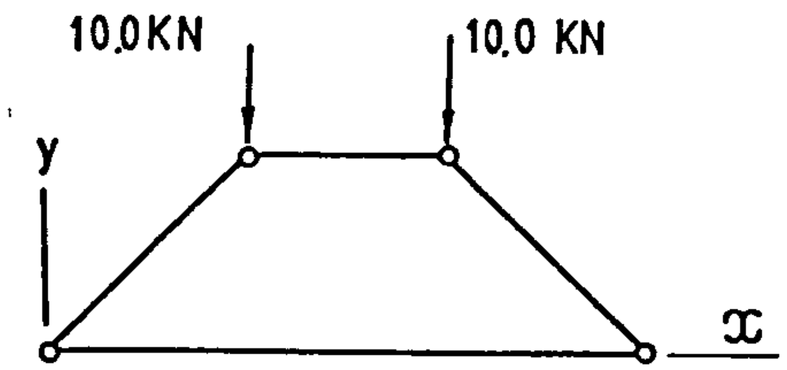

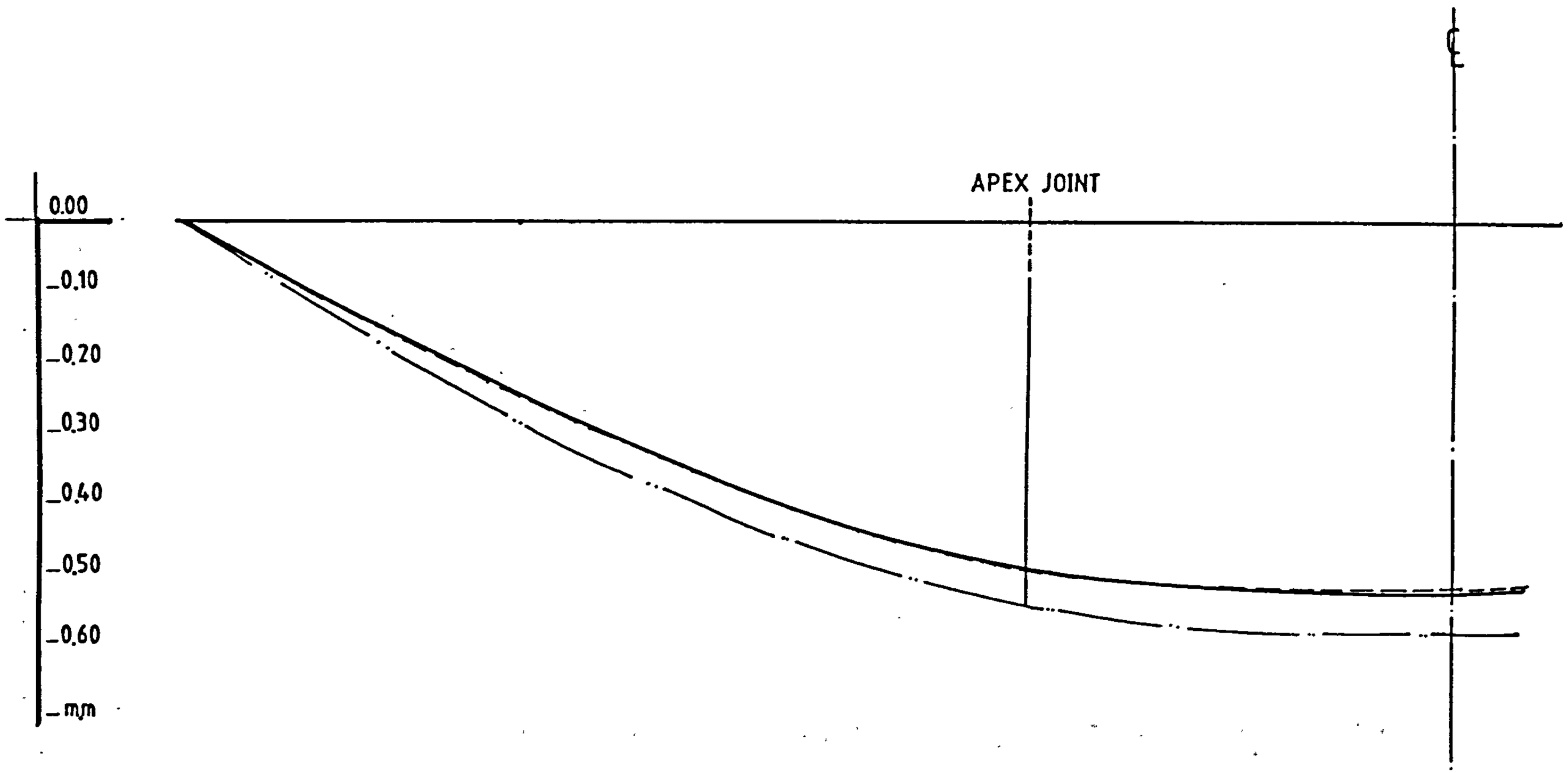

Fig.9.17 Case Of Two Vertical Loads 10.0 Kn Each At Apex Joint
In-Plane Displacements Of Bottom Flange
(Corner Joints Are Hinged)

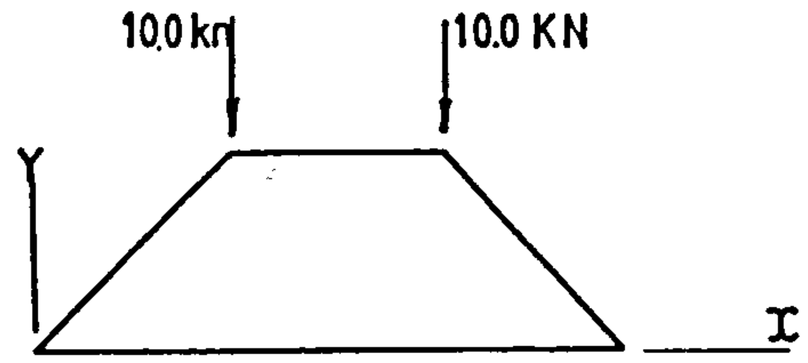

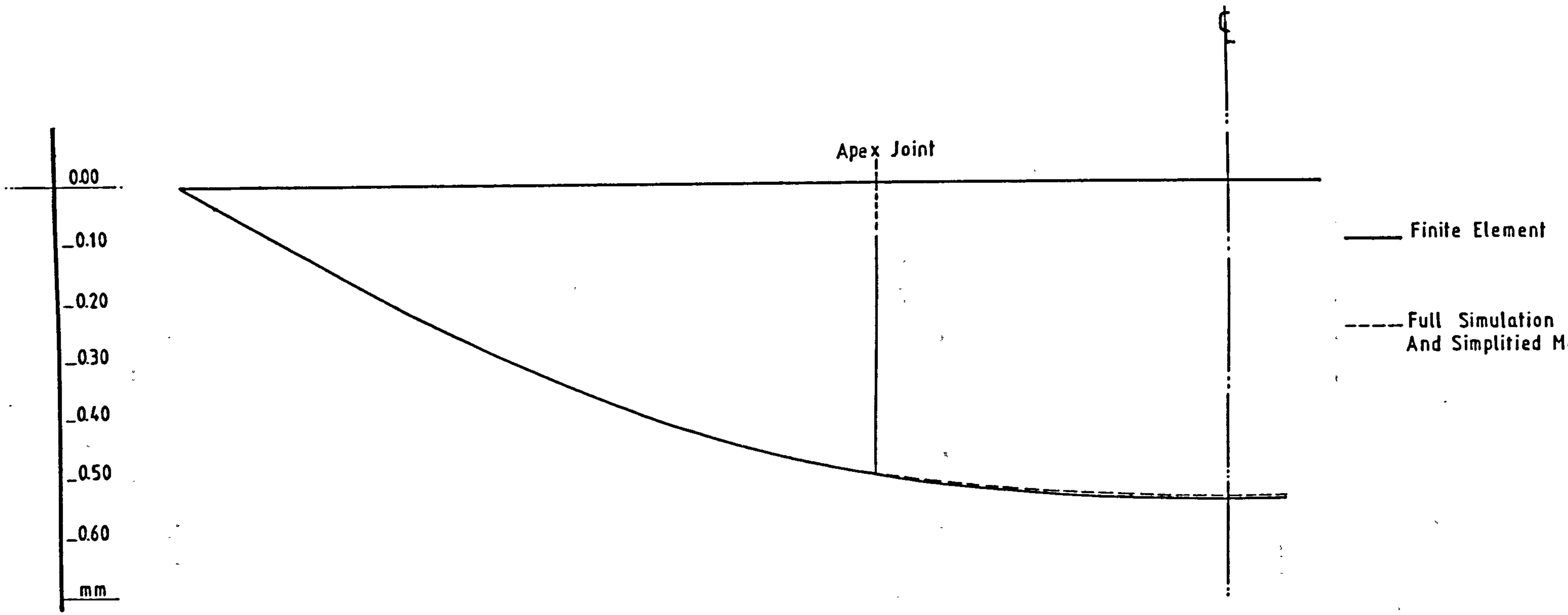

Fig.9.18 Case Of Two Vertical Loads 10.0 Kn Each At Apex Joint
In-Plane Displacements Of Bottom Flange
(Corner Joints Are Fixed)

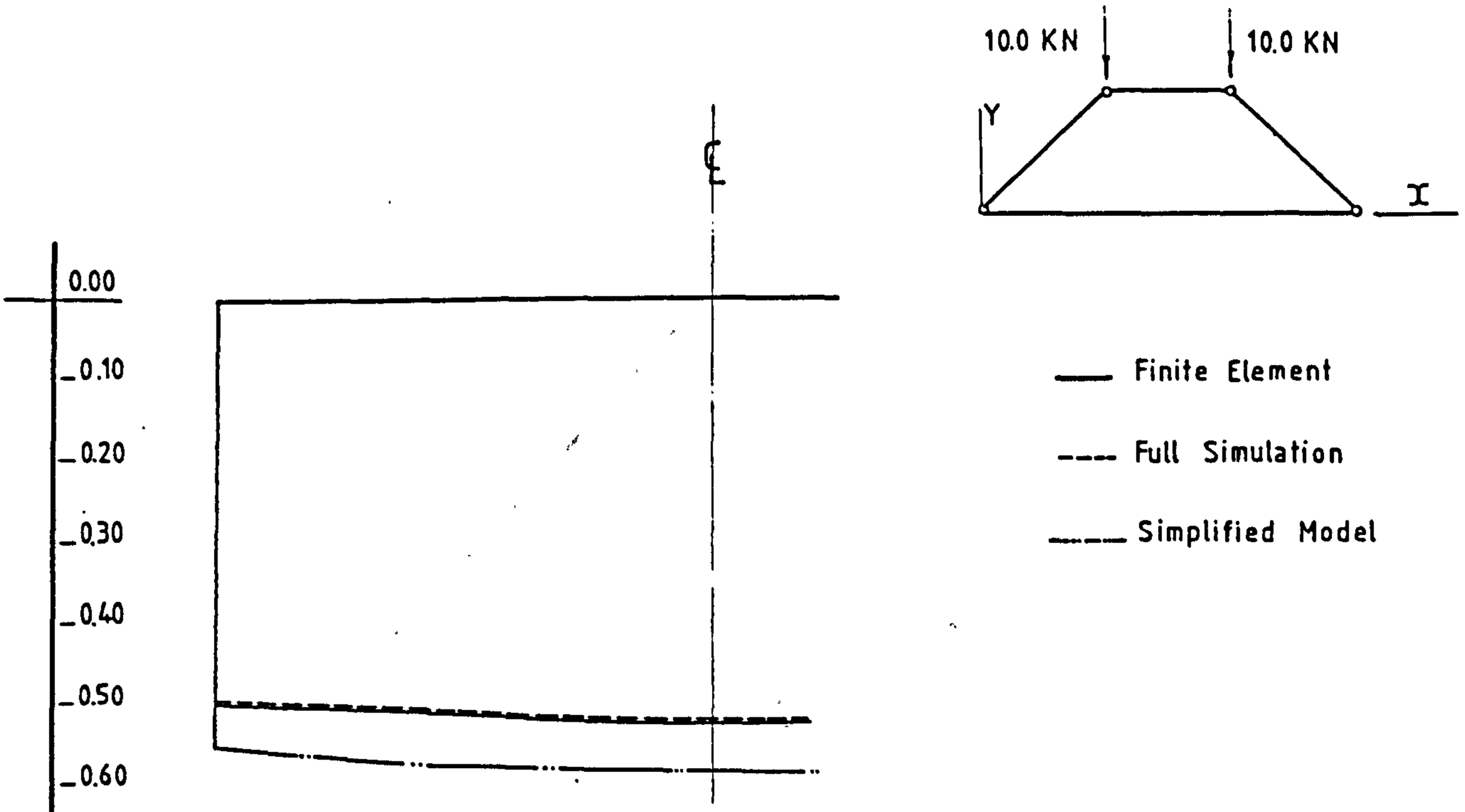

Fig.9.19 Case Of Two Vertical Loads 10.0 KN Each At Apex Joint
In_Plane Displacements Of Top Flange
(Corner Joints Are Fixed)

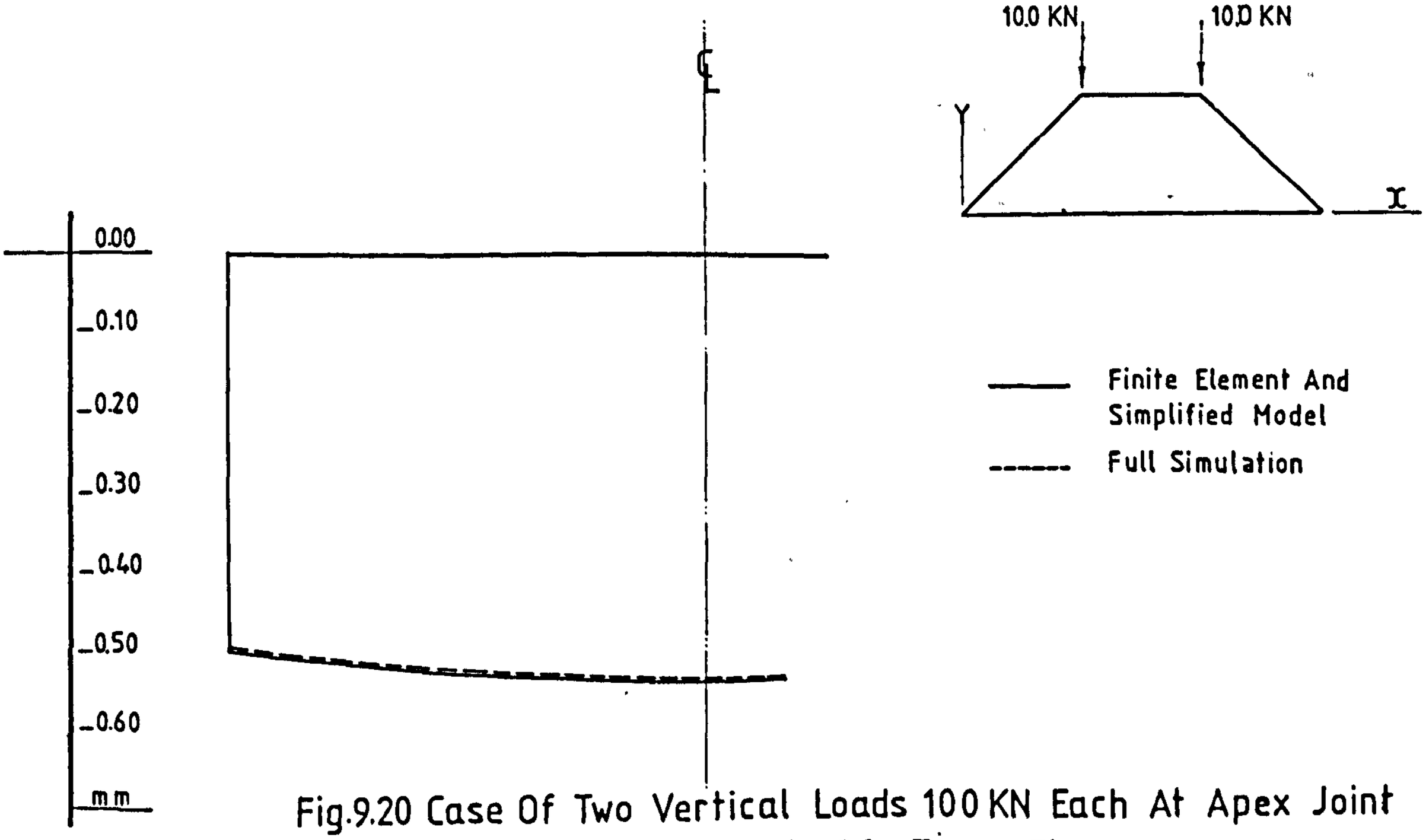

Fig.9.20 Case Of Two Vertical Loads 100 KN Each At Apex Joint
In.Plane Displacements Of Top Flange
(Corner Joints Are Fixed)

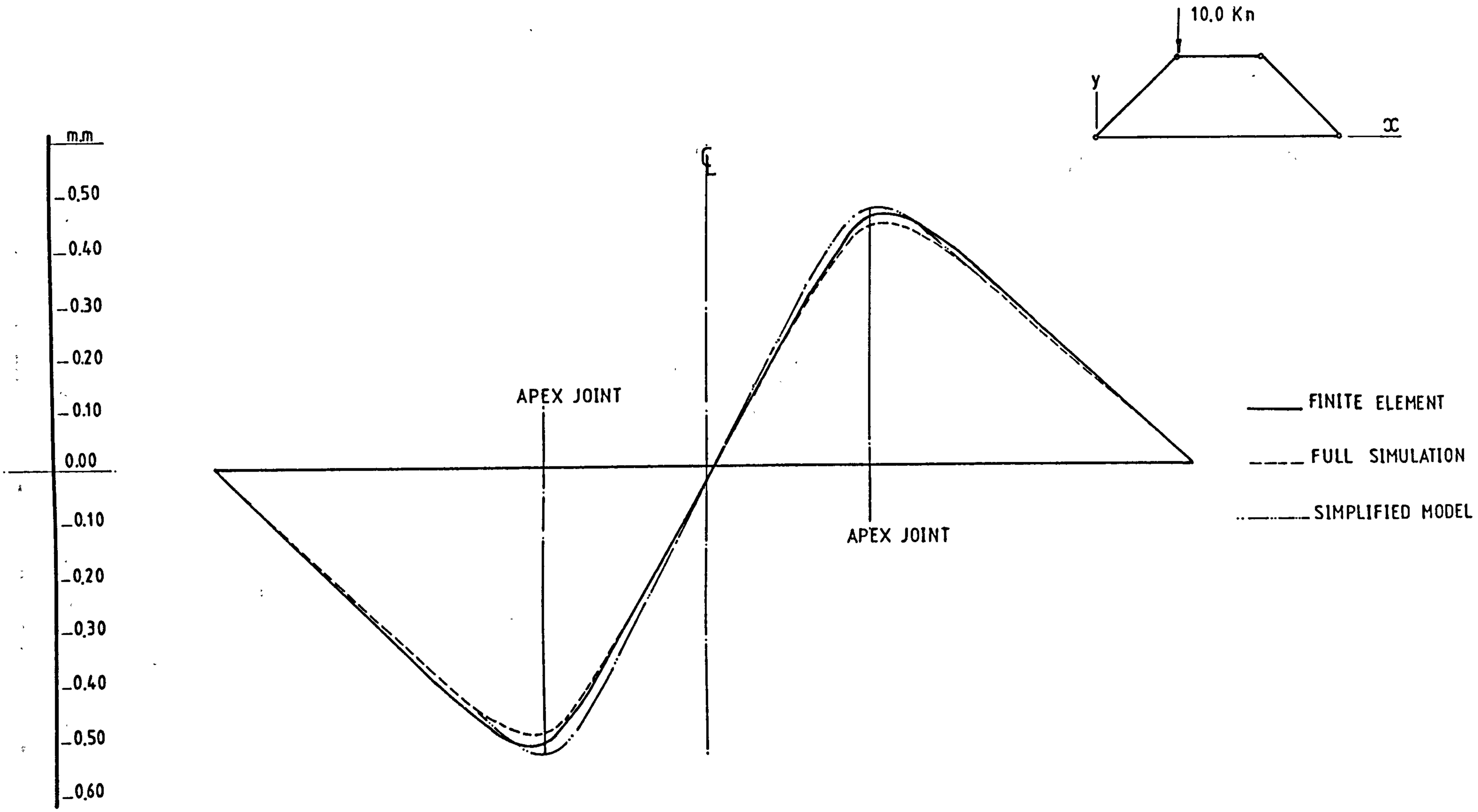

Fig.9.21 Case Of One Vertical Load 10.0 kn At Apex Joint
In-Plane Displacements Of Bottom Flange
(Corner Joints Are Hinged)

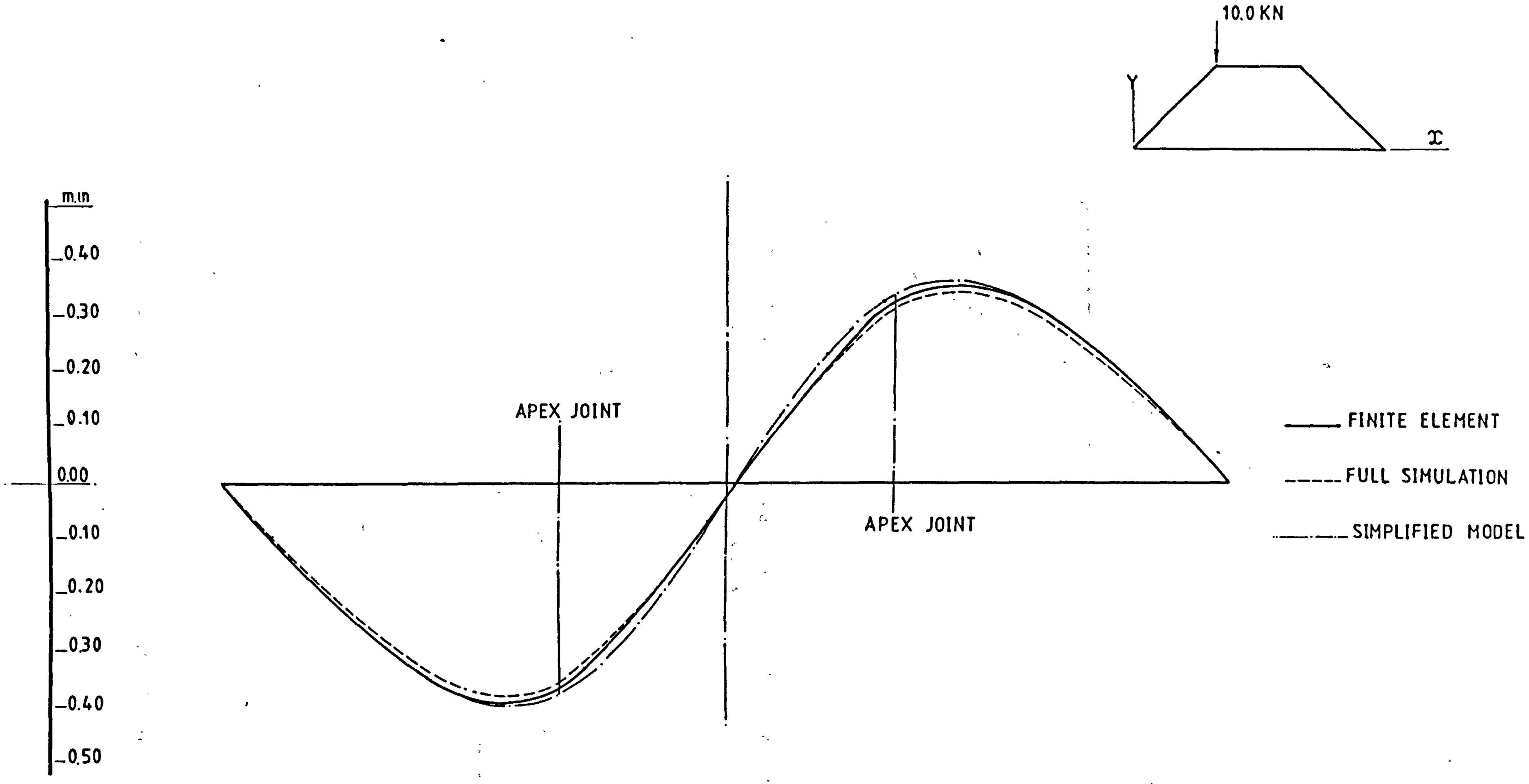

Fig. 9.22 Case Of One Vertical Load 10.0 kn At Apex Joint
In-Plane Displacements Of Bottom Flange
(Corner Joints Are Fixed)

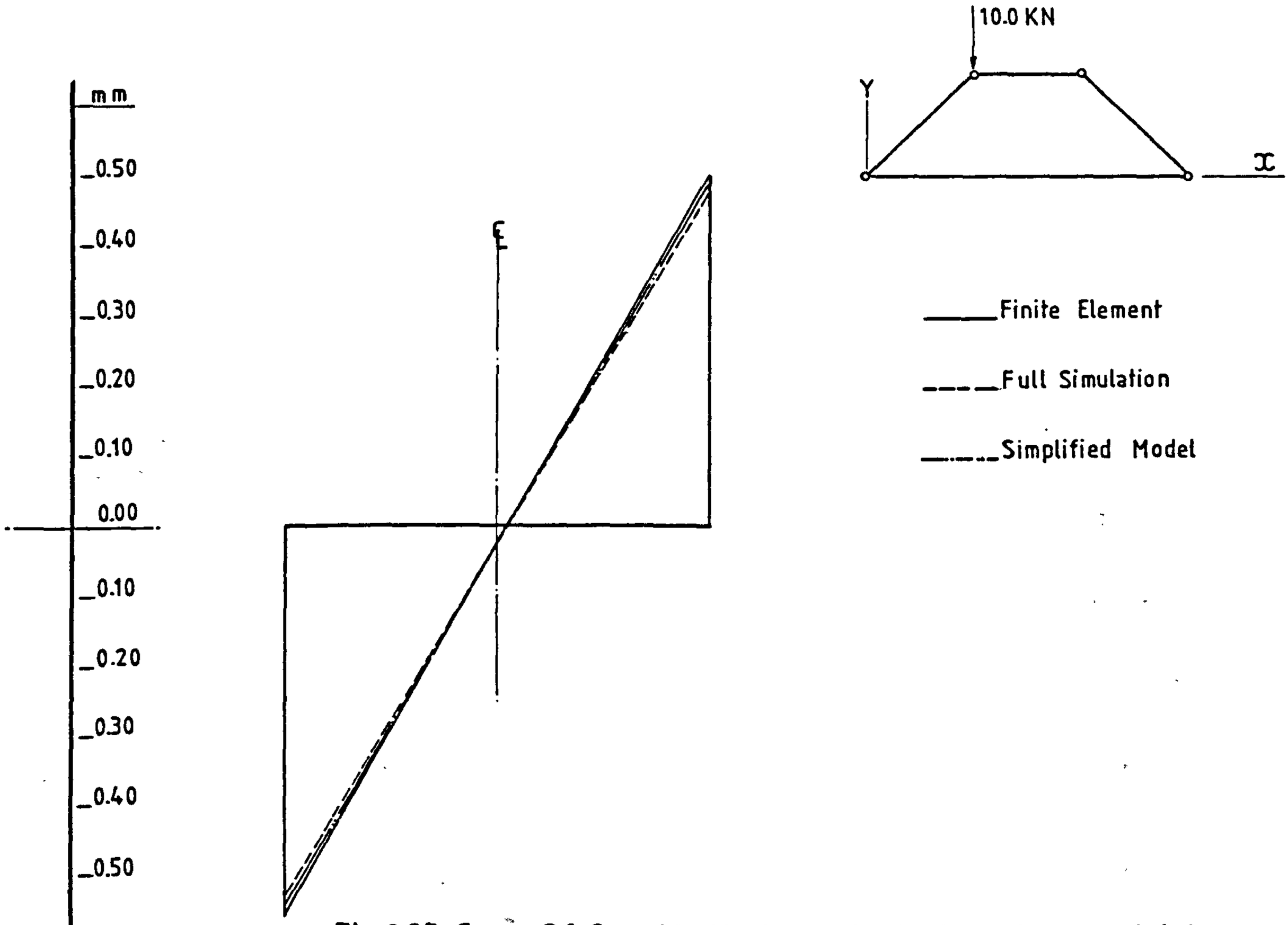

Fig.9.23 Case Of One Vertical Load 10.0 kn At Apex Joint
In Plane Displacements Of Top Flange
(Corner Joints Are Hinged)

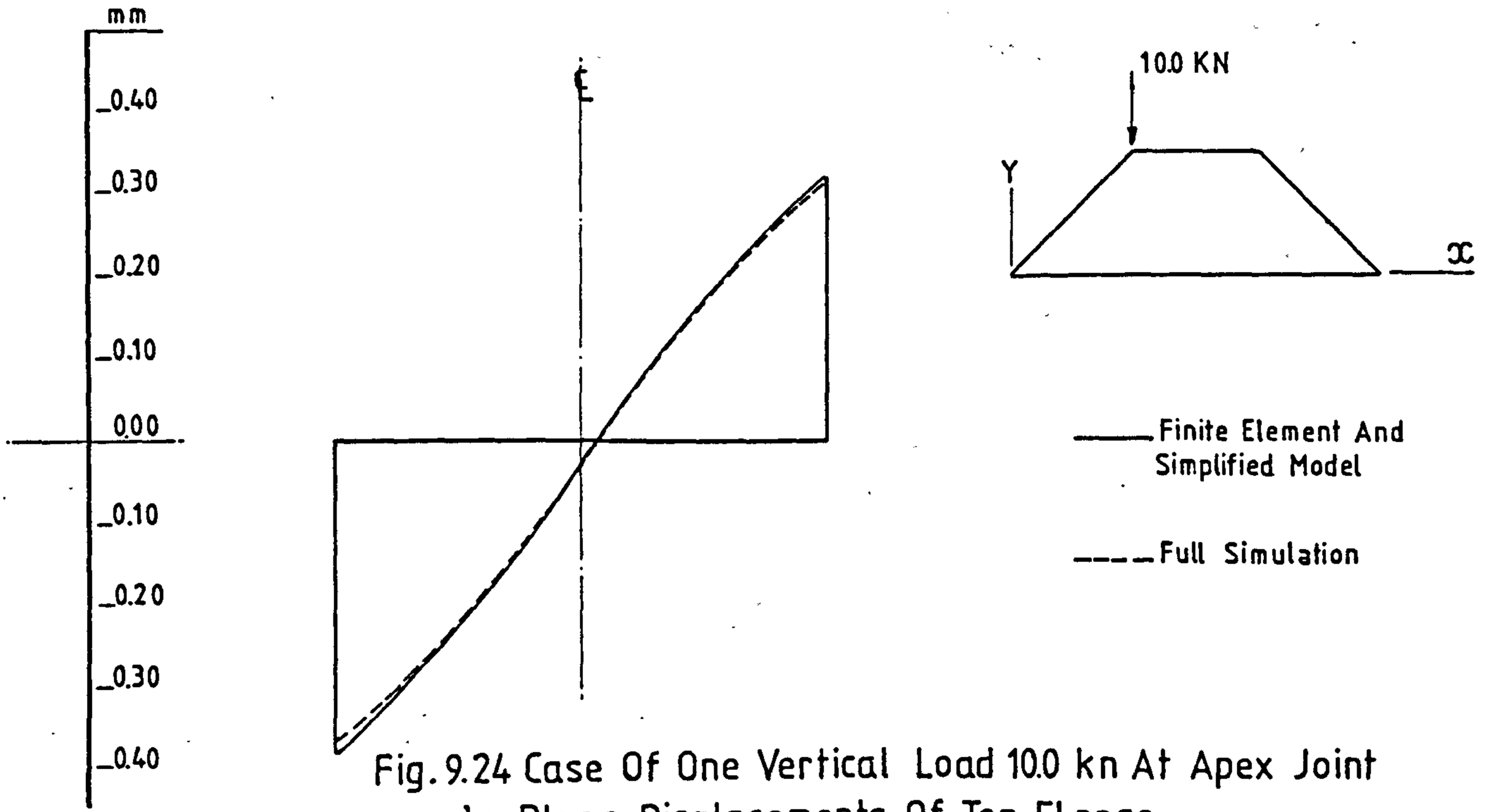

Fig. 9.24 Case Of One Vertical Load 10.0 kn At Apex Joint
In_Plane Displacements Of Top Flange
(Corner Joints Are Fixed).

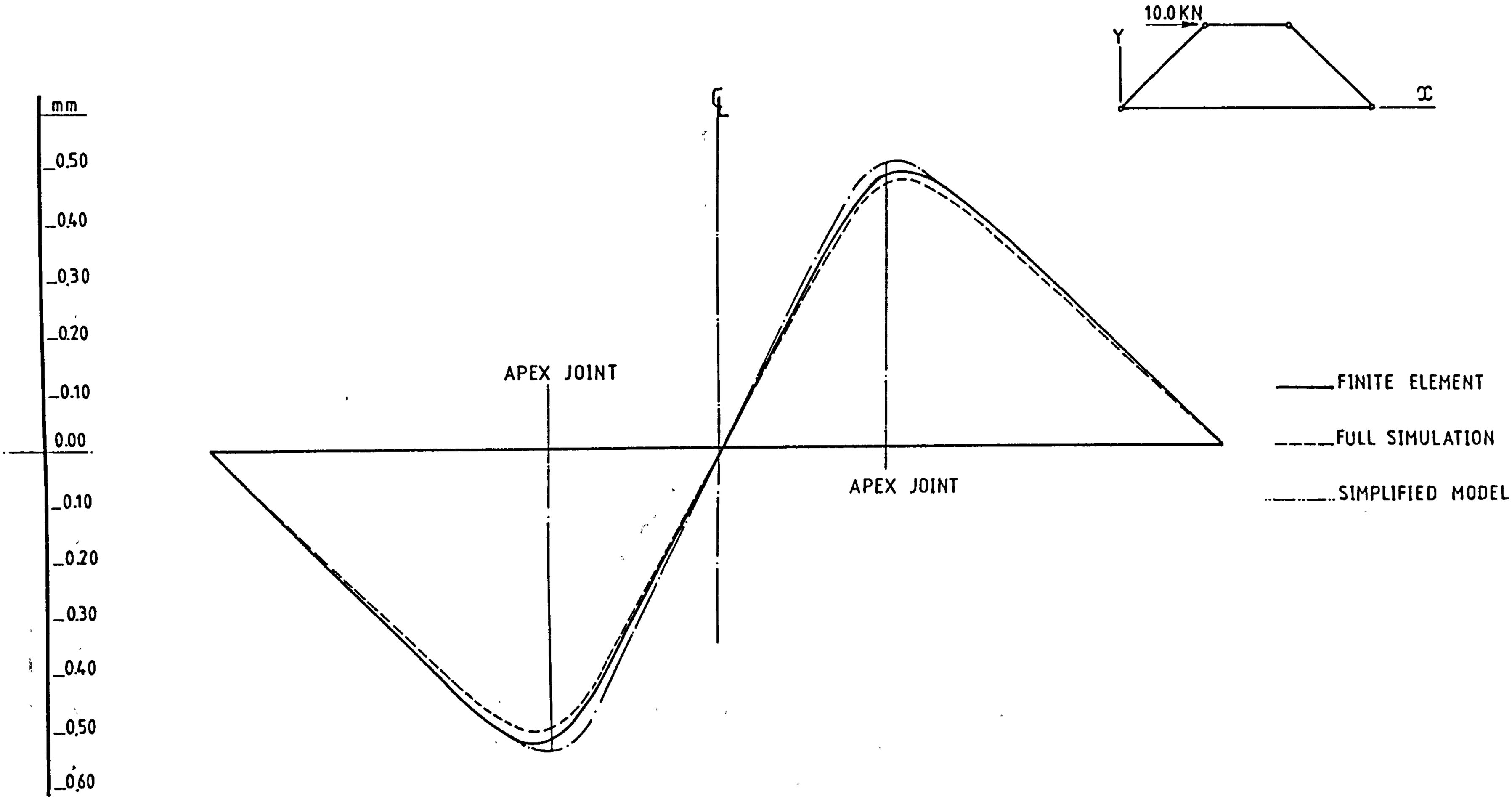

Fig.9.25 Case Of A Side Load 10.0 kn At Apex Joint
In Plane Displacements Of Bottom Flange
(Corner Joints Are Linged)

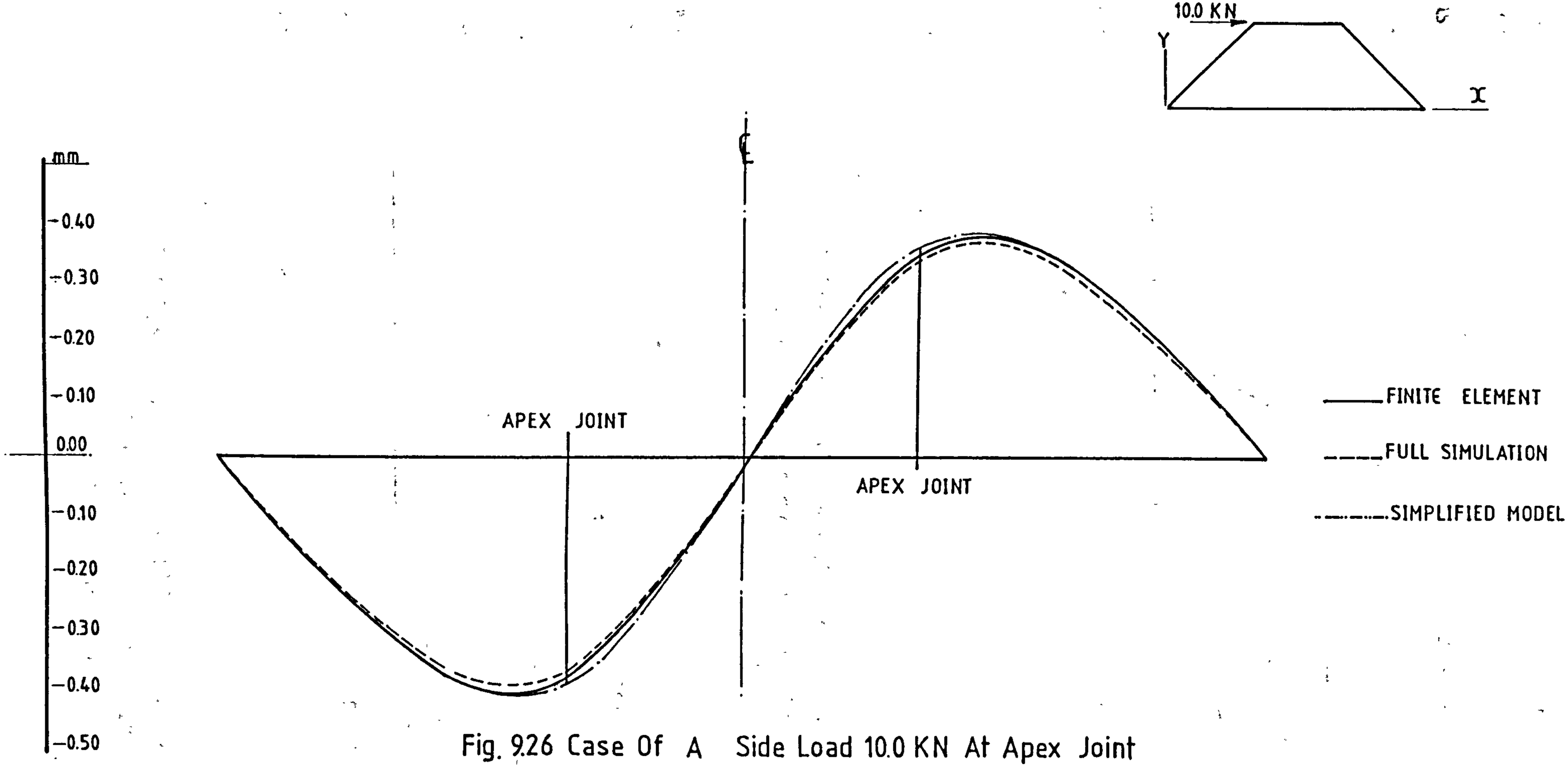

Fig. 9.26 Case Of A Side Load 10.0 KN At Apex Joint
In-Plane Displaecements Of Bottom Flange
(Corner Joints. Are Fixed)

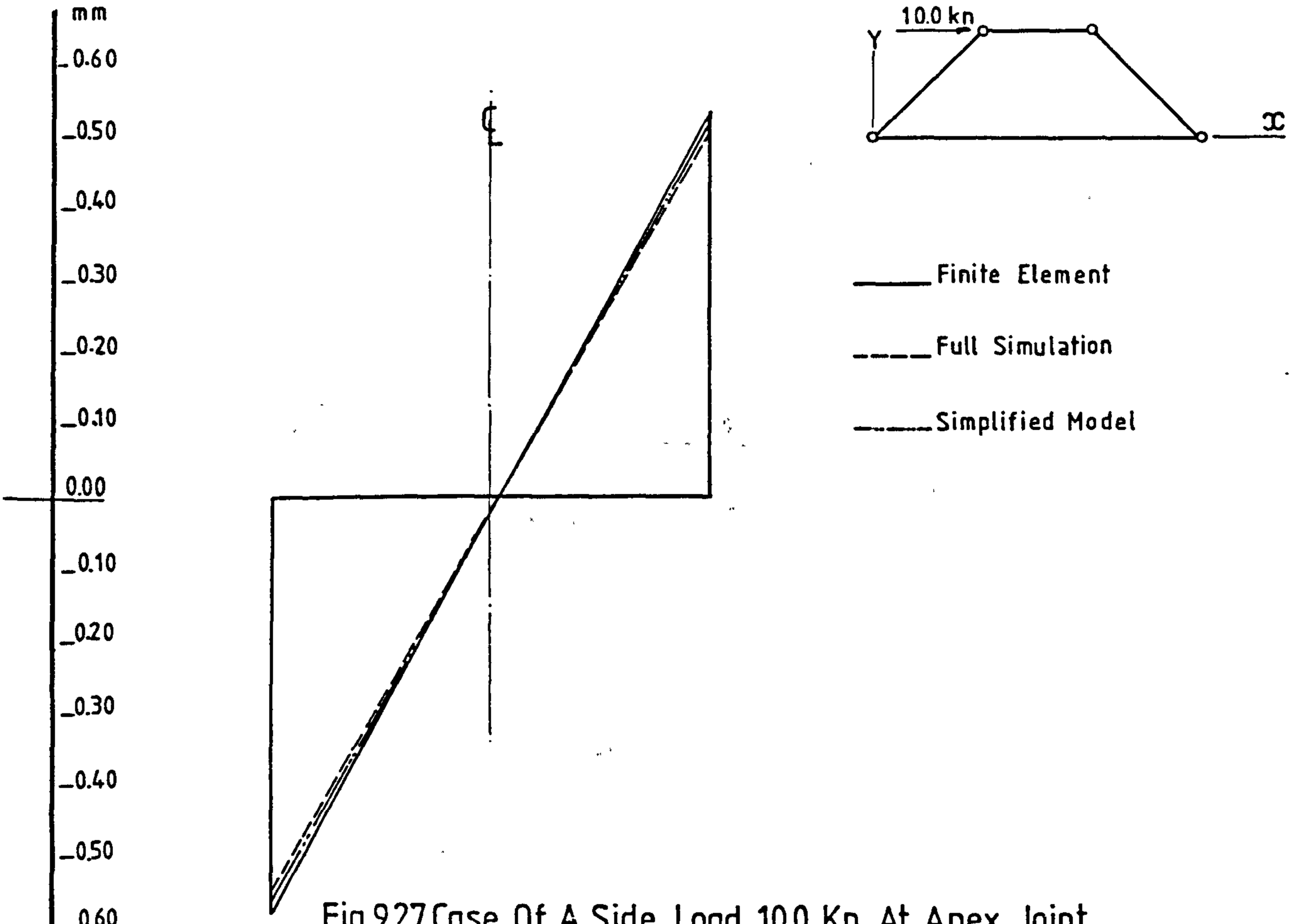

Fig.9.27 Case Of A Side Load 10.0 Kn At Apex Joint
In-Plane Displacements Of Top Flange
(Corner Joints Are Hinged)

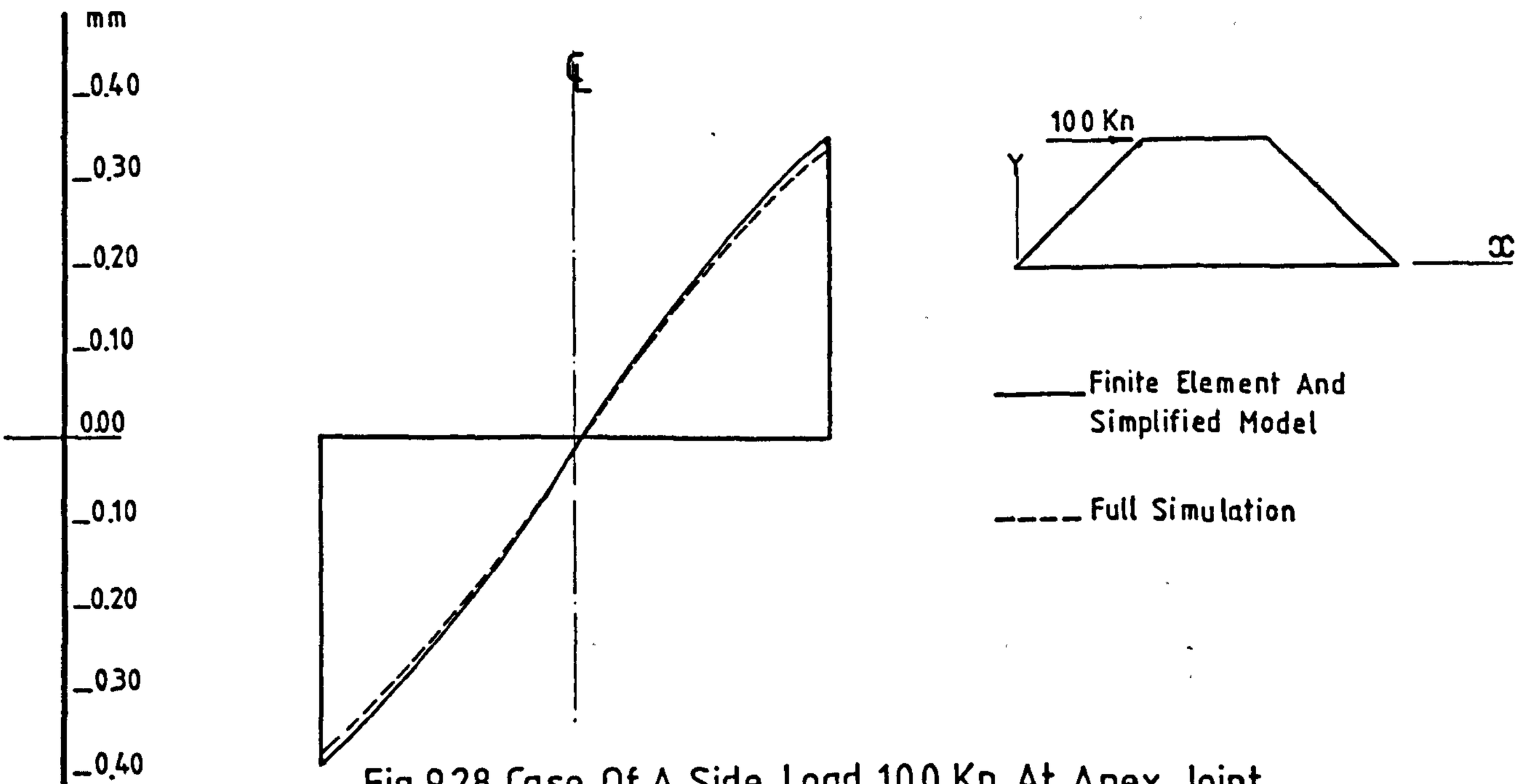

Fig.9.28 Case Of A Side Load 10.0 Kn At Apex Joint
In-Plane Displacements Of Top Flange
(Corner Joints Are Fixed)

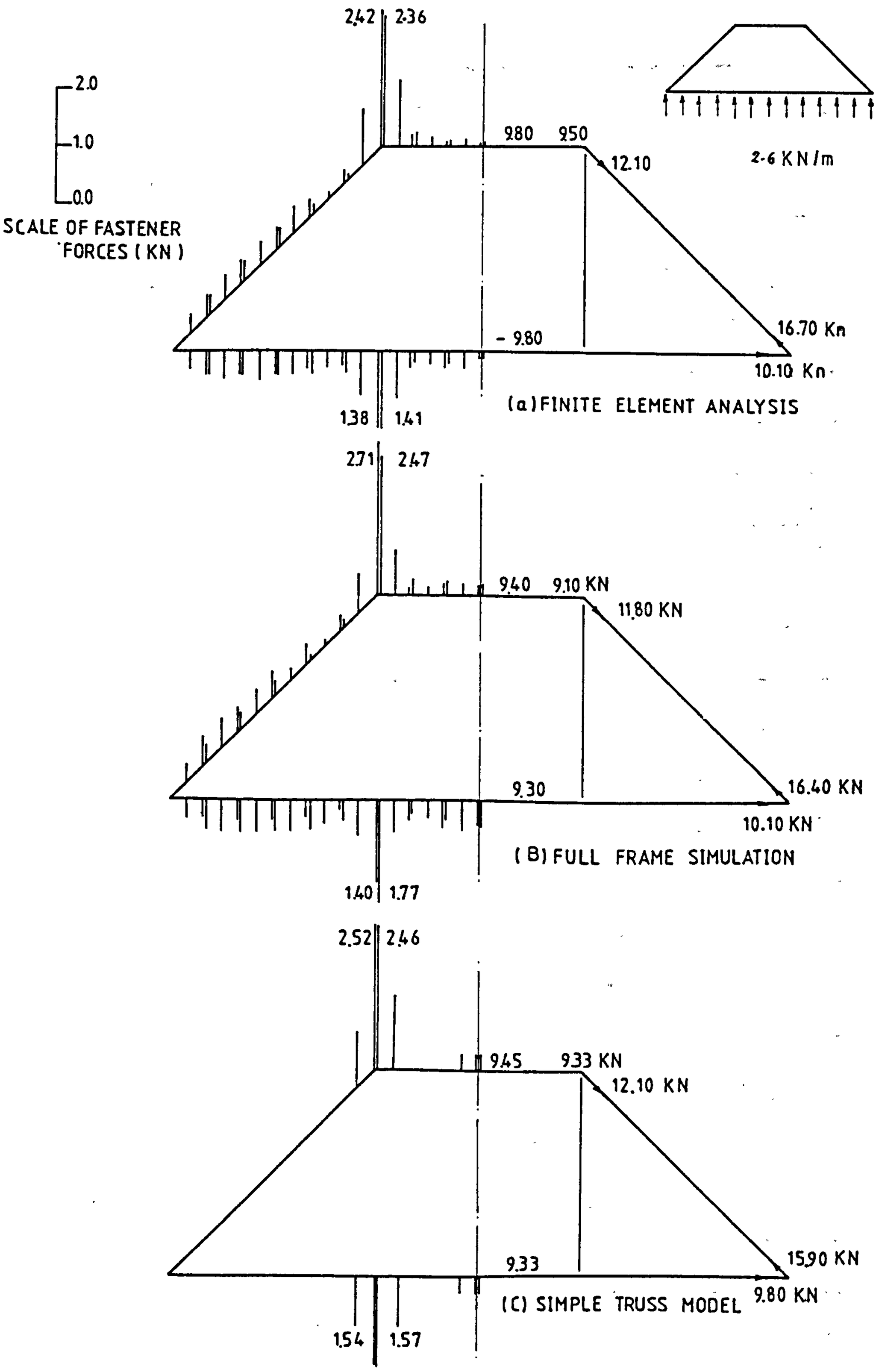

Fig. 9.29 Fastener Forces Due To Wind Load
(Hinged Corners Model)

H=Hinged Corners

R=Rigid Corners

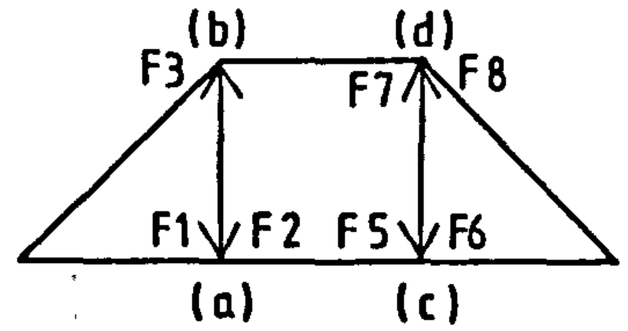

LOADING CASE / MODEL / FASTENERS		Wind Load 2.60 KN/m						10.0 KN 10.0 KN						10.0 KN						10.0 KN					
		Finite Element		Full Frame Simulation		Simple Truss		Finite Element		Full Frame Simulation		Simple Truss		Finite Element		Full Frame Simulation		Simple Truss		Finite Element		Full Frame Simulation		Simple Truss	
		H.	R.	H.	R.	H.	R.	H.	R.	H.	R.	H.	R.	H.	R.	H.	R.	H.	R.	H.	R.	H.	R.	H.	R.
JOINT a	F1	1.38	0.59	1.40	0.58	1.54	0.77	0.012	0.004	0.013	0.004	0.014	0.004	0.73	0.104	0.89	0.192	0.72	0.100	0.77	0.105	0.93	0.198	0.75	0.100
	F2	1.41	0.62	1.77	0.75	1.57	0.81	0.013	0.005	0.019	0.008	0.015	0.005	0.60	0.063	0.83	0.015	0.60	0.062	0.63	0.067	0.87	0.022	0.62	0.064
JOINT b	F3	2.42	0.81	2.71	0.95	2.52	1.04	0.027	0.010	0.031	0.012	0.029	0.010	1.56	0.26	1.74	0.23	1.63	0.33	1.63	0.26	1.82	0.23	1.71	0.33
	F4	2.36	0.77	2.47	0.81	2.46	0.99	0.025	0.009	0.027	0.009	0.027	0.010	1.65	0.35	1.93	0.47	1.72	0.44	1.72	0.36	2.02	0.49	1.81	0.45
JOINT c	F5	1.41	0.62	1.77	0.75	1.57	0.81	0.013	0.005	0.019	0.008	0.015	0.005	0.59	0.063	0.81	0.023	0.58	0.060	0.62	0.067	0.86	0.025	0.61	0.64
	F6	1.38	0.59	1.40	0.58	1.54	0.77	0.012	0.004	0.013	0.004	0.014	0.004	0.72	0.100	0.88	0.187	0.71	0.095	0.76	0.105	0.92	0.196	0.74	0.100
JOINT d	F7	2.36	0.77	2.47	0.81	2.46	0.99	0.025	0.009	0.027	0.009	0.027	0.010	1.62	0.34	1.90	0.46	1.70	0.43	1.71	0.36	2.00	0.49	1.79	0.45
	F8	2.42	0.81	2.71	0.95	2.52	1.04	0.027	0.010	0.031	0.012	0.029	0.010	1.53	0.25	1.71	0.22	1.61	0.32	1.61	0.26	1.79	0.23	1.68	0.33

Table 9.1 Critical Fastener Forces For Hinged And Fixed Models

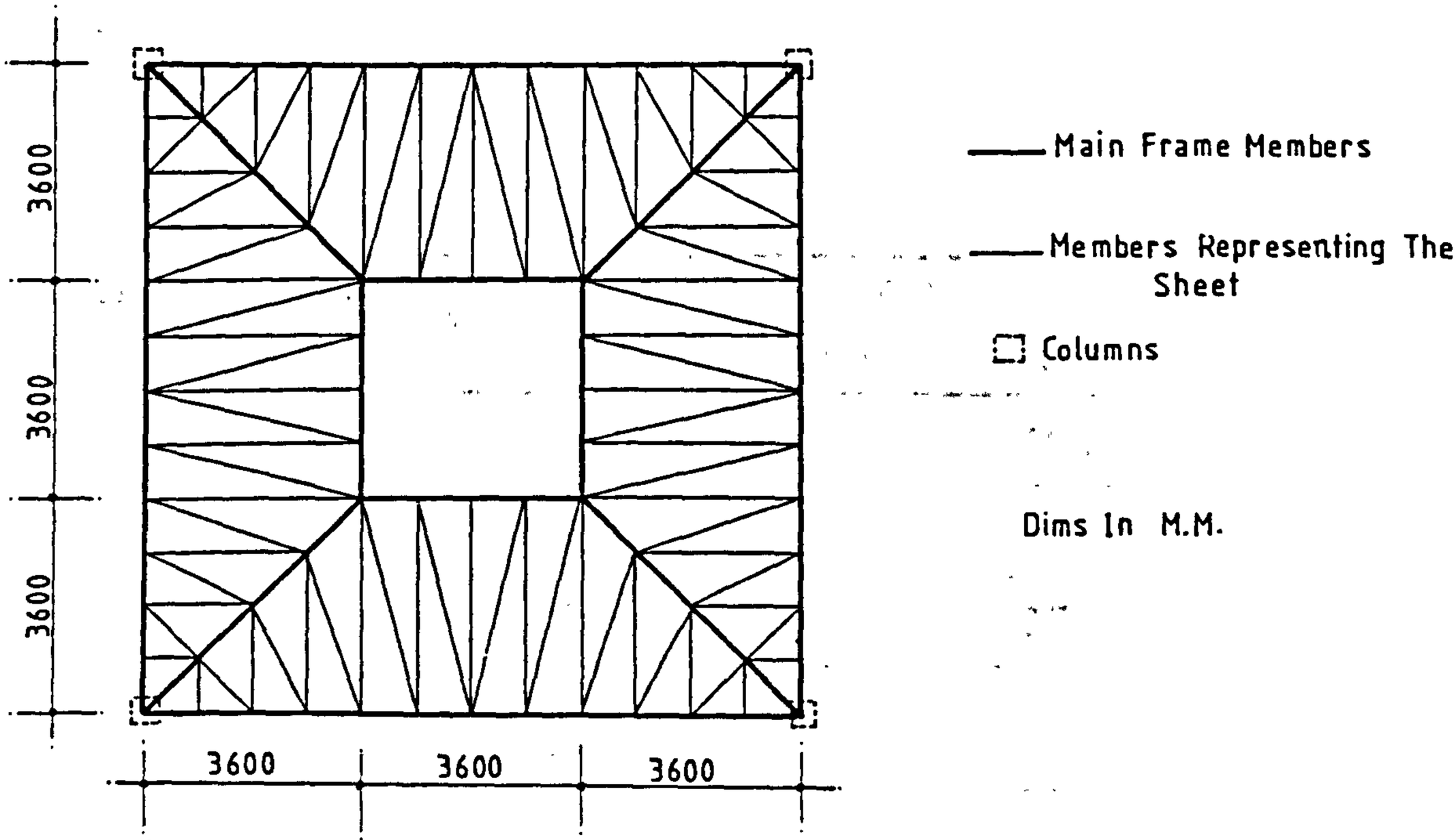

Fig.9.30 The Model Used To Analyse The MACE Unit

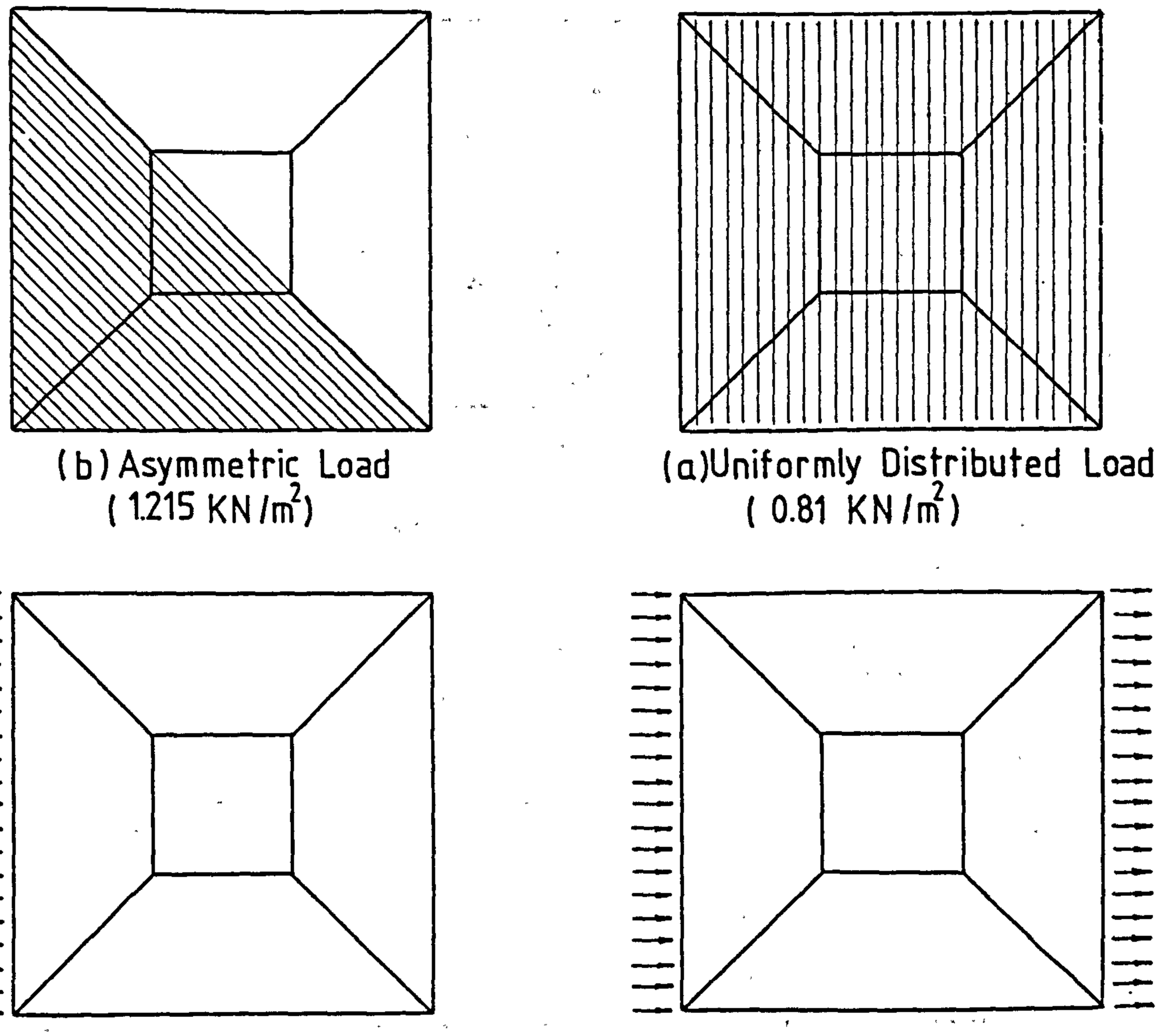

(b) Asymmetric Load
(1.215 KN/m^2)

(a)Uniformly Distributed Load
(0.81 KN/m^2)

(C)Wind Load On One Side
(2.46 KN/m)

(d) Wind Load On Both Sides
(1.23 KN/m/Side)

Fig. 9.31 Cases Of Loading On The MACE Structure

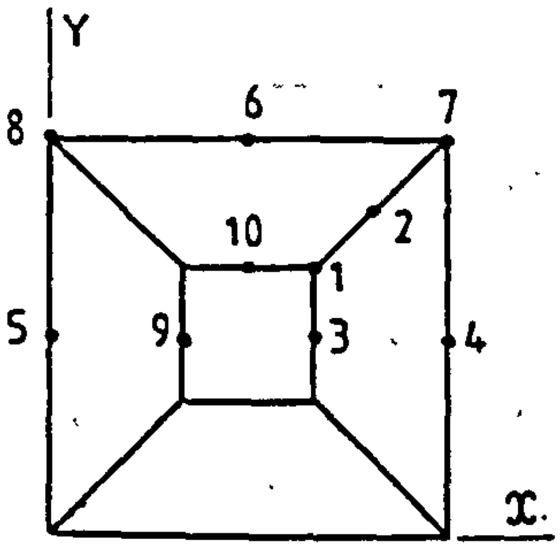

DISPL. IN mm

JOINT	DIRECTION	EXPERIMENTAL RESULTS	THEORETICAL	
			HINGED	FIXED
1	Z	12.60	9.26	9.06
2	Z	7.50	10.50	5.75
3	Z	13.90	12.60	10.78
3	X	0.95	0.65	0.19
4	X	4.17	3.50	3.35
7	Z	0.11	0.28	0.25
7	X	0.92	1.05	1.02

Table 9.2 Experimental And Theoretical Displacements Under U.D.L. 0.81 KN/m^2

JOINT	DIRECTION	CASE "C" "WIND ON ONE SIDE"			CASE "D" "WIND ON BOTH SIDES"		
		EXPERIME.	THEORETICAL		EXPERIME.	THEORETICAL	
			HINGED	FIXED		HINGED	FIXED
3	X	1.80	2.23	2.14	2.65	3.54	2.73
4	X	2.43	1.72	1.68	6.23	3.92	2.95
5	X	9.85	6.14	4.21	4.94	3.92	2.95
6	Y	-0.15	-0.50	-0.55	-0.05	0.0	0.0
7	X	1.50	1.62	1.57	2.17	1.82	1.76
8	X	1.90	2.02	1.95	1.75	1.82	1.76
9	X	3.35	4.94	3.23	2.42	3.54	2.73
10	Y	-0.10	-0.04	-0.04	-0.02	0.0	0.0

Table 9.3 Experimental And Theoretical Displacements Under Wind Load Cases

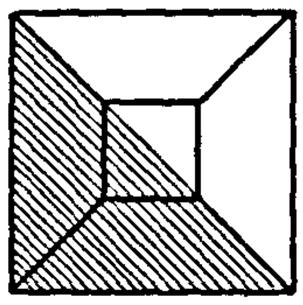

Asymmetric Load
(1.215 Kn/m^2)

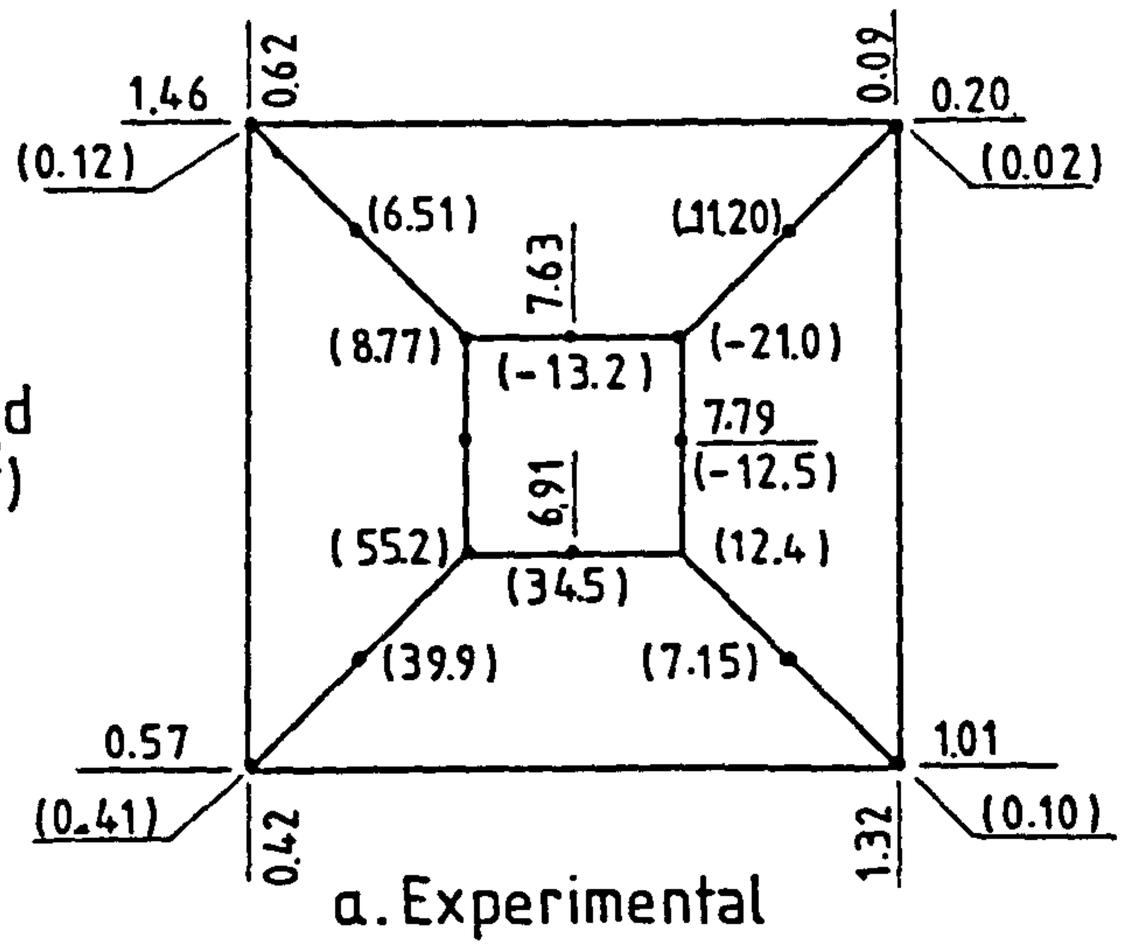

DISPL IN MM
-Ve = UPWARD
(VERTICAL)

a. Experimental

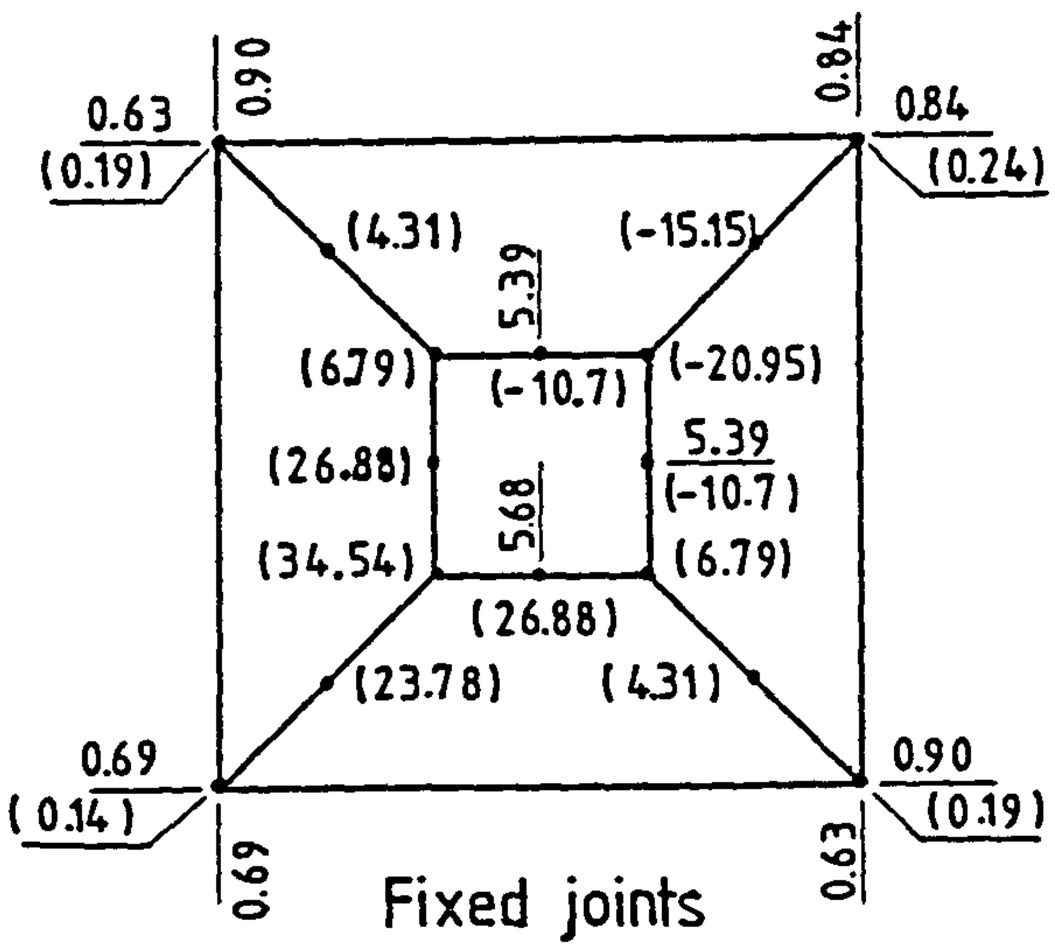

Fixed joints

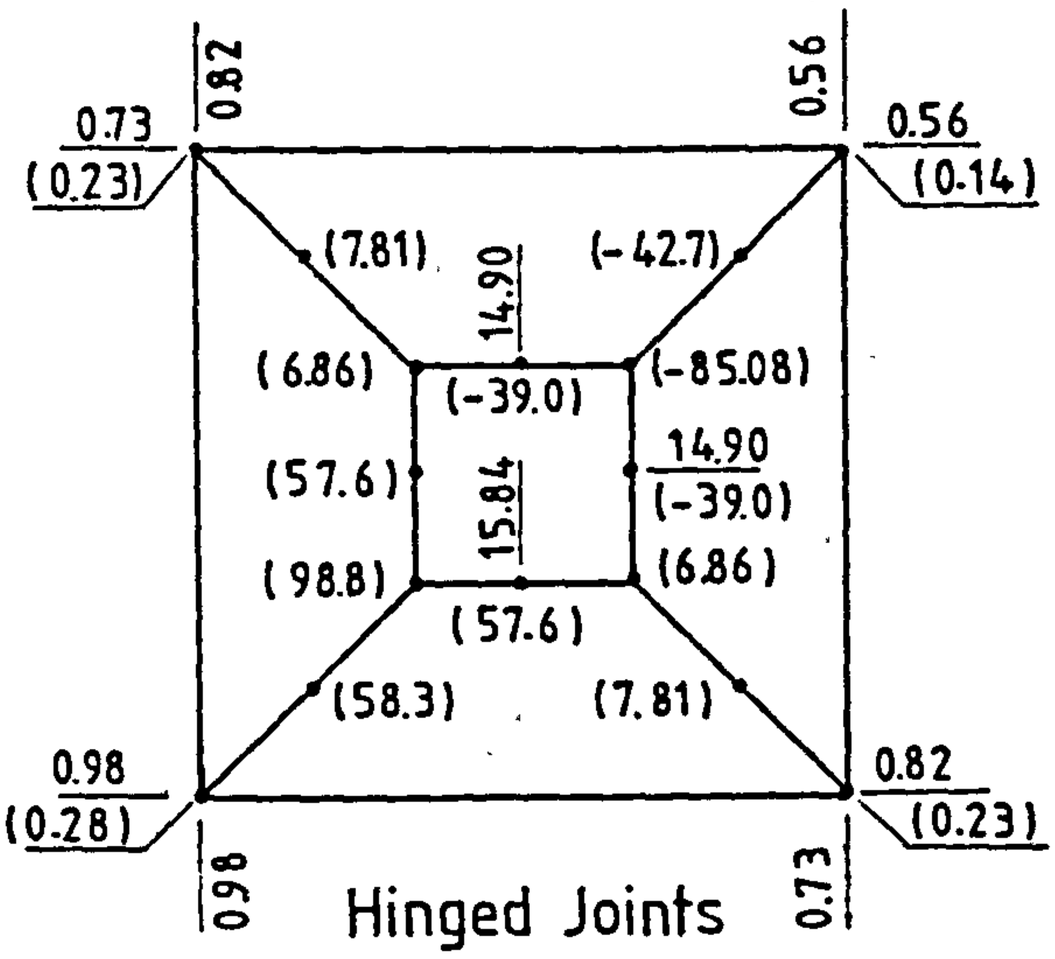

Hinged Joints

b. Simple Truss Model

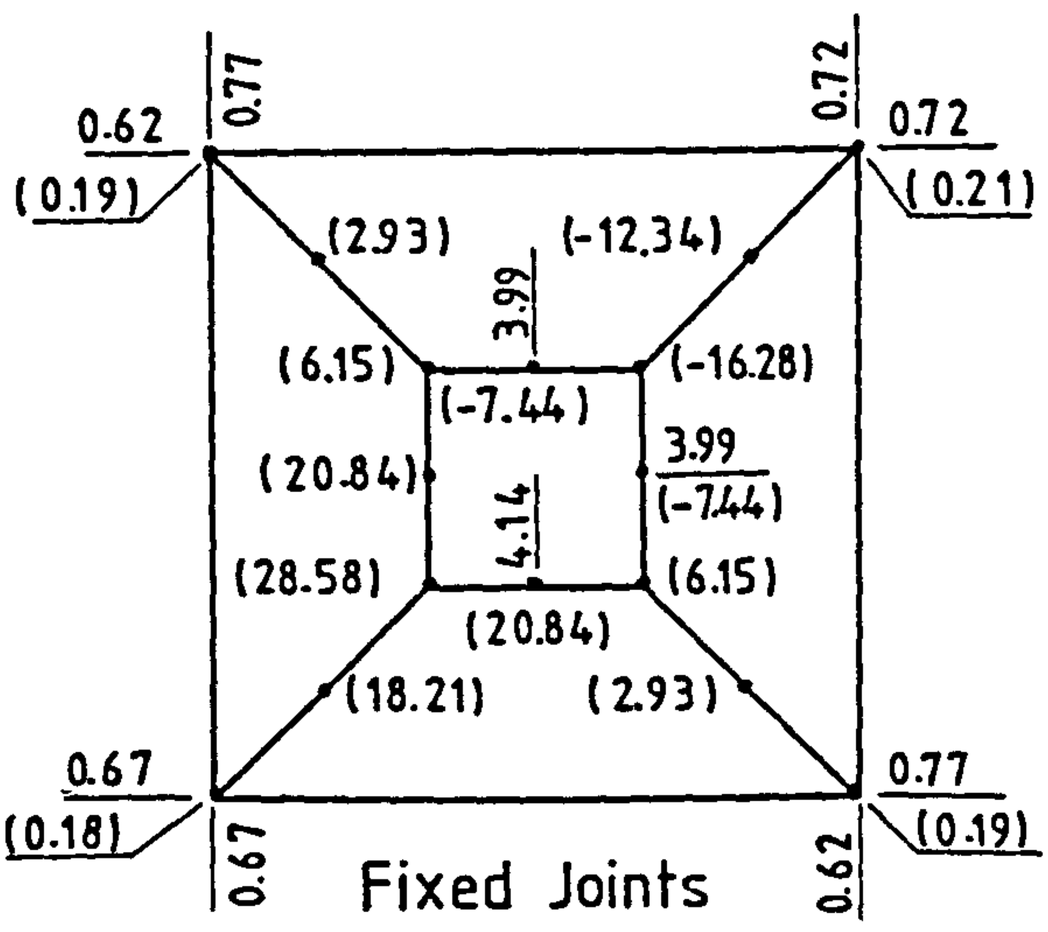

Fixed Joints

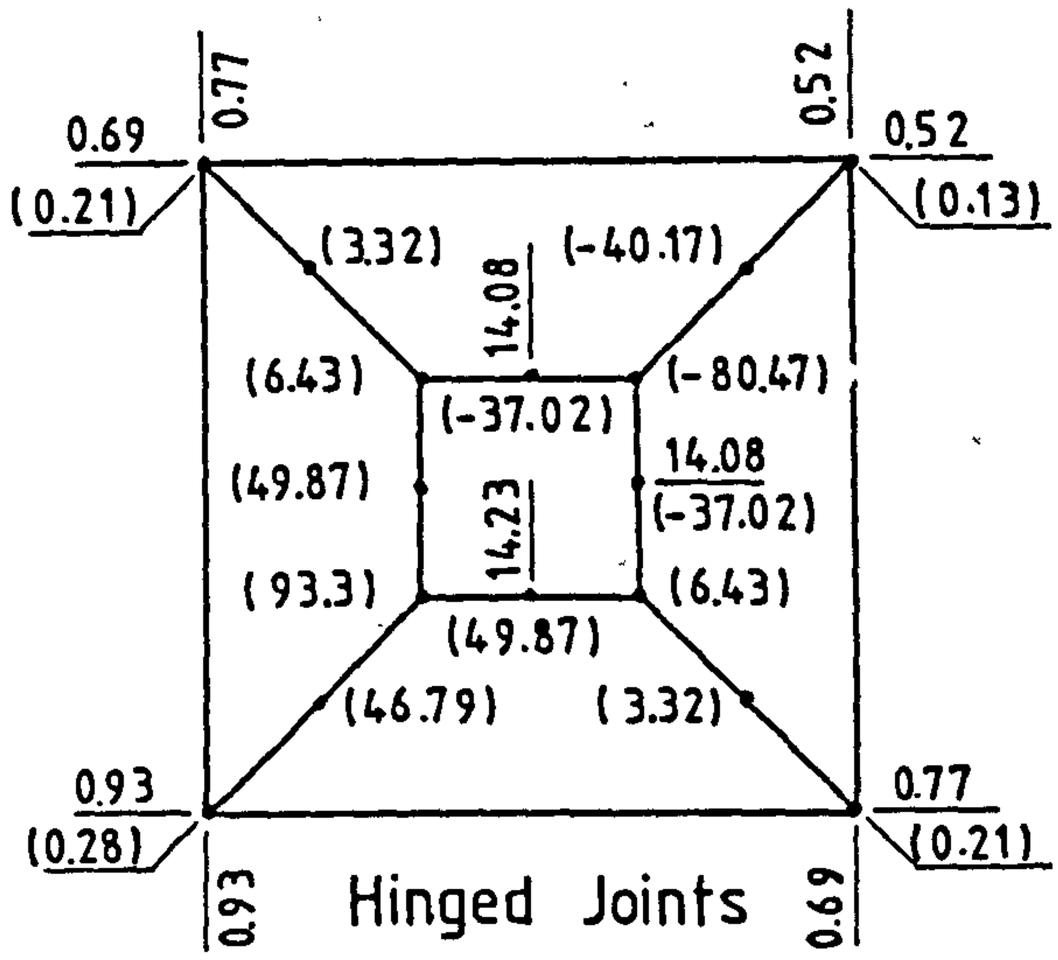

Hinged Joints

C. Simplified X. Diagonals Model

Fig. 9.32 Comparison Between Experimental And Theoretical Displacements In The Case Of Asymmetric Load

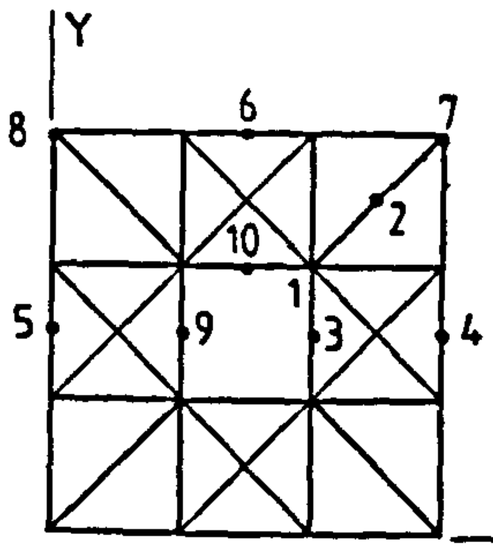

X-DIAGONALS MODEL

DISPL. IN mm

JOINT	DIRECTION	EXPERIMENTAL RESULTS	THEORETICAL	
			HINGED	FIXED
1	Z	12.60	8.57	8.20
2	Z	7.50	4.42	3.91
3	Z	13.90	8.93	8.57
3	x	0.95	0.10	0.10
4	x	4.17	3.15	2.50
7	Z	0.11	0.27	0.26
7	x	0.92	0.97	0.93

Table 9.4 Comparison Between Experimental Results And The Results Of The X-Diagonals Model (U.D.L 0.81 KN/m^2)

JOINT	DIRECTION	CASE "C" "WIND ON ONE SIDE"			CASE 'D' "WIND ON BOTH SIDES"		
		EXPERIME.	THEORETICAL		EXPERIME.	THEORETICAL	
			HINGED	FIXED		HINGED	FIXED
3	x	1.80	2.34	2.27	2.65	2.59	2.27
4	x	2.43	1.82	1.67	6.23	3.69	3.47
5	x	9.85	5.67	5.27	4.94	3.69	3.47
6	Y	-0.15	-0.41	-0.61	-0.05	-0.14	0.0
7	x	1.50	1.57	1.58	2.17	1.77	1.77
8	x	1.90	1.70	1.96	1.75	1.77	1.77
9	x	3.35	3.56	2.27	2.42	2.59	2.27
10	Y	-0.10	0.0	-0.02	-0.02	-0.02	0.0

Table 9.5 Comparison Between Experimental Results And The Results Of The X-Diagonals Model (Wind Load Cases)

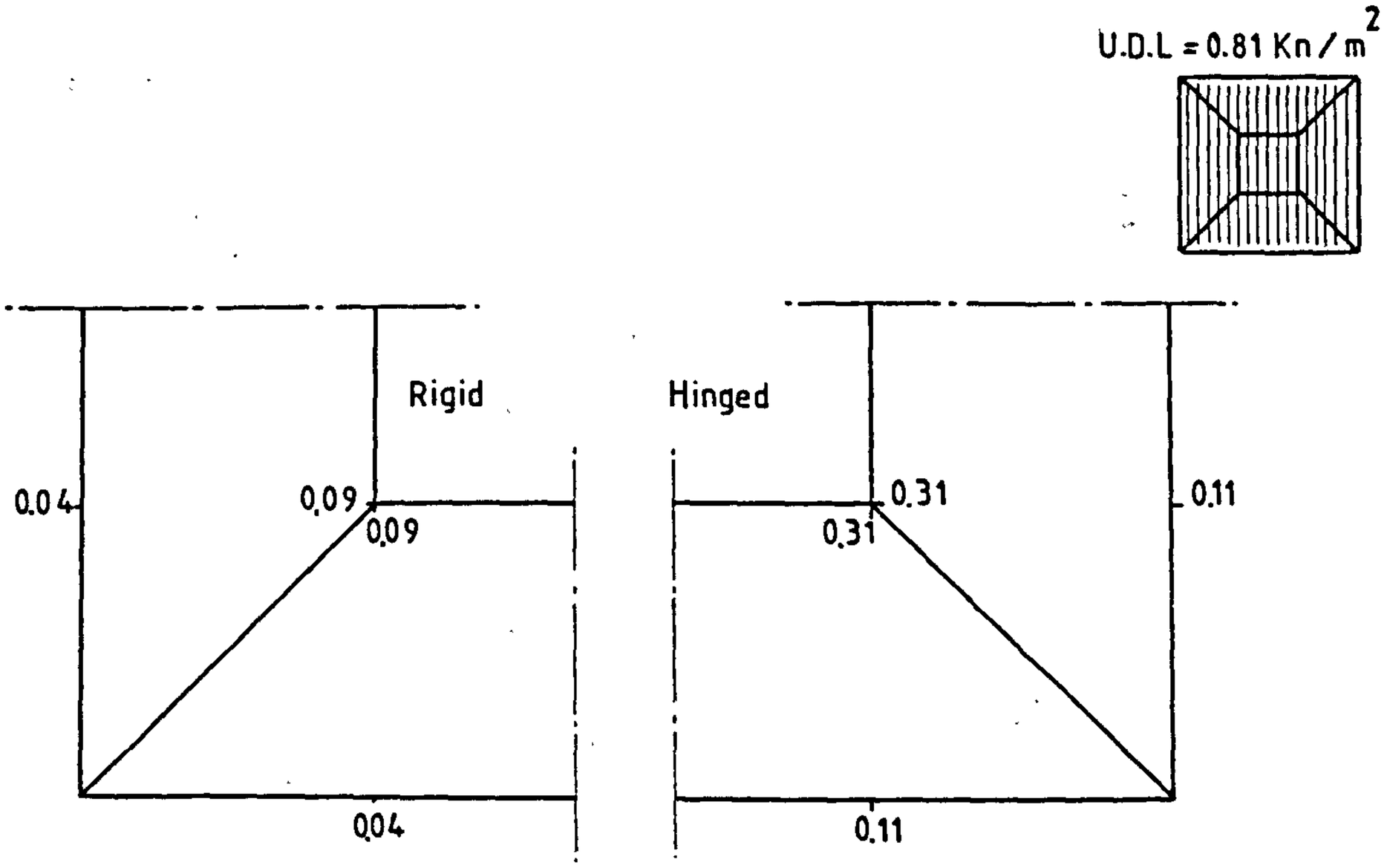

Fig. 9.33 Fastener Forces (In Kn) Due To U.D.L Of 0.81 Kn/m^2

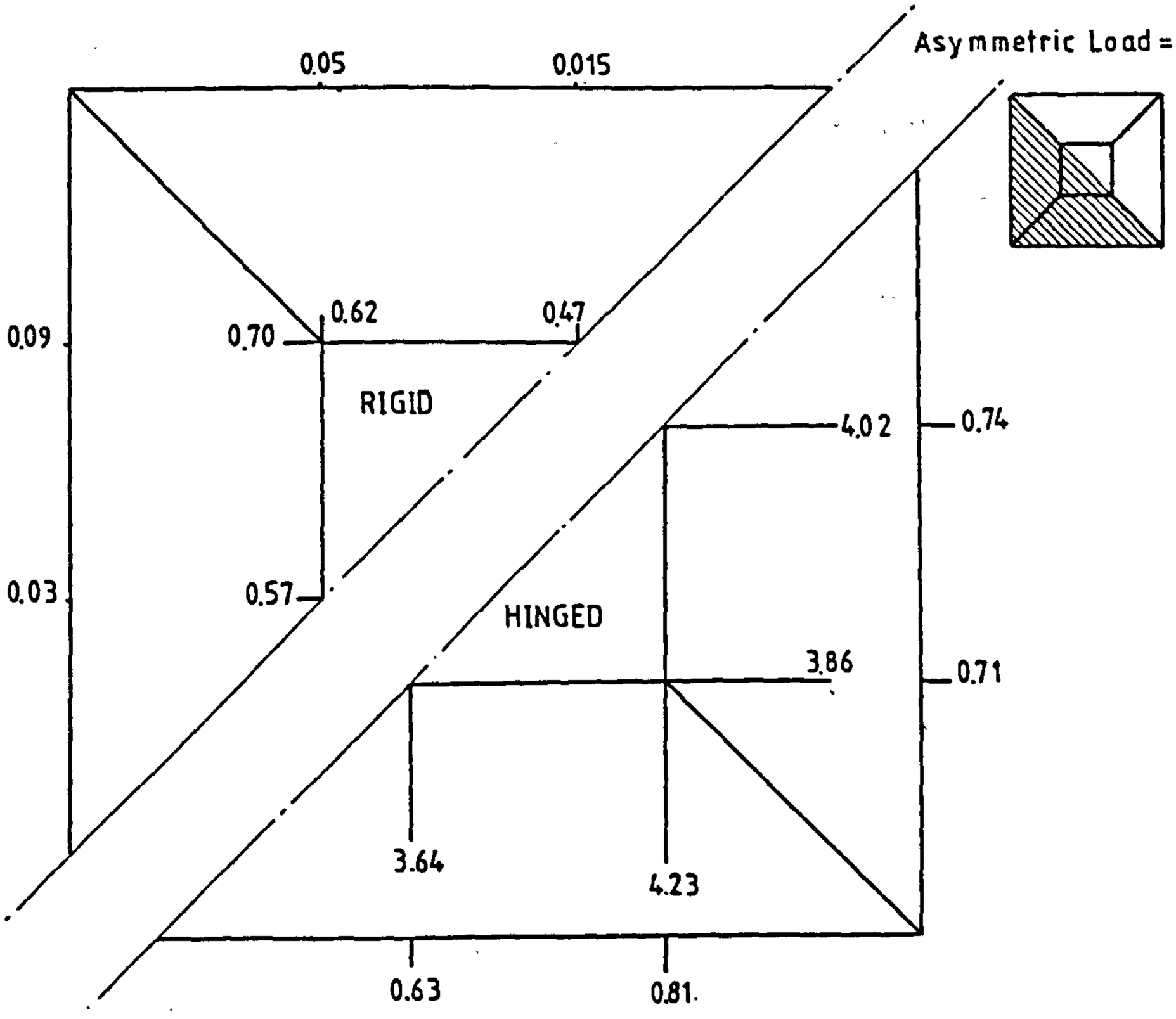

Fig. 9.34 Fastener Forces (In Kn) Due To Asymmetric Load Of 1.215 Kn/m^2

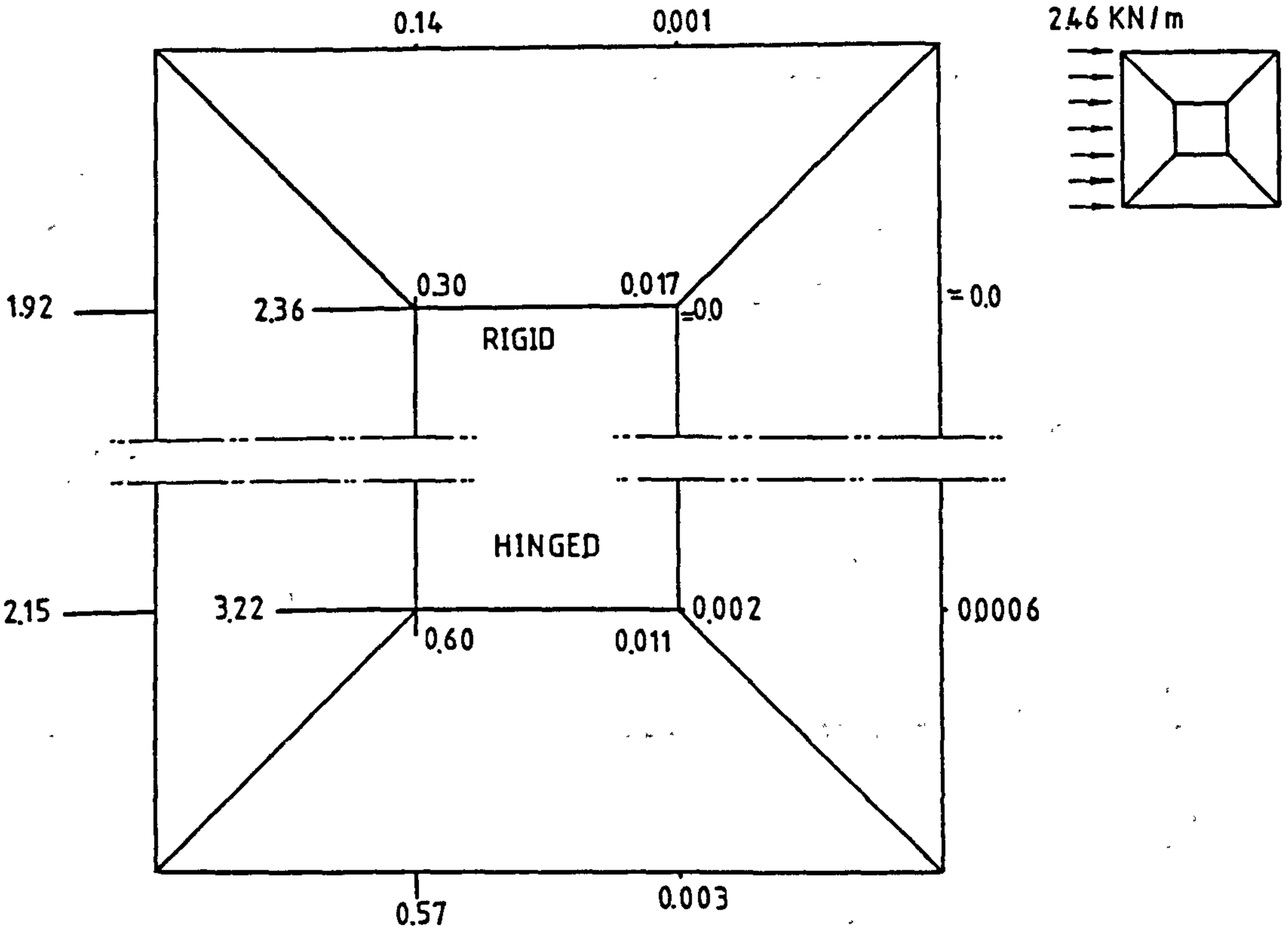

Fig.9.35 Fastener Forces (In kn) Due To Wind Load Case 'c'

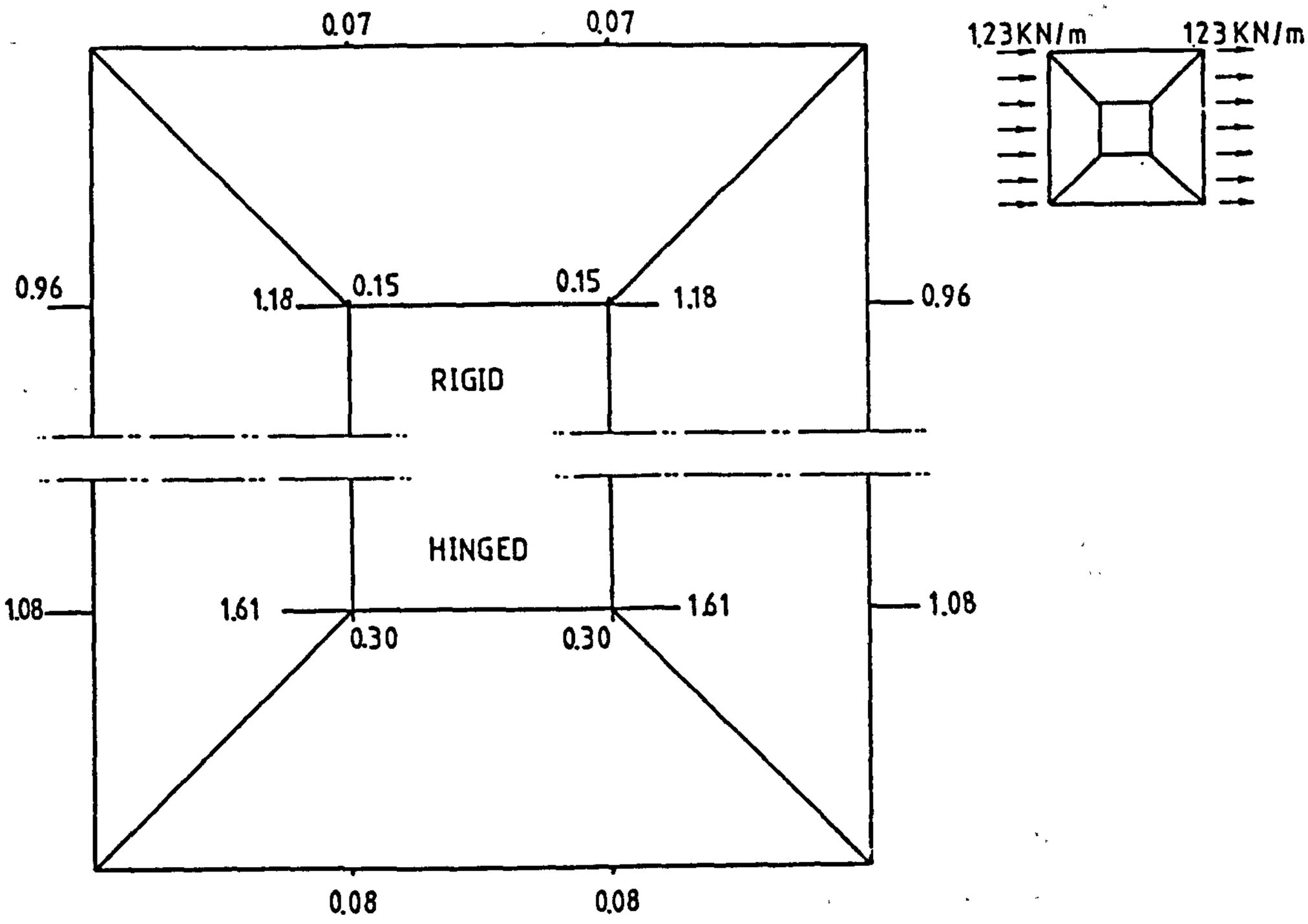

Fig.9.36 Fastener Forces (In kn) Due To Wind Load Case 'd'

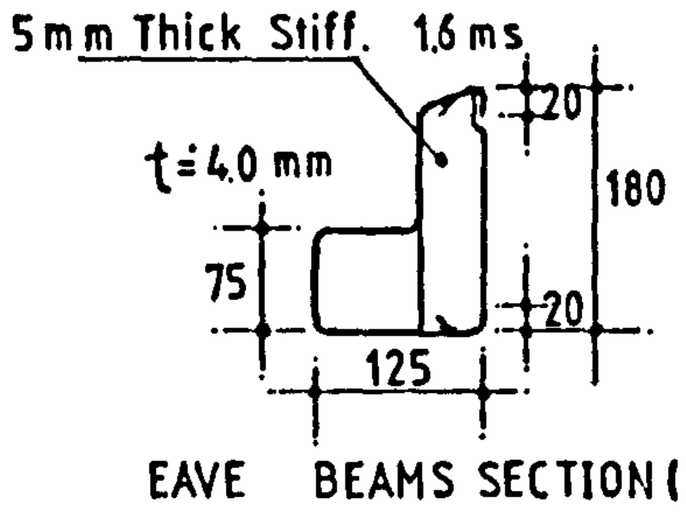

EAVE BEAMS SECTION (A_A)

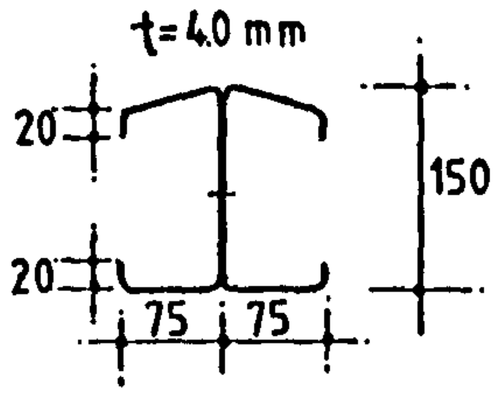

HIP MEMBERS

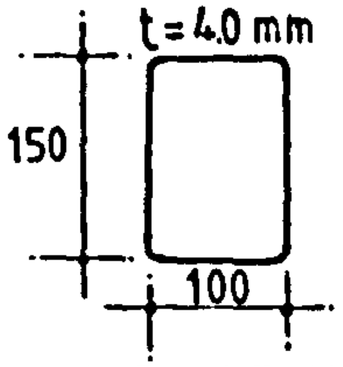

APEX BEAMS

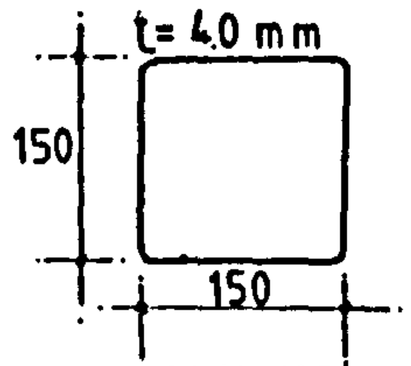

COLUMNS

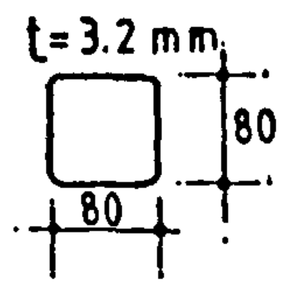

INTERMIDIATE POSTS 'C'

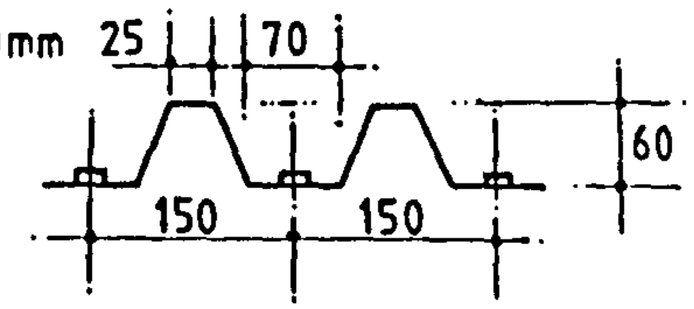

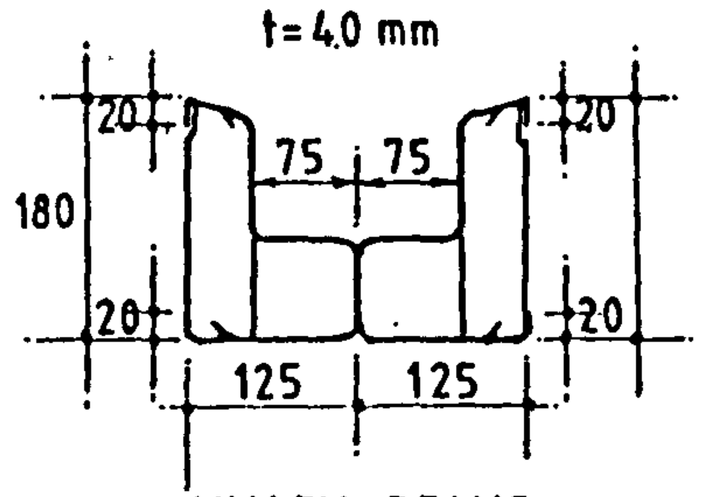

VALLEY BEAMS

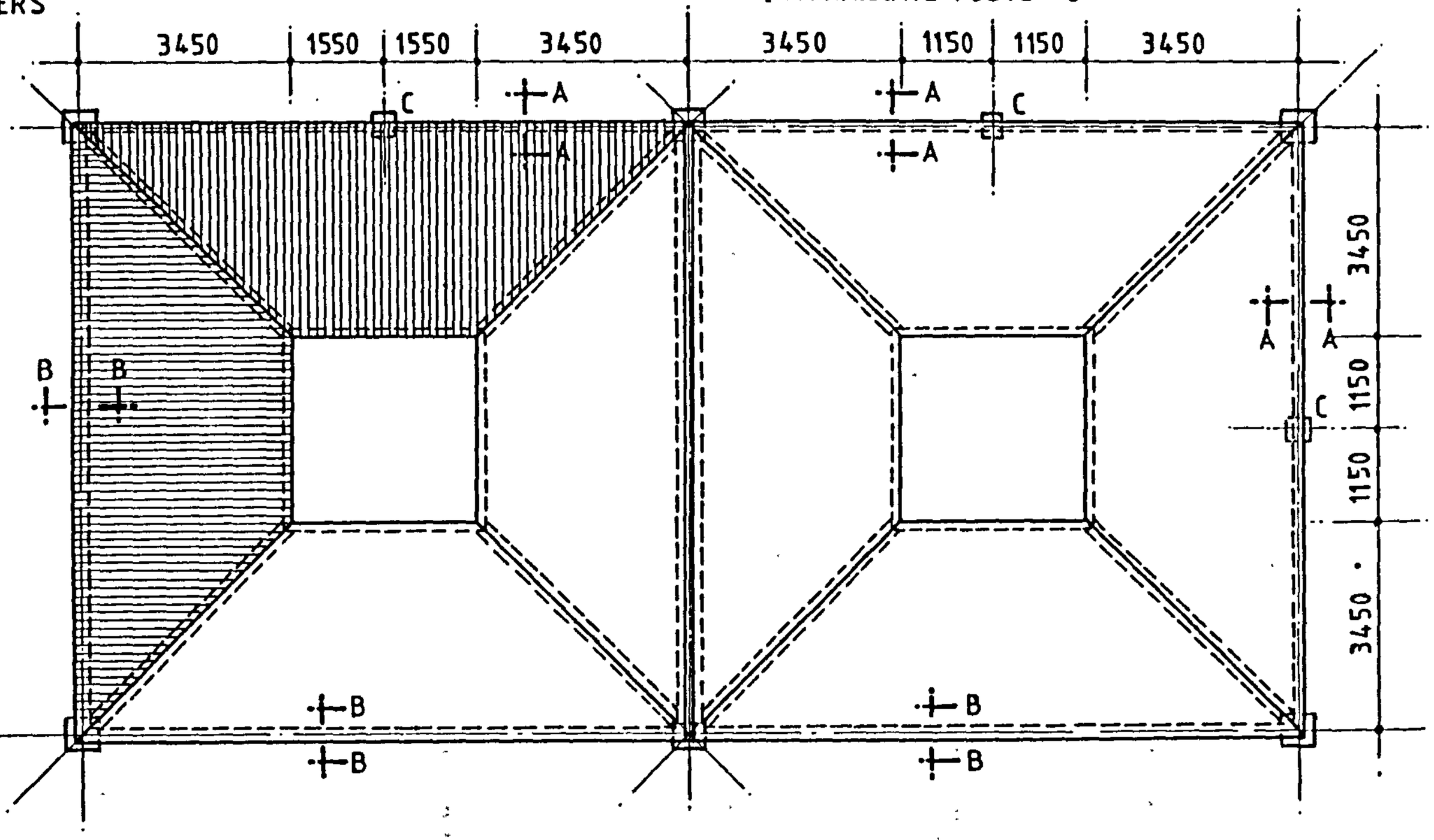

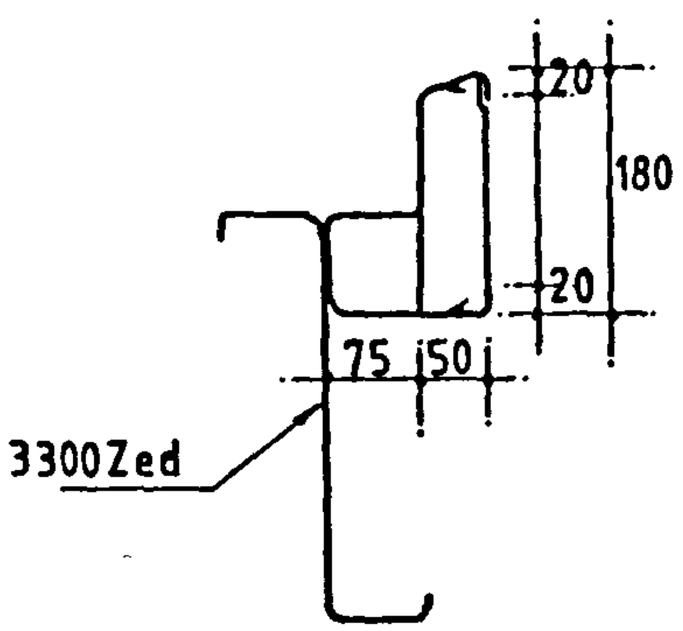

EAVE BEAMS SECTION (B_B)

Fig.9.37 Details Of The Two Bay Pyradome Structure

ALL DIMS IN M.M.

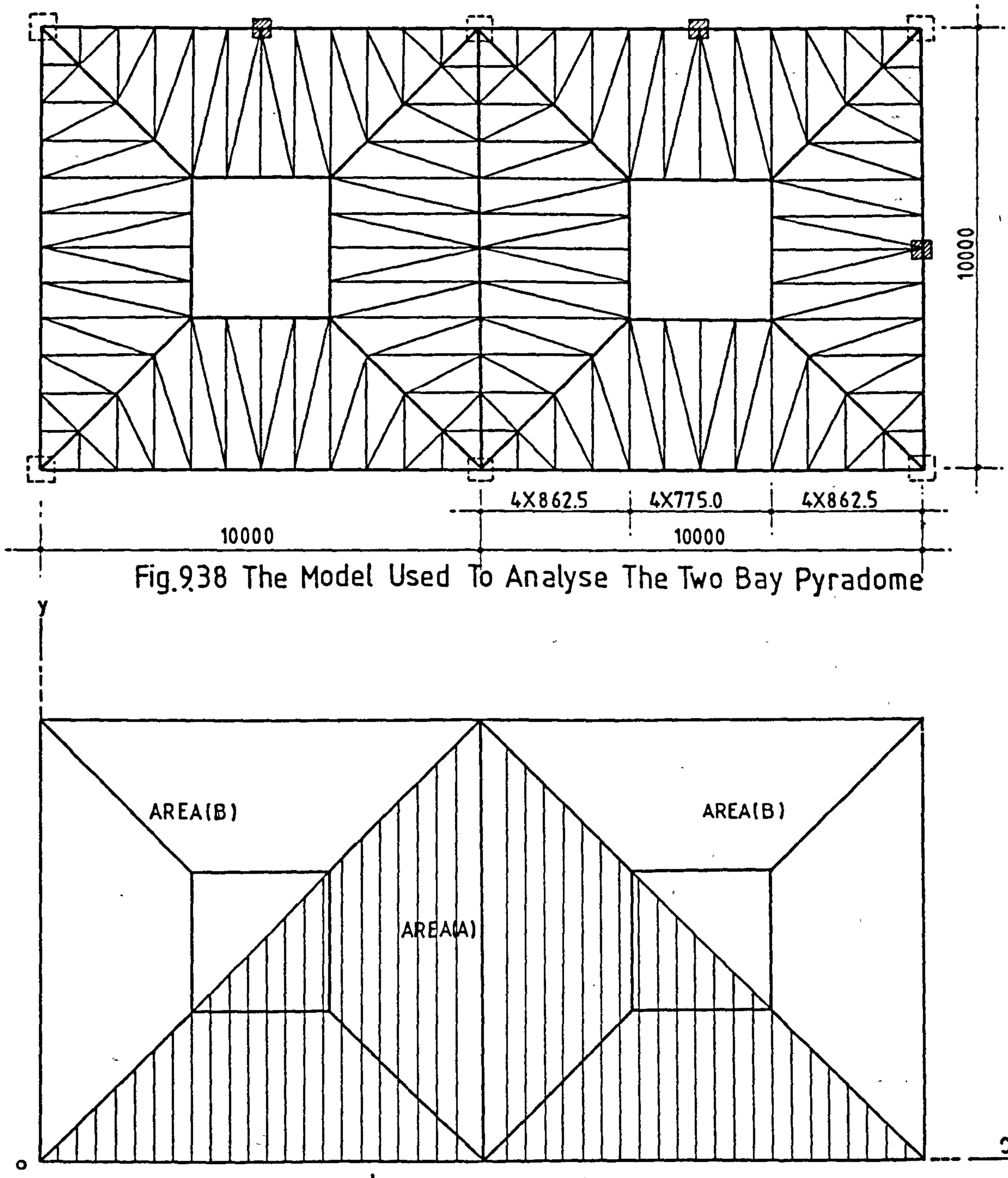

Fig.9.38 The Model Used To Analyse The Two Bay Pyradome

a-Uniformly Distributed v^{al} Load = 0.80 Kn/m^2 Over The Entire Area

b-U.D.L. 0.80 Kn/m Over Area (A) While
Area (B) Is Loaded By 0.40 Kn/m^2

Fig. 9.39 Vertical Loads On The Pyradome

DIMS IN MM

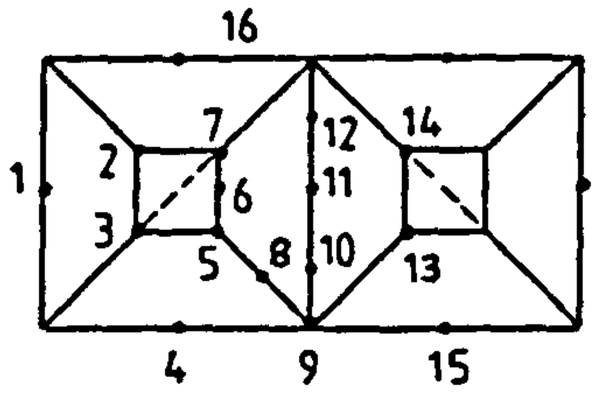

JOINT	CASE(A)			CASE(B)		
	EXPER. RESULTS	THEORETICAL RESULTS		EXPER. RESULTS	THEORETICAL RESULTS	
		HINGED	FIXED		HINGED	FIXED
1	12.0	15.95	8.31	5.50	8.00	4.06
2	7.0	7.28	7.19	3.50	-0.94	2.028
3	7.0	7.96	7.47	4.50	6.24	5.44
4	12.0	16.01	5.17	12.0	15.98	5.19
5	9.0	8.16	7.52	9.0	10.89	9.45
6	8.50	10.80	6.68	8.0	12.01	9.50
7	9.0	9.22	7.77	5.0	9.18	6.55
8	8.50	9.63	5.35	8.50	11.03	6.81
9	2.0	0.17	0.16	1.50	0.17	0.17
10	13.50	9.28	7.01	13.0	9.44	7.18
11	19.50	11.69	9.86	18.0	10.64	8.8
12	12.50	9.20	6.81	11.0	7.30	5.30
13	9.0	8.00	8.02	8.0	11.80	9.85
14	9.50	10.01	8.24	5.50	8.70	6.76
15	12.0	16.00	5.40	16.50	15.97	5.31
16	2.0	2.04	1.20	2.50	1.26	0.81

Table. 9.6 Vertical Deflections-U.D.L. And Asymmetric Load For The Two-Bay Pyradome

- Def. in m.m.
- -ve Upward

APPENDIX A.2.1.

The second-order stiffness matrix given by Renton (9)

This matrix is valid for skew and doubly symmetrical cross sections. The submatrices a_{11} , a_{12} ,....,a_{44} of the second order stiffness matrix K in eq. 2.68 as given by Renton (9), are,

$$\left[a_{11}\right] = \begin{bmatrix} \frac{EA}{\ell} & o & o \\ o & \frac{12EI_z}{\ell^3}\phi_5 & o \\ o & o & \frac{12EI_y}{\ell^3}\rho_5 \end{bmatrix} \quad \left[a_{12}\right] = \begin{bmatrix} o & o & o \\ o & o & \frac{-6EI_y}{\ell^2}\rho_2 \\ o & \frac{6EI_z}{\ell^2}\phi_2 & o \end{bmatrix} \qquad (A.2.1)$$

$$\left[a_{13}\right] = -\left[a_{11}\right] = -\left[a_{33}\right] \ , \quad \left[a_{14}\right] = \left[a_{12}\right] = -\left[a_{43}\right] \qquad (A.2.2)$$

$$\left[a_{22}\right] = \begin{bmatrix} \zeta_x & o & o \\ o & \frac{4EI_y}{\ell}\rho_3 & o \\ o & o & \frac{4EI_z}{\ell}\phi_3 \end{bmatrix} \quad \left[a_{23}\right] = \begin{bmatrix} o & o & o \\ o & o & \frac{-6EI_z}{\ell^2}\phi_2 \\ o & \frac{6EI_y}{\ell^2}\rho_2 & o \end{bmatrix}$$

$$\left[a_{24}\right] = \begin{bmatrix} -\zeta_x & o & o \\ o & \frac{2EI_y}{\ell}\rho_4 & o \\ o & o & \frac{2EI_y}{\ell}\phi_4 \end{bmatrix} \quad \text{and} \quad \left[a_{44}\right] = \left[a_{22}\right] \qquad (A.2.4)$$

in which,

$$\phi_1 = \frac{\tau_z}{2} \cdot \cot \frac{z}{2} \ , \ \phi_2 = \frac{\tau_z^2}{12(1-\phi_1)} \ , \ \phi_3 = \frac{3}{4}\ \phi_2 + \frac{1}{4}\ \phi_1 \quad \text{(A.2.5)}$$

$$\phi_4 = \frac{3}{4}\ \phi_2 - \frac{1}{2}\ \phi_1 \ , \ \phi_5 = \phi_1\ \phi_2 \quad \text{and} \quad \tau_z^2 = \frac{P_x\ \ell^2}{EI_z} \quad \text{(A.2.6)}$$

values $\rho_1, \rho_2, \ldots,$ and ρ_5 can be calculated from

$$\tau_y = \frac{P_x\ \ell^2}{EI_y} \quad \text{and,}$$

$$\zeta_x = \frac{GJ - P_x\ i_o^2}{\ell\left(1 - \frac{2}{\mu_x \ell} \tanh \frac{\mu_x \ell}{2}\right)} \quad \text{where } \mu_z = \sqrt{\frac{1}{EI_\omega}\left(GJ - P_x i_o^2\right)} \quad \text{(A.2.7)}$$

APPENDIX A.3.1

SUBROUTINE BIMOM

```
      SUBROUTINE BIMOM(II)
      DOUBLE PRECISION FA,EA,CA,DA,FEA,FCA,FDA,ECA,
     1 EDA,CDA,F1,E1,Y1,Z1,X2,X3
      DOUBLE PRECISION CFM,FM,CC(110)
      DOUBLE PRECISION R1,R2,R3,R4,R5,R6,R7,R8,R9,R10
      DOUBLE PRECISION SUMR1,SUMR2,SUMR3,SUMR4,SUMR5,SUMR6,
     1 SUMR7,SUMR8,SUMR9,SUMR10
      DIMENSION FA(110),EA(110),CA(110),DA(110),FEA(110),
     1 FCA(110),FDA(110),ECA(110),EDA(110),CDA(110)
      DIMENSION R1(110),R2(110),R3(110),R4(110),R5(110),
     1   R6(110),R7(110),R8(110),R9(110),R10(110)
      DIMENSION SUMR1(110),SUMR2(110),SUMR3(110),SUMR4(110),
     1   SUMR5(110),SUMR6(110),SUMR7(110),SUMR8(110),SUMR9(110),
     2   SUMR10(110)
      COMMON/FUNCT/FA,EA,CA,DA,FEA,FCA,FDA,ECA,EDA,CDA,E1,E1
     1 Y1,Z1,X1,X3
      COMMON/FACTOR/R1,R2,R3,R4,R5,R6,R7,R8,R9,R10
      COMMON/SUMM/SUMR1,SUMR2,SUMR3,SUMR4,SUMR5,SUMR6,SUMR7
     1 ,SUMR8,SUMR9,SUMR10
        COMMON/FORCS/FM(35000),CFM(35000)
      DO 10 I=1,81
      X1=0.0125*(I-1)
      X2=X1*X1
      X3=X2*X1
      F1=6.0*(X2-X1)
      E1=-F1
      Y1=(-3.0*X2+4.0*X1-1.0)
      Z1=(2.0*X1-3.0*X2)
      FA(I)=F1*F1
      EA(I)=E1*E1
      CA(I)=Y1*Y1
      DA(I)=Z1*Z1
      FEA(I)=F1*E1
      FCA(I)=F1*Y1
      FDA(I)=F1*Z1
      ECA(I)=E1*Y1
      EDA(I)=E1*Z1
      CDA(I)=Y1*Z1
      IF(I.LT.2)GO TO 8
      CC(I)=-CFM(14*(I-1))
      SL=0.50*(CC(I)-CC(I-1))
      R1(I)=(FA(I-1)*CC(I-1)+FA(I)*CC(I)+0.50*FA(I-1)*CC(I)+
     1 0.50*FA(I)*CC(I-1))/240.0
      R2(I)=(EA(I-1)*CC(I-1)+EA(I)*CC(I)+0.50*EA(I-1)*CC(I)+
     1 0.50*EA(I)*CC(I-1))/240.0
      R3(I)=(CA(I-1)*CC(I-1)+CA(I)*CC(I)+0.50*CA(I-1)*CC(I)+
     1 0.50*CA(I)*CC(I-1))/240.0
      R4(I)=(DA(I-1)*CC(I-1)+DA(I)*CC(I)+0.50*DA(I-1)*CC(I)+
     1 0.50*DA(I)*CC(I-1))/240.0
      R5(I)=(FEA(I-1)*CC(I-1)+FEA(I)*CC(I)+0.50*FEA(I-1)*CC(I)+
     1 0.50*FEA(I)*CC(I-1))/240.0
      R6(I)=(FCA(I-1)*CC(I-1)+FCA(I)*CC(I)+0.50*FCA(I-1)*CC(I)+
     1 0.50*FCA(I)*CC(I-1))/240.0
      R7(I)=(FDA(I-1)*CC(I-1)+FDA(I)*CC(I)+0.50*FDA(I-1)*CC(I)+
```

```
     1 0.50*FDA(I)*CC(I-1))/240.0
       R8(I)=(ECA(I-1)*CC(I-1)+ECA(I)*CC(I)+0.50*ECA(I-1)*CC(I)+
     1 0.50*ECA(I)*CC(I-1))/240.0
       R9(I)=(EDA(I-1)*CC(I-1)+EDA(I)*CC(I)+0.50*EDA(I-1)*CC(I)+
     1 0.50*EDA(I)*CC(I-1))/240.0
       R10(I)=(CDA(I-1)*CC(I-1)+CDA(I)*CC(I)+0.50*CDA(I-1)*CC(I)+
     1 0.50*CDA(I)*CC(I-1))/240.0
       SUMR1(I)=SUMR1(I-1)+R1(I)
       SUMR2(I)=SUMR2(I-1)+R2(I)
       SUMR3(I)=SUMR3(I-1)+R3(I)
       SUMR4(I)=SUMR4(I-1)+R4(I)
       SUMR5(I)=SUMR5(I-1)+R5(I)
       SUMR6(I)=SUMR6(I-1)+R6(I)
       SUMR7(I)=SUMR7(I-1)+R7(I)
       SUMR8(I)=SUMR8(I-1)+R8(I)
       SUMR9(I)=SUMR9(I-1)+R9(I)
       SUMR10(I)=SUMR10(I-1)+R10(I)
       GO TO 10
     8 CC(I)=0.0
       SUMR1(1)=0.0
       SUMR2(1)=0.0
       SUMR3(1)=0.0
       SUMR4(1)=0.0
       SUMR5(1)=0.0
       SUMR6(1)=0.0
       SUMR7(1)=0.0
       SUMR8(1)=0.0
       SUMR9(1)=0.0
       SUMR10(1)=0.0
    10 CONTINUE
       WRITE(8,100)SUMR1(81)
   100 FORMAT(//4H RR1,E15.6)
       WRITE(8,101)SUMR2(81)
   101 FORMAT(//4H RR2,E15.6)
       WRITE(8,102)SUMR3(81)
   102 FORMAT(//4H RR3,E15.6)
       WRITE(8,103)SUMR4(81)
   103 FORMAT(//4H RR4,E15.6)
       WRITE(8,104)SUMR5(81)
   104 FORMAT(//4H RR5,E15.6)
       WRITE(8,105)SUMR6(81)
   105 FORMAT(//4H RR6,E15.6)
       WRITE(8,106)SUMR7(81)
   106 FORMAT(//4H RR7,E15.6)
       WRITE(8,107)SUMR8(81)
   107 FORMAT(//4H RR8,E15.6)
       WRITE(8,108)SUMR9(81)
   108 FORMAT(//4H RR9,E15.6)
       WRITE(8,109)SUMR10(81)
   109 FORMAT(//5H RR10,E15.6)
       RETURN
       END
```

APPENDIX A.3.2.

Coefficients K_b and K_t of the geometric matrix

Fact.	K_{b1}	K_{b2}	K_{b3}	K_{b4}	K_{t1}	K_{t2}	K_{t3}	K_{t4}
0.01	0.5999	0.0652	0.0501	0.0166	0.30	0.0334	0.0250	0.0083
0.05	0.5995	0.0652	0.0500	0.0166	0.30	0.0333	0.0250	0.0083
0.10	0.5979	0.0650	0.0499	0.0166	0.299	0.0332	0.0249	0.0083
0.25	0.5869	0.0640	0.0489	0.0163	0.292	0.0326	0.0243	0.0081
0.50	0.5513	0.0607	0.0456	0.0155	0.2700	0.0297	0.0223	0.0076
0.75	0.5014	0.0561	0.0410	0.0144	0.2396	0.0268	0.0196	0.0069
1.0	0.4463	0.0510	0.0359	0.0132	0.2063	0.0236	0.0166	0.0061
2.0	0.2642	0.0347	0.0190	0.0094	0.1006	0.0132	0.0072	0.0036
3.0	0.1642	0.0263	0.0	0.0074	0.0495	0.0079	0.0029	0.0022
4.0	0.1091	0.0218	0.0040	0.0063	0.0263	0.0053	0.0010	0.0015
5.0	0.0760	0.0192	0.0012	0.0055	0.0150	0.0038	0.0002	0.0011
6.0	0.0548	0.0173	0.0006	0.0050	0.0090	0.0029	0.0	0.0008
7.0	0.0406	0.0159	-0.0016	0.0045	0.0058	0.0023	-0.0002	0.0006
8.0	0.0308	0.0147	-0.0022	0.0040	0.0038	0.0018	-0.0002	0.0005
9.0	0.0238	0.0138	-0.0025	0.0036	0.0026	0.0015	-0.0003	0.0004
10.0	0.0188	0.0130	-0.0026	0.0033	0.0019	0.0013	-0.0003	0.0003

Table A.5.2. Bimoment coefficients K_{b1}-K_{t4}

APPENDIX A.4.1

MAIN SUBROUTINE

```
C
C
C
C
C   FIRST AND SECOND ORDER ANALYSIS OF SPACE FRAMES
      DOUBLE PRECISION A,BM,CM,DM,EM,FM,WJ,CFM
      INTEGER*4 JDF
      CHARACTER*10  RESFIL,DATFIL
      DIMENSION XL(1000),YL(1000),ZL(1000),NM(1000),
     1 JS(1000),JDF(3000)
      DIMENSION ITN(5000),JA(5000),JB(5000),JC(5000),
     1 QC(5000),RC(5000)
      DIMENSION DM(8000),EM(8000),PCA(5000),PCB(5000)
      DIMENSION NT(400),MAP(1000,500),WJ(6000),A(8000),
     1 BM(8000),CM(80000)
      DIMENSION EY(50),GR(50),AR(50),GQ(50),GQR(50),GJ(50),
     1 QS(50),RS(50)
      INTEGER ADDR(1000),WADDR(1000),ORD(1000),NST(1000),P,Q
      DIMENSION GG(50,5),FFW(50,8),PAY(50),PAZ(50),
     1 WLO(1000),JLO(2000)
      COMMON/FORCS/FM(35000),CFM(35000)
      COMMON/BARMS/GG,FFW,PAY,PAZ,JLO,WLO
      COMMON/SPMTS/EY,AR,GR,GQ,GQR,GJ,QS,RS
      COMMON/JOINT/XL,YL,ZL,WJ
      COMMON/MISC/A,BM,CM,DM,EM
      COMMON/INTS/NM,JS,JDF,NT,MAP,WADDR,ADDR,ORD,NST
      COMMON/SPMEM/ITN,JA,JB,JC,QC,RC,PCA,PCB
       COMMON/NITS/NJS,NPMS,NPMTS,NILS,NJOLD,NPREV,NMS,
     1  NE,ISTOR,NSTOR,ISTOW,NSTOW,IM,JOB,NPRMS,DET
     2 ,NBMS,NBMTS,MODE,JCN,JCDF,CRD,FLAM,NLJS,TOL
     3 ,NMTS,NINTS
C
C   MODE 0 = SINGLE ANALYSIS - SEVERAL LOAD VECTORS
C   MODE 1 = STABILITY ANALYSIS AT SINGLE LOAD LEVEL
C   MODE 2 = REPEATED CYCLES TO CRITICAL LOAD
C
C   ADD 10 TO MODE FOR INCREMENTAL LOADING USING INPUT
C   LOAD AS FIRST STEP
C
      IOBUFFER=16384
      DO 9123 IJK=1,23
      PRINT*
9123  CONTINUE
      WRITE (*,'(''                                        '',$)')
      WRITE (*,'(''PROGRAMME SPACE'')')
      PRINT*
      PRINT*
      PRINT*
C
C
777   PRINT*
      PRINT*
      WRITE (*,'(''NAME OF RESULTS FILE                    '',$)')
      READ  (*,'(A)') RESFIL
      OPEN  (UNIT=8,FILE=RESFIL,STATUS='UNKNOWN',ERR=777)
```

```
888     PRINT*
        PRINT*
        WRITE (*,'(''NAME OF DATA FILE                    '',$)')
        READ  (*,'(A)') DATFIL
        OPEN  (UNIT=9,FILE=DATFIL,STATUS='OLD',ERR=888)
        OPEN  (UNIT=10,STATUS='SCRATCH',FORM='UNFORMATTED')
        OPEN  (UNIT=11,STATUS='SCRATCH',FORM='UNFORMATTED')
      NPRINT=0
  100 FORMAT(1H1//47X,34HSTABILITY ANALYSIS OF
     + SPACE FRAMES/47X,34(1H*)
     +//////43X,23(2H* )/43X,1H*,43X,1H*/
     +43X,45H* PROGRAM TO ANALYSE THE TORSIONAL/FLEXURAL *
     +/43X,45H* BEHAVIOUR OF SPACE FRAMES CONTAINING:     *
     +/43X,1H*,43X,1H*/
     +43X,45H*   [1] BARSOUM TYPE MEMBERS WITH SEVEN     *
     +/43X,45H*       DEGREES OF FREEDOM.                 *
     +/43X,1H*,43X,1H*/
     +43X,45H*   [2] MEMBERS WITH OFFSET SHEAR CENTRES   *
     +/43X,45H*       AND NEUTRAL AXES.                   *
     +/43X,1H*,43X,1H*/43X,23(2H* ))///)
      WRITE(8,100)
  101 FORMAT(I5,18A4)
  900 READ(9,101)JOB,(A(I),I=1,18)
      IF(JOB.LE.-1)GO TO 999
  102 FORMAT(13H1JOB NUMBER  ,I6/1X,10(1H*))
  103 FORMAT(1X,12HJOB NUMBER  ,I6/11(1H*))
      IF(NPRINT)3,3,4
    3 WRITE(8,103)JOB
      GOTO 9
    4 WRITE(8,102)JOB
    9 CONTINUE
      NPRINT=NPRINT+1
  112 FORMAT(//1H ,18A4//)
      WRITE(8,112)(A(I),I=1,18)
  770 FORMAT(//13H SPACE FRAMES/1X,12(1H*))
      WRITE(8,770)
      NMS=0
      NPRMS=0
      NPREV=0
      NJOLD=0
      NSTOR=0
      NSTOW=0
      FLAM=1.0
C   ICOUNT COUNTS NUMBER OF DIFFERENT LOAD LEVELS
C   NI COUNTS CYCLES AT A GIVEN LOAD
C   NIT COUNTS TOTAL NUMBER OF CYCLES
C   NEG COUNTS NUMBER OF NEGATIVE DETERMINANT CONDITIONS
C       ENCOUNTERED
C  ICREV COUNTS NUMBER OF REVERSALS OF SIGN OF CRITICAL
C       DEFLECTION
      ICOUNT=0
      NI=0
      NIT=0
      NEG=0
      ICREV=0
      DET1=1.0
      CRDO=0.0
      WNEG=1000000000.0
      NCY=20
```

```
      REWIND 10
      REWIND 11
      IM=50
  301 CALL MAPP(ISTEP)
C
      IF(NBMS.EQ.0)GO TO 7
      J=14*NBMS
      DO 2 I=1,J
      CFM(I)=0.0
    2 FM(I)=0.0
    7 I=0
      IF(NMS.GT.0)CALL SPACE(I)
      IF(NBMS.GT.0)CALL BARS(I,NIT)
C
      B=10.0
      CALL SOLVE(B)
      IF(NIT.EQ.0.OR.DET1.EQ.1.0)DET1=DET
      IF(DET.LT.0.0)GO TO 991
      IF(NINTS.GT.0)GO TO 301
C
    5 I=10
      IF(NMS.GT.0)CALL SPACE(I)
      IF(NBMS.GT.0)CALL BARS(I,NIT)
C
C  RECOVER BLOCK DATA FROM TAPE
      IF(NPREV.LT.1)GO TO 200
      DO 250 I=1,7
  250 BACKSPACE 10
      READ(10)NMS,NJS,NMTS,NJOLD,NPREV,NINTS,NE,ISTOR,ISTOW,
     1 NSTOR,NSTOW
      CALL STORE(7,1,ISTOR-NSTOR,A,1)
      READ(10)(ITN(I),JA(I),JB(I),JC(I),QC(I),RC(I),PCA(I),
     1 PCB(I),I=1,NMS)
      READ(10)(JS(I),JDF(I),ORD(I),ADDR(I),WADDR(I),NST(I),
     1 XL(I),YL(I),ZL(I),I=1,NJS)
      READ(10)(EY(I),AR(I),GR(I),GQ(I),GQR(I),GJ(I),QS(I),
     1 RS(I),I=1,NMTS)
      J=NJS-NINTS
      READ(10)((MAP(I,K),K=1,IM),I=1,J)
      J=ISTOW-NSTOW
      DO 260 I=1,NSTOW
  260 CM(I)=WJ(I)
      DO 255 I=1,NSTOW
  255 WJ(WADDR(1+NJS-NINTS)+I-1)=CM(I)
      READ(10)(WJ(I),I=1,J)
      DO 253 I=1,7
  253 BACKSPACE 10
      IF(JOB.LT.30000)GO TO 257
      CALL STORE(9,1,ISTOR,A,1)
      IF(ISTOW.LE.100)WRITE(8,256)(WJ(I),I=1,ISTOW)
  256 FORMAT(//10(1H ,10E12.4/))
  257 B=0.0
      CALL SOLVE(B)
      GO TO 5
C
C  SEQUENCE FOR SECOND ORDER ITERATIONS
C  FM(I) HOLDS MEMBER FORCES AT LAST CONVERGENCE.
C       LOAD FACTOR = WAL
C  FM(I) ARE FACTORED TO PREDICTION SO DIRECTLY COMPARABLE
```

```
C       WITH CFM(I)
C  CURRENT VALUES OF FORCES ARE IN CFM(I)
  200 IF(MODE.EQ.0)GO TO 900
      NI=NI+1
      NIT=NIT+1
      Z=DET/DET1
      WRITE(8,107)NI,CRD,DET,Z
      IF(CRD.EQ.0.0.AND.CRDO.EQ.0.0.AND.NI.GE.2)GO TO 902
  107 FORMAT(/20H CRITICAL DEFLECTION,I3,E15.6,15H    DET
     1 ERMINANT,E15.6,F10.5)
      IF(CRD.EQ.0.0)GO TO 315
      IF(ABS((CRD-CRDO)/CRD).LT.TOL)GO TO 313
  315 IF(CRD*CRDO.LT.0.0)ICREV=ICREV+1
      IF(ICREV.GE.3)GO TO 973
      IF(NI.GE.NCY.AND.MODE.EQ.2)GO TO 973
      IF(NI.GE.NCY)GO TO 900
      CRDO=CRD
      IF(MODE.NE.3)GO TO 15
      J=14*NBMS
      DO 383 I=1,J
  383 CFM(I)=FM(I)
      GO TO 15
C
C  ARRIVES AT LABEL 313 IF CONVERGED AT GIVEN LOAD FACTOR
  313 ICOUNT=ICOUNT+1
      IF(MODE.EQ.1)GO TO 900
      WRITE(8,108)
  108 FORMAT(//26H CALCULATION HAS CONVERGED)
      Z=FLAM/CRD
      WNEW=5.0*FLAM/3.0
      IF(ICOUNT.EQ.1)GO TO 319
      IF(NIT.EQ.0)GO TO 319
      ZO=WWO/CO
      Y=ZO-Z
      IF(Y.EQ.0.0)GO TO 993
      WNEW=FLAM+(FLAM-WWO)*Z/Y
      WRITE(8,109)WNEW
  109 FORMAT(//11H PREDICTION,E15.6)
      IF(ABS((WNEW-PRED)/PRED).LT.TOL.AND.ISTEP.EQ.0)
     1 GO TO 900
      IF(WNEW.LT.WNEG)GO TO 319
      WRITE(8,147)WNEG
  147 FORMAT(/32H PREDICTION TOO HIGH - REDUCE TO,E15.6)
      WNEW=WNEG
  319 IF(ICOUNT.GT.NCY)GO TO 900
      WWO=FLAM
      FLAM=0.75*WNEW+0.25*WWO
C
      IF(ISTEP.EQ.0)GO TO 411
      X=WWO+1.0
      IF(X.GT.FLAM.AND.ICOUNT.GE.2)GO TO 411
      IF(ISTEP.GT.20)GO TO 411
      ISTEP=ISTEP+1
      FLAM=X
      GO TO 412
  411 ISTEP=0
  412 CONTINUE
C
      FACTOR=FLAM/WWO
```

```
      PRED=WNEW
      CO=CRD
      CRDO=CRD*FACTOR
      NI=0
      ICREV=0
      WAL=FLAM
      J=14*NBMS
      DO 371 I=1,J
      CFM(I)=CFM(I)*FACTOR
  371 FM(I)=CFM(I)
      WRITE(8,110)FLAM,FACTOR,FM(1),FM(2),FM(3),FM(4)
  110 FORMAT(/16H NEW LOAD FACTOR,E12.5,9H   FACTOR,
     1 E12.5,10X,4E13.5)
C   ***
C   TAPE RECOVERY REQUIRED (REWIND)
C   ***
C   PREPARE FOR RECYCLING
   15 DO 10 I=1,ISTOW
   10 WJ(I)=0.0
      CALL STORE(4,1,ISTOR,A,1)
      IF(NLJS.EQ.0)GO TO 7
      DO 11 I=1,NLJS
      KA=JLO(2*I-1)
      K=WADDR(KA)+JLO(2*I)-1
      DO 11 J=1,NILS
      IW=K+(J-1)*JS(KA)
   11 WJ(IW)=WJ(IW)+WLO(I)*FLAM
      IF(JOB.LT.20000)GO TO 7
      WRITE(8,385)
      J=14*NBMS
      WRITE(8,386)(CFM(I),I=1,J)
  385 FORMAT(/13H FORCE MATRIX/1H )
  386 FORMAT(7E13.5)
  390 FORMAT(1H )
      WRITE(8,390)
      GO TO 7
C
C   ARRIVES IF NEGATIVE DETERMINANT HAS BEEN FOUND
  991 WRITE(8,992)
  992 FORMAT(//30H HALTED - NEGATIVE DETERMINANT)
      IF(MODE.EQ.0)GO TO 900
C   ***
C   TAPE RECOVERY REQUIRED (REWIND)
C   ***
  973 ICREV=0
      IF(NIT.GT.150)WRITE(8,974)
  974 FORMAT(//16H TOO MANY CYCLES)
      IF(NIT.GT.150)GO TO 900
      NEG=NEG+1
      IF(NEG.GT.NCY)GO TO 900
      IF(FLAM.LT.WNEG)WNEG=FLAM
      IF(ICOUNT.EQ.0)GO TO 8
      FLAM=FLAM-0.24*(WNEW-WWO)
      FACTOR=FLAM/WAL
      GO TO 387
    8 FLAM=0.5*FLAM
      FACTOR=0.5
  387 NI=0
      J=14*NBMS
```

```
      DO 388 I=1,J
  388 CFM(I)=FM(I)*FACTOR
      WRITE(8,110)FLAM,FACTOR,CFM(1),CFM(2),CFM(3),CFM(4)
      GO TO 15
C
  993 WRITE(8,111)
  111 FORMAT(///14H NO PREDICTION)
      GO TO 900
  902 WRITE(8,903)
  903 FORMAT(//34H REPEATED ZERO CRITICAL DEFLECTION)
      GO TO 900
  999 CLOSE (8)
      CLOSE (9)
      CLOSE (10)
      CLOSE (11)
      STOP
      END
```

APPENDIX A.4.2

SUBROUTINE MAPP

```
C
C
C
C
C
      SUBROUTINE MAPP(ISTEP)
      DOUBLE PRECISION A,BM,CM,DM,EM,WJ
      INTEGER*4 JDF
       DIMENSION XL(1000),YL(1000),ZL(1000),NM(1000),
     1 JS(1000),JDF(3000)
       DIMENSION ITN(5000),JA(5000),JB(5000),JC(5000),
     1 QC(5000),RC(5000)
       DIMENSION EY(50),GR(50),AR(50),GQ(50),GQR(50),GJ(50),
     1 QS(50),RS(50),BW(50)
       DIMENSION NT(400),MAP(1000,500),WJ(6000),A(8000),
     1 BM(8000),CM(80000)
       DIMENSION DM(8000),EM(8000),PCA(5000),PCB(5000)
       INTEGER ADDR(1000),WADDR(1000),ORD(1000),NST(1000),
     1 P,Q,S,T
       DIMENSION GG(50,5),FFW(50,8),PAY(50),PAZ(50),
     1 WLO(1000),JLO(2000)
       COMMON/BARMS/GG,QZZ,PAY,PAZ,JLO,WLO
       COMMON/JOINT/XL,YL,ZL,WJ
       COMMON/NITS/NJS,NPMS,NPMTS,NILS,NJOLD,NPREV,NMS,
     1   NE,ISTOR,NSTOR,ISTOW,NSTOW,IM,JOB,NPRMS,DET
     2 ,NBMS,NBMTS,MODE,JCN,JCDF,CRD,FLAM,NLJS,TOL
     3 ,NMTS,NINTS
       COMMON/INTS/NM,JS,JDF,NT,MAP,WADDR,ADDR,ORD,NST
       COMMON/MISC/A,BM,CM,DM,EM
       COMMON/SPMEM/ITN,JA,JB,JC,QC,RC,PCA,PCB
       COMMON/SPMTS/EY,AR,GR,GQ,GQR,GJ,QS,RS,BW
       IW=NSTOW+1
       DO 7 I=IW,600
     7 WJ(I)=0.0
       NE=0
C  READ ROUTINE FOR SPACE FRAMES
       NPRMS=NPRMS+NMS
       IF(NPREV.GT.0)READ(9,160)NJS,NMS,NBMS
       IF(NPREV.EQ.0)READ(9,160)NJS,NMS,NMTS,NBMS,NBMTS,
      1 JCN,JCDF,TOL,MODE
   160 FORMAT(8I5,F10.0)
       WRITE(8,193)NJS,NMS,NMTS,NBMS,NBMTS
   193 FORMAT(/I5,7H JOINTS,I12,14H SPACE MEMBERS,I4,6H TY
     1 PES,I2,16H BARSOUM MEMBERS,I4,6H TYPES/)
       IF(NPREV.GT.0)GO TO 3
       IF(JCN.EQ.0)JCDF=1
       IF(JCN.EQ.0)JCN=1
       IF(TOL.EQ.0.0)TOL=0.005
   172 FORMAT(5H MODE,I2/)
       WRITE(8,172)MODE
   173 FORMAT(15H CRITICAL JOINT,I5,5X,26HCRITICAL DEGREE O
     1 F FREEDOM,I5/)
       IF(MODE.NE.0)WRITE(8,173)JCN,JCDF
   174 FORMAT(10H TOLERANCE,F12.6//)
```

```
C
      ISTEP=0
      IF(MODE.LE.9)GO TO 270
      MODE=MODE-10
      ISTEP=1
  270 CONTINUE
C
      WRITE(8,174)TOL
  175 FORMAT(19H JOINT CO-ORDINATES/1X,18(1H*)//)
      WRITE(8,175)
    3 NJS=NJS+NPREV
  161 FORMAT(I1,I9,3F10.0)
  162 FORMAT(8F10.0)
      IW=NPREV+1
      DO 401 I=IW,NJS
      NST(I)=0
      NM(I)=0
      READ(9,161)JS(I),JDF(I),XL(I),YL(I),ZL(I)
  195 FORMAT(6H JOINT,2I4,3X,I8,3E18.6)
      WRITE(8,195)I,JS(I),JDF(I),XL(I),YL(I),ZL(I)
      DO 401 J=1,IM
  401 MAP(I,J)=0
  163 FORMAT(4I5,4F10.0)
      IF(NPREV.GT.0)GO TO 304
      IW=NMTS+NBMTS
      WRITE(8,500)
  500 FORMAT(//19H MEMBER INFORMATION/1X,18(1H*)/)
      DO 402 I=1,IW
      READ(9,162)EY(I),AR(I),GR(I),GQ(I),GQR(I),GJ(I),
     1 QS(I),RS(I)
  196 FORMAT(/5H TYPE,I2,8E14.6)
      WRITE(8,196)I,EY(I),AR(I),GR(I),GQ(I),GQR(I),GJ(I),
     1 QS(I),RS(I)
      IF(I.GT.NBMTS)GO TO 402
      READ(9,662)(GG(I,J),J=1,5),PAY(I),PAZ(I),BW(I)
      WRITE(8,665)(GG(I,J),J=1,5),PAY(I),PAZ(I),BW(I)
      READ(9,662)(FFW(I,J),J=1,8)
      WRITE(8,661)(FFW(I,J),I=1,8)
C  NOTE THAT GG(I,1) IS POLAR M OF I ABOUT SHEAR CENTRE
  665 FORMAT(13H BARSOUM TYPE,4X,8E12.5)
  661 FORMAT(17H BIMOMENT FACTORS,4X,8E12.5)
  662 FORMAT(8F10.0)
  402 CONTINUE
  304 T=NMS+NBMS
      WRITE(8,176)
  176 FORMAT(//1H )
      DO 404 I=1,T
      READ(9,163)ITN(I),JA(I),JB(I),JC(I),QC(I),RC(I),
     1 PCA(I),PCB(I)
  197 FORMAT(7H MEMBER,I4,I12,3I5,12X,4E15.6)
      WRITE(8,197)I,ITN(I),JA(I),JB(I),JC(I),QC(I),RC(I),
     1 PCA(I),PCB(I)
      J=ABS(JA(I))-NJOLD+NPREV
      K=ABS(JB(I))-NJOLD+NPREV
      IF(JS(K).EQ.0)GO TO 403
      IW=NST(J)
      DO 43 L=1,IW
      IF(MAP(J,L).EQ.K)GO TO 403
   43 CONTINUE
```

```
      NST(J)=NST(J)+1
      NM(J)=NM(J)+JS(K)
      MAP(J,NST(J))=K
  403 IF(JS(J).EQ.0)GO TO 404
      IW=NST(K)
      DO 44 L=1,IW
      IF(MAP(K,L).EQ.J)GO TO 404
   44 CONTINUE
      NST(K)=NST(K)+1
      NM(K)=NM(K)+JS(J)
      MAP(K,NST(K))=J
  404 CONTINUE
      READ(9,160)NLJS,NILS,NINTS
C  PRELIMINARY STORE MAP COMPLETE - END OF SPACE FRAME DATA
C  START FINAL STORE MAP OR CONSIDER NEXT REDUCTION
      WRITE(8,129)
  129 FORMAT(///1X,15HSTORAGE DETAILS/1X,15(1H*)//)
  200 J=1000
      IW=NJS-NINTS
      DO 13 I=1,IW
      IF(JS(I).EQ.0)GOTO13
      IF(NM(I).GE.J)GOTO13
      IF(NM(I).LT.0)GOTO13
      J=NM(I)
      K=I
   13 CONTINUE
      IF(J.EQ.0)GO TO 57
      IF(J.LT.999)GO TO 19
      WRITE(8,113)
  113 FORMAT(/26H ELIMINATION PLAN COMPLETE/)
      GO TO 21
   57 WRITE(8,123)K,J,S
  123 FORMAT(11H LAST JOINT,3I6)
      NE=NE+1
      ORD(NE)=K
      GO TO 21
   19 S=NST(K)+1
  111 FORMAT(16H ELIMINATE JOINT,I4,14H    MEMBERS     ,I4
     1 9H STORING ,I4)
      WRITE(8,111)K,J,S
      NE=NE+1
      ORD(NE)=K
      NM(K)=-NM(K)
      J=NST(K)
      DO 14 I=1,J
      N=MAP(K,I)
      IF(N.LT.0)GOTO14
      IW=NST(N)
      DO 18 Q=1,IW
      IF(MAP(N,Q).NE.K)GOTO18
      MAP(N,Q)=-MAP(N,Q)
      NM(N)=NM(N)-JS(K)
   18 CONTINUE
      DO 85 L=1,J
      IF(MAP(K,L).LT.0)GOTO85
      IF(I.EQ.L)GOTO85
      S=0
      IW=NST(N)
      DO 16 P=1,IW
```

```
      IF(MAP(N,P).NE.MAP(K,L))GOTO16
      S=2
   16 CONTINUE
      IF(S.GT.1)GOTO85
      NM(N)=NM(N)+JS(MAP(K,L))
      NST(N)=NST(N)+1
      MAP(N,NST(N))=MAP(K,L)
      IF(NST(N).LT.IM-3)GO TO 85
      NM(N)=1
  120 FORMAT(28H FORCED ELIMINATION REQUIRED,2I6)
      WRITE(8,120)N,NST(N)
   85 CONTINUE
   14 CONTINUE
C  CONSIDER NEXT REDUCTION
      GO TO 200
C     STORE MAP LAID OUT COMPILE ADDRESSES
   21 S=1
      P=1
      DO 20 I=1,NJS
      WADDR(I)=P
      ADDR(I)=S
      P=P+JS(I)*NILS
  114 FORMAT(I6,9HADDRESS  ,I6,2I10)
      WRITE(8,114)I,NST(I),ADDR(I),WADDR(I)
      IF(NST(I).LT.1)GO TO 20
      IW=NST(I)
      DO 22 J=1,IW
      IF(IABS(MAP(I,J)).LT.I)GO TO 22
      S=S+JS(I)*JS(IABS(MAP(I,J)))
   22 CONTINUE
   20 S=S+JS(I)*JS(I)
      S=S-1
      P=P-1
  115 FORMAT(10H STORAGE  ,2I10)
      WRITE(8,115)S,P
C  FINAL STORE MAP COMPLETE
      ISTOW=P
      ISTOR=S
      DO 50 I=1,NJS
  116 FORMAT(3H JS,I5,6H  MAP ,20I4)
   50 WRITE(8,116)NM(I),(MAP(I,J),J=1,20)
      IF(NLJS.EQ.0)GO TO 53
C  READ IN LOAD VECTORS
  916 FORMAT(///16H LOADING DETAILS/1X,15(1H*))
      WRITE(8,916)
  127 FORMAT(//5H NLJS,I5,7H   NILS,I5,8H   NINTS,I5//)
      WRITE(8,127)NLJS,NILS,NINTS
      DO 24 I=1,NLJS
  105 FORMAT(2I5,7F10.5)
      READ(9,105)K,L,(BM(J),J=1,NILS)
      WRITE(8,194)K,L,(BM(J),J=1,NILS)
  194 FORMAT(6H JOINT,I4,I2,7E15.6)
      K=K-NJOLD+NPREV
      WLO(I)=BM(1)
      JLO(2*I-1)=K
      JLO(2*I)=L
      DO 24 J=1,NILS
      M=WADDR(K)+L-1+(J-1)*JS(K)
      WJ(M)=BM(J)+WJ(M)
```

```
   24 CONTINUE
      WRITE(8,128)
  128 FORMAT(1H ///1H )
   53 CALL STORE(4,NSTOR+1,ISTOR-NSTOR,A,1)
C  ADJUST INTERFACE TERMS TO CONFORM TO NEW ADDRESSES
      IF(NPREV.LT.1)GO TO 256
      DO 255 I=1,NPREV
      J=NPREV+1-I
      K=NT(J+1)-NT(J)
      CALL STORE(3,NT(J),K,A,1)
      CALL STORE(4,NT(J),K,A,1)
  255 CALL STORE(2,ADDR(J),K,A,1)
  256 RETURN
      END
```

APPENDIX A.4.3

SUBROUTINE BARS

```
C
C
C
C
C
C
      SUBROUTINE BARS(IC,NI)
      DOUBLE PRECISION A,BM,CM,DM,EM,FM,WJ,CFM
      DOUBLE PRECISION XLG,X,Y,Z,AA,AB,B1,B2,SO,FSS,XX,XXX,
     1 BB,CC,DD,CL1,CM1,CN1,CL2,CM2,CN2,CL3,CM3,CN3
      INTEGER*4 JDF
      DIMENSION XL(1000),YL(1000),ZL(1000),NM(1000),JS(1000)
     1  ,ITN(5000),JA(5000),JB(5000),JC(5000),QC(5000)
     2  ,EY(50),GR(50),AR(50),GQ(50),GQR(50),GJ(50),QS(50)
     3  ,NT(400),MAP(1000,500),WJ(6000),A(8000),BM(8000)
     4  ,DM(8000),EM(8000),PCA(5000),PCB(5000),JDF(3000),
     5  GG(50,5),BW(50),PAY(50),PAZ(50),JLO(2000),WLO(1000)
     6 ,RC(5000),RS(50),CM(80000),FFW((50,8)
      INTEGER ADDR(1000),WADDR(1000),ORD(1000),NST(1000),
     1 P,Q,R,T
      REAL MX,MY,MZ,MY1,MY2,MZ1,MZ2,MW,MW1,MW2
      COMMON/FORCS/FM(35000),CFM(35000)
      COMMON/JOINT/XL,YL,ZL,WJ
      COMMON/NITS/NJS,NPMS,NPMTS,NILS,NJOLD,NPREV,NMS,NMTS,
     1  NE,ISTOR,NSTOR,ISTOW,NSTOW,IM,JOB,NPRMS,DET,NINTS
     2 ,NBMS,NBMTS,MODE,JCN,JCDF,CRD,FLAM,NLJS,TOL
      COMMON/INTS/NM,JS,JDF,NT,MAP,WADDR,ADDR,ORD,NST
      COMMON/BARMS/GG,FFW,PAY,PAZ,JLO,WLO
      COMMON/MISC/A,BM,CM,DM,EM
      COMMON/SPMEM/ITN,JA,JB,JC,QC,RC,PCA,PCB
      COMMON/SPMTS/EY,AR,GR,GQ,GQR,GJ,QS,RS,BW
      IF(IC.GT.5.AND.JOB.GT.999)WRITE(8,150)
  150 FORMAT(//14H MEMBER FORCES/1X,13(1H*))
      DO 459 II=1,NBMS
      I=II
C  EVALUATE LENGTH AND DIRECTION COSINES - MEMBER I
      P=ABS(JA(I))-NJOLD+NPREV
      Q=ABS(JB(I))-NJOLD+NPREV
      R=ABS(JC(I))-NJOLD+NPREV
      XLG=SQRT((XL(Q)-XL(P))**2+(YL(Q)-YL(P))**2+(ZL(Q)-
     1 ZL(P))**2)
      CL1=(XL(Q)-XL(P))/XLG
      CM1=(YL(Q)-YL(P))/XLG
      CN1=(ZL(Q)-ZL(P))/XLG
      AA=(CL1*(XL(R)-XL(P))+CM1*(YL(R)-YL(P))+CN1*(ZL(R)-
     1 ZL(P)))/XLG
      X=XL(P)+AA*(XL(Q)-XL(P))
      Y=YL(P)+AA*(YL(Q)-YL(P))
      Z=ZL(P)+AA*(ZL(Q)-ZL(P))
      AB=SQRT((XL(R)-X)**2+(YL(R)-Y)**2+(ZL(R)-Z)**2)
      CL2=(XL(R)-X)/AB
      CM2=(YL(R)-Y)/AB
      CN2=(ZL(R)-Z)/AB
      CL3=CM1*CN2-CM2*CN1
      CM3=CN1*CL2-CN2*CL1
      CN3=CL1*CM2-CL2*CM1
```

```
  164 FORMAT(/3E15.6,26H  DIRECTION COSINES MEMBER,I5,
     1 9H   LENGTH,E15.6)
  165 FORMAT(3E15.6)
      IF(IC.GT.5.OR.NI.GT.0)GO TO 449
      WRITE(8,164)CL1,CM1,CN1,I,XLG
      WRITE(8,165)CL2,CM2,CN2
      WRITE(8,165)CL3,CM3,CN3
      IF(I.EQ.NBMS)WRITE(8,166)
  166 FORMAT(1H /1H )
C
C  BUILD TRANSFORMATION MATRIX IN DM(14*14)
C
  449 DO 450 J=1,196
  450 DM(J)=0.0
      CR=RC(I)
      CQ=QC(I)
      PA=PCA(I)
      PB=PCB(I)
      DM(1)=CL1
      DM(2)=CM1
      DM(3)=CN1
      DM(15)=CL2
      DM(16)=CM2
      DM(17)=CN2
      DM(29)=CL3
      DM(30)=CM3
      DM(31)=CN3
      DO 447 J=1,3
      DO 447 K=1,3
      L=J+3+14*(K+2)
      M=J+14*(K-1)
      DM(L)=DM(M)
  447 CONTINUE
      DM(74)=-CL3
      DM(75)=-CM3
      DM(76)=-CN3
      DM(4)=-CR*CL2-CQ*CL3
      DM(5)=-CR*CM2-CQ*CM3
      DM(6)=-CR*CN2-CQ*CN3
      DM(18)=-CR*CL1+PA*CL3
      DM(19)=-CR*CM1+PA*CM3
      DM(20)=-CR*CN1+PA*CN3
      DM(32)=CQ*CL1+PA*CL2
      DM(33)=CQ*CM1+PA*CM2
      DM(34)=CQ*CN1+PA*CN2
      DM(106)=CL1
      DM(107)=CM1
      DM(108)=CN1
      DM(120)=CL2
      DM(121)=CM2
      DM(122)=CN2
      DM(134)=CL3
      DM(135)=CM3
      DM(136)=CN3
      DM(151)=CL1
      DM(152)=CM1
      DM(153)=CN1
      DM(165)=CL2
      DM(166)=CM2
```

```
      DM(167)=CN2
      DM(179)=-CL3
      DM(180)=-CM3
      DM(181)=-CN3
      DM(109)=-CR*CL2-CQ*CL3
      DM(110)=-CR*CM2-CQ*CM3
      DM(111)=-CR*CN2-CQ*CN3
      DM(123)=-CR*CL1+PB*CL3
      DM(124)=-CR*CM1+PB*CM3
      DM(125)=-CR*CN1+PB*CN3
      DM(137)=CQ*CL1+PB*CL2
      DM(138)=CQ*CM1+PB*CM2
      DM(139)=CQ*CN1+PB*CN2
      DM(91)=1.0
      DM(196)=1.0
      IF(IC.LE.5.AND.NI.LE.0.AND.II.LE.1)WRITE(8,399)(DM(J)
     1 ,J=1,196)
  399 FORMAT(/22H TRANSFORMATION MATRIX/14(/1H ,14F8.4))
C
C  BUILD STIFFNESS MATRIX IN MEMBER COORDINATES IN A(14X14)
C
      I=ITN(II)
      DO 451 J=1,196
  451 A(J)=0.0
      E=EY(I)
      AA=AR(I)
      GZ=GR(I)
      GY=GQ(I)
      GK=GJ(I)
      ECW=E*GQR(I)
      GO=GG(I,1)
      G1=GG(I,2)
      G2=GG(I,3)
      G3=GG(I,4)
      G4=GG(I,5)
      J=14*(II-1)
      FX=-CFM(J+1)
      QY1=-CFM(J+2)
      QZ1=-CFM(J+3)
      MX=-CFM(J+4)
      MY1=-CFM(J+5)
      MZ1=-CFM(J+6)
      MW1=-CFM(J+7)
      QY2=-CFM(J+9)
      QZ2=-CFM(J+10)
      MY2=-CFM(J+12)
      MZ2=-CFM(J+13)
      MW2=-CFM(J+14)
      PY=-PAY(I)*FLAM
      PZ=-PAZ(I)*FLAM
      ZO=RS(I)
      YO=QS(I)
      B1=(G1+G2)/GY-2.0*ZO
      B2=(G3+G4)/GZ-2.0*YO
      SO=GO/AA+YO*B1+ZO*B2
      FSS=FX*SO
      XX=XLG*XLG
      XXX=XX*XLG
      A(1)=E*AA/XLG
```

```
      AA=1.2*FX/XLG
      BB=-FX/10.0
      CC=FX*XLG/7.5
      DD=-FX*XLG/30.0
      MY=MY1-MY2
      MZ=MZ1-MZ2
      MW=MW1-MW2
      A(8)=-A(1)
      A(16)=12.0*E*GZ/XXX+AA
      A(18)=0.6*MY/XLG+0.05*QZ1+0.55*QZ2
      A(20)=-6.0*E*GZ/XX+BB
      A(21)=-0.05*MY-0.05*QZ2*XLG
      A(23)=-A(16)
      A(25)=-0.6*MY/XLG-0.55*QZ1-0.05*QZ2
      A(27)=A(20)
      A(28)=-0.05*MY-0.05*QZ1*XLG
      A(31)=12.0*E*GY/XXX+AA
      A(32)=-0.6*MZ/XLG-0.05*QY1-0.55*QY2
      A(33)=-6.0*E*GY/XX+BB
      A(35)=0.05*MZ+0.05*QY2*XLG
      A(38)=-A(31)
      A(39)=0.6*MZ/XLG+0.55*QY1+0.05*QY2
      A(40)=A(33)
      A(42)=0.05*MZ+0.05*QY1*XLG
      A(46)=1.2*GK/XLG+12.0*ECW/XXX+1.2*FSS/XLG+0.3*(2.0*MY/
     1 XLG+QZ1+QZ2)*B1+0.3*(2.0*MZ/XLG+QY1+QY2)*B2+(FFW1*MW
     2 /XLG+FFW5*MX)*BW
      A(47)=0.55*MZ+0.1*QY1*XLG+0.45*QY2*XLG
      A(48)=-0.55*MY-0.1*QZ1*XLG-0.45*QZ2*XLG
      A(49)=-GK/10.0-6.0*ECW/XX-FSS/10.0-0.05*(MY+QZ1*XLG)
     1 *B1-0.05*(MZ+QY1*XLG)*B2-(FFW3*MW+FFW7*MX*XLG)*BW
      A(51)=-0.6*MY/XLG-0.05*QZ1-0.55*QZ2
      A(52)=0.6*MZ/XLG+0.05*QY1+0.55*QY2
      A(53)=-A(46)
      A(54)=0.05*MZ-0.05*QY1*XLG+0.1*QY2*XLG
      A(55)=-0.05*MY+0.05*QZ1*XLG-0.1*QZ2*XLG
      A(56)=-GK/10.0-6.0*ECW/XX-FSS/10.0-0.05*(MY+QZ2*XLG)*
     1 B1-0.05*(MZ+QY1*XLG)*B2-(FFW3*MW+FFW7*MX*XLG)*BW
      A(61)=4.0*E*GY/XLG+CC
      A(63)=-MZ*XLG/15.0-QY1*XX/60.0-0.05*QY2*XX
      A(66)=-A(33)
      A(67)=-0.05*MZ-0.1*QY1*XLG+0.05*QY2*XLG
      A(68)=2.0*E*GY/XLG+DD
      A(70)=MZ*XLG/60.0+QY2*XX/60.0
      A(76)=4.0*E*GZ/XLG+CC
      A(77)=MY*XLG/15.0+QZ1*XX/60.0+0.05*QZ2*XX
      A(79)=-A(20)
      A(81)=0.05*MY+0.1*QZ1*XLG-0.05*QZ2*XLG
      A(83)=2.0*E*GZ/XLG+DD
      A(84)=-MY*XLG/60.0-QZ2*XX/60.0
      A(91)=GK*XLG/7.5+4.0*ECW/XLG+FSS*XLG/7.5+(MY*XLG/15.0
     1 +QZ1*XX/60.0+QZ2*XX/20.0)*B1+(MZ*XLG/15.0+QY1*XX/60.0
     2 +QY2*XX/20.0)*B2+(FFW2*MW*XLG+FFW6*MX*XX)*BW
      A(93)=0.05*MY+0.05*QZ2*XLG
      A(94)=-0.05*MZ-0.05*QY2*XLG
      A(95)=-A(56)
      A(96)=MZ*XLG/60.0+QY1*XX/60.0
      A(97)=-MY*XLG/60.0-QZ1*XX/60.0
      A(98)=-GK*XLG/30.0+2.0*ECW/XLG-FSS*XLG/30.0-(MY*XLG/60.0
```

```
     1 +(QZ1+QZ2)*XX/120.0)*B1-(MZ*XLG/60.0+(QY1+QY2)*XX/120.0
     2 )*B2-(FFW4*MW*XLG+FFW8*MX*XX)*BW
       A(106)=A(1)
       A(121)=A(16)
       A(123)=0.6*MY/XLG+0.55*QZ1+0.05*QZ2
       A(125)=-A(20)
       A(126)=0.05*MY+0.05*QZ1*XLG
       A(136)=A(31)
       A(137)=-0.6*MZ/XLG-0.55*QY1-0.05*QY2
       A(138)=-A(33)
       A(140)=-0.05*MZ-0.05*QY1*XLG
       A(151)=A(46)+(PY+PZ)
       A(152)=-0.55*MZ-0.45*QY1*XLG-0.1*QY2*XLG
       A(153)=0.55*MY+0.45*QZ1*XLG+0.1*QZ2*XLG
       A(154)=-A(49)
       A(166)=A(61)
       A(168)=-MZ*XLG/15.0-0.05*QY1*XX-QY2*XX/60.0
       A(181)=A(76)
       A(182)=MY*XLG/15.0+0.05*QZ1*XX+QZ2*XX/60.0
       A(196)=A(91)+(QZ1-QZ2)*XX*B1/30.0+(QY1-QY2)*XX*B2/30.0
       DO 452 J=1,14
       DO 452 K=1,14
       IF(J.GE.K)GO TO 452
       A(J+14*(K-1))=A(K+14*(J-1))
   452 CONTINUE
       IF(IC.GT.5)GO TO 480
C
C    FORM T.K.T(TRANS)
C
       CALL XMULT(14,14,14,DM,A,BM)
       CALL XTRAN(14,14,DM,A)
       CALL XMULT(14,14,14,BM,A,EM)
C   TRANSFORMED STIFFNESS MATRIX IS NOW IN EM.  SPLIT INTO
C   INTO 7X7 BLOCKS AND ADD INTO STORE
C
       IF(JS(P).EQ.0)GO TO 454
       DO 456 J=1,7
       DO 456 K=1,7
   456 A(K+7*(J-1))=EM(K+14*(J-1))
  1101 FORMAT(7H SORTSQ,10I8)
       IF(JOB.GE.20000)WRITE(8,1101)P,JS(P),JDF(P),ADDR(P)
       IF(JS(P).NE.7)CALL SORTSQ(7,JDF(P),A)
       CALL STORE(1,ADDR(P),JS(P)**2,A,1)
       IF(JS(Q).EQ.0)GO TO 459
       IF(Q.LT.P)GO TO 454
       DO 460 J=1,7
       DO 460 K=1,7
   460 A(K+7*(J-1))=EM(K+98+14*(J-1))
  1102 FORMAT(7H  SORTG,10I8)
       IF(JOB.GE.20000)WRITE(8,1102)P,JS(P),JDF(P),Q,JS(Q),JDF(Q)
       IF(JS(P)*JS(Q).NE.49)CALL SORTG(7,JDF(P),7,JDF(Q),A)
       K=0
       IW=NST(P)
       DO 462 J=1,IW
       IF(IABS(MAP(P,J)).LT.P)GO TO 462
       IF(IABS(MAP(P,J)).NE.Q)GO TO 463
       T=K
   463 K=K+JS(P)*JS(IABS(MAP(P,J)))
   462 CONTINUE
```

```
      T=T+JS(P)*JS(P)+ADDR(P)
      CALL STORE(1,T,JS(P)*JS(Q),A,1)
C   CONSIDER TERMS FOR END 2
C
  454 IF(JS(Q).EQ.0)GO TO 459
      DO 465 J=1,7
      DO 465 K=1,7
  465 A(K+7*(J-1))=EM(K+105+14*(J-1))
      IF(JOB.GE.20000)WRITE(8,1101)Q,JS(Q),JDF(Q),ADDR(Q)
      IF(JS(Q).NE.7)CALL SORTSQ(7,JDF(Q),A)
      CALL STORE(1,ADDR(Q),JS(Q)**2,A,1)
      IF(JS(P).EQ.0)GO TO 459
      IF(P.LT.Q)GO TO 459
      DO 467 J=1,7
      DO 467 K=1,7
  467 A(K+7*(J-1))=EM(K+7+14*(J-1))
      IF(JOB.GE.20000)WRITE(8,1102)Q,JS(Q),JDF(Q),P,JS(P),JDF(P)
      IF(JS(P)*JS(Q).NE.49)CALL SORTG(7,JDF(Q),7,JDF(P),A)
      K=0
      IW=NST(Q)
      DO 469 J=1,IW
      IF(IABS(MAP(Q,J)).LT.Q)GO TO 469
      IF(IABS(MAP(Q,J)).NE.P)GO TO 470
      T=K
  470 K=K+JS(Q)*JS(IABS(MAP(Q,J)))
  469 CONTINUE
      T=T+JS(Q)*JS(Q)+ADDR(Q)
      CALL STORE(1,T,JS(Q)*JS(P),A,1)
      GO TO 459
C   STIFFNESS MATRIX TERMS ENTERED - NEXT SEQUENCE EVALUATES
C   MEMBER FORCES
C
  480 IW=NILS*JS(P)
      DO 484 J=1,IW
  484 EM(J)=WJ(WADDR(P)+J-1)
      IF(JS(P).NE.7)CALL UNSORT(7,JDF(P),NILS,EM)
      IW=NILS*JS(Q)
      DO 486 J=1,IW
  486 BM(J)=WJ(WADDR(Q)+J-1)
      IF(JS(Q).NE.7)CALL UNSORT(7,JDF(Q),NILS,BM)
      DO 488 K=1,NILS
      DO 488 J=1,7
      L=NILS-K
      EM(J+14*L)=EM(J+7*L)
  488 EM(J+7+14*L)=BM(J+7*L)
C   MEMBER DISPLACEMENTS END 1 AND END 2 NOW CONSECUTIVE IN EM
      CALL XTRAN(14,14,DM,BM)
      CALL XMULT(14,14,14,A,BM,DM)
      CALL XMULT(14,14,NILS,DM,EM,A)
  100 L=II+NPRMS
      DO 489 J=1,NILS
  489 WRITE(8,170)L,(A((J-1)*14+K),K=1,14)
  170 FORMAT(I4,7E15.6/4X,7E15.6/1H )
C   EVALUATION OF MEMBER FORCES COMPLETE - COLLECTED IN CFM
C
      DO 490 J=1,14
  490 CFM(14*(II-1)+J)=A(J)
  459 CONTINUE
      WRITE(8,167)
```

```
  167 FORMAT(1H )
      IF(IC.LT.5)GO TO 211
      IW=NBMS*14
      WRITE(11)(CFM(I),I=1,IW)
C   STORE CURRENT MEMBER FORCES ON TAPE 1
  211 IF(JOB.GT.10000.AND.IC.LT.5)CALL STORE(9,1,ISTOR,A,1)
      RETURN
      END
```

APPENDIX A.4.4

SUBROUTINE SOLV(B)

```
      SUBROUTINE SOLVE(B)
      DOUBLE PRECISION A,BM,CM,DM,EM,WJ
      INTEGER*4 JDF
      DIMENSION XL(1000),YL(1000),ZL(1000),NM(1000),JS(1000)
     1 ,JDF(3000)
      DIMENSION ITN(5000),JA(5000),JB(5000),JC(5000),QC(5000)
     1 ,RC(5000)
      DIMENSION EY(50),GR(50),AR(50),GQ(50),GQR(50),GJ(50),
     1 QS(50),RS(50),BW(50)
      DIMENSION NT(400),MAP(1000,500),WJ(6000),A(8000),
     1 BM(8000),CM(80000)
      DIMENSION DM(8000),EM(8000),PCA(5000),PCB(5000)
      INTEGER ADDR(1000),WADDR(1000),ORD(1000),NST(1000),
     1 P,Q,R,S,T
      DIMENSION GG(50,5),FFW(50,8),PAY(50),PAZ(50),
     1 WLO(1000),JLO(2000)
      COMMON/BARMS/GG,FFW,PAY,PAZ,JLO,WLO
      COMMON/JOINT/XL,YL,ZL,WJ
      COMMON/NITS/NJS,NPMS,NPMTS,NILS,NJOLD,NPREV,NMS,NMTS,
     1  NE,ISTOR,NSTOR,ISTOW,NSTOW,IM,JOB,NPRMS,DET,NINTS
     2 ,NBMS,NBMTS,MODE,JCN,JCDF,CRD,FLAM,NLJS,TOL
      COMMON/INTS/NM,JS,JDF,NT,MAP,WADDR,ADDR,ORD,NST
      COMMON/MISC/A,BM,CM,DM,EM
      COMMON/SPMEM/ITN,JA,JB,JC,QC,RC,PCA,PCB
      COMMON/SPMTS/EY,AR,GR,GQ,GQR,GJ,QS,RS,BW
C  BASIC INVERSION BLOCK
  263 DO 60 I=1,NE
      IF(B.LT.5.0)GO TO 240
      K=ORD(I)
C  EXTRACT AND INVERT KBB, WRITE BACK INVERT, STORE INVERT
C      IN BM
      T=ADDR(K)
      CALL STORE(3,T,JS(K)*JS(K),BM,1)
      CALL XINVT(JS(K),BM,A ,DET)
      IF(DET.LT.0.0)RETURN
      CALL STORE(2,T,JS(K)*JS(K),A,1)
C  EVALUATE (INVERT KBB)*WB AND WRITE BACK TO WB
      R=WADDR(K)
      IW=JS(K)*NILS
      DO 63 J=1,IW
   63 DM(J)=WJ(R+J-1)
      CALL XMULT(JS(K),JS(K),NILS,A ,DM,BM)
      DO 64 J=1,IW
   64 WJ(R+J-1)=BM(J)
      IF(I.EQ.NE.AND.NINTS.EQ.0)GO TO 60
C  EXTRACT KBA BLOCK BY BLOCK, STORE BLOCKS END TO END IN CM
   90 NS=0
      NB=0
      T=ADDR(K)+JS(K)*JS(K)
      R=0
      IW=NST(K)
      DO 65 J=1,IW
      N=IABS(MAP(K,J))
      IF(MAP(K,J).LT.0)GO TO 66
      NB=NB+1
```

```
      NS=NS+JS(N)
      NT(NB)=N
      IF(N.LT.K)GO TO 67
      CALL STORE(3,T,JS(K)*JS(N),CM,R+1)
      R=R+JS(K)*JS(N)
   66 IF(N.LT.K)GO TO 65
      T=T+JS(K)*JS(N)
      GO TO 65
   67 IC=ADDR(N)+JS(N)*JS(N)
      IV=NST(N)
      DO 69 P=1,IV
      IF(IABS(MAP(N,P)).LT.N)GO TO 69
      IF(IABS(MAP(N,P)).NE.K)GO TO 70
      CALL STORE(3,IC,JS(K)*JS(N),EM,1)
      IU=JS(K)
      IY=JS(N)
      DO 71 Q=1,IU
      DO 71 L=1,IY
   71 CM(R+Q+JS(K)*(L-1))=EM(L+JS(N)*(Q-1))
      R=R+JS(N)*JS(K)
   70 IC=IC+JS(N)*JS(IABS(MAP(N,P)))
   69 CONTINUE
   65 CONTINUE
      IF(B.LT.5.0)GO TO 91
      IF(NS.EQ.0)GO TO 60
C  EVALUATE KAB(INVERT KBB)WB AND SUBTRACT FROM WA
      CALL XTRAN(JS(K),NS,CM,DM)
      CALL XMULT(NS,JS(K),NILS,DM,BM,CM)
      NR=0
      DO 82 J=1,NB
      DO 72 P=1,NILS
      IW=JS(NT(J))
      DO 72 Q=1,IW
      AA=WJ(WADDR(NT(J))-1+Q+JS(NT(J))*(P-1))
      WJ(WADDR(NT(J))-1+Q+JS(NT(J))=AA-CM(NR+Q+NS*(P-1))
     1 *(P-1))
   72 CONTINUE
   82 NR=NR+JS(NT(J))
C  EVALUATE KAB(INVERT KBB)KBA AND SUBTRACT BLOCK BY BLOCK
C      FROM KAA
      CALL XMULT(NS,JS(K),JS(K),DM,A,BM)
      CALL XTRAN(NS,JS(K),DM,A)
      CALL XMULT(NS,JS(K),NS,BM,A,CM)
      NC=0
      DO 73 Q=1,NB
      NR=0
      DO 74 P=1,NB
      IF(NT(Q).LT.NT(P))GO TO 76
      IW=JS(NT(Q))
      IV=JS(NT(P))
      DO 75 N=1,IW
      DO 75 M=1,IV
   75 BM(M+JS(NT(P))*(N-1))=CM(NR+M+NS*(NC+N-1))
      IF(NT(Q).NE.NT(P))GO TO 77
      CALL STORE(5,ADDR(NT(P)),JS(NT(P))*JS(NT(P)),BM,1)
      GO TO 76
   77 IC=ADDR(NT(P))+JS(NT(P))**2
      IW=NST(NT(P))
      DO 79 N=1,IW
```

```
      IF(IABS(MAP(NT(P),N)).LT.NT(P))GO TO 79
      IF(IABS(MAP(NT(P),N)).NE.NT(Q))GO TO 80
      CALL STORE(5,IC,JS(NT(P))*JS(NT(Q)),BM,1)
   80 IC=IC+JS(NT(P))*JS(IABS(MAP(NT(P),N)))
   79 CONTINUE
   76 NR=NR+JS(NT(P))
   74 CONTINUE
      NC=NC+JS(NT(Q))
   73 CONTINUE
C  REDUCTION OF JOINT K COMPLETE
C  END OF BASIC INVERSION BLOCK
      GO TO 60
C
C  EVALUATE DISPLACEMENTS IN REVERSE ORDER OF REDUCTION
  240 K=ORD(NE-I+1)
      IF(I.EQ.1.AND.NINTS.EQ.0)GO TO 98
      GO TO 90
C  EXTRACT KBA BLOCK BY BLOCK INTO CM,PUT (INVERT KBB) IN
C  BM, WA IN DM
   91 IF(NS.EQ.0)GO TO 98
      CALL STORE(3,ADDR(K),JS(K)*JS(K),BM,1)
      NR=0
      DO 93 L=1,NB
      DO 94 P=1,NILS
      IW=JS(NT(L))
      DO 94 Q=1,IW
   94 DM(NR+Q+NS*(P-1))=WJ(WADDR(NT(L))+Q-1+JS(NT(L))*(P-1))
   93 NR=NR+JS(NT(L))
C  EVALUATE (INVT.KBB)KBA(WA) RESULT IN CM. DISPLACEMENTS
C   IN DM AND WJ
      CALL XMULT(JS(K),JS(K),NS,BM,CM,A)
      CALL XMULT(JS(K),NS,NILS,A,DM,CM)
      IV=JS(K)*NILS
      DO 92 J=1,IV
      DM(J)=WJ(WADDR(K)+J-1)-CM(J)
   92 WJ(WADDR(K)+J-1)=DM(J)
   98 CONTINUE
   60 CONTINUE
C
C  EVALUATION OF JOINT DISPLACEMENTS COMPLETE
C
      IF(JOB.GT.30000)CALL STORE(9,1,ISTOR,A,1)
      IF(JOB.GT.30000.AND.ISTOW.LE.100)WRITE(8,256)(WJ(I),
     1 I=1,ISTOW)
  256 FORMAT(//10(1H ,10E12.4/))
      IF(B.LT.5.0)GO TO 261
      IF(NINTS.LT.1)B=0.0
      IF(NINTS.LT.1)GO TO 263
  141 FORMAT(I4,7E15.6/)
C  TRANSFER ALL BLOCK DATA TO TAPE
C
      NSTOR=ISTOR+1-ADDR(1+NJS-NINTS)
      NSTOW=ISTOW+1-WADDR(1+NJS-NINTS)
  155 FORMAT(/10H RETAINING,2I6/)
      WRITE(8,155)NSTOR,NSTOW
      WRITE(10)NMS,NJS,NMTS,NJOLD,NPREV,NINTS,NE,ISTOR,ISTOW
     1 ,NSTOR,NSTOW
      CALL STORE(6,1,ISTOR-NSTOR,A,1)
      WRITE(10)(ITN(I),JA(I),JB(I),JC(I),QC(I),RC(I),PCA(I),
```

```
     1 PCB(I),I=1,NMS)
      WRITE(10)(JS(I),JDF(I),ORD(I),ADDR(I),WADDR(I),NST(I),
     1 XL(I),YL(I),ZL(I),I=1,NJS)
      WRITE(10)(EY(I),AR(I),GR(I),GQ(I),GQR(I),GJ(I),QS(I),
     1 RS(I),I=1,NMTS)
      J=NJS-NINTS
      WRITE(10)((MAP(I,K),K=1,IM),I=1,J)
      J=ISTOW-NSTOW
      WRITE(10)(WJ(I),I=1,J)
C
C   MOVE ALL INTERFACE TERMS TO BASE OF STORAGE
      DO 272 I=1,NINTS
      S=NST(I)
      K=I+NJS-NINTS
      NM(I)=NM(K)
      NST(I)=NST(K)
      JS(I)=JS(K)
      JDF(I)=JDF(K)
      XL(I)=XL(K)
      YL(I)=YL(K)
      ZL(I)=ZL(K)
      NT(I)=1+ADDR(K)-ADDR(1+NJS-NINTS)
      P=NJS-NINTS
      Q=0
      T=NST(I)
      IF(T.LE.0)GO TO 271
      DO 84 J=1,T
      N=IABS(MAP(K,J))
      IF(N.LE.P)GO TO 59
      Q=Q+1
      MAP(I,Q)=(N-P)*MAP(K,J)/N
      GO TO 84
   59 NST(I)=NST(I)-1
   84 CONTINUE
  271 IW=Q+1
      IF(IW.GT.S)GO TO 272
      DO 85 J=IW,S
   85 MAP(I,J)=0
  272 CONTINUE
      NT(NINTS+1)=NSTOR+1
      DO 86 I=1,NSTOW
   86 WJ(I)=WJ(WADDR(1+NJS-NINTS)+I-1)
      CALL STORE(8,ADDR(1+NJS-NINTS),NSTOR,A,1)
      NJOLD=NJOLD+NJS-NPREV
      NPREV=NINTS
      IF(JOB.GT.30000)CALL STORE(9,1,ISTOR,A,1)
      IF(JOB.GT.30000.AND.ISTOW.LE.100)WRITE(8,256)(WJ(I),I=1,ISTOW)
      RETURN
  261 WRITE(8,140)
  140 FORMAT(///24H DISPLACEMENTS AT JOINTS/1X,24(1H*)/1H )
      Q=7
      IF(NBMS.LE.0)Q=6
      DO 23 K=1,NJS
      IF(JS(K).EQ.0)GO TO 23
      P=K+NJOLD-NPREV
      IV=JS(K)*NILS
      DO 22 I=1,IV
   22 BM(I)=WJ(WADDR(K)+I-1)
      IF(JS(K).NE.Q)CALL UNSORT(Q,JDF(K),NILS,BM)
```

```
      DO 21 J=1,NILS
      N=Q*(J-1)+1
      IW=N+Q-1
   21 WRITE(8,141)P,(BM(M),M=N,IW)
      IF(P.EQ.JCN)CRD=BM(JCDF)
   23 CONTINUE
      END
```

SUBROUTINE STORE

```
      SUBROUTINE STORE(IT,IADDR,ISIZE,ARG,II)
      DOUBLE PRECISION ST,ARG
      DIMENSION ST(16000),ARG(800)
      COMMON/XST/ST
      IF(ISIZE.EQ.0)RETURN
      GO TO(1,2,3,4,5,6,7,8,9),IT
    1 DO 10 I=1,ISIZE
   10 ST(IADDR+I-1)=ST(IADDR+I-1)+ARG(II+I-1)
      GO TO 99
    2 DO 11 I=1,ISIZE
   11 ST(IADDR+I-1)=ARG(II+I-1)
      GO TO 99
    3 DO 12 I=1,ISIZE
   12 ARG(II+I-1)=ST(IADDR+I-1)
      GO TO 99
    4 DO 13 I=1,ISIZE
   13 ST(IADDR+I-1)=0
      GO TO 99
    5 DO 14 I=1,ISIZE
   14 ST(IADDR+I-1)=ST(IADDR+I-1)-ARG(II+I-1)
      GO TO 99
    6 WRITE(10)(ST(IADDR+I-1),I=1,ISIZE)
      GO TO 99
    7 READ(10) (ST(IADDR+I-1),I=1,ISIZE)
      GO TO 99
    8 DO 15 I=1,ISIZE
   15 ST(II+I-1)=ST(IADDR+I-1)
      GO TO 99
  140 FORMAT(/12H PRINT STORE)
    9 WRITE(8,140)
  179 FORMAT(I5,2H   ,9E12.4)
      IW=(ISIZE+8)/9
      DO 144 I=1,IW
      J=9*I-8
  144 WRITE(8,179)J,(ST(J+9*(I-1)),J=1,9)
      WRITE(8,141)
  141 FORMAT(1H )
   99 RETURN
      END
```

SUBROUTINE UNSORT

```
      SUBROUTINE UNSORT(JS,IJDF,NILS,B)
      DOUBLE PRECISION B,C
      INTEGER*4 IJDF,JDF,K,IL,IM
      DIMENSION B(49),C(49),IT(7)
      COMMON/US/C
      JDF=IJDF
      M=0
      IL=JS
      IM=10
      K=IM**(IL-1)
      DO 5 I=1,JS
      IT(I)=0
      IF(JDF.LT.K)GO TO 5
      M=M+1
      IT(I)=2
      JDF=JDF-K
    5 K=K/IM
      IB=0
      DO 3 J=1,JS
      IF(IT(J).GT.1)GO TO 8
      DO 2 I=1,NILS
    2 C(J+JS*(I-1))=0.0
      GO TO 3
    8 IB=IB+1
      DO 7 I=1,NILS
    7 C(J+JS*(I-1))=B(IB+M*(I-1))
    3 CONTINUE
      IW=JS*NILS
      DO 4 I=1,IW
    4 B(I)=C(I)
      RETURN
      END
```

SUBROUTINE SORTSQ

```
      SUBROUTINE SORTSQ(IQ,IJR,TERM)
      DOUBLE PRECISION TERM
      INTEGER*4 IR,IJR,K,L,M
      DIMENSION TERM(49),I(7)
      L=IQ
      M=10
      IR=IJR
      K=M**(L-1)
      DO 3 J=1,IQ
      I(J)=0
      IF(IR.LT.K)GO TO 2
      IR=IR-K
      I(J)=2
    2 K=K/M
    3 CONTINUE
      IC=0
      DO 6 J=1,IQ
      IF(I(J).LT.1)GO TO 6
      DO 5 KK=1,IQ
      IF(I(KK).LT.1)GO TO 5
      IC=IC+1
      TERM(IC)=TERM(KK+IQ*(J-1))
    5 CONTINUE
    6 CONTINUE
      RETURN
      END
```

SUBROUTINE SORTG

```
      SUBROUTINE SORTG(IAQ,JAR,IBQ,JBR,TERM)
      DOUBLE PRECISION TERM
      INTEGER*4 IAR,JAR,IBR,JBR,K,L,LB,M
      DIMENSION TERM(49),IA(7),IB(7)
      L=IAQ
      LB=IBQ
      M=10
      IAR=JAR
      IBR=JBR
      K=M**(L-1)
      DO 6 J=1,IAQ
      IA(J)=0
      IF(IAR.LT.K)GO TO 2
      IAR=IAR-K
      IA(J)=2
    2 K=K/M
    6 CONTINUE
      K=M**(LB-1)
      DO 3 J=1,IBQ
      IB(J)=0
      IF(IBR.LT.K)GO TO 4
      IBR=IBR-K
      IB(J)=2
    4 K=K/M
    3 CONTINUE
      IC=0
      DO 7 KK=1,IBQ
      IF(IB(KK).LT.1)GO TO 7
```

```
      DO 5 J=1,IAQ
      IF(IA(J).LT.1)GO TO 5
      IC=IC+1
      TERM(IC)=TERM(J+IAQ*(KK-1))
    5 CONTINUE
    7 CONTINUE
      RETURN
      END
```

SUBROUTINE XTRAN

```
      SUBROUTINE XTRAN(M,N,B,C)
      DOUBLE PRECISION B,C
      DIMENSION B(M,N),C(N,M)
      DO 2 I=1,M
      DO 2 J=1,N
    2 C(J,I)=B(I,J)
      RETURN
      END
```

SUBROUTINE XMULT

```
      SUBROUTINE XMULT(L,M,N,A,B,C)
      DOUBLE PRECISION A,B,C
      DIMENSION A(L,M),B(M,N),C(L,N)
      DO 2 I=1,L
      DO 2 J=1,N
      C(I,J)=0
      DO 2 K=1,M
    2 C(I,J)=C(I,J)+A(I,K)*B(K,J)
      RETURN
      END
```

SUBROUTINE XINVT

```
      SUBROUTINE XINVT(IP,B,C,DET)
      DOUBLE PRECISION B,C,AP,AT
      DIMENSION B(49),C(49)
      IF(IP.EQ.1)GO TO 9
      IW=IP*IP
      DO 2 I=1,IW
    2 C(I)=0
      DO 3 I=1,IP
    3 C(I+IP*(I-1))=1.0
      IW=IP-1
      DO 5 IQ=1,IW
      K=IP-IQ+1
      AP=B(K+IP*(K-1))
      IK=K-1
      DO 5 I=1,IK
      AT=B(I+IP*(K-1))/AP
      DO 5 J=1,IP
      B(I+IP*(J-1))=B(I+IP*(J-1))-B(K+IP*(J-1))*AT
    5 C(I+IP*(J-1))=C(I+IP*(J-1))-C(K+IP*(J-1))*AT
C   MATRIX NOW REDUCED TO UPPER TRIANGLE FORM
      DO 6 IQ=1,IW
      AP=B(IQ+IP*(IQ-1))
      IK=IQ+1
      DO 6 I=IK,IP
```

```
      AT=B(I+IP*(IQ-1))/AP
      DO 6 J=1,IP
      B(I+IP*(J-1))=B(I+IP*(J-1))-B(IQ+IP*(J-1))*AT
    6 C(I+IP*(J-1))=C(I+IP*(J-1))-C(IQ+IP*(J-1))*AT
C   MATRIX NOW REDUCED TO DIAGONAL FORM
      DET=1.0
      DO 7 I=1,IP
      DO 12 J=1,IP
   12 C(I+IP*(J-1))=C(I+IP*(J-1))/B(I+IP*(I-1))
    7 DET=DET*B(I+IP*(I-1))
      GO TO 8
    9 DET=B(1)
      C(1)=1.0/B(1)
    8 RETURN
      END
```

APPENDIX A.5.1.

Calculation of warping stiffness ρ and carry-over factor C

Three cases were considered by Khan and Tottenham (79) as follows:

(i) Beam fully restrained at the far end

The boundary conditions are:

at $x = o$: $\theta_x = o$, and $\theta'_x = 1$ (A.5.1.a)

at $x = \ell$: $\theta_x = o$, and $\theta'_x = o$ (A.5.1.b)

The warping stiffness ρ is given by,

$$\rho = \frac{k\ell(k\ell \cosh k\ell - \sinh k\ell)}{k\ell \sinh k\ell + 2(1 + \cosh k\ell)} \cdot \frac{EI_\omega}{\ell} \qquad (A.5.2.)$$

and the carry-over factor C is,

$$C = \frac{\sinh k\ell - k\ell}{k\ell \cosh k\ell - \sinh k\ell} \qquad (A.5.3.)$$

(ii) Beam with far end restrained against rotation θ_x

The boundary conditions for this case are,

at $x = o$: $\theta_x = o$, and $\theta'_x = 1$ (A.5.4.a)

at $x = \ell$: $\theta_x = o$, and $B = o$ (A.5.4.b)

The warping stiffness ρ is given by,

$$\rho = \frac{(k\ell)^2 \sinh k\ell}{k\ell \cosh k\ell - \sinh k\ell} \quad \frac{EI_\omega}{\ell} \qquad (A.5.5.)$$

The carry-over factor C is equal to zero in this case.

(iii) Beam with far end free

The boundary conditions of this case are,

at $x = o$: $\theta_x = o$, and $\theta'_x = 1$ (A.5.6.a)

at $x = \ell$: $B = o$, and $T = o$ (A.5.6.b)

The warping stiffness is given by,

$$\rho = \frac{k\ell \sinh k\ell}{\cosh k\ell} \frac{EI_\omega}{\ell} \quad \text{(A.5.7.)}$$

The carry-over factor C is equal to zero in this case.

APPENDIX A.5.2.

The constant functions ϕ_1 - ϕ_4 in the bimoment-warping matrix

These functions are given by,

$$\phi_1 = 2S\ (1 + C) + \pi^2 \quad \text{(A.5.8.a)}$$

$$\phi_2 = S\ (1 + C) \quad \text{(A.5.8.b)}$$

$$\phi_3 = SC \quad \text{(A.5.8.c)}$$

$$\phi_4 = S \quad \text{(A.5.8.d)}$$

where, the functions S and C are given by,

$$S = \tau\ (\frac{1 + 2\tau \coth 2\tau}{\tanh \tau - \tau}) \quad \text{(A.5.9.a)}$$

$$\text{and} \quad C = \frac{2\tau - \sinh 2\tau}{\sinh 2\tau - 2\tau \cosh 2\tau} \quad \text{(A.5.9.b)}$$

$$\text{where} \quad \tau = \frac{\ell}{2} \sqrt{GJ/EI_\omega} \quad \text{(A.5.10.)}$$

APPENDIX A.9.1.

Calculation of diaphragm flexibility

A.9.1.1. Notations

a : Length of panel in the direction perpendicular to the corrugations (mm).

b : Depth of panel in the direction parallel to the corrugations (mm).

α_1, α_4: Correction factors to allow for intermediate perpendicular members.

$\bar{K}$: Non-dimensional sheeting constant for distortional flexibility.

E : Modulus of elasticity.

γ : Poisson's ratio of the frame members material.

S_p : Flexibility of sheet to perpendicular member fastener (mm/kN).

S_s : Flexibility of a seam fastener (mm/kN).

n_{sh} : Number of sheet widths per panel.

n_s : Number of seam fasteners per seam line.

n_p : Total number of perpendicular members.

β_1 : Factor depends upon whether the profile is fixed as a sheeting or decking and on the number of sheet to a perpendicular member fasteners in a sheet width.

A_f : Cross sectional area (mm^2) of an edge member.

θ : Angle of inclination of a diagonal member of the model with respect to the direction perpendicular to the corrugations.

d : Pitch of corrugations (mm).

h : Height of profile (mm).

t : Net thickness of sheeting.

A.9.1.2. Flexibility due to distortion of the sheeting profile

$$C_{1.1} = \frac{a\ d^{2.5}\ \alpha_1\ \alpha_4\ \bar{K}}{E\ t^{2.5}\ b^2} \qquad (A.9.1)$$

Tables for the correction factors α_1 and α_4 and for the non-dimensional factor $\bar{K}$ are presented in reference (13).

A.9.1.3. Flexibility due to shear strain in the sheet

$$C_{1.2} = \frac{2a(1+\nu)\ [1+(2h/d)]}{E\ t\ b} \qquad (A.9.2)$$

A.9.1.4. Flexibility due to movement at the sheet to perpendicular member fasteners

$$C_{2.1} = \frac{2a \cdot S_p \cdot p}{b^2} \qquad (A.9.3)$$

A.9.1.5. Flexibility due to movement in the seam fasteners

$$C_{2.2} = \frac{2S_p \cdot S_p(n_{sh} - 1)}{2n_s S_p + \beta_1\ n_p S_s} \qquad (A.9.4)$$

A.9.1.6. Flexibility due to axial strain in the frame members

$$C_3 = \frac{2a^3}{3E \cdot A_f \cdot b^2} \qquad (A.9.5)$$

A.9.1.7. Area of the diagonal simulating the overall shear flexibility of a sheet panel

As shown in fig. 1.d. the vertical component of the force in the diagonal member is given by,

$$Q = \frac{E \cdot A_d}{\ell_d}\ \Delta \cdot \cos\theta \qquad (A.9.6)$$

$$\Delta = C \cos\theta \quad \text{when } Q = 1.0 \text{ kN}$$

then subsituting f r Δ, the area of the diagonal member takes the form,

$$A_d = \frac{\ell_d}{E\ C\ \cos^2\theta} \qquad (A.9.7)$$

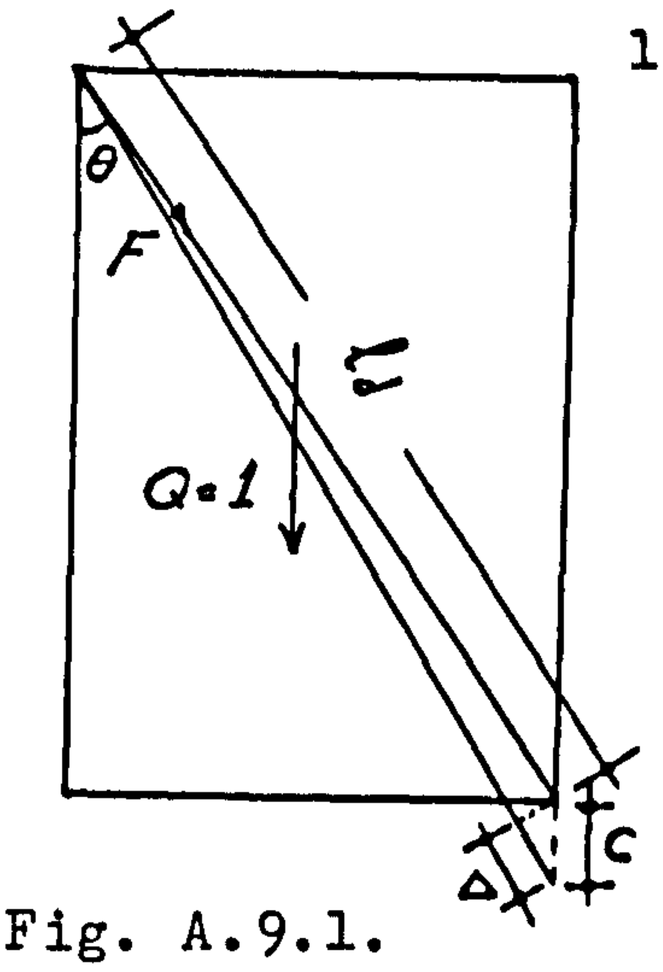

Fig. A.9.1.

It should be noted that equation (A.9.7) has been derived for the case when the two edge chords are parallel. In this case the axial strain of the edge members is due to in-plane bending. In the trapezoidal panels of the truss simulating the diaphragm, the inclined edge member has its own share in carrying the shearing force in the panel. As the axial stiffness of this member is large in comparison to that of the diagonal member, the vertical component of the strain caused by shear can be neglected and the area of the diagonal member can be calculated using equation (A.9.7).

APPENDIX A.9.2.

Calculation of fastener forces from the results of the simple truss model

F, F_l, F_r and F_L are the fastener forces given by the finite element method;

V is the vertical component of the force between the sheet and the frame members at joint 'C',

$$V = F_D \cos\theta - F_V \qquad (A.9.8)$$

$$R = 1 + \frac{1}{F}\left[(F_r + F_L)\frac{\bar{x}}{\rho} + F_l\right] \qquad (A.9.9)$$

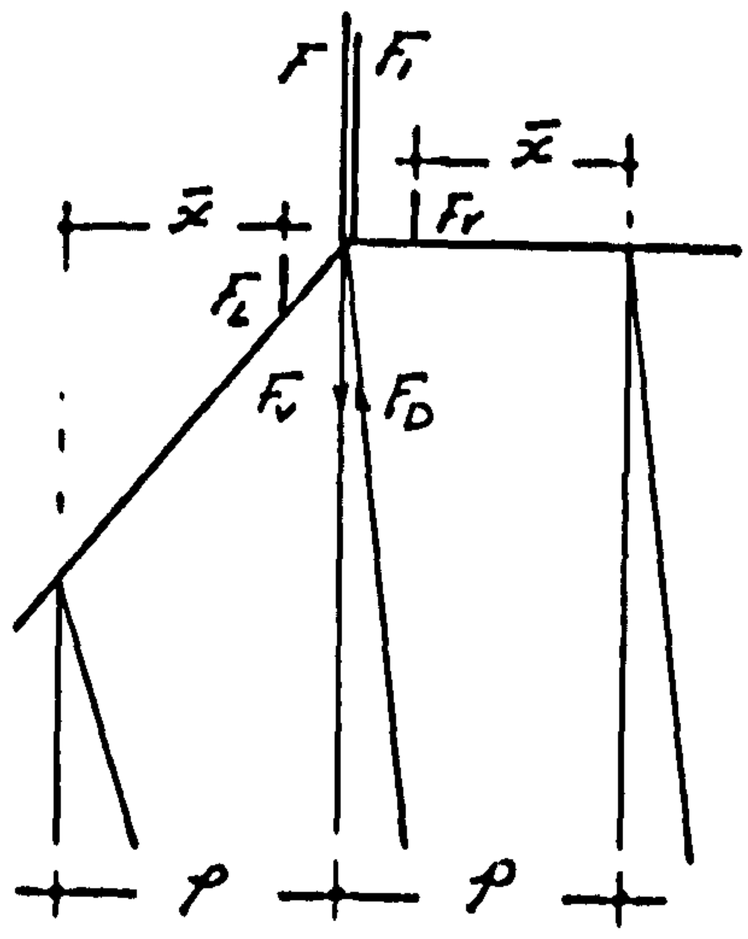

Fig. A.9.2.

The maximum fastener force at joint 'C' takes the value,

$$F_m = \frac{V}{R} \qquad (A.9.10)$$

REFERENCES (I)

1. Vlasov, V.Z., "Thin Walled Elastic Beams", 2nd Edition, National Science Foundation, Washington D.C., 1961.

2. Timoshenko, S.P., and Gere, J.M., "Theory of Elastic Stability", 2nd Edition, McGraw-Hill Book Co., New York, N.Y., 1961.

3. Bleich, F., "Buckling Strength of Metal Structures", McGraw-Hill Book Co., New York, N.Y., 1952.

4. Trahair, N.S., "Elastic Stability of Frame Structures", thesis presented to the University of Sydney in fulfilment of the requirements for the degree of Doctor of Philosophy, Nov. 1967.

5. Brown, P.T., and Trahair, N.S., "Finite Integral Solution of Differential Equations", Civil Engineering Transactions, Institution of Engineers, Australia, Vol. CE10, No. 2, Oct. 1968, pp.193-196.

6. Trahair, N.S., "Elastic Stability of Propped Cantilevers", Civil Engineering Transactions, Institution of Engineers, Australia, Vol. CE10, No. 1, Apr. 1968, pp.94-100.

7. Vacharajittiphan, P., and Trahair, N.S., "Analysis of Lateral Buckling in Plane Frames", Journal of the Structural Division, ASCE, Vol. 101, No. ST7, July 1975, pp.1497-1516.

8. Livesley, R.K., "The Application of an Electronic Digital Computer to some problems of Structural Analysis", The Structural Engineer, vol. 34, No. 1, January 1956, pp.1-12.

9. Renton, J.D., "Stability of Space Frames by Computer Analysis", Journal of the Structural Division, ASCE, Vol.88, No. ST4, August 1962, pp.81-103.

10. Chu, K.H., and Rampetsreiter, R.H., "Large Deflection Buckling of Space Frames", Journal of the Structural Division, ASCE, vol. 98, No. ST12, December 1972, pp.2701-2722.

11. Razzaq, Z., and Naim, M.M., "Elastic Instability of Unbraced Space Frames", Journal of the Structural Division, ASCE, Vol. 106, No. ST7, July 1980, pp.1389-1400.

12. Chaudhary, A.B., "Generalized Stiffness Matrix for Thin-Walled Beams", Journal of the Structural Division, ASCE, Vol. 108, No. ST3, March 1982, pp.559-577.

13. Aly, G.A., and Sato, N., Discussion of "Generalized Stiffness matrix for Thin-Walled Beams - by Chaudhary, A.B", Journal of the Structural Division, ASCE, Vol. 110, No. 2, Feb. 1984, pp.421-422.

14. Kappus, R., "Drillknicken zentrisch gedrückter Stäbe mit offenem Profil im elastischen Bereich", Luftfahrt-Forschung, 1937. Translated in N.A.C.A. Tech. Mem. 851, 1938.

15. Rodden, W.P., Jones, J.P., and Bhuta, P.G., "A Matrix Formulation of the Transverse Structural Influence Coefficients of an Axially Loaded Timoshenko Beam", Journal of the American Institute of Aeronautics and Astronautics, vol. 1, No. 1, January 1963, pp.225-227.

16. Gallagher, R.H., and Padlog, J., "Discrete Element Approach to Structural Instability Analysis", Journal of the American Institute of Aeronautics and Astronautics, vol. 1, No. 6, June 1963, pp.1437-1439.

17. Archer, J.S., "Consistent Matrix Formulations for Structural Analysis Using Finite Element Techniques", Journal of the American Institute of Aeronautics and Astronautics, vol. 3, No. 10, October 1965, pp.1910-1918.

18. Hartz, B.J., "Matrix Formulation of Structural Stability Problems", Journal of the Structural Division, ASCE, vol. 91, No. ST6, December 1965, pp.141-157.

19. Hicks, G.W., "Finite Element Elastic Buckling Analysis", Journal of the Structural Division, ASCE, vol. 93, No. ST6, December 1967, pp.71-80.

20. Mallett, R.H., and Marcal, P.V., "Finite Element Analysis of nonlinear Structures", Journal of the Structural Division, ASCE, vol. 94, No. ST9, September 1968, pp.2081-2105.

21. Krahula, J.L., "Analysis of Bent and Twisted Bars Using the Finite Element Method", Journal of American Institute of Aeronautics and Astronautics, vol. 5, No. 7, June 1967, pp.1194-1197.

22. Krajcinovic, D., "A Consistent Discrete Element Technique for Thin-Walled Assemblages", International Journal of Solids and Structures, vol. 5, 1969, pp.639-662.

23. Krajcinovic, D., "Matrix Force Analysis of Thin-Walled Structures", Journal of the Structural Division, ASCE, vol. 96, No. ST1, January 1970, pp.107-121.

24. Barsoum, R., and Gallagher, R., "Finite Element Analysis of Torsional and Torsional-Flexural Stability Problems", International Journal of Numerical Methods in Engineering, vol. 2, 1970, pp.335-352.

25. Nethercot, D.A., and Rockey, K.C., "Finite Element Solutions for the Buckling of Columns and Beams", International Journal of Mechanical Science, vol. 13, 1971, pp.945-949.

26. Powell, G., and Klingner, R., "Elastic Lateral Buckling of Steel Beams", Journal of the Structural Division, ASCE, vol. 96, No. ST9, September 1970, pp.1919-1932.

27. Alwis, W.A.M., and Usmi, T., "Elastic Lateral Torsional Buckling of Unbraced and Braced Planar Frames", Journal of Computers and Structures, vol. 10, 1979, pp.517-529.

28. Tebedge, N., and Tall, L., "Linear Stability Analysis of Beam-Column", Journal of the Structural Division, ASCE, vol. 99, No. ST12, December 1973, pp.2439-2458.

29. Chajes, A., and Winter, G., "Torsional-Flexural Buckling of Thin-Walled Members", Journal of the Structural Division, ASCE, vol. 91, No. ST4, August 1965, pp.103-124.

30. Horne, M.R., Hoh, K.E., and Poskitt, T.J., "The Torsional-Flexural Behaviour of Thin-Walled Prismatic Members", International Journal of Mechanical Science, vol. 13, 1971, pp.641-657.

31. Culver, C.G., "Exact Solution of the Biaxial Bending Equations", Journal of the Structural Division, ASCE, vol. 92, No. ST2, April 1966, pp.63-83.

32. Renton, J.D., "A Direct Solution of the Torsional-Flexural Buckling of Axially Loaded Thin-Walled Bars", The Structural Engineer, vol. 38, No. 9, September 1960, pp.273-276.

33. Pekoz, T.B., and Winter, G., "Torsional-Flexural Buckling of Thin-Walled Sections Under Eccentric Load", Journal of the Structural Division, ASCE, vol. 95, No. ST5, May 1969, pp.941-963.

34. Salvadori, M.G., "Lateral Buckling of I-Beams", Transactions, ASCE, vol. 118, October 1953, pp.1165-1182.

35. Lee, G.C., "A Survey of Literature on the Lateral Instability of Beams", Welding Research Council Bulletin, Series No. 63, Aug. 1960.

36. Nethercot, D.A., "The Lateral Stability of Beams Supported by Corrugated Sheeting", Ph.D. Thesis presented to the University of Wales, 1970.

37. Nethercot, D.A., and Rockey, K.C., "A unified approach to the elastic lateral buckling of beams", The Structural Engineer, vol. 49, No. 7, July 1971, pp.321-329.

38. Trahair, N.S., and Kitipornchai, S., "Elastic Lateral Buckling of Stepped I-Beams", Journal of the Structural Division, ASCE, vol. 97, No. ST10, October 1971, pp.2535-2548.

39. Kitipornchai, S., and Trahair, N.S., "Elastic Stability of Tapered I-Beams," Journal of the Structural Division, ASCE, vol. 98, No. ST3, March 1972, pp.713-728.

40. Anderson, J.M., and Trahair, N.S., "Stability of Monosymmetric Beams and Cantilevers", Journal of the Structural Division, ASCE, vol. 98, No. ST1, January 1972, pp.269-286.

41. Kitipornchai, S., and Trahair, N.S., "Buckling Properties of Monosymmetric I-Beams", Journal of the Structural Division, ASCE, vol. 106, No. ST5, May 1980, pp.941-957.

42. Nethercot, D.A., and Rockey, K.C., "Lateral Buckling of beams with mixed end conditions", The Structural Engineer, vol. 51, No. 4, April 1973, pp.133-139.

43. Roberts, T.M., "Second Order Strains and Stability of Thin-Walled Bars of Open Cross Section", International Journal of Mechanical Science, vol. 23, 1981, pp.297-306.

44. Roberts, T.M., and Azizian, Z.G., "Nonlinear Analysis of Thin-Walled Bars of Open Cross Section", International Journal of Mechanical Science, vol. 25, 1983, pp.565-577.

45. Flint, A.R., "The Influence of Restraints on the Stability of Beams", The Structural Engineer, vol. 29, No. 9, September 1951, pp.235-246.

46. Austin, W.J., Yegian, S., and Tung, T.P., "Lateral Buckling of Elastically End-Restrained I-Beams", Transactions, ASCE, vol. 120, April 1955, pp.374-390.

47. Trahair, N.S., "Stability of I-Beams with Elastic End Restraints", The Journal of the Institution of Engineers, Australia, vol. 37, No. 6, June 1965, pp.157-168.

48. Salvadori, M.G., "Lateral Buckling of Beams of Rectangular Cross Section Under Bending and Shear", Proceedings 1st U.S. National Congress of Applied Mechanics, 1951, p.403-406.

49. Trahair, N.S., "Elastic Stability of I-Beam Elements in Rigid-Jointed Structures", The Journal of the Institution of Engineers, Australia, vol. 38, No. 7-8, July-Aug. 1966, pp.171-180.

50. Trahair, N.S., "Interaction Buckling of Narrow Rectangular Continuous Beams", Civil Engineering Transactions Institution of Engineers, Australia, vol. CE10, No. 2, October 1968, pp.167-172.

51. Trahair, N.S., "Elastic Stability of Continuous Beams", Journal of the Structural Division, ASCE, vol. 95, No. ST6, June 1969, pp.1295-1312.

52. Hartmann, A.J., "Flexural-Torsional Buckling of Planar Structures", Thesis presented to the University of Illinois, at Urbana, in 1964, in partial fulfilment of the requirements for the degree of Doctor of Philosophy.

53. Hartmann, A.J., and Munse, W.H., "Flexural-Torsional Buckling of Planar Frames", Journal of the Structural Division, ASCE, vol. 92, No. EM2, April 1966, pp.37-59.

54. Hartmann, A.J., "Elastic Lateral Buckling of Continuous Beams", Journal of the Structural Division, ASCE, vol. 93, No. ST4, August 1967, pp.11-26.

55. Hartmann, A.J., "Experimental Study of Flexural-Torsional Buckling", Journal of the Structural Division, ASCE, vol. 96, No. ST7, July 1970, pp.1481-1493.

56. Trahair, N.S., Discussion of "Elastic Lateral Buckling of Continuous Beams - by Hartmann, A.J.", Journal of the Structural Division, ASCE, vol. 94, No. ST3, March 1968, pp.845-848.

57. Nethercot, D.A., and Trahair, N.S., "Lateral buckling approximations for elastic beams", The Structural Engineer, vol. 54, No. 6, June 1976, pp.197-204.

58. Dux, P.F., and Kitipornchai, S., "Elastic Buckling of Laterally Continuous I-Beams", Journal of the Structural Division, ASCE, vol. 108, No. ST9, September 1982, pp.2099-2116.

59. Trahair, N.S., "Restrained Elastic Beam-Columns", Journal of the Structural Division, ASCE, vol. 95, No. ST12, December 1969, pp.2641-2664.

60. Vacharajittiphan, P., and Trahair, N.S., "Elastic Lateral Buckling of Portal Frames", Journal of the Structural Division, ASCE, vol. 99, No. ST5, May 1973, pp.821-835.

61. Vacharajittiphan, P., and Trahair, N.S., "Analysis of Lateral Buckling in Plane Frames", Journal of the Structural Division, ASCE, vol. 101, No. ST7, July 1975, pp.1497-1516.

62. Morino, S., "Analysis of Space Frames", Thesis presented to Lehigh University, in 1970, in partial fulfilment of the requirements of the degree of Doctor of Philosophy.

63. Citipitioglu, E., "Stability of Rigid-Jointed Space-Frames", dissertation presented to Oklahoma State University, in 1965, in partial fulfilment of the requirements of the degree of Doctor of Philosophy.

64. Vacharajittiphan, P., and Trahair, N.S., "Warping and Distortion at I-Section Joints", Journal of the Structural Division, ASCE, vol. 100, No. ST3, March 1974, pp.547-564.

65. Birnstiel, C., and Iffland, S.B., "Factors Influencing Frame Stability", Journal of the Structural Division, ASCE, vol. 106, No. ST2, Feb. 1980, pp.491-504.

66. Chilver, A.H., "Thin-walled Structures", A collection of papers on the stability and strength of tin-walled structures, Chatto, Windus Ltd., London 1967.

67. Jennings, A., and Majid, K.I., "The computer analysis of space frames using sparse matrix techniques", International Conference on Space Structures, 1966, Dept. of Civil Engr. University of Surrey.

68. Zbirohowshi-Koscia, K., "Thin-walled Beams from theory to practice", Crosby Lockwood & Son Ltd., London 1967.

69. Rao, S.S., "The Finite Element Method in Engineering", A. Wheaton & Co. Ltd., Exeter, first edition 1982.

70. Cope, R.J., Sawko, F., and Tickell, R.G., "Computer Methods for Civil Engineer", McGraw Hill, London, First Edition 1982.

71. Brebbia, C.A., and Ferrante, A.J., "Computational Methods for the Solution of Engineering Problems", Pentech Press London, 2nd Edition 1979.

72. Southwell, R.V., "An Introduction to the Theory of Elasticity", 2nd Edition 1941.

73. Leicester, R.H., "Southwell Plot for Beam-Column", Journal of the Structural Division, ASCE, vol. 95, No. EM6, December 1970, pp.945-965.

74. Ariaratnam, S.T., "The Southwell Method for Predicting Critical Loads of Elastic Structures", Quart. Journ. Mech. and Applied Math., vol. XIV, Pt.2, 1961, pp.137-153.

75. Roorda, J., "Some Thoughts on the Southwell Plot", Journal of the Structural Division, ASCE, vol. 92, No. EM6, December 1967, pp.37-48.

76. Davies, J.M., "Stability of Unbraced Pallet Racks", Fifth International Speciality Conference on Cold-Formed Steel Structures, Missouri, U.S.A., November 18-19, 1980, pp.409-427.

77. Horne, M.R., and Merchant, W., "The Stability of Frames", Pergaman Press Ltd., London 1965.

78. Coates, R.C., Coutie, M.G., and Kong, F.K., "Structural Analysis, 2nd Edition, Thomas Nelson Ltd., London 1980.

79. Black, M.M., "The Analysis and Design of Thin-Walled Open-Section Beams", Thin walled Steel Structures. Their design and use in building, Edited by Rockey, K.C., and Hill, H.V., Crosby Lockwood Ltd., 1969, pp.173-209.

80. Black, M.M. and Semple, H.M., "Torsion-Bending Analysis of Continuous Thin-Walled Beams", Int. J. Mech. Sci. Pergamon Press 1969, vol.11, pp.791-810.

81. Walker, A.C., "Design and Analysis of Cold-Formed Sections", International Textbook Company Ltd., London 1975.

82. Khan, A.H., and Tottenham, H., "The method of bimoment distribution for the analysis of continuous thin-walled structures subjected to torsion", Proc. Instn. Civ. Engrs., Part 2, Dec. 1977, pp.843-863.

83. Medwadowski, S., J., "Warping Moment Distribution", Journal of the Structural Division, ASCE, vol. 110, No. 2, Feb. 1985, pp.453-466.

84. Davies, J.M., "Torsion-Bending Analysis Made Easy", Paper TN 454 to be published Proc. ICE, Part 2.

85. Ramm, E., and Osterrieder, P., "Ultimate Load Analysis of Three-Dimensional Beam Structures with Thin-Walled Cross Sections Using Finite Elements", Stability of metal structures - Paris 16-17 Nov. 1983, Preliminary report, pp.201-210.

REFERENCES (II)

1. Bryan, E.R., Davies, J.M., Young, J.G. and Lawson, R.M., "MACE Nursery unit Load Tests". University of Salford, Department of Civil Engineering Report Ref. No. 74/51, December 1974.

2. Davies, J.M., Lawson, R.M., Young, J.G., "Calculated and observed behaviour of folded plate roof of a nursery school". Proc. Conf. on the performance of Building Structures, Glasgow Mar., 1974, pp.31-44.

3. BS449: part 2, 1969 "Specification for the use of structural steel in building". Appendix A. Loading Tests.

4. University of Salford, "Loading Tests on Pyradomes", Dept. of Civil Engineering Report Ref. No. 80/142, March 1980.

5. Nilson, A.H.,"Shear Diaphragms of Light Gauge Steel" Journal of the Structural Division, ASCE, Proc. vol. 86, No. ST11, Nov. 1960.

6. Ammar, A.R., and Nilson, A.H., "Analysis of Light Gauge Steel Shear Diaphragms, Parts I and II", Research Reports Nos. 350 and 351, Department of Civil Engineering, Cornell University, Ithaca, N.Y. Aug, 1972, Apr. 1973.

7. Nilson, A.H., "Analysis of Light Gauge Steel Shear Diaphragms", Proc., 2nd Specialty Conference on cold-formed steel structures, University of Missouri-Rolla, Rolla, Mo., Oct. 1973, pp.325-363.

8. Bryan, E.R., "The Stressed Skin Design of Steel Buildings", CONSTRADO Monograph, Crosby Lockwood Staples, London, England, 1973.

9. Davies, J.M., and Lawson, R.M., "The Shear Flexibility of Corrugated Steel Sheeting", Proc., 3rd International Specialty Conference on cold-formed Steel Structures, University of Missouri-Rolla, Rolla, Mo., Nov. 1975, pp.535-568.

10. Davies, J.M., and Lawson, R.M., "The Shear Deformation of Profiled Metal Sheeting". International Journal for Numerical Methods in Engineering, vol. 12, 1978, pp.1507-1541.

11. Davies, J.M., "A General Solution for the Shear Flexibility of Profiled Sheets", University of Salford, Department of Civil Engineering Report Ref. No. 82/173, Aug. 1982.

12. Davies, J.M., "Simplified Diaphragm Analysis", Journal of the Structural Division, ASCE, Proc., vol. 103, No. ST11, Nov. 1977, pp.2093-2109.

13. Davies, J.M. and Bryan, E.R., "Manual of Stressed Skin Diaphragm Design", Granada publishing, Great Britain 1982.

14. Davies, J.M., "Calculation of Steel Diaphragm Behaviour", Journal of the Structural Division, ASCE, Vol. 102, No. ST7, July 1976, pp.1411-1430.

15. SAP4: A computer program for static and dynamic analysis of linear systems. University of Manchester Regional Computer Center.